Physiological contribution and molecular details of GIRK-dependent signaling in the heart

A THESIS
SUBMITTED TO THE FACULTY OF THE
UNIVERSITY OF MINNESOTA
BY

Allison Diane Anderson

IN PARTIAL FULFILLMENT OF THE REQUIREMENTS
FOR THE DEGREE OF
DOCTOR OF PHILOSOPHY

Advisor: Kevin Wickman, PhD

July 2020

Acknowledgements

First and foremost, I must thank my advisor, Dr. Kevin Wickman. Your guidance and patience, in addition to the wonderfully supportive training environment you have cultivated, has been invaluable to my scientific and professional training. I also thank the members of my thesis committee, Dr. Stanley Thayer, Dr. Timothy Walseth, and Dr. John Osborn for their insights and encouragement these past years

Thank you, also, to the members of the Wickman lab, both past and present. This includes Dr. Ezequiel Marron Fernandez de Velasco, Dr. Megan Tipps, Dr. Lei Zhang, Dr. Nora McCall, Baovi Vo, Tim Rose, Margot DeBaker, Shirley (Haichang) Luo, Eric Mitten, Manini Mantri, Bushra Haider, Nicholas Carlblom, Hannah Oberle, Zhilian Xia, JingYing Zhang, and Melody Truong, Courtney Wright, and Mehrsa Zahiremami. Words cannot begin to describe the deep gratitude I have for the amazing sense of community and support (both technical and emotional) you all have provided. A special thank you to Dr. Nora McCall, who provided insightful feedback on the writing of this dissertation.

In addition to the Wickman lab, I have been fortunate to have amazing colleagues in the graduate students in the Department of Pharmacology, who I would also like to thank. My gratitude is also extended towards the Pharmacology Graduate Student Organization (PGSO) for providing an additional avenue for community within our program.

I would also like to thank my collaborators from the labs of Dr. Elena Tolkacheva, Dr. David Weaver, Dr. Kirill Martemyanov. It has been an immense pleasure to work with such esteemed researchers throughout the course of my graduate career. Additionally, I thank Dr. Nakano and Dr. Birnbaumer for the valuable mouse lines included in this work. My research and training experience has been incredibly enriched by these collaborations.

Thank you also to my mentors at the University of Minnesota Morris, Dr. Timna Wyckoff, Dr. Nancy Carpenter, Dr. Jennifer Goodnough, and Dr. Ted Pappenfus for introducing me to the wonderful world of research and guiding me towards graduate school (and away from medical school).

To my friends and family, I thank you all for the years of encouragement and comfort you have given to me. Special thanks to my biggest cheerleaders, my parents Jackie and Keith Peterson, and my incredible husband, Matt Anderson. Thank you all for the years of unwavering support and encouragement.

Lastly, I would like to thank my funding sources which supported this work. This includes grants from the National Institute of Health (NIH) to AA (HL139090), KW and KAM (HL105550), SWL (HL129544), AN (HL124503), ET (HL128790), CDW and KW (MH107399), and LB (NIH Intramural Research Program Project Grant Z01-ES-101643) and additional funding from the National Science Foundation to ET (CAREER PHY-125541 and DCSD 1662250).

Dedication

This dissertation is dedicated to my brother Michael Peterson, whose ongoing journey with Cystic Fibrosis is what inspired my passion for biomedical research and sparked my interest in ion channel biology.

Abstract

Activation of parasympathetic signaling to the heart results in a slowing of heart rate (HR) and an increase in heart rate variability (HRV). Perturbations in parasympathetic signaling to the heart contributes to the pathogenesis of cardiac arrhythmias such as atrial fibrillation. Accordingly, understanding the molecular mechanisms that facilitate the effects of parasympathetic signaling to the heart may provide insight for novel therapeutic interventions for related rhythm disorders. Parasympathetic signaling to the heart is carried largely by the vagus nerve which, when activated, results in activation of muscarinic receptors (M_2R) on cardiomyocytes. M_2R activation results in the modulation of several ion channels and enzymes, including activation of G protein gated inwardly rectifying potassium (GIRK) channels. The work in this thesis provides a thorough investigation into the physiological relevance of GIRK-dependent signaling in the heart while also probing the details of the underlying signaling architecture.

Previous work with parasympathomimetic compounds and global GIRK knockout mice suggested that GIRK channels mediate approximately 50% of the effects of parasympathetic signaling on HR and HRV. Here, we found that mice lacking GIRK channels selectively in atrial and sinoatrial nodal (SAN) tissue displayed absent responses to the HR slowing and HRV increases upon direct vagus nerve stimulation (VNS). Furthermore, GIRK channel ablation in atrial/SAN tissue conferred resistance to VNS-induced arrhythmias. Thus, GIRK channels in the atria represent an attractive therapeutic target for parasympathetic-mediated arrhythmias.

Unlike in the atria, the details and relevance of GIRK-dependent signaling in the ventricles are less well known. Electrophysiological recordings in isolated mouse ventricular myocytes revealed a similar GIRK channel subunit composition to those in the atria, however, many attributes (amplitude, sensitivity, kinetics, regulation) were distinct

from atrial/SAN counterparts. Furthermore, while GIRK channels mediated the effects of muscarinic stimulation on isolated ventricular myocyte excitability, specific ventricular ablation of GIRK channels in mice showed no impact on the mouse QT interval or ventricular arrhythmia susceptibility. In summary, disruption of ventricular GIRK channel dependent signaling does not appear to predispose the heart to arrhythmias.

Work presented here, and in the literature, supports the contention that inhibition of GIRK channel activity has promising therapeutic implications for supraventricular arrhythmias. Accordingly, we characterized a novel GIRK channel inhibitor, VU0468554. VU0468554 afforded dose-dependent block of GIRK channel activation in SAN cells with only minimal antagonism of GIRK channel activity in neurons, which express a different subunit composition. In the isolated mouse heart, VU0468554 exhibited a moderate, yet significant reversal of GIRK-mediated bradycardia elicited by muscarinic activation. Therefore, VU0468554 represents a novel pharmacological tool with therapeutic implications.

In addition to M_2R activation, GIRK channels are also activated by adenosine 1 receptor (A_1R) activation which is exploited clinically for the diagnosis and treatment of certain arrhythmias. We noted that M_2R- and A_1R-GIRK channel signaling exhibit distinct characteristics and are uniquely regulated by regulator of G protein signaling 6 (RGS6) in mouse SAN cells. These differences appear to arise from a combination of distinct G protein preferences by M_2R and A_1R and a strong substrate preference by RGS6.

Altogether, the GIRK channel signaling network present in the heart represents a critical mediator of cardiac parasympathetic signaling with promising therapeutic implications.

Table of Contents

List of Tables

List of Figures

List of Abbreviations

A_1R	Adenosine 1 receptor
AC	Adenylyl cyclase
AChE	Acetylcholinesterase
Ado	Adenosine
ADP	Action potential duration
AF	Atrial fibrillation
AGS	Activator of G protein signaling
AMPA	α-amino-3-hydroxy-5-methyl-4-isoxazolepropionic acid
ANS	Autonomic nervous system
AVN	Atrioventricular node
BCL	Basic cycle lengths
BRET	Bioluminescence Resonance Energy Transfer
bpm	Beats per minute
cAMP	Cyclic adenosine monophosphate
CCh	Carbachol
ChaT	Choline acetyltransferase
CN X	Cranial nerve 10
CNS	Central nervous system
CPA	N6-Cyclopentyladenosine
D_2R	Dopamine 2 receptor
DAG	Diacylglycerol
ECG	Electrocardiogram
ER	Endoplasmic reticulum
ERP	Effective refractory period
ESDC	Embryonic stem cell-derived cardiomyocytes
GAP	GTPase-activating protein
GEF	Guanine exchange factor
GIRK	G protein gated inwardly rectifying K^+
GPCR	G-protein coupled receptors
GRK	G protein coupled receptor kinase
HCN	Hyperpolarization-activated cyclic nucleotide-gated
HR	Heart rate
HRV	Heart rate variability
IP	Inositolphosphate
IRK	Inward rectifying K^+ channels
IVC	Inferior vena cava
LQTS13	Long QT Syndrome 13
M_1R, M_2R, M_3R, M_4R, M_5R	Muscarinic receptor subtypes 1, 2, 3, 4, 5
MOR	Mu opioid receptor
nAChR	Nicotinic receptor
NMDA	N-Methyl-d-aspartate
NTS	Nucleus tractus solitarius
PIP_2	Phosphatidylinositol 4,5-bisphosphate
PLC	Phospholipase C
PSVT	Paroxysmal supraventricular tachycardia
PVN	Paraventricular nucleus
RGS	Regulator of G protein signaling
RMP	Resting membrane potential

RMSSD	Root mean square of successive differences
RPV	Right pulmonary vein
S1P	Sphingosine-1-phosphate
SAN	Sinoatrial node
SCD	Sudden cardiac death
SR	Sarcoplasmic reticulum
SVC	Superior vena cava
TTQ	Tertiapin Q
VF	Ventricular fibrillation
VNS	Vagus nerve stimulation
VT	Ventricular tachycardia

Chapter 1

Introduction

1.1 Cardiac Arrhythmia and the Autonomic Nervous System

1.1.1 Normal cardiac conduction and cardiac arrhythmia

The cardiovascular system is responsible for providing the tissues and organ systems of body with the blood and nutrients necessary for survival. This function is driven by the electrical activity of the heart, which is responsible for pumping the blood through the vasculature. Normal conduction of electrical impulses throughout the heart (**Figure 1.1**) begins in the sinoatrial node (SAN), the pacemaker of the heart (Kennedy et al., 2016). The impulse generated in the SAN then instigates a wave of depolarization that travels throughout the top chambers of the heart, the left and right atria, until it reaches the atrioventricular node (AVN). From there, the impulse advances through the HIS-Purkinje system, which then distributes this conduction throughout the bottom chambers, the left and right ventricles, in an organized fashion. This well-orchestrated conduction pathway is what underlies each heartbeat, at a rate of typically 60-100 beats per minute (bpm) at rest in humans.

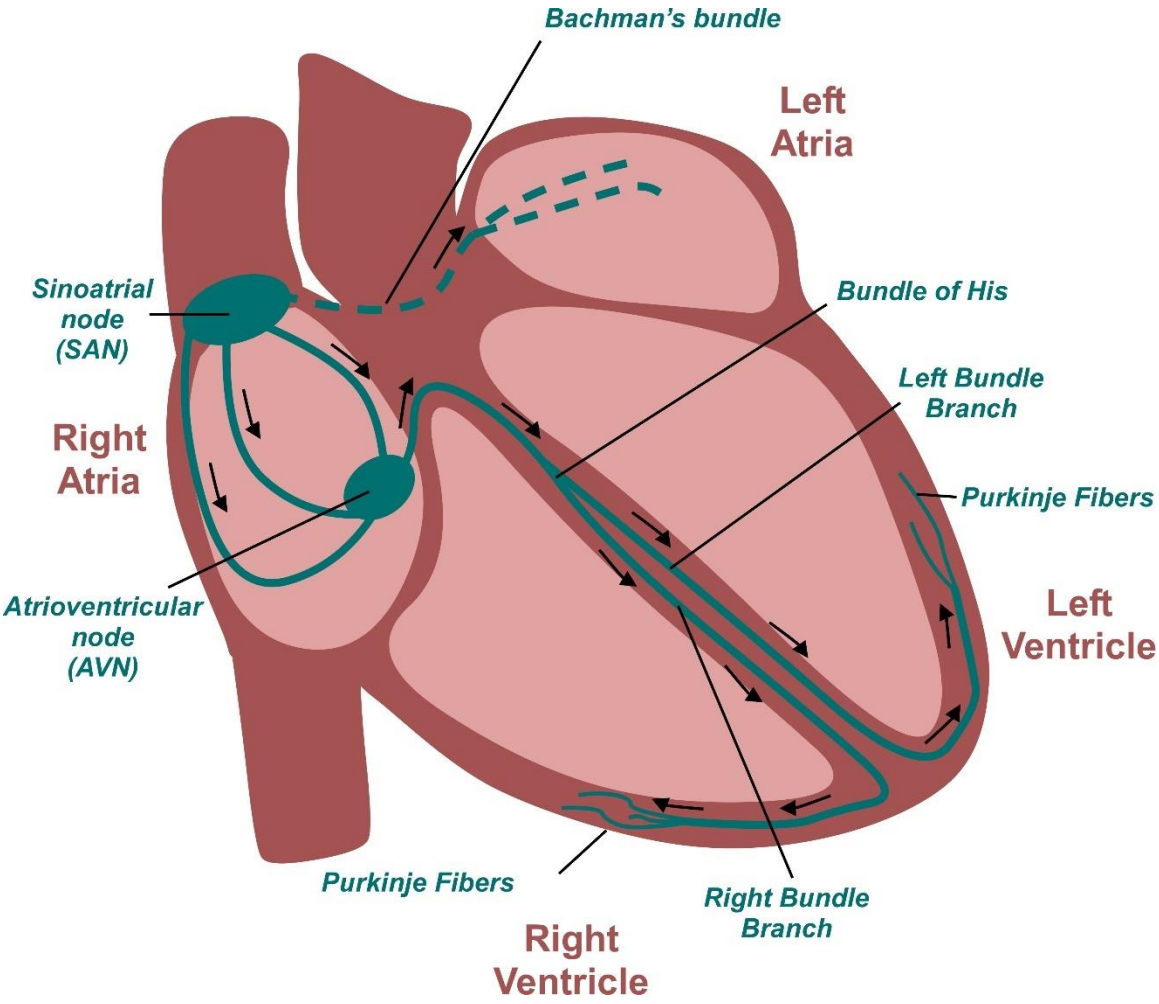

Figure 1.1. The cardiac conduction system
A coronal view of the heart depicting the main conduction pathways. The blue/green indicate conduction centers and pathways while the black arrows denote the direction. The impulse starts in the SAN and travels throughout the right atria (and through the Bachman's bundle to the left atria). The electrical signal then converges onto the AVN, which transmits the impulse throughout the ventricles by way of the Bundle of His, left and right bundle branches, and purkinje fibers.

Perturbations in this conduction pathway that result in a heart rate (HR) that is either too fast (>100 bpm, tachycardia), too slow (<60 bpm, bradycardia), or irregular (fibrillation) are designated as cardiac arrhythmias (Padeletti and Bagliani, 2017). Cardiac arrhythmias are largely classified by the area/region of the heart in which they arise and use the following broad, classifications: premature beats, bradyarrhythmias, supraventricular arrhythmia, and ventricular arrhythmias.

Premature beats. Premature beats refer to additional or extra heartbeats which arise from the cardiac impulse signal arriving early in either the atria (premature atrial contraction) or the ventricle (premature ventricular contraction) (Bagliani et al., 2018). Premature beats can sometimes cause a “fluttering” feeling in the chest and are largely harmless in the absence of structural heart disease (Gorenek et al., 2020; You and Liu, 2019).

Bradyarrhythmias. Any HR lower than normal (<60 bpm) is classified as a bradyarrhythmia. Sinus bradycardia may be an indicator of efficient cardiovascular health, seen more commonly in younger individuals or people who are physically fit (Aksu et al., 2018). However, in some cases, a low HR is the consequence of underlying disease such as heart failure, tissue damage, and hypothyroidism, resulting in poor cardiac output (Aksu et al., 2018). Whether or not bradycardia alone is pathogenic, a slower HR in general is responsible for a phenomenon known as “short-long-short” sequence (El-Sherif et al., 1999; Manolis et al., 2020; Sweeney et al., 2007). Essentially, the longer time between each heartbeat, known as cycle length, causes a heterogeneous prolongation of repolarization throughout the myocardium, creating a pro-arrhythmic environment.

Supraventricular tachyarrhythmias. Tachyarrhythmias, or arrhythmias resulting in a faster than normal (>100bpm) HR, that originate in the top two chambers of the heart are called supraventricular tachycardia. The most common supraventricular arrhythmias are atrial fibrillation (AF), atrial flutter, and paroxysmal supraventricular tachycardia

(PSVT). AF is an irregular and/or fast arrhythmia that occurs in the atria. In contrast to typical cardiac conduction, in AF the conduction spreads in a disorganized fashion, causing the atria to quiver or “fibrillate” (Dahya and Taigen, 2019). Similar to AF, atrial flutter results in a fast rhythm; however, it is organized, in contrast to the disorganized signals seen with AF (Stancák, 1998; Tai and Chen, 2009). PSVT is a tachyarrhythmia that starts and stops very abruptly due to the signals re-entering the atria from the ventricle (Al-Zaiti and Magdic, 2016).

Ventricular arrhythmias. Typically the most dangerous arrhythmias, ventricular arrhythmias arise from the ventricular tissue of the heart (AlMahameed and Ziv, 2019). Ventricular tachycardia (VT) is a fast, yet organized rhythm in the ventricles. On its own, VT may last only seconds and is relatively harmless. However, it can turn into a far more dangerous arrhythmia known as ventricular fibrillation (VF). VF occurs when the conduction in the ventricles becomes disorganized and instead of a coordinated contraction, the ventricles quiver. Given that the ventricles supply the body with blood, a loss of ventricular contraction can be fatal.

Cardiac arrhythmias are both pervasive and debilitating. Indeed, AF is the most common cardiac arrhythmia with approximately 2.7-6.1 million cases in the United States ((Chatterjee et al., 2017; Go et al., 2001; Miyasaka et al., 2006); the lifetime risk of developing AF is approximately 1 in 4 (Heeringa et al., 2006; Lloyd-Jones et al., 2004). AF is associated with an increased risk for ischemic stroke, renal disease, and death (Odutayo et al., 2016). Furthermore, ventricular arrhythmias are thought to be the underlying cause of nearly 80% of sudden cardiac death (SCD) cases (Chugh et al., 2008). Therefore, having adequate therapeutic interventions for individuals suffering from cardiac arrhythmias is imperative.

1.1.2 Current pharmacotherapy for the treatment of cardiac arrhythmias

Currently available anti-arrhythmic drugs target the molecules and machinery underlying the cardiac action potential. The action potential of the typical cardiomyocyte (atrial or ventricular) can be divided into 4 phases (Shih, 1994) (**Figure 1.2**). The standard action potential of a cardiomyocyte begins in Phase 4, when the cell is at rest with a membrane potential around -90 mV. This membrane potential is largely maintained by inward rectifying K^+ channels (IRK/Kir), mostly Kir2.1 or I_{K1}(Anumonwo and Lopatin, 2010). Inward rectification refers to an intracellular block of the pore of IRK channels at positive membrane potentials by cations like Mg^{2+} and polyamines, stopping K^+ efflux (Hibino et al., 2010). At negative, physiological membrane potentials, IRK channels allow K^+ out of the cell, maintaining the membrane potential around the Nernst potential of K^+ (-90 mV). When an action potential from a neighboring cardiomyocyte passes through a gap junction, Phase 0 beings, triggering a rapid depolarization of the cell membrane as voltage-gated Na^+ channels (I_{Na} ; $Na_v1.5$) open (Balse and Eichel, 2018). This is followed by the characteristic “notch” of Phase 1, where quick deactivation of the Na^+ channels is followed by the brief opening of transient outward K^+ channels, I_{to1}. Phase 2 or the “plateau phase” follows, where a balance of charge flow occurs due to delayed rectifier K^+ channels (I_{Kr} & I_{Ks}) opening and resulting in K^+ efflux (Charpentier et al., 2010). At the same time, L-type calcium ($I_{Ca,L}$) channels open, allowing Ca^{2+} influx (Bodi et al., 2005). The Ca^{2+} influx during this phase binds to ryanodine receptors located on the sarcoplasmic reticulum (SR), allowing further Ca^{2+} release from the SR which facilitates myocyte contraction (Eisner et al., 2017). Phase 3 begins when the $I_{Ca,L}$ channels close and further potassium (I_{Kr}, I_{Ks}, I_{K1}) channels open. This K^+ efflux results in membrane repolarization. At the resting membrane potential (RMP; -90 mV), the delayed rectifiers close, but I_{K1} remain open and the cell enters Phase 4 again.

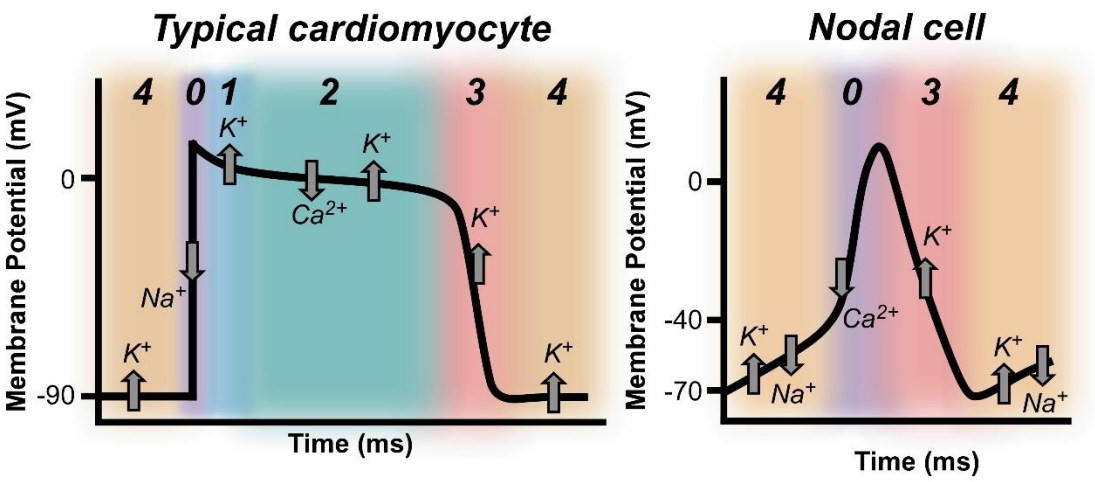

Figure 1.2. The cardiac action potential
Representation of the different phases of a typical cardiomyocyte (left) and nodal cell (right) action potential. Different phases of the cardiac action potential are denoted as follows: Phase 4:orange, Phase 0:purple, Phase 1:blue, Phase 2:green, Phase 3:red. The black line indicates the membrane potential over time in each phase. The gray arrows indicate the direction of ion flow during each phase.

The action potentials of pacemaker cells in the SAN and AVN are distinct in several aspects (Shih, 1994). As their name indicates, pacemaker cells are never completely at rest. Instead of having a stable membrane potential in Phase 4, nodal cells slowly depolarize until they reach approximately -40 mV due to the presence of hyperpolarization-activated cyclic nucleotide-gated (HCN) channels. HCN channels, often referred to as the I "funny" current (I_f), are a mixed Na^+ and K^+ current which are active at voltages under -40/-45 mV with a reversal potential at approximately -10/-20 mV (Difrancesco, 2010). Once the slow depolarization arrives at approximately -40 mV, the activation of L-type Ca^{2+} channels marks the beginning of Phase 0, a notably slower (2 ms vs. 10/20 ms) depolarization than observed in a typical human cardiomyocyte. While, Phase 1 and Phase 2 are notably absent in pacemaking cells, Phase 3 is similar to that of a typical cardiomyocyte action potential.

Deviations in the initiation and/or repolarization of cardiac action potentials and effective refractory period (ERP), the duration of time when the cell cannot respond to new stimulus, are key substrates in the formation of cardiac arrhythmias (Nerbonne and Kass, 2005). Anti-arrhythmic drugs are classified into 4 different groups (Class I, II, III and IV) based on the mechanism of action and the resulting influence on APD and ERP (Shu et al., 2009). The first class (Class I) of anti-arrhythmic drugs is comprised of Na^+ channel blockers and are split into 3 groups (1a, 1b,1c) based on their relative potencies and impact on re-shaping cardiac action potential duration (APD) (1a: APD prolongation, 1b: APD shortening, 1c: No effect on APD length). The next class, Class II, of anti-arrhythmic agents are the β-adrenergic receptor blockers, or "β-blockers" (Ogrodowczyk et al., 2015). Unlike the other classes, the β-blockers do not block ion channel activity directly, but rather, act by blocking β-adrenergic receptor signaling. Stimulation of β-adrenergic signaling results in an increase in cyclic adenosine monophosphate (cAMP) formation (Wallukat, 2002). cAMP increases the open probability of both L-type Ca^{2+} channels and HCN4 channels (Kumari et al., 2018). Thus, β-blockers decrease $I_{Ca,L}$ and I_f currents through by decreasing intracellular cAMP. Class III is a heterogenous group of anti-arrhythmic drugs that share the common broad mechanism of APD and ERP prolongation. These actions are primarily through blocking K^+ channel activity, specifically I_{Kr}, however the members of this class of drugs vary in their selectivity for this channel and may have additional actions on other cardiac ion channels. Lastly, Class IV anti-arrhythmia agents are comprised of the Ca^{2+} channel blockers which impact the slow calcium dependent action potentials in the SAN and AVN, therefore slowing the depolarization and firing rate (Szentandrassy et al., 2015). Altogether, the different anti-arrhythmic drug classes available afford several options for treating diverse patient populations.

While anti-arhythmic pharmacotherapy is widely used in the clinical management of cardiac arrhythmia, there are issues with limited efficacy and the potential to induce

arrhythmia. For example, the most efficacious drug for treating AF is amiodarone, is 60% successful in maintaining normal sinus rhythm within a year, in comparison to 50% for other anti-arrhythmic drugs (Dahya and Taigen, 2019). However, amiodarone also carries major adverse effects including the risk of developing a ventricular repolarization disorder known as Long QT. Long QT can develop into a life-threatening arrhythmia known as Torsades de Pointes (Turker et al., 2017). Due to these limitations, other therapeutic interventions, such as catheter ablation, defibrillation, and pacemaker implantation are frequently required in the treatment of cardiac arrhythmias (Fu, 2015; Macle and Nattel, 2016). Therefore, gaining a further understanding of how HR is regulated is necessary for the development of improved, sophisticated pharmacotherapeutic options. One such avenue of emerging research involves interventions targeted at the autonomic nervous system (ANS), which plays a key role in both regulation of HR and the development of cardiac arrhythmias (Dusi et al., 2019; Manolis et al., 2020).

1.1.3 Autonomic control of heart rate and role in arrhythmogenesis

While the heart has its own intrinsic beating rate, due to the underlying automaticity of the pacemaker cells of the SAN, the ANS tightly regulates this beating rate. The ANS consists of the sympathetic branch and the parasympathetic branch, which generally work antagonistically to modulate HR dynamics (Manolis et al., 2020; Shen and Zipes, 2014). Activation of the sympathetic nervous system results in what is colloquially known as the “flight-or-fight” response and results in an increase in HR (Coote and Chauhan, 2016). Conversely, parasympathetic activation is associated with “rest-and-digest” physiological responses which include a decrease in HR and an increase in the beat-to-beat variability, *i.e.*, heart rate variability (HRV) (Dyavanapalli et al., 2016). While these two branches largely work to oppose one another, a well-described interaction, known as accentuated antagonism, exists in which the effects of one branch of the ANS is amplified in the

presence of the other (Lujan et al., 2016; Uijtdehaage and Thayer, 2000). For example, the bradycardia elicited upon activation of the parasympathetic nervous system dramatically increases when given under concurrent sympathetic activation (Uijtdehaage and Thayer, 2000).

Dysregulation of autonomic signaling has been linked to a number of debilitating cardiac arrhythmias (Manolis et al., 2020). As might be expected, supraventricular tachyarrhythmias are typically associated with enhanced sympathetic activity, while bradyarrhythmias are linked to increased or abnormal parasympathetic tone. The role of autonomic dysfunction in AF is more complex, however (Chen and Tan, 2007; Hou et al., 2016). Stimulation of the vagus nerve, which carries much of the parasympathetic signaling to the heart, is associated with AF due to the resulting heterogenous prolongment of APD in the atria. However, simultaneously triggered activation of parasympathetic (vagus nerve) and sympathetic activity (left stellate ganglia) has been observed at the onset of AF. In line with these observations, neural ablation of either sympathetic input to the heart and or parasympathetic input to the heart result has been shown to eliminate paroxysymal AF episodes.

Ventricular arrhythmias, including VF, are known causes of SCD and sympathetic stimulation has been shown, both experimentally and clinically to provoke such arrhythmias (Hou et al., 2016; Huang et al., 2017). Additionally, damaged myocardium, either through ischemia and/or infarction, can serve a substrate for arrhythmic triggers due to the heterogeneity of sympathetic innervation of the ventricles. Similarly, a phenomenon known as “nerve sprouting” also occurs, where patients with myocardial infarction increased sympathetic nerve sprouting associated with increased VF episode.

Given the complex role the ANS plays in arrhythmogenesis, understanding the molecular components which mediate these effects may afford new targets to exploit for

novel therapeutic interventions. The focus of this dissertation is on the inhibitory branch of the ANS, the parasympathetic nervous system.

1.2 Parasympathetic Regulation of Cardiac Function

1.2.1 Brainstem origin of the vagus nerve

The parasympathetic signaling to the heart is carried by the vagus nerve (cranial nerve 10; CN X), which originates in the brainstem (Gourine et al., 2016; Huang et al., 2015) (**Figure 1.3**). Vagal nerve activity is modulated by three main centers of the medulla oblongata: the dorsal motor nucleus, the nucleus ambiguus, and nucleus tractus solitarius (NTS). The dorsal motor nucleus lies near the fourth ventricle in the medulla and contains vagal efferent fibers which carry signaling to the heart (Standish et al., 1994). The nucleus ambiguus, which resides in the lowest part of the brainstem (the reticular formation of the medulla oblongata) is another primary site of origin for the vagal efferent fibers which innervate the heart. The cardiac vagal neurons of the nucleus ambiguus are typically silent, and do not possess pacemaker activity (Mendelowitz, 1996). However, only small depolarizing currents (100 pA) are necessary to evoke firing of these neurons with relatively little delay (Mendelowitz, 1996). Studies have shown that excitatory, glutamatergic input from the NTS (Wang et al., 2006) activates post-synaptic N-Methyl-d-aspartate (NMDA) and α-amino-3-hydroxy-5-methyl-4-isoxazolepropionic acid (AMPA) receptors in the cardiac vagal neurons of the nucleus ambiguus (Neff et al., 1998). The NTS is located in the dorsomedial medulla and is largely responsible for facilitating the baroreceptor reflex, which is how the body regulates blood pressure by modulating HR (Andresen and Kunze, 1994). This process of regulation involves chemoreceptors and mechanoreceptors located in the carotid sinus and aortic arch which activate baroreceptors afferents in the NTS which relays these signals to the nucleaus ambiguus.

While not directly involved in vagal signaling to the heart, signaling in the paraventricular nucleus (PVN), while largely seen as sympathoexcitatory, also contains axonal projections to the nucleus ambiguus and can indirectly influence vagal nerve activity (Geerling et al., 2010; Stuesse and Fish, 1984). These various pathways present in the central nervous system (CNS) modulate the activity of the vagus nerve, which carries the main branches of parasympathetic pre-ganglionic fibers.

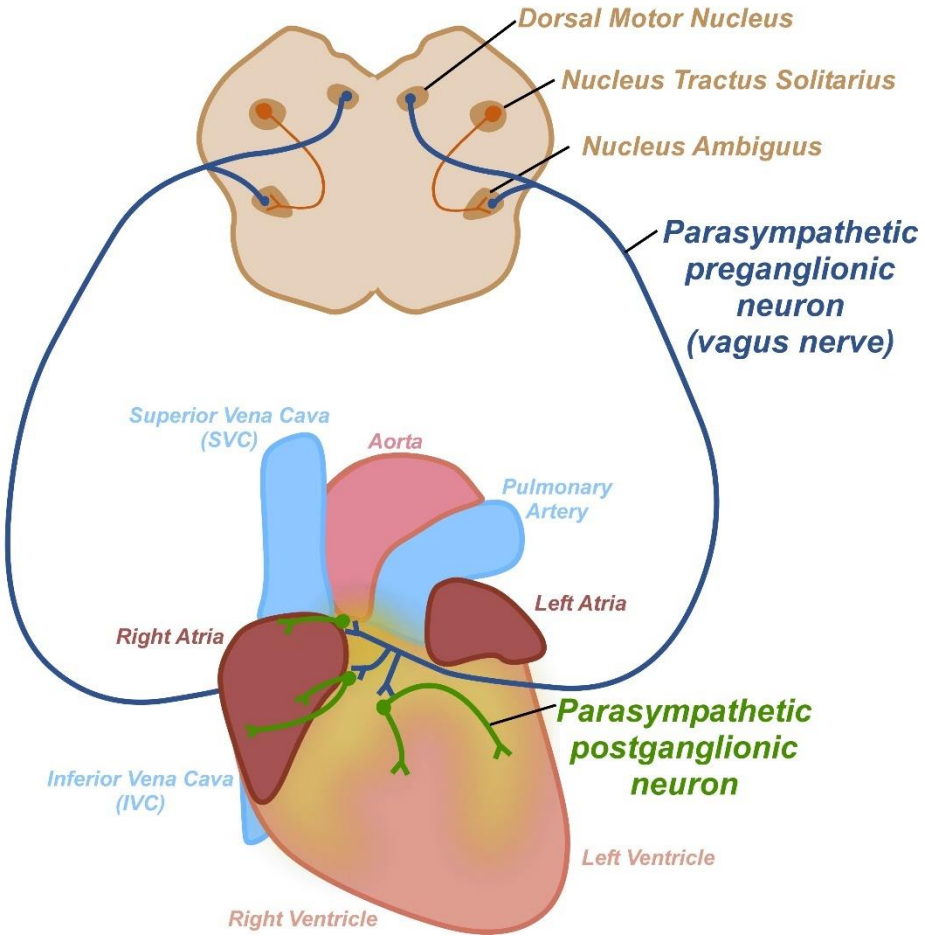

Figure 1.3. Parasympathetic innervation of the heart
Representation of vagal input to the heart. The vagus nerve originates in the brainstem and its activity is modulated by the dorsal motor nucleus, nucleus tractus solitarius, and nucleus ambiguus (depicted above in a coronal section of the medulla). The branches of vagus nerve act as parasympathetic preganglionic neurons, terminating on the intrinsic cardiac ganglia located on epicardial fat pads (yellow). The preganglionic neuron releases ACh onto parasympathetic postganglionic neurons present in the cardiac ganglia which extensively innervate the myocardium (Huang et al., 2015).

1.2.2 Vagal innervation of the heart

Parasympathetic input to the heart via the vagus nerve terminates with synaptic connection to post-ganglionic neurons within intracardiac ganglia, an intricate network of synaptic connectivity across the heart. The pattern of parasympathetic innervation of cardiac tissue differs greatly between the different chambers of the heart.

Work including histology, surgical dissection and epicardial radiofrequency catheter ablation have demonstrated rich vagal innervation of atrial and nodal tissue (Coote, 2013). An area of particularly high vagal innervation include a fat pad located between the medial superior vena cava (SVC) and aortic root (Chiou et al., 1997). The rich vagal innervation at the SVC-aortic root fat pad then proceeds to innervate fat pads located between the inferior vena cava (IVC)-left atria and the right pulmonary veins (RPV)-left atria (Chiou et al., 1997; Randall et al., 1987). While the majority of vagal input passes through the SVC-aortic root fat pad, there is evidence of direct innervation of the IVC-left atria fat pad, RPV-left atria fat pad, and atrial myocardium as well.

Until recently, it was thought that vagal innervation of the ventricles was either sparse or entirely absent. However, current work has shown that vagal efferent fibers are, indeed, present in ventricular tissue and play an important role in regulating ventricular physiology (Coote, 2013). Histological work looking at markers of cholinergic nerve terminals (acetylcholinesterase (AChE) and choline acetyltransferase (ChaT)) highlighted the existence of an extensive network of post-ganglionic ventricular innervation throughout ventricular muscle fibers. The post-ganglionic vagal fibers that innervate the ventricles are largely fibers which originate from the principle supraventricular fat pads discussed above, in addition to sites located at the interventricular groove, the interatrial and interventricular septa (Blomquist et al., 1987; Gatti et al., 1997).

Both pre-ganglionic and post-ganglionic parasympathetic neurotransmission is mediated by the neurotransmitter acetylcholine (ACh). Activation of the vagus nerve

results in the release of ACh onto nicotinic receptors (nAChR) present on post-ganglionic parasympathetic neurons present in the intracardiac ganglia (De Biasi, 2002). Thus, nAChRs represent a critical intermediary of the effects of parasympathetic signaling on the heart. nAChRs are ligand-gated non-selective ion channels with permeability primarily to Na^+ and K^+ and moderately to Ca^{2+} (Papke, 2014). Activation of nAChRs requires the binding of ACh which instigates rapid membrane depolarization and neuronal activation (Papke, 2014). nAChRs are pentameric channels consisting of various combinations of the following subunits: 9 alpha subunits (α2-α10) and 3 beta subunits (β2-4) (Papke, 2014). Rat intracardiac neurons have been shown to express α2–α9 and β2–β4 subunits, though not all of the neurons within ganglion express all these subunits (Poth et al., 1997). The α3 nAChR subunit is highly expressed in all autonomic ganglia, including cardiac ganglia, and is likely a critical component of many AChR subtype compositions (Rust et al., 1994). The use of sub-type specific blockers and knockout mice has shown that while α7-containing nAChRs appear to mediate the effects of sympathetic signaling to the heart, α4β2-containing nAChRs mediate the bradycardic effects of parasympathetic signaling to the heart (Li et al., 2009b). Therefore, it appears distinct receptors subtypes mediate parasympathetic and sympathetic ganglionic synaptic transmission. The activation of nAChRs in parasympathetic postganglionic neurons in the cardiac ganglia ultimately results in the release of ACh onto muscarinic receptors present in the surface membrane of cardiomyocytes.

1.2.3 Muscarinic-dependent signaling in the heart

Muscarinic receptors represent the main molecular mediator for parasympathetic actions on cardiac tissue. Thus, understanding the details of muscarinic signaling in the heart is critical to understanding parasympathetic regulation of HR dynamics.

Muscarinic receptors belong to the large protein family of seven-transmembrane receptors known as G-protein coupled receptors (GPCR) (Dhein et al., 2001; Katritch et al., 2013). As their name suggests, these receptors are coupled to heterotrimeric G proteins consisting of a G alpha ($G\alpha$) subunit bound to a tightly coupled, G beta-gamma ($G\beta\gamma$) dimer (Weis and Kobilka, 2018). When the receptor is in the inactive state, the α subunit of this complex is bound to GDP. Upon ligand binding, the receptor undergoes a conformational change that is transmitted to the G protein complex. This conformational change results in the GDP bound to the α subunit being exchanged with cytosolic GTP. This GDP-to-GTP exchange in combination with a decreased affinity of α-GTP for $G\beta\gamma$ resulting in the dissociation of the α-GTP from the $G\beta\gamma$ dimer. Subsequently, both α-GTP and $G\beta\gamma$ interact with various downstream effectors. Eventual reassociation of $G\alpha$ and $G\beta\gamma$ occurs due to intrinsic GTP hydrolysis activity of $G\alpha$. This process is often facilitated by Regulator of G protein Signaling (RGS) proteins that accelerate the rate of GTP hydrolysis (Stewart and Fisher, 2015; Willars, 2006).

Five different muscarinic receptor subtypes have been identified in mammals: M_1R, M_2R, M_3R, M_4R, and M_5R (Caulfield, 1993; Dhein et al., 2001). Differences between muscarinic receptor sub-types reside primarily in the third intracellular loop, a region shown to be critical for G protein coupling (Wess et al., 1997), resulting in the two distinct groupings for the subtypes. M_1R, M_3R, M_5R are G_q coupled receptors which classically activate phospholipase C (PLC), resulting in the production of diacylglycerol (DAG) and inositolphosphate (IP), whereas, M_2R and M_4R are $G_{i/o}$ coupled receptors, whose activation results in the inhibition adenylyl cyclase (AC). $G_{i/o}$ coupled receptors are characterized by a sensitivity to pertussis toxin, which prevents the coupling of $G\alpha$ subunits of the $G_{i/o}$ subfamily to receptors through ADP ribosylation (Mangmool and Kurose, 2011). A combination of studies involving relative expression of muscarinic sub-

types and the use of sub-type specific modulators has shown that M_2R is the predominant muscarinic isoform expressed in cardiac tissue (Dhein et al., 2001; Peralta et al., 1987; Saternos et al., 2018). Indeed, HR slowing to cholinergic stimulation is absent in atria from mice lacking M_2R, further suggesting that M_2R is predominant subtype mediating the effects of parasympathetic signaling in cardiac tissue (Stengel et al., 2000).

Upon agonist-induced activation of muscarinic receptors, desensitization occurs in a matter of seconds. A major contributor to the initial desensitization is the rapid phosphorylation of the activated (ligand-bound) receptors by G protein-coupled receptor kinases (GRKs) (Gurevich and Gurevich, 2019). The phosphorylation of the receptors results in an increased affinity for cytosolic β-arrestin, which conformationally restricts the receptors from coupling to G proteins. Four different GRKs have been shown to be expressed in the heart (GRK2, GRK3, GRK5, and GRK6 (Hullmann et al., 2016)) and each demonstrate varying degrees of M_2R phosphorylation *in vitro* (Marlene Hosey et al., 1995). Thus, M_2R desensitization is likely the result of a combination of GRK-M_2R interactions.

Muscarinic receptor-dependent signaling has a profound effect on supraventricular physiology (Harvey, 2012; Harvey and Belevych, 2003). M_2R activation in SAN cells results in membrane hyperpolarization, which slows the spontaneous depolarization and ultimately reduces the firing rate of SAN cells. In the AVN, membrane hyperpolarization upon muscarinic activation decreases impulse conduction. In atrial myocytes, activation of M_2R shortens APD and reduces contractile force. Similar effects are seen in ventricular tissue, although to a much lesser extent and largely in the presence of background cAMP-dependent signaling. These effects are mediated by both direct and indirect influences on several downstream ion channels (Harvey and Belevych, 2003), detailed in **Figure 1.4**.

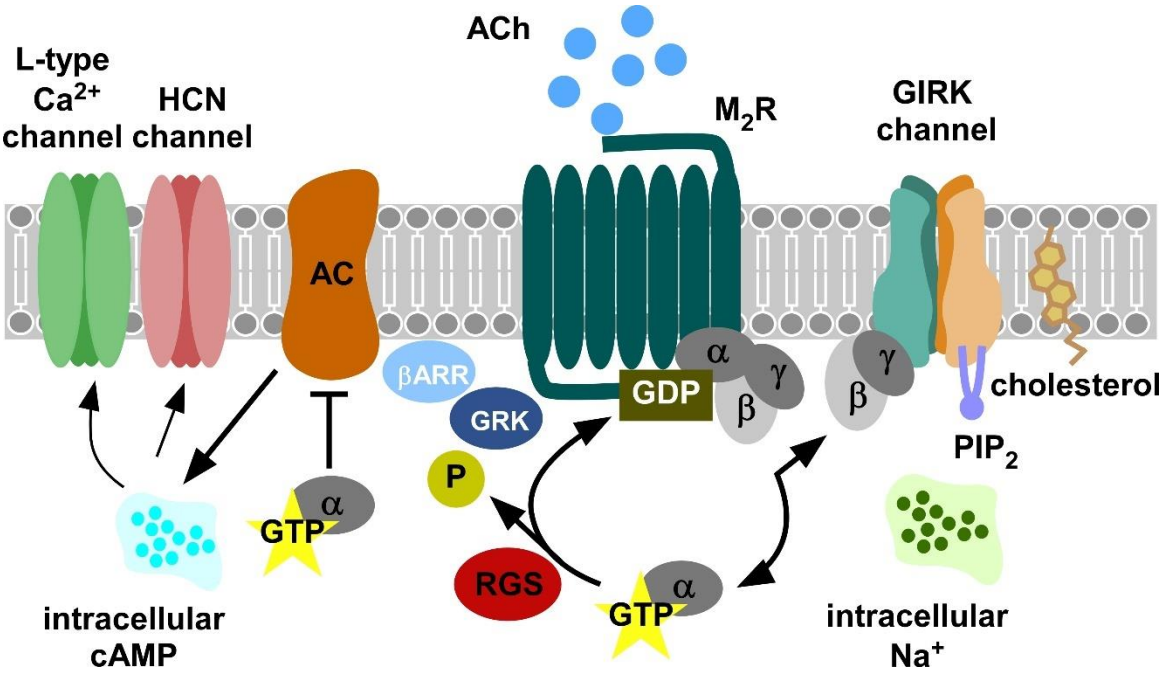

Figure 1.4. Details and downstream effectors of muscarinic signaling in cardiomyocytes.
Post-ganglionic parasympathetic release of ACh activates M_2R receptors present on cardiomyocytes. Activation of M_2R results in the dissociation of $G\alpha$ and $G\beta\gamma$. $G\alpha$ inhibits AC which results in a decrease in intracellular cAMP. This results in the inhibition of cAMP-dependent $I_{Ca,L}$ and I_f currents. $G\beta\gamma$ activates GIRK channels, a process dependent on the cofactor PIP_2 and modulated by cholesterol and intracellular Na^+. Reassociation of $G\alpha$ and $G\beta\gamma$ occurs due to intrinsic GTP hydolysis activity present in $G\alpha$, process facilitated by RGS proteins. Desensitization of M_2R is mediated by phosphorylation by GRKs resulting in an increase affinity for β-arrestin.

The indirect influence of muscarinic activation in cardiomyocytes is due to inhibition of AC, which decreases intracellular cAMP. Reduction of intracellular cAMP inhibits the gating of two conductances which play a critical role in cardiomyocyte excitability and contraction, I_f (HCN4) and $I_{Ca,L}$ (L-type Ca^{2+} channels). As discussed in section **1.1.2**, I_f is responsible for the diastolic depolarization phase of action potentials in nodal cells and has been, accordingly, called the "pacemaker current" (Difrancesco, 2010). Inhibition of I_f via muscarinic activation results in decreased diastolic depolarization of nodal cells. Activation of $I_{Ca,L}$ is responsible for both cardiomyocyte excitation-contraction coupling and nodal cellular depolarization (Bodi et al., 2005), therefore, muscarinic activation results in

an inhibition of these processes. Interestingly, while muscarinic suppression of $I_{Ca,L}$ in the atria is observed the absence of elevated cAMP, it seems that elevated cAMP is required for muscarinic inhibition of ventricular $I_{Ca,L}$, representing a molecular mechanism of accentuated antagonism (Harvey and Belevych, 2003). The direct effects of muscarinic activation involve the acetylcholine activated K^+ conductance, I_{KACh}, mediated by activation of G protein-gated inwardly rectifying K^+ (GIRK) channels, and is the focus of this dissertation. The next section describes GIRK channel function and what is currently known about its role in mammalian cardiac physiology.

1.3 GIRK channels in the heart

1.3.1 GIRK channel structure, function, and activation

GIRK channels were first identified in nodal cells as a unique, ACh-dependent K^+ conductance with gating and conductance characteristics that were distinct from resting inwardly rectifying K^+ channels (I_{K1}) (Sakmann et al., 1983). The cDNA for the GIRK subunit GIRK1 (Kir3.1) was the first GIRK channel subunit to be isolated (Dascal et al., 1993a; Kubo et al., 1993) followed by the identification of cDNAs for additional GIRK subunits GIRK2, GIRK3, and GIRK4 (Doupnik et al., 1995; Kofuji et al., 1995; Krapivinsky et al., 1995a; Lesage et al., 1994). GIRK channel subunits are conserved across mouse, rat and human and each share similar core structure, including intracellular N- and C-terminal domains, two transmembrane segments, and a hydrophobic pore domain (Hibino et al., 2010). Native GIRK channels are tetrameric complexes made up of various combinations of these 4 subunits (GIRK1, GIRK2, GIRK3, and GIRK4). While GIRK1, GIRK2, and GIRK3 are broadly expressed in the CNS, GIRK4 expression in the brain is extremely limited. Prominent GIRK4 expression is restricted to discrete neuronal populations present in cortex, thalamus, and hypothalamus (Wickman et al., 2000).

In contrast, GIRK1 and GIRK4 are highly expressed in cardiac tissue while GIRK2 and GIRK3 are absent. Indeed, the predominant GIRK channel subtype in cardiomyocytes is a heterotetrametric complex containing GIRK1 and GIRK4 in 1:1 stoichiometry (Bettahi et al., 2002). While GIRK1 and GIRK4 share similar core structures, GIRK1 lacks an endoplasmic reticulum (ER) export motif and is unable to form functional channels on its own. Therefore, GIRK1 requires co-expression with other subunits which contain an ER export motif, such as GIRK4, for proper membrane translocation (Dascal et al., 1993b; Hedin et al., 1996; Kennedy et al., 1999). GIRK4, on the other hand, can form functional GIRK4 homo-tetrameric complexes and there is evidence of their presence in atrial myocytes (Corey and Clapham, 1998).

GIRK channels are activated specifically by $G_{i/o}$ coupled GPCRs. Initial studies of GPCR-dependent activation of cardiac GIRK channels identified that activation was dependent on trimeric G proteins rather than secondary messenger systems (Breitwieser and Szabo, 1985; Pfaffinger et al., 1985). Further studies identified $G\beta\gamma$, not $G\alpha$, as the critical activator of cardiac GIRK channels, where binding of $G\beta\gamma$ increases the open probability of the channel. (Huang et al., 1997; Krapivinsky et al., 1995b; Nemec et al., 1999; Wickman et al., 1994). $G\beta\gamma$ can bind directly to both cardiac GIRK channel subunits with potential binding sites for $G\beta\gamma$ are located at both the N- and C- termini of GIRK1 and GIRK4 (He et al., 1999; Huang et al., 1995, 1997; Takao et al., 1994). The selective activation of GIRK channels by G proteins of the $G_{i/o}$ family is thought to be related to the rapid $G\beta\gamma$ release rate of this G protein subfamily, resulting in higher concentrations of $G\beta\gamma$ available for GIRK channel activation (Touhara and MacKinnon, 2018).

$G_{i/o}$ coupled GPCRs present in the heart known to activate GIRK channels include M_2R as well as the adenosine 1 receptor, A_1R, which mediates the effects of the autacoid adenosine (Ado) on cardiac electrophysiology. GIRK channel activity in the absence of GPCR activation, known as constitutive GIRK channel activity, does exist, albeit at a much

lower opening frequency than agonist-dependent activity (Ito et al., 1994; Sakmann et al., 1983). Expression of proteins which bind $G\beta\gamma$ ($G\alpha_i$ and myristoylated phosducin) in rat atrial myocytes revealed that basal GIRK channel activity is indeed independent of free $G\beta\gamma$ (Kienitz et al., 2014). In this study, basal GIRK activity was defined as the amount of current sensitive to the bee venom peptide tertiapin-Q (TTQ), which preferentially inhibits GIRK channels over other IRK channels at nanomolar concentrations (Kanjhan et al., 2005). Thus, basal and GPCR-activated GIRK channel gating are the result of separate processes.

1.3.2 GIRK channel cofactors and regulation

The dynamics of GIRK channel gating are the result of an expansive signaling architecture of interwoven interactions between various co-factors, intracellular conditions, and regulatory proteins. Below, I summarize the key regulatory factors involved in GIRK-dependent signaling in cardiomyocytes, which include phosphatidylinositol 4,5-bisphosphate (PIP_2), channel phosphorylation, intracellular Na^+, cholesterol, activator of G protein signaling (AGS) proteins, and RGS proteins.

PIP_2. PIP_2 is a phospholipid found in the cytoplasmic leaflet which modulates the activity of a number of membrane-delimited proteins including ion channels such as GIRK channels (Suh and Hille, 2008). Indeed, studies in which PIP_2 is depleted from the membrane using anti-PIP_2 antibodies results in a decrease in channel activity (Huang et al., 1998). Conversely, restoring PIP_2 to the membrane also restores GIRK channel activity (Huang et al., 1998). In addition to being required for $G\beta\gamma$ activation, there is also evidence of direct activation of GIRK channel by PIP_2 (Huang et al., 1998). The PIP_2 binding site is located near the interface of the transmembrane domain and cytoplasmic domain of each GIRK channel subunit (Whorton and MacKinnon, 2011). This interaction is maintained by positively charged lysines present at his interface which associate with the negative

charged phosphates on PIP_2. It is known that agonist-independent GIRK activity is PIP_2-dependent, as PIP_2 alone can maximally activate GIRK channels in the absence of $G\beta\gamma$ (Huang et al., 1998). Though it is intact PIP_2 which plays a direct role in the gating of GIRK channels, PIP_2 is a substrate for PLC; the products of PIP_2 cleavage being IP_3 and DAG. Therefore, PLC-dependent processes effectively deplete the amount of PIP_2 present in the membrane, which may regulate GIRK-dependent signaling.

Phosphorylation. Work in both recombinant systems and cardiomyocytes has revealed the necessary role phosphorylation of GIRK channels plays in channel activity. Bath application of phosphatase inhibitors results in a reduction in constitutive GIRK channel activity, suggesting that basal activity seems to be influenced in part by phosphorylation levels (Berlin et al., 2011; Voigt et al., 2014). De-phosphorylation of GIRK channels using protein phosphatases can prevent channel activation by $G\beta\gamma$ as well, an effect rescued by the addition of ATP (Medina et al., 2000). Putative Ser/Thr sites between amino acid 373 and 419 located on the C-terminus of GIRK1 are critical for channel phosphorylation and regulation of the channel by protein phosphatases (Medina et al., 2000). Notably, these sites are absent on GIRK4, demonstrating that GIRK1 is indeed the site of channel phosphorylation.

Intracellular Na^+. Intracellular Na^+ can activate GIRK channels through both direct and indirect actions. Intracellular Na^+ has been shown to bind to cardiac GIRK channels and increase responsiveness to $G\beta\gamma$ activation. A negatively charged Asp residue in the C-terminus of GIRK4 seems to be a critical site for the direct actions of Na^+ on gating of GIRK channels (Zhang et al., 1999). Na^+ also reduces the affinity of the interaction between $G\alpha$GDP and $G\beta\gamma$ (Rishal et al., 2003), which enhances GIRK-dependent signaling by increasing free $G\beta\gamma$. Interestingly, impaired Na^+ regulation of GIRK channels has been observed in atrial myocytes isolated from human patients with chronic AF (Voigt

et al., 2013). This decrease has been linked to a decrease in GIRK4 relative to GIRK1 in atrial tissue from chronic AF patients (Voigt et al., 2013).

Cholesterol. Cholesterol is a critical component of the cell membrane and it plays a central role in membrane dynamics and cell signaling. Indeed, cholesterol impacts the function of a variety of ion channels, including GIRK channels, through both direct interaction as well as indirect actions on membrane fluidity/rigidity. Studies in planar lipid bilayers demonstrated that cholesterol enrichment increases the open probability of cardiac GIRK channels, an effect that was not due to an increase in GIRK channel surface expression (Bukiya et al., 2015). Indeed, cholesterol has been shown to work synergistically with PIP_2 to activate atrial GIRK channels (Bukiya and Rosenhouse-Dantsker, 2017). Mutagenesis studies have identified 5 residues in the hydrophobic surface of the transmembrane domain which may be responsible for the actions of cholesterol on GIRK channels (Bukiya and Rosenhouse-Dantsker, 2017). Enrichment of rabbit atrial myocytes with cholesterol resulted in an increase in ACh-induced GIRK currents (Deng et al., 2012). Similarly, atrial myocytes isolated from rats fed a high cholesterol diet displayed a similar increase in ACh-induced GIRK currents (Deng et al., 2012). In line with these findings, pharmacological inhibition of cholesterol production using statins attenuates GIRK channels activity in mouse atrial myocytes (Cho et al., 2014). As a whole, these studies highlight the modulatory role cholesterol plays in GIRK channel activity.

AGS proteins. AGS proteins are receptor-independent activators of G protein-dependent signaling (Blumer et al., 2005; Blumer and Lanier, 2014). AGS proteins 1-3 each have distinct molecular mechanisms from one another (Blumer et al., 2005; Cismowski et al., 2001). AGS1 acts as a guanine exchange factor (GEF) for $G_{i/o}$ G proteins, similar to the actions of a GPCR. Indeed, in oocytes injected with GIRK1, GIRK4 and M_2R cDNA, co-injection of AGS1 cDNA results in a reduction in ACh-induced current

amplitudes (Takesono et al., 2002). Thus, AGS proteins, namely AGS1, can negatively modulate GPCR/GIRK dependent responses by altering the available pool of activatable G proteins.

RGS proteins. RGS proteins accelerate the termination of G-protein dependent signaling through their GTPase-activating protein (GAP) activity. Various RGS proteins are expressed in cardiac tissue, including RGS2, RGS3, RGS4, RGS6, RGS10, RGS-Gα-interacting protein (GAIP), and RGSZ2 (Doupnik et al., 2001). Embryonic derived stem cells (EDSCs) containing either mutant $G\alpha_{i2}$ or $G\alpha_o$ that are insensitive to RGS regulation revealed exaggerated GIRK-dependent signaling, suggesting a negative regulatory role for RGS proteins in GPCR-GIRK signaling (Fu et al., 2006). RGS6 in particular has emerged as the critical negative regulator of cardiac M_2R-GIRK signaling. RGS6 is a member of the R7 RGS family which forms obligate dimers with the atypical Gβ subunit Gβ5. Ablation of RGS6 results in delayed GIRK channel deactivation kinetics and increased channel sensitivity to muscarinic receptor activation (Posokhova et al., 2010; Wydeven et al., 2014b; Yang et al., 2010a).

In addition to RGS6, both RGS4 and RGS5 have been identified as potential regulators of cardiac GIRK signaling. RGS4 has been shown to associate with GIRK channels and regulate GIRK-dependent signaling in reconstituted cell systems (Inanobe et al., 2001). SAN cells from mice lacking RGS4 display decreased GRK-independent 7desensitization and prolonged activation and deactivation of GIRK-dependent currents compared to recordings in SAN cells from wild-type mice (Cifelli et al., 2008). However, an additional study was not able to replicate these findings and identified RGS6 as the dominant regulator of GIRK dependent signaling in nodal/atrial tissue (Wydeven et al., 2014b). Intriguingly, concurrent genetic ablation of RGS4 along with RGS6 results in a partial rescue of the phenotypes observed in *Rgs6*$^{-/-}$ SAN cells (Wydeven et al., 2014b). In addition to RGS4 and RGS6, RGS5 and RGS10 have also been suggested to play a

role in GIRK-dependent signaling (Bender et al., 2008; Qin et al., 2016). Altogether, RGS proteins have an interwoven set of roles in modulating GIRK signaling in cardiac tissue.

1.3.3 Role of GIRK channels in cardiomyocyte excitability

GIRK channels are highly expressed in SAN and AVN cells and are critical mediators of $G_{i/o}$ coupled GPCRs present in these tissues (DiFrancesco et al., 1989; Meijler and Janse, 1988; Mesirca et al., 2013; Nishimura et al., 1988; Noma and Trautwein, 1978). Activation of muscarinic receptors in SAN cells results in hyperpolarization and a reduction in the firing rate, ultimately slowing HR. GIRK channels are also the main mediators of the hyperpolarization and firing rate slowing effects of A_1R activation in rabbit SAN cells (Belardinelli et al., 1988). Initial electrophysiological assessments aimed at teasing out the HR slowing actions of ACh in rabbit SAN cells revealed a reversal potential of ACh-induced currents which resembled a K^+ conductance distinct in gating and conductance properties from resting IRK channels in atrial and ventricular cells (Noma and Trautwein, 1978; Sakmann et al., 1983) with similar observations in rabbit and guinea pig AVN cells (Nishimura et al., 1988; Yuill and Hancox, 2002). DiFrancesco and colleagues later identified a concentration-dependence of ACh on downstream effectors where low concentrations predominantly inhibit I_f yet approximately 20 times higher concentrations are required for GIRK channel activation (DiFrancesco et al., 1989). More recent work using *Girk4*$^{-/-}$ mice showed that SAN cells lacking GIRK4 displayed significantly blunted pacemaker rate reduction upon application of ACh (Mesirca et al., 2013).

In addition to their role in modulating the beating rate and conduction of nodal cells, GIRK channels are highly expressed in atrial tissue and play a critical role in mediating atrial myocyte excitability (Calloe et al., 2013; Gaborit et al., 2007; Wang et al., 2013b). Single channel recordings in isolated mouse atrial myocytes revealed classic

rectification characteristics and GIRK single channel properties (Wickman et al., 1998). Furthermore, this current was activated by either ACh or GTPγS and absent in atrial myocytes from mice lacking GIRK4 (Wickman et al., 1998). Studies in isolated canine and rat atrial preparations revealed profound shortening of APD, ERP, and lowering of RMP upon application of ACh or the A_1R agonist N6-Cyclopentyladenosine (CPA) (Calloe et al., 2013; Wang et al., 2013b). CPA elicits a similar impact on rat atrial APD, ERP and RMP (Wang et al., 2013b) Notably, the effects of ACh and CPA perfusion on rat atrial preparations were reversed upon application of TTQ, suggesting GIRK-dependence (Wang et al., 2013b).

While it is commonly accepted that GIRK channels contribute to the actions of ACh in nodal cells and atrial myocytes, the degree to which GIRK channels mediate the effects of parasympathetic activation on HR dynamics and associated arrhythmias is less clear. As detailed in **Figure 1.4**, muscarinic receptor activation results in the modulation of a number of ion channels which include I_f and $I_{Ca,L}$. The degree to which I_f and $I_{Ca,L}$ modulation regulates HR remains unclear. The use of parasympathetic mimetic compounds or indirect activation of the vagus nerve via the baroflex in global *Girk4*$^{-/-}$ mice has suggested that approximately half of the effects of parasympathetic signaling on HR are mediated through cardiac GIRK channels (Mesirca et al., 2013; Wickman et al., 1998). However, these results are confounded by compound selectivity issues and constitutive knockout models. Therefore, more specific and direct manipulations are necessary to fully elucidate the contribution of GIRK channels to parasympathetic regulation of HR dynamics.

Similar to initial observations reporting minimal or absent vagal innervation of the ventricles, GIRK channels were thought to be expressed solely in atrial and nodal tissue, therefore playing little to no role in ventricular function. However, more recent work has called this point into contention. **Table 1** summarizes key previous efforts to investigate

the expression of GIRK channel subunits in ventricular tissue of various mammalian species. While some studies reported no detectable GIRK subunit expression levels, others utilizing more sensitive techniques found evidence of low expression in some mammalian species. For example, efforts to locate GIRK1 subunit expression using immunofluorescence in tissue sections from rat, ferret and guinea pigs showed no signaling for GIRK1 (Dobrzynski et al., 2001, Dobrzynski et al., 2002). However, immunocytochemistry on isolated ventricular myocytes from ferrets and rats did show labeling for GIRK1 (Dobrzynski et al., 2001, Dobrzynski et al., 2002). Furthermore, single channel recordings in mammalian isolated ventricular myocytes have revealed ACh-dependent responses with gating characteristics resembling GIRK channels (Koumi and Wasserstrom, 1994). Notably, these responses were significantly less sensitive to ACh in recordings from isolated human ventricular myocytes as compared to atrial counterparts (Koumi and Wasserstrom, 1994). Therefore, it appears that GIRK channels may be present in mammalian ventricular tissue, although at far more sparse levels in comparison to levels found in atrial and nodal tissue.

Table 1.1: Summary of key previous efforts investigating GIRK channel presence in the mammalian ventricle

Species	Technique	Conclusion	Reference(s)
Mouse	Immunohistochemistry	Yes, ventricular detection	(Liang et al., 2014)
Rat	Northern blot analysis of Kir3.1 mRNA	No presence/detection	(Dobrzynski et al., 2002)
	Western blot	Yes, if total protein increased	(Dobrzynski et al., 2001)
	RT-PCR	Yes, ventricular detection	(McGrath and de Bold, 2009)
	Immunocytochemistry	Weak/to no detection	(Dobrzynski et al., 2001)
	Immunohistochemistry	Yes, ventricular detection	(Liang et al., 2014)
	Immunohistochemistry	No presence/detection	(Dobrzynski et al., 2001)
	Whole-cell electrophysiology	Presence of ACh-dependent response	(Beckmann et al., 2008)
	Whole-cell electrophysiology	Presence of ACh-dependent response	(McMorn et al., 1993)
Guinea pig	Northern blot analysis of Kir3.1 mRNA	No presence/detection	(Dobrzynski et al., 2002)
	Immunohistochemistry	No presence/detection	(Dobrzynski et al., 2001)
	Whole-cell electrophysiology	Presence of ACh-dependent response	(Koumi and Wasserstrom, 1994)
Cat	Whole-cell electrophysiology	Presence of ACh-dependent response	(Koumi and Wasserstrom, 1994)
Dog	Kir3.1 PCR products	Yes, ventricular detection	(Dobrzynski et al., 2002)
Ferret	Kir3.1 PCR products	Yes, ventricular detection	(Dobrzynski et al., 2002)
	Immunohistochemistry	No presence/detection	(Dobrzynski et al., 2002)
	Immunohistochemistry	No presence/detection	(Dobrzynski et al., 2001)
	Immunocytochemistry	Yes, ventricular detection	(Dobrzynski et al., 2002)
	Whole-cell electrophysiology	Presence of ACh-dependent response	(Boyett et al., 1988)
Human	Western blot	Yes, ventricular detection	(Yang et al., 2010b)
	Immunohistochemistry	Yes, ventricular detection	(Liang et al., 2014)
	Whole-cell electrophysiology	Presence of ACh-dependent response	(Koumi and Wasserstrom, 1994)

The degree of which GIRK channels in contribute to the effects of muscarinic activation on ventricular myocyte contractility and excitability is less clear. Initial work characterized the actions of muscarinic receptor activation in ventricular tissue being largely dependent on indirect inhibition of Ca^{2+} channels and were only observed in the presence of β-adrenergic stimulation (Harvey and Belevych, 2003). More recent work, however, has shown that recordings from isolated mouse right ventricle demonstrated perfusion of ACh shortened APD and lowered RMP (Liang et al., 2014). This effect was reversed by the selective GIRK channel inhibitor TTQ and absent in parallel recordings from *Girk4*$^{-/-}$ mice. In isolated rat papillary muscle, a similar shortening of APD and decrease in RMP was seen upon perfusion of CPA (Liang et al., 2014). Again, these effects were reversed upon perfusion of TTQ. Further experiments investigating basal activity of GIRK channels in the isolated papillary muscle perfused only TTQ and observed a slight, yet significant, prolongation of APD and rise in RMP. Similar results were seen in Langendorf-perfused isolated rat hearts. A reduction in APD and ERP was seen upon perfusion of either ACh or CPA which was reversed by the co-perfusion of TTQ (Liang et al., 2014). ECG recordings in anesthetized mice both showed ventricular ERP was prolonged at baseline and after muscarinic stimulation upon genetic ablation of GIRK4 (Kovoor et al., 2001). Together, these results suggest that GIRK channels may contribute to the effects of inhibitory G protein activation in ventricular tissue.

1.3.4 Cardiac GIRK channels as novel therapeutic targets

GIRK channel activity in the atria has been widely implicated in the pathogenesis of AF. Direct vagus nerve stimulation (VNS) has been used to both provoke and sustain AF in many mammalian species, due to heterogenous shortening of APD and ERP (Manolis et al., 2020; Zhu et al., 2019). Interestingly, application of TTQ has been shown to terminate both pharmacologically- and VNS- induced AF, suggesting that GIRK

channels may be mediators of the arrhythmic effects of parasympathetic activation (Hashimoto et al., 2006). Further evidence includes observations that higher levels of constitutive GIRK channel activity, yet reduced GPCR-induced GIRK channel activity, are observed in human patients with AF (Voigt et al., 2014). Work using a combination of optical mapping and immunoblotting found that regions of the human atria with Ado-induced AF initiation are localized to areas with high A_1R and GIRK expression (Li et al., 2016). These observations are in line with findings in *Rgs6*$^{-/-}$ mice, which display an increased susceptibility to pacing-induced AF linked to increased GIRK channel activity (Posokhova et al., 2013). Conversely, genetic ablation of *Girk4* in mice has been shown to confer resistance to pacing-induced AF (Kovoor et al., 2001). Overall, these studies suggest that GIRK channels play a role in the pathogenesis of AF.

In addition to AF, GIRK channel activity has been linked to nodal rhythm disorders. Recent work in human patients with familial sinus node dysfunction has revealed a mutation in GNB2, which encodes Gβ2 and results in exaggerated GIRK dependent signaling (Kuß et al., 2019; Stallmeyer et al., 2017). Additional work in rodent models of nodal dysfunction has demonstrated the therapeutic potential of cardiac GIRK channel inhibition. Sinus bradycardia in the rat, elicited by chemical ablation of the SAN, is partially recovered upon genetic knockdown of GIRK1 (Li et al., 2017). Furthermore, mice lacking L-type Ca^{2+} channel 1.3 (*Cav1.3*$^{-/-}$) display many hallmarks of sick sinus syndrome such as bradycardia and AV (Mesirca et al., 2016a, 2016b) which are rescued upon genetic ablation of *Girk4*. Similarly, expression of a dominant-negative, non-conductive HCN4-channel subunit (hHCN4-AYA) resulting in a loss of I_f activity results in severe nodal dysfunction which is also rescued upon removal of GIRK4 (Mesirca et al., 2014, 2016a). Collectively, these studies highlight the potential of targeting cardiac GIRK channels as a therapeutic intervention for nodal dysfunction.

It has long been assumed that due to the minimal/lack of GIRK channel expression in the ventricle, targeted inhibition of cardiac GIRK channels could provide a safe, selective treatment for supraventricular arrhythmias. However, recent work has identified a mutation in GIRK4 that impairs membrane trafficking of the channel (Yang et al., 2010b). This trafficking impairment results in a loss of channel function associated with type 13 Long QT syndrome (LQTS13) (Wang et al., 2013a; Yang et al., 2010b). Therefore, thorough investigation of the impact of GIRK channels on ventricular physiology is necessary to fully understand the therapeutic potential of targeting cardiac GIRK channels.

1.4 Summary

GIRK channels represent a crucial downstream effector of parasympathetic signaling to the heart; however, several gaps in knowledge in the current literature still remain. The goal of my thesis work is to investigate the details of GIRK-dependent signaling in the context of cardiac physiology. In **Chapter 2**, I probe the specific contribution of atrial GIRK channels in mediating the effects of direct VNS on HR, HRV, and arrhythmia susceptibility in the mouse using a novel atrial-specific knockout line. I next present work in **Chapter 3** which characterizes GIRK-dependent signaling in the mouse ventricle and utilized a novel ventricular-specific knockout line to determine its contribution to *ex vivo* and *in vivo* ventricular physiology. Based on evidence of therapeutic potential of GIRK channels described in **Chapters 2** and **3**, GIRK channels represent an attractive therapeutic target for the treatment of relevant cardiac rhythm disorders. Therefore, in **Chapter 4**, I provide an initial, preclinical assessment of a novel inhibitor that is selective to cardiac GIRK channels over neuronal GIRK channels. Lastly, in **Chapter 5**, I expand on previous work detailing regulation of M_2R-GIRK signaling by RGS6 in the SAN to explore its role in mediating A_1R-GIRK signaling. These studies revealed intriguing

insights into the role of RGS6 in mediating functional compartmentalization of GPCR-GIRK channel signaling in the SAN. Altogether, work contained in this dissertation highlights the integral role GIRK channel signaling plays in mediating parasympathetic influence on HR and represents an attractive therapeutic target for the development of efficacious and safe treatments for cardiac arrhythmias.

Chapter 2

Atrial GIRK channels mediate the effects of vagus nerve stimulation on heart rate dynamics and arrhythmogenesis.

Lee S*, Anderson A*, Guzman PA, Nakano A, Tolkacheva E, Wickman K (2018). Atrial GIRK channels mediate the effects of vagus nerve stimulation on heart rate dynamics and arrhythmogenesis. Front. Physiol. 9:943. (*equal contributors)

Author Contributions: S.W.L., A.A., E.T, and K.W. were responsible for the conception of this study, wrote and prepared the manuscript. All authors contributed to experimental design, execution of experiments, and data analysis. All authors reviewed the manuscript.

2.1 Introduction

The parasympathetic and sympathetic branches of the ANS work antagonistically to maintain cardiovascular homeostasis (Gordan et al., 2015). Autonomic dysregulation, characterized by excessive sympathetic activation and diminished parasympathetic influence, is central to the pathogenesis of cardiovascular diseases including heart failure and hypertension (Bibevski and Dunlap, 2011; Mancia and Grassi, 2014; Schwartz and De Ferrari, 2011). Efferent fibers of the vagus nerve provide the parasympathetic innervation to the heart, and VNS has shown promise in the treatment of cardiovascular diseases, including heart failure and hypertension (Beaumont et al., 2015; Petkovich et al., 2015; Premchand et al., 2016; Smith et al., 2016; Xie et al., 2014). As a result, there is renewed interest in understanding the cell signaling pathways that mediate the impact of VNS on cardiac physiology.

Parasympathetic regulation of HR is mediated via release of ACh, which activates cardiac muscarinic M2 receptors (M_2R) on SAN and AVN cells, and atrial myocytes (Dhein et al., 2001). M_2R activation stimulates inhibitory G proteins, which suppress the activity of the HCN (pacemaker or "funny" current, I_f) and L-type Ca^{2+} channels ($I_{Ca,L}$) (Difrancesco, 2010; DiFrancesco et al., 1989; DiFrancesco and Borer, 2007; Kozasa et al., 2018; Mangoni and Nargeot, 2008; Zaza et al., 1996), and activate GIRK channels (Dhein et al., 2001; Logothetis et al., 1987; Wickman et al., 1994). The atrial GIRK channel, often referred to as I_{KACh}, is a heterotetrameric complex composed of homologous subunits – GIRK1/Kir3.1 and GIRK4/Kir3.4 – in 1:1 stoichiometry (Corey et al., 1998; Krapivinsky et al., 1995a). Ventricular myocytes also express a GIRK1/GIRK4 channel, albeit at lower levels than in atrial myocytes, and this channel mediates the impact of cholinergic agonists on APD and the excitability of ventricular myocytes (Anderson et al., 2018 (**Chapter 3**);

Dobrzynski et al., 2001, 2002; Koumi et al., 1997; Liang et al., 2014; Posokhova et al., 2010).

The extent to which the various cardiac conductances (I_f, $I_{Ca,L}$, GIRK) contribute to the parasympathetic influence on HR dynamics is unclear. Previous studies investigating the role of GIRK channels have used pharmacological tools to mimic parasympathetic activation in constitutive/global knockout mice lacking either GIRK1 (*Girk1*$^{-/-}$; (Bettahi et al., 2002)) or GIRK4 (*Girk4*$^{-/-}$; (Wickman et al., 1998)). Loss of either subunit eliminates the GIRK current in atria and ventricular myocytes (Anderson et al., 2018; Bettahi et al., 2002; Mesirca et al., 2013; Posokhova et al., 2013; Wickman et al., 1998), and yields a comparable attenuation of HR responses to systemic administration of parasympathomimetic agents (Bettahi et al., 2002). For example, experiments involving the administration of the α1 adrenergic receptor agonist methoxamine, which evokes a baroreflex-mediated increase in parasympathetic input to the heart, suggested that GIRK channel activation accounts for approximately half of the bradycardic effect of indirect parasympathetic activation in awake mice (Bettahi et al., 2002; Wickman et al., 1998). While direct perfusion of isolated hearts from wild-type and *Girk4*$^{-/-}$ mice with relatively high concentrations of ACh (0.3–10 μM) yielded similar results, the bradycardic effect of lower ACh concentrations was comparable in these hearts (Mesirca et al., 2013). Thus, the mediators of parasympathetic influence on HR dynamics may differ depending on the type and intensity of pharmacological stimulation, and the model systems used to evaluate their impact.

While the vagal nerve innervation of atrial and nodal tissue is well-established, vagal innervation of the ventricle has also been reported (Coote, 2013). The relative contribution of atrial and ventricular GIRK channels to the parasympathetic regulation of the heart has not been fully elucidated. Moreover, GIRK1 and GIRK4 are expressed in the hypothalamus, and GIRK4 has been detected specifically in the PVN of the hypothalamus

(Karschin et al., 1996; Luján and Aguado, 2015; Perry et al., 2008; Wickman et al., 2000), a region that regulates cardiac vagal neurons in the brainstem (Dyavanapalli et al., 2016; Piñol et al., 2014). Thus, the impact of *Girk1* or *Girk4* ablation on HR dynamics following pharmacological stimulation of the baroreflex could be due to loss of GIRK channel activity in a central regulator(s) of autonomic function. In this study, we used direct VNS, and new atrial- and ventricle-specific models of GIRK channel ablation, to probe the contribution of cardiac GIRK channels to the parasympathetic regulation of HR, HRV, and arrhythmogenesis. Our findings suggest that the impact of direct VNS on cardiac physiology in anesthetized mice is attributable primarily to activation of atrial GIRK channels.

2.2 Methods

Animals. All experiments were performed in accordance with the guidelines set forth by the National Institutes of Health Guide for the Care and Use of Laboratory Animals and were approved by the University of Minnesota Institutional Animal Care and Use Committee. C57BL/6J mice and B6.Cg-Gt(ROSA)26Sortm14(CAG-tdTomato)Hze/J (Ai14-tdTomato) reporter mice were purchased from The Jackson Laboratory (Bar Harbor, ME, United States). The generation of constitutive *Girk4*$^{-/-}$ mice, as well as mice lacking GIRK1 in ventricular tissue (MLC2VCre(+):*Girk1*$^{fl/fl}$) and their control littermates (MLC2VCre(-):*Girk1*$^{fl/fl}$), was described previously (Anderson et al., 2018 (**Chapter 3**); Wickman et al., 1998). To generate mice lacking GIRK1 in atrial tissue, conditional Girk1 knockout mice (*Girk1*$^{fl/fl}$ mice; (Marron Fernandez de Velasco et al., 2017a)) were crossed with an atrial-specific Cre driver line (SLNCre mice; (Nakano et al., 2011)). SLNCre(+):*Girk1*$^{fl/fl}$ mice, and their control littermates (SLNCre(-):*Girk1*$^{fl/fl}$), were used in this study. All mice were housed in a quiet, temperature- and humidity-controlled room with a 12:12 h light-dark cycle. Food and water were available ad libitum.

Microscopy. Mice were injected intraperitoneally (I.P.) with heparin (250 U) and then anesthetized with ketamine (100 mg/kg) and xylazine (10 mg/kg). Hearts were then excised, fixed, and sectioned as described (Anderson et al., 2018) (**Chapter 3**). Once sections were mounted and stained with ProLong Gold Antifade reagent with DAPI (Thermo Fisher Scientific, Waltham, MA, United States), fluorescent images were captured and processed as described (Anderson et al., 2018) (**Chapter 3**).

Cardiomyocyte Culture and Electrophysiology. Adult (8–12 weeks) SAN cells and ventricular myocytes were isolated as described (Anderson et al., 2018) (**Chapter 3**) and used within 8 h of isolation. Coverslips containing SAN cells or ventricular myocytes were transferred to a perfusion chamber and electrophysiological recordings were conducted

as described (Anderson et al., 2018). In brief, whole-cell access was obtained in a bath consisting of (in mM): 130 NaCl, 5.4 KCl, 1 $CaCl_2$, 1 $MgCl_2$, 5.5 glucose, 5 HEPES/NaOH (pH 7.4). CCh-currents (holding potential of -70 mV) were measured in a high-K^+ bath solution consisting of (in mM): 120 NaCl, 25 KCl, 1 $CaCl_2$, 1 $MgCl_2$, 5.5 glucose, 5 HEPES/NaOH (pH 7.4). CCh was applied via ValveLink 8.2 rapid perfusion system (AutoMate Scientific, Berkeley, CA, United States). $BaCl_2$ (5 μM) was included in the bath solution for ventricular myocyte recordings to block I_{K1}, which has been shown to mask GIRK-dependent currents (Beckmann et al., 2008). Studies using these recording conditions, and *Girk1*$^{-/-}$ and/or *Girk4*$^{-/-}$ mice, have shown definitively that the inward currents evoked by cholinergic agonists are mediated entirely by GIRK channel activation (Anderson et al., 2018 (**Chapter 3**); Bettahi et al., 2002; Posokhova et al., 2013). Steady-state CCh-induced currents (pA) were normalized to cell capacitance (pF), and experiments that did not have stable, low access resistances (<20 MΩ) were not included.

ECG Recordings in SLNCre:Girk1$^{fl/fl}$ *Mice.* Male and female SLNCre(-):*Girk1*$^{fl/fl}$ and SLNCre(+):*Girk1*$^{fl/fl}$ mice (8–12 weeks) were anesthetized with 1.5% isoflurane supplemented with an air mixture of 40% O_2/60% N_2 to sustain stable HR. ECG electrodes were placed subcutaneously into the limbs, and ECG data were acquired with an IX-ECG-12 ECG recorder (iWorx Systems, Inc., Dover, NH, United States). Baseline ECG data were recorded for 10 min, at which point CCh was administered (1.0 mg/kg IP). Baseline (9–10 min) and post-CCh (15–16 min) HR and HRV analysis was performed using Kubios HRV software (Tarvainen et al., 2014). Artifact detection/correction was utilized to detect RR intervals and reduce the impact of ectopic beats and instances of AV block on HR and HRV analysis.

Vagus Nerve Bipolar Cuff Electrode Implantation and ECG Recording. Male and female mice (8–12 weeks) were anesthetized with isoflurane (5% for induction and 1.5% for maintenance). After hair removal and skin cleaning, aseptic technique was used to

make a ventral midline incision in the neck, and the skin and muscles were retracted. After identifying and isolating the right vagus nerve, a custom helical lead bipolar cuff electrode (Cyberonics, Inc., Houston, TX, United States) was implanted around the nerve (Lee et al., 2016; Xie et al., 2014). The electrode was then connected to the Demipulse Model 103 VNS pulse generator (Cyberonics, Inc.). For VNS experiments, 1 min of baseline ECG was recorded (PRE). Subsequently, VNS (0.25 mA, 10 Hz, and 500 μs) was delivered for 1 min (ON). ECG data were then acquired for 1 min immediately after VNS cessation (POST). Each experiment concluded with PRE, ON, and POST ECG measurements conducted 10 min after administration of atropine (2.0 mg/kg IP).

Analysis of VNS ECG Recordings. ECG recordings were used to quantify changes in HR and HRV due to VNS throughout the study using Kubios HRV software. All values were averaged over 1 min PRE and ON periods of VNS stimulation. Noisy data segments, premature atrial complexes, and arrhythmic episodes were excluded, and only steady-state data after initial adjustment of the HR to VNS were used for analysis. To account for inter-subject variations in baseline HR, the chronotropic effect of VNS was determined by calculating a relative change in HR (ΔHRON) as follows: $\Delta HRON=(HRON-HRPREHRPRE)\times 100\%$ where HRON and HRPRE are the mean HR during the VNS ON and PRE periods, respectively. HRV was calculated as the ratio between the standard deviation of RR intervals (SDRR) to mean of RR intervals (mean RR), as described (McIntyre et al., 2014): $HRV=(SDRRMean\ RR)\times 100\%$. The number of mice that exhibited arrhythmic episodes was also quantified during both PRE and ON periods. An arrhythmic episode was defined as any of the following episodes: (i) skipped beats, (ii) bigeminy, (iii) bradycardia (HR at least 25 bpm less than the mean PRE or ON HR, lasting for more than 2 s), and (iv) tachycardia (HR at least 25 bpm more than the mean PRE or ON HR, lasting for more than 2 s). Premature atrial complexes were not

considered arrhythmic episodes as they were observed during VNS regardless of genotype, and frequently occur under healthy conditions (Shindler and Kostis, 2009).

Statistical Analysis. All data are presented as mean ± SEM. Student's t-test, two-way ANOVA with repeated measures, and Fisher's exact test were used as appropriate (GraphPad Software, Inc., La Jolla, CA, United States). For studies involving two-way ANOVA analysis, interactions are reported if detected. Post hoc analysis (Bonferroni multiple comparison) was used when appropriate. The level of significance was set at $P < 0.05$.

2.3 Results

2.3.1 Generation and Characterization of an Atrial-Specific *Girk*$^{-/-}$ Mouse Line

In a recent study, we reported the development and characterization of a ventricle-specific *Girk1*$^{-/-}$ mouse (MLC2VCre:*Girk1*$^{fl/fl}$) that lacked ventricular GIRK channel activity (Anderson et al., 2018) (**Chapter 3**). To generate an atrial-specific *Girk1*$^{-/-}$ line, we crossed conditional Girk1 knockout mice (*Girk1*$^{fl/fl}$; (Marron Fernandez de Velasco et al., 2017a)) with an atrial-specific Cre driver line (SLNCre; (Nakano et al., 2011)). The atrial specificity of Cre-dependent recombination in the SLNCre driver line was validated by crossing this line with a Cre-dependent fluorescent reporter mouse (Ai14-tdTomato) (**Figure 2.1A,B**).

To test whether atrial GIRK channel activity was lost in SLNCre(+):*Girk1*$^{fl/fl}$ mice, we measured whole-cell currents evoked by the non-selective muscarinic receptor agonist carbachol (CCh) in SAN cells from adult Cre(+) and Cre(-) littermates. CCh-induced current density was significantly smaller in SAN cells from SLNCre(+):*Girk1*$^{fl/fl}$ mice when compared to SLNCre(-):*Girk1*$^{fl/fl}$ littermates (**Figure 2.1C,D**). The small residual CCh-induced current seen in SLNCre(+):*Girk1*$^{fl/fl}$ SAN cells is likely due to the presence of residual GIRK4 homomeric channels (Corey and Clapham, 1998)). Importantly, CCh-induced current densities were comparable in adult ventricular myocytes from SLNCre(+):*Girk1*$^{fl/fl}$ and SLNCre(-):*Girk1*$^{fl/fl}$ mice (**Figure 2.1E**).

Constitutive *Girk1*$^{-/-}$ and *Girk4*$^{-/-}$ mice exhibit blunted HR and HRV responses to cholinergic agonists (Anderson et al., 2018; Bettahi et al., 2002; Kovoor et al., 2001; Wickman et al., 1998). To discern whether these effects are mediated by activation of atrial GIRK channels, we recorded ECGs in anesthetized SLNCre(-):*Girk1*$^{fl/fl}$ and SLNCre(+):*Girk1*$^{fl/fl}$ mice, before and after administration of CCh (1.0 mg/kg I.P.) (**Figure 2.2A**). We observed no differences in baseline HR or HRV between SLNCre(-):*Girk1*$^{fl/fl}$

and SLNCre(+):*Girk1*$^{fl/fl}$ mice (**Figure 2.2B,C**). CCh-induced bradycardia, while present, was smaller in SLNCre(+):*Girk1*$^{fl/fl}$ mice than in SLNCre(-):*Girk1*$^{fl/fl}$ littermates (**Figure 2.2B**). In addition, the CCh-induced increase in HRV in control SLNCre(-):*Girk1*$^{fl/fl}$ mice was absent in SLNCre(+):*Girk1*$^{fl/fl}$ mice (**Figure 2.2C**). Thus, mice lacking atrial GIRK channels exhibit diminished HR and absent HRV responses to CCh challenge, reminiscent of phenotypes reported in *Girk1*$^{-/-}$ and *Girk4*$^{-/-}$ mice.

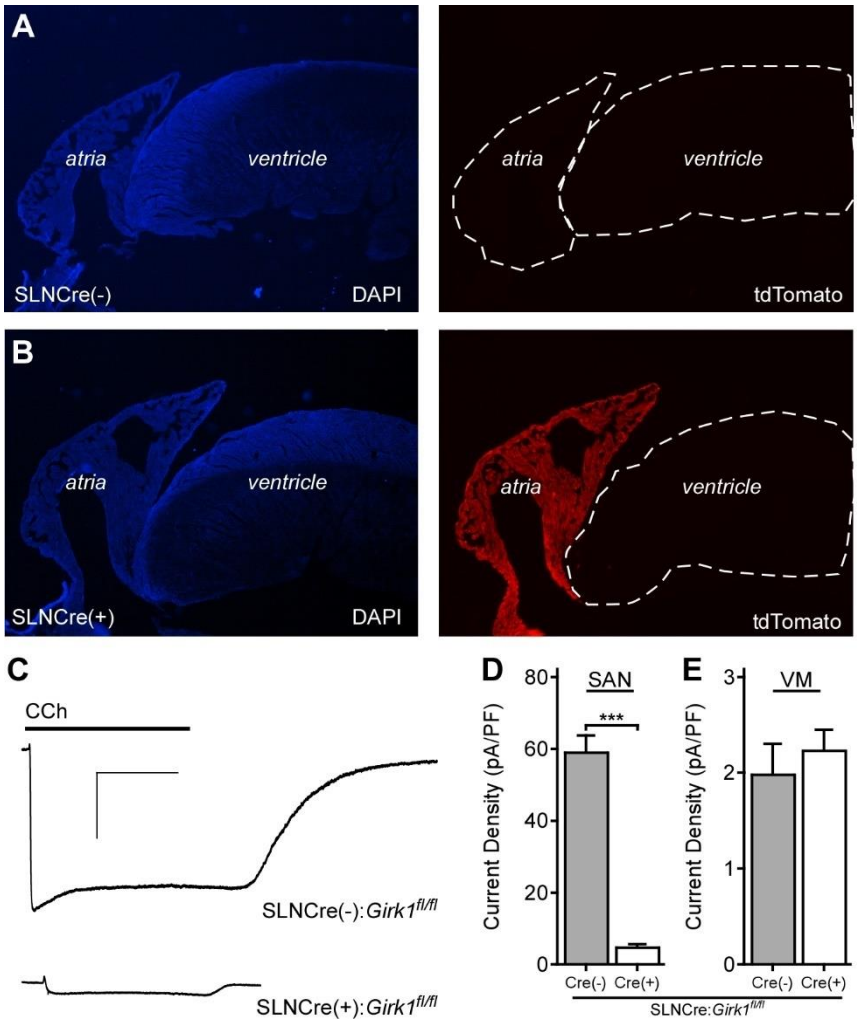

Figure 2.1. Characterization of an atrial-specific *Girk*$^{-/-}$ mouse line.
(**A,B**) SLNCre(–) and SLNCre(+) mice were crossed with the Cre-dependent fluorescent reporter strain, Ai14-tdTomato. Representative sections stained with DAPI (Left), and associated tdTomato fluorescence (Right), in hearts from SLNCre(–) (Top) and SLNCre(+) (Bottom) offspring. (C) Representative whole-cell currents (V_{hold} = –70 mV) evoked by carbachol (CCh, 10 μM) in a high-K^+ bath solution in adult SAN cells from SLNCre(–):*Girk1*$^{fl/fl}$ and SLNCre(+):*Girk1*$^{fl/fl}$ mice. Scale bars: 1 nA/10 s. (D,E) Summary of CCh-induced currents in adult SAN cells (t_{47} = 11.3; ***P < 0.001; n = 24–25/genotype) and ventricular myocytes (VM; t_{21} = 0.6; P = 0.54; n = 11–12/genotype) from SLNCre(–):*Girk1*$^{fl/fl}$ and SLNCre(+):*Girk1*$^{fl/fl}$ mice.

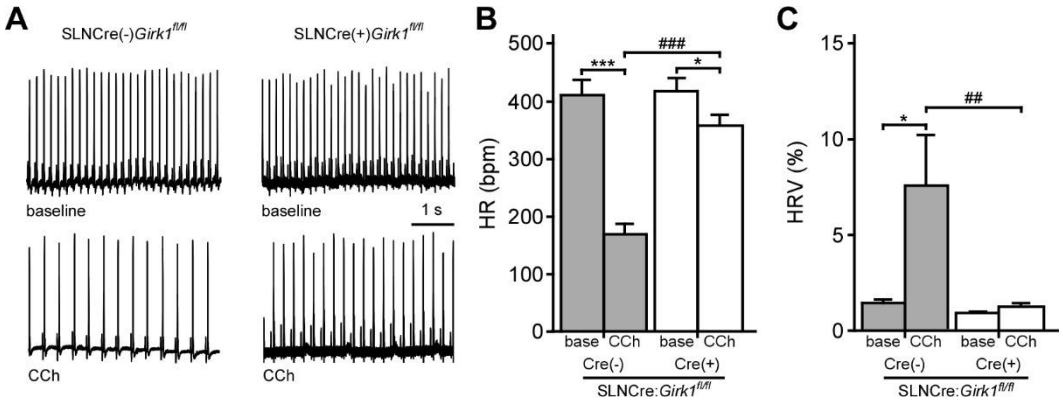

Figure 2.2. Impact of atrial GIRK channel ablation on HR and HRV responses to carbachol.

(**A**) Representative segments of ECG recordings from anesthetized SLNCre(–):*Girk1*$^{fl/fl}$ and SLNCre(+):*Girk1*$^{fl/fl}$ mice, at baseline (Top) and following administration of CCh (1.0 mg/kg I.P.; Bottom). (**B**) Summary of HR data at baseline (base) and after CCh injection for SLNCre(–):*Girk1*$^{fl/fl}$ (n = 7) and SLNCre(+):*Girk1*$^{fl/fl}$ (n = 8) mice. Two-way ANOVA analysis revealed an interaction between genotype and treatment ($F_{1,13} = 38.6$; $P < 0.001$). Symbols: $^{*}P < 0.05$ and $^{***}P < 0.001$, vs. baseline (within genotype); $^{\#\#\#}P < 0.001$ vs. SLNCre(–):*Girk1*$^{fl/fl}$ (within treatment). (**C**) Summary of HRV data at baseline (base) and after CCh injection for SLNCre(–):*Girk1*$^{fl/fl}$ (n = 7) and SLNCre(+):*Girk1*$^{fl/fl}$ (n = 8) mice. HRV was calculated as the ratio of standard deviation of RR to mean RR (see section "**3.2 Materials and Methods**"). Two-way ANOVA analysis revealed an interaction between genotype and treatment ($F_{1,13} = 5.4$; $P < 0.05$). Symbols: $^{*}P < 0.05$ vs. baseline (within genotype); $^{\#\#}P < 0.01$ vs. SLNCre(–):*Girk1*$^{fl/fl}$ mice (within treatment).

2.3.2 Impact of Whole-Heart and Tissue-Specific GIRK Channel Ablation on Baseline HR and HRV

We next evaluated HR and HRV prior to and during acute VNS in anesthetized SLNCre(+):*Girk1*$^{fl/fl}$ and SLNCre(-):*Girk1*$^{fl/fl}$ mice, and MLC2VCre(+):*Girk1*$^{fl/fl}$ and MLC2VCre(-):*Girk1*$^{fl/fl}$ mice. These studies also involved wild-type and constitutive *Girk4*$^{-/-}$ mice, which lack cardiac GIRK channels (whole-heart ablation). We did not observe a difference in baseline HR or HRV between wild-type and *Girk4*$^{-/-}$ mice (**Figure 2.3A,B**). Similarly, there were no significant differences in baseline HR and HRV between SLNCre(-):*Girk1*$^{fl/fl}$ and SLNCre(+):*Girk1*$^{fl/fl}$ mice, or MLC2VCre(-):*Girk1*$^{fl/fl}$ and MLC2VCre(+):*Girk1*$^{fl/fl}$ mice (**Figure 2.3A,B**).

2.3.3 Whole-Heart and Tissue-Specific GIRK Channel Ablation and VNS-Induced Bradycardia

We next assessed the impact of whole-heart or tissue-specific GIRK channel ablation on the bradycardic effects of acute VNS, by comparing the relative change in HR evoked by VNS (ΔHR_{ON}). Acute VNS suppressed HR by more than 40% in anesthetized wild-type mice, but had little impact on HR in *Girk4*$^{-/-}$ mice (**Figure 2.4C**). SLNCre(+):*Girk1*$^{fl/fl}$ mice also displayed minimal VNS-induced bradycardia relative to SLNCre(-):*Girk1*$^{fl/fl}$ controls (**Figure 2.4A–C**). In contrast, the VNS-induced decrease in HR was comparable between MLC2VCre(+):*Girk1*$^{fl/fl}$ and MLC2VCre(-):*Girk1fl/fl* mice (**Figure 2.4C**). After VNS was terminated, HR values returned to baseline for all genotypes (data not shown). To determine if the bradycardic effect of VNS was dependent on muscarinic receptor activation, we also evaluated the impact of VNS on HR following administration of atropine (2.0 mg/kg I.P.). In the presence of atropine, VNS had no effect on HR in any of the genotypes evaluated (**Figure 2.4D**). Collectively, these findings

suggest that VNS-induced bradycardia in anesthetized mice is mediated predominantly by the muscarinic receptor-dependent activation of atrial GIRK channels.

2.3.4. Whole-Heart and Tissue-Specific GIRK Channel Ablation and VNS-Induced Increase in HRV

We next examined the impact of VNS on HRV in whole-heart and tissue-specific *Girk*$^{-/-}$ mice. VNS evoked a significant increase in HRV in wild-type and SLNCre(-):*Girk1*$^{fl/fl}$ mice, and this effect was absent in both constitutive *Girk4*$^{-/-}$ and SLNCre(+):*Girk1*$^{fl/fl}$ mice (**Figure 2.5A,B**). In contrast, the increase in HRV induced by VNS was similar in both MLC2VCre(-):*Girk1*$^{fl/fl}$ and MLC2VCre(+):*Girk1*$^{fl/fl}$ mice (**Figure 2.5B**). Atropine blocked the VNS-induced increase in HRV in wild-type, SLNCre(-):*Girk1*$^{fl/fl}$, MLC2VCre(-):*Girk1*$^{fl/fl}$, and MLC2VCre(+):*Girk1*$^{fl/fl}$ mice (**Figure 2.5C**). Thus, the VNS-induced increase in HRV in mice appears to be mediated predominantly through the muscarinic receptor-dependent activation of atrial GIRK channels.

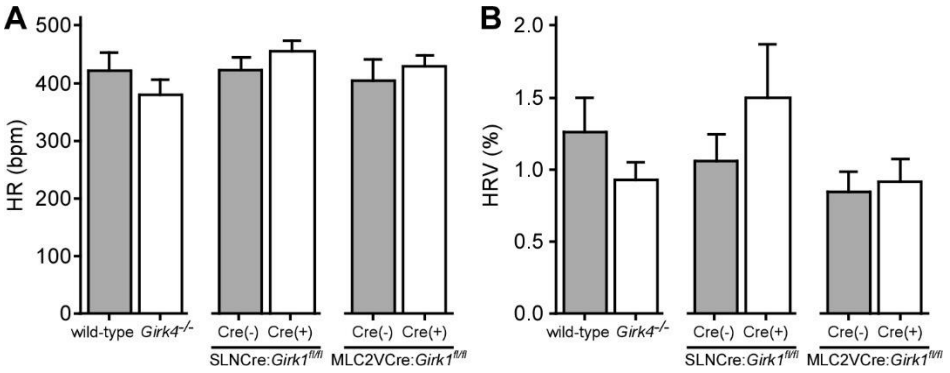

Figure 2.3. Impact of whole-heart and tissue-specific GIRK channel ablation on baseline HR and HRV.

(**A**) Summary of baseline HR data. There were no significant differences in baseline HR between wild-type (n = 10) and *Girk4*$^{-/-}$ (n = 10) mice (t_{18} = 1.0; P = 0.32), SLNCre(–):*Girk1*$^{fl/fl}$ (n = 6) and SLNCre(+):*Girk1*$^{fl/fl}$ (n = 5) mice (t_9 = 1.1; P = 0.29), or MLC2VCre(–):*Girk1*$^{fl/fl}$ (n = 6) and MLC2VCre(+):*Girk1*$^{fl/fl}$ (n = 8) mice (t_{12} = 0.7; P = 0.51). (**B**) Summary of baseline HRV data. There were no significant differences in HRV between wild-type (n = 10) and *Girk4*$^{-/-}$ (n = 10) mice (t_{18} = 1.2; P = 0.23), SLNCre(–):*Girk1*$^{fl/fl}$ (n = 5) and SLNCre(+):*Girk1*$^{fl/fl}$ (n = 5) mice (t_8 = 1.1, P = 0.32), or MLC2VCre(–):*Girk1*$^{fl/fl}$ (n = 6) and MLC2VCre(+):*Girk1*$^{fl/fl}$ (n = 8) mice (t_{12} = 0.32; P = 0.76).

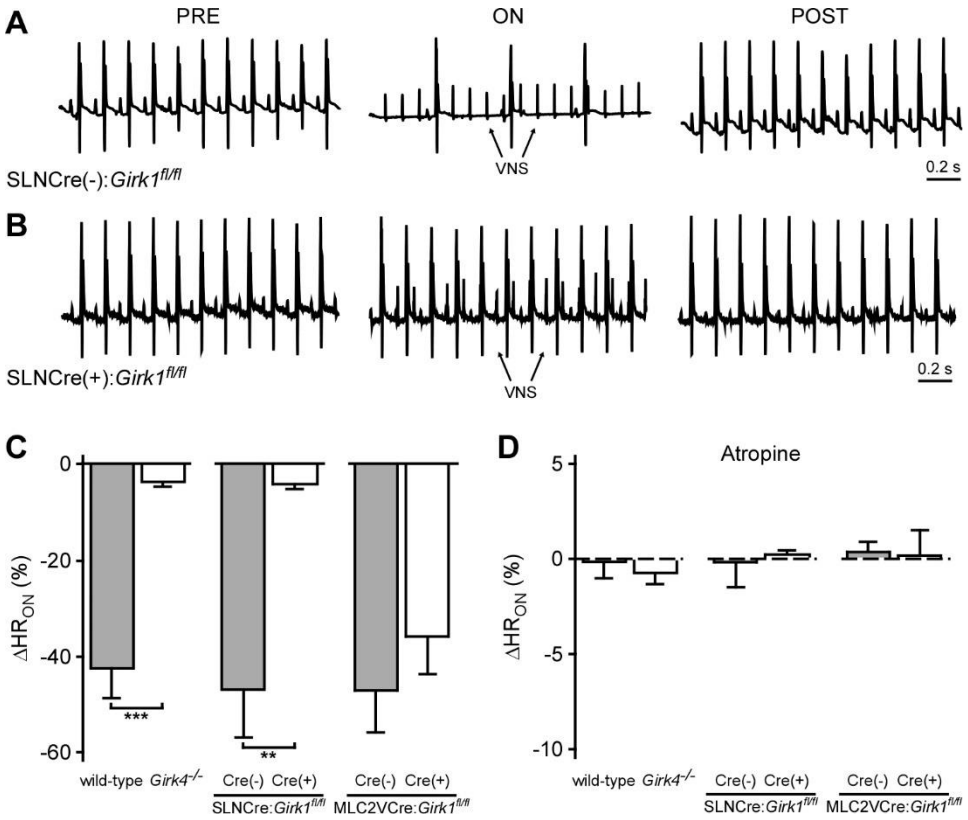

Figure 2.4. Impact of whole-heart and tissue-specific GIRK channel ablation on VNS-induced decrease in HR.

(**A**,**B**) Representative ECG segments from anesthetized SLNCre(–):*Girk1*$^{fl/fl}$ (Top) and SLNCre(+):*Girk1*$^{fl/fl}$ (Bottom) mice prior to (PRE, Left), during (ON, Middle), and after (POST, Right) VNS. The small spikes observed during VNS (ON) correspond to electrical stimulation artifacts. (**C**) Relative change in HR (ΔHR_{ON}) during VNS. A significant difference in ΔHR_{ON} was observed between wild-type (n = 9) and *Girk4*$^{-/-}$ (n = 10) mice (t_{17} = 6.5; ***P < 0.001), as well as SLNCre(–):*Girk1*$^{fl/fl}$ (n = 6) and SLNCre(+):*Girk1*$^{fl/fl}$ (n = 5) mice (t_9 = 3.9; **P < 0.01). No difference was seen between MLC2VCre(–):*Girk1*$^{fl/fl}$ (n = 6) and MLC2VCre(+):*Girk1*$^{fl/fl}$ (n = 8) mice (t_{12} = 0.95; P = 0.36). (**D**) Relative change in HR (ΔHR_{ON}) during VNS, in the presence of atropine (2.0 mg/kg I.P.). There were no significant differences between wild-type (n = 4) and *Girk4*$^{-/-}$ (n = 6) mice (t_8 = 0.6; P = 0.59), SLNCre(–):*Girk1*$^{fl/fl}$ (n = 6) and SLNCre(+):*Girk1*$^{fl/fl}$ (n = 4) mice (t_8 = 0.2; P = 0.82), and MLC2VCre(–):*Girk1*$^{fl/fl}$ (n = 6) and MLC2VCre(+):*Girk1*$^{fl/fl}$ (n = 4) mice (t_8 = 0.2, P = 0.88).

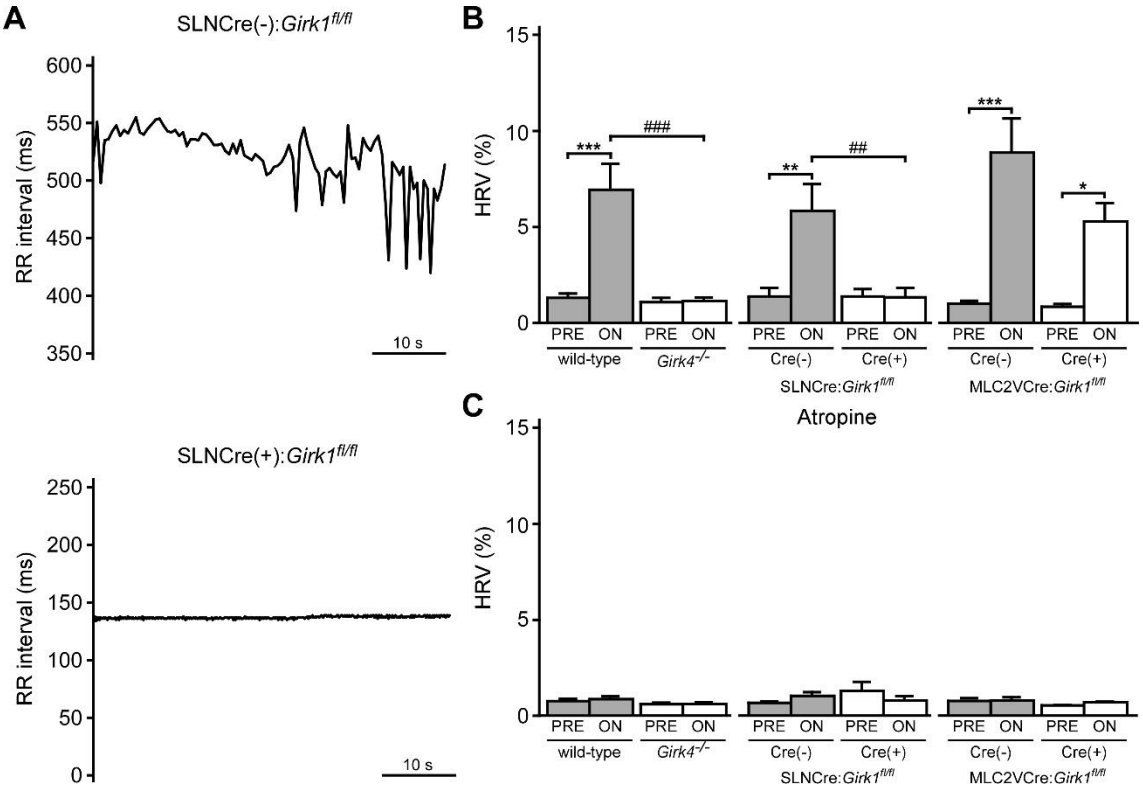

Figure 2.5. Impact of whole-heart and tissue-specific GIRK channel ablation on VNS-induced increase in HRV.

(**A**) Typical RR tachograms extracted from ECG recordings while VNS was on, comparing beat-to-beat changes in RR intervals between SLNCre(–):*Girk1*$^{fl/fl}$ (Top) and SLNCre(+):*Girk1*$^{fl/fl}$ (Bottom) mice. (**B**) Summary of mean HRV data at baseline and during VNS. Two-way ANOVA analysis revealed an interaction between genotype and treatment between wild-type (n = 8) and *Girk4*$^{-/-}$ (n = 10) mice ($F_{1,16} = 20.3$; $P < 0.001$), and between SLNCre(–):*Girk1*$^{fl/fl}$ (n = 6) and SLNCre(+):*Girk1*$^{fl/fl}$ (n = 5) mice ($F_{1,9} = 12.8$; $P < 0.01$). There was a significant main effect of treatment ($F_{1,12} = 44.0$; $P < 0.001$) between MLC2VCre(–):*Girk1*$^{fl/fl}$ (n = 6) and MLC2VCre(+):*Girk1*$^{fl/fl}$ (n = 8) littermates, but no main effect of genotype ($F_{1,12} = 4.2$; $P = 0.06$) or interaction between genotype and treatment ($F_{1,12} = 3.2$; $P = 0.10$). Symbols: *$P < 0.05$, **$P < 0.01$, and ***$P < 0.001$, vs. PRE (within genotype); $^{###}P < 0.001$, wild-type vs. *Girk4*$^{-/-}$ (within treatment); $^{##}P < 0.01$, SLNCre(–):*Girk1*$^{fl/fl}$ vs. SLNCre(+):*Girk1*$^{fl/fl}$ (within treatment). (**C**) Summary of mean HRV data at baseline and during VNS, following atropine administration. In wild-type (n = 4) and *Girk4*$^{-/-}$ (n = 6) mice, there was a main effect of treatment ($F_{1,8} = 5.7$, $P < 0.05$), however, post hoc analysis did not reveal any significance within either genotype. There was no main effect of genotype ($F_{1,8} = 2.0$, $P = 0.19$), or interaction between genotype and treatment ($F_{1,8} = 3.2$; $P = 0.11$), in wild-type and *Girk4*$^{-/-}$mice as well. There was no main effect of treatment ($F_{1,8} = 0.1$, $P = 0.76$) or genotype ($F_{1,8} = 0.53$, $P = 0.49$), and no interaction between treatment and genotype ($F_{1,8} = 3.5$, $P = 0.1$), in SLNCre(–):*Girk1*$^{fl/fl}$ (n = 6) and SLNCre(+):*Girk1*$^{fl/fl}$ (n = 4) mice. There was no main effect of treatment ($F_{1,7} = 0.45$, $P = 0.52$) or genotype ($F_{1,7} = 0.79$, $P = 0.40$), and no interaction between treatment and genotype ($F_{1,7} = 0.3$; $P = 0.62$), in MLC2VCre(–):*Girk1*$^{fl/fl}$ (n = 6) and MLC2VCre(+):*Girk1*$^{fl/fl}$ (n = 4) mice.

2.3.5. Whole-Heart and Tissue-Specific GIRK Channel Ablation and VNS-Induced Arrhythmias

Direct VNS has been utilized extensively in previous studies to induce and maintain arrhythmias in various large mammalian species (Zhang and Mazgalev, 2011). To probe the involvement of GIRK channel activation on VNS-induced arrhythmogenesis, we quantified arrhythmic episodes prior to and after VNS in whole-heart and tissue-specific *Girk*$^{-/-}$ mice, and their respective controls (**Figure 2.6**). No mice displayed arrhythmic episodes prior to VNS, nor were arrhythmic episodes seen in mice given atropine (data not shown). Arrhythmic episodes were frequently observed, however, during VNS in wild-type and SLNCre(-):*Girk1*$^{fl/fl}$ mice (**Figure 2.6B**). In contrast, *Girk4*$^{-/-}$ and SLNCre(+):*Girk1*$^{fl/fl}$ mice did not exhibit VNS-induced arrhythmias (**Figure 2.6B**). VNS-induced arrhythmogenesis was comparable in MLC2VCre(+):*Girk1*$^{fl/fl}$ and MLC2VCre(-):*Girk1*$^{fl/fl}$ mice. Overall, these findings suggest that atrial GIRK channels play a critical role in the induction of arrhythmias during VNS.

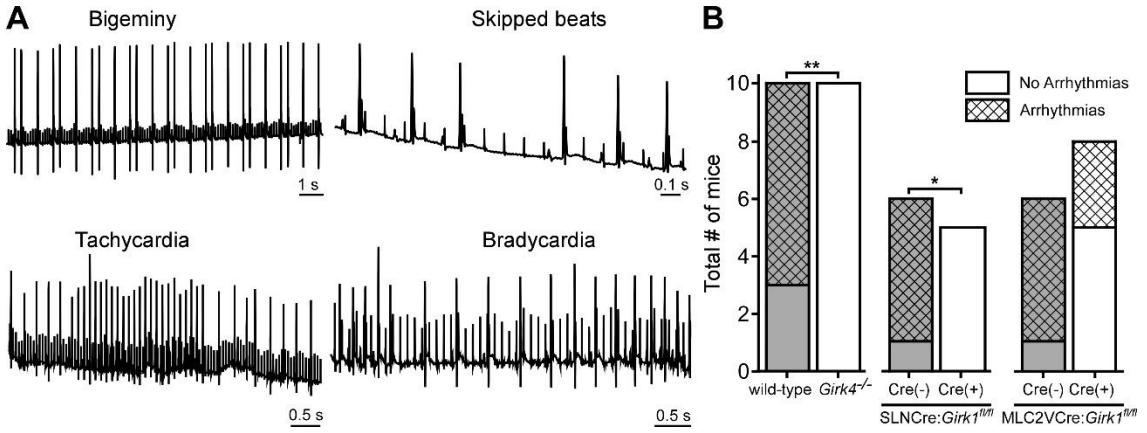

Figure 2.6. Impact of whole-heart and tissue-specific GIRK channel ablation on VNS-induced arrhythmogenesis.

(**A**) Representative segments of ECG recordings of arrhythmias (bigeminy, skipped beats, bradycardia, and tachycardia) observed during VNS. (**B**) Total number of mice exhibiting arrhythmic episodes during VNS. Fisher's exact test revealed a significant difference in arrhythmia incidence between wild-type (n = 10) and *Girk4*$^{-/-}$ (n = 10) mice (**P < 0.01), and SLNCre(–):*Girk1*$^{fl/fl}$ (n = 6) and SLNCre(+):*Girk1*$^{fl/fl}$ (n = 5) mice (*P < 0.05), but no difference between MLC2VCre(–):*Girk1*$^{fl/fl}$ (n = 6) and MLC2VCre(+):*Girk1*$^{fl/fl}$ (n = 8) mice (P = 0.14).

2.4 Discussion

Parasympathetic regulation of cardiac physiology is thought to involve muscarinic-dependent and independent actions on atrial and ventricular tissue, and multiple enzymes and ion channels (Coote, 2013; Gordan et al., 2015). While previous studies have suggested that GIRK channels, $I_{Ca,L}$, and I_f mediate the muscarinic receptor-dependent effects of parasympathetic activation on the heart, their relative contributions remain unclear. Here, we demonstrate that the impact of direct VNS on HR, HRV, and arrhythmogenesis in anesthetized mice is mediated primarily by the muscarinic receptor-dependent activation of atrial GIRK channels. Notably, this study is the first to evaluate the impact of GIRK channel ablation, either in whole-heart or in tissue-specific fashion, on the effects of direct VNS in mice.

Constitutive *Girk1*$^{-/-}$ and *Girk4*$^{-/-}$ mice display blunted HR and HRV responses to pharmacologic treatments that stimulate or mimic parasympathetic activity (Bettahi et al., 2002; Kovoor et al., 2001; Mesirca et al., 2013; Wickman et al., 1998). However, the degree of bradycardia conferred by GIRK channel activation that has been reported in these studies has varied. For example, the bradycardic effect evoked by methoxamine activation of the baroreflex was ~50% smaller in *Girk4*$^{-/-}$ mice (Bettahi et al., 2002; Wickman et al., 1998), whereas experiments involving direct perfusion of ACh onto SAN tissue, or of isolated mouse hearts, have suggested that the GIRK channel contribution to the bradycardic effect of cholinergic agonists is concentration-dependent (Mesirca et al., 2013). Consistent with this premise, DiFrancesco et al. (1989) showed a concentration-dependent effect of ACh in modulation of I_f and I_{KACh} in SAN cells: whereas nanomolar concentrations of ACh inhibited I_f, 20-fold higher concentrations were required to activate I_{KACh}.

In this study, we found that nearly all of the HR and HRV response to electrical stimulation of the vagus nerve was absent in constitutive *Girk4*$^{-/-}$ mice, and in mice lacking only atrial GIRK channels. Atropine blocked VNS-induced HR and HRV responses, indicating that these effects are dependent on muscarinic receptor activation. While the prominent contribution of GIRK channels revealed in this study could reflect our utilization of a relatively strong VNS protocol, or the fact that all recordings were made in anesthetized mice, it was nevertheless surprising that minimal residual impact of VNS stimulation on HR or HRV was observed in *Girk4*$^{-/-}$ mice and SLNCre(+):*Girk1*$^{fl/fl}$ mice. Given that $I_{Ca,L}$ and I_f conductances have been recorded in SAN cells from *Girk4*$^{-/-}$ mice (Mesirca et al., 2013), and that residual cholinergic-induced bradycardia was seen in *Girk4*$^{-/-}$ mice (Anderson et al., 2018; Bettahi et al., 2002; Mesirca et al., 2013; Wickman et al., 1998), we do not believe that the lack of VNS-induced effects in *Girk4*$^{-/-}$ or SLNCre(+):*Girk1*$^{fl/fl}$ mice reflects a loss of muscarinic receptor expression and/or function. Notably, our findings are consistent with those of a recent study showing that while knockdown of HCN4 exaggerated the bradycardic response to VNS in mice, over-expression of HCN4 only blunted VNS-induced bradycardia in the presence of isoproterenol (Kozasa et al., 2018). Thus, muscarinic-dependent activation of atrial GIRK channels appears to play the primary role in the effect of VNS on HR dynamics, at least in the anesthetized mouse.

The VNS-induced reduction of atrial ERP and increase in heterogeneity throughout the atria has been linked to atrial arrhythmogenesis (Prystowsky et al., 1983; Shen and Zipes, 2014; Zhang and Mazgalev, 2011). Indeed, VNS is frequently utilized for the induction and maintenance of AF in large mammalian species (Katsouras et al., 2009; Zhang and Mazgalev, 2011). Additionally, high vagal tone is associated with various bradyarrhythmias, including AV block and sinus node dysfunction, in human patients (Aksu et al., 2018). Here, we demonstrated that VNS is also pro-arrhythmic in the mouse,

as arrhythmic episodes were only observed during VNS. Moreover, the arrhythmogenic effect of VNS in the anesthetized mouse is primarily attributable to the muscarinic receptor-dependent activation of atrial GIRK channels.

VNS has been shown to exhibit anti-inflammatory effects by decreasing pro-inflammatory and/or increasing anti-inflammatory cytokine levels in various animal models (Calvillo et al., 2011; Mihaylova et al., 2012; Zhang et al., 2009). Thus, it will be interesting to test whether VNS confers a therapeutic benefit in heart diseases characterized by pro-inflammatory cytokines (Hedayat et al., 2010). In addition, although GIRK channel activation appears to mediate most of the VNS-induced influence on HR dynamics, further studies are needed to discern whether VNS-induced activation of atrial GIRK-channels underlies its cardioprotective benefit in diseases such as heart failure. As part of this effort, experiments should be conducted to determine whether it is possible to identify VNS parameters that deliver therapeutic benefits without promoting arrhythmogenesis.

Notably, neither *Girk4*$^{-/-}$ nor SLNCre(+):*Girk1*$^{fl/fl}$ mice exhibited arrhythmic episodes during VNS. These findings are consistent with a previous report showing that *Girk4* ablation confers resistance to pacing-induced AF in mice (Kovoor et al., 2001), and can restore normal cardiac rhythm in mouse models of sick sinus syndrome and AV block (Mesirca et al., 2014, 2016a). Interestingly, a recent study reported that increased GIRK channel activity secondary to a mutation in the gene encoding the G protein β2 subunit (Gβ2; GNB2) is associated with AV nodal dysfunction in humans (Stallmeyer et al., 2017). Collectively, these insights highlight the clinical potential of pharmacologic or genetic suppression of atrial GIRK channels for the treatment of supraventricular arrhythmias.

In summary, we conclude that the muscarinic receptor-dependent activation of atrial GIRK channels is the dominant mediator of VNS-induced effects on HR, HRV, and arrhythmogenesis in mice. Our findings highlight the potential therapeutic benefit of

selectively targeting this branch of the parasympathetic signaling for the management of atrial arrhythmias.

Chapter 3

Expression and relevance of the G protein-gated K^+ channel in the mouse ventricle

Anderson A, Kulkarni K, Marron Fernandez de Velasco E, Carlblom N, Xia Z, Xie X, Nakano A, Martemyanov K, Tolkacheva E, Wickman K (2018). Expression and relevance of the G protein-gated K^+ channel I_{KACh} in the mouse ventricle. Sci. Rep. 8(1):1192.

Author Contributions: A.A., K.A.M. and K.W. designed the overall scope of the study. A.A., K.K., E.M.F.d.V., N.C., Z.X., A.N., E.T. and K.W. were responsible for experimental design, execution of experiments, and/or data analysis. A.A. and K.W. wrote the manuscript. All authors reviewed the manuscript.

3.1 Introduction

Increased output of the parasympathetic branch of the ANS leads to the slowing of HR and an increase in HRV, an indicator of beat-to-beat fluctuations in HR (Draghici and Taylor, 2016; Lombardi and Stein, 2011). Abnormal parasympathetic regulation of cardiac output has been linked to multiple cardiac disorders, including AF, AV block, heart failure, and SCD (Alboni et al., 2013; Bigger et al., 1992; La Rovere et al., 2009; Munger et al., 2014; Schwartz, 1998)

The parasympathetic influence on the heart involves ACh acting on SAN and AVN cells, as well as atrial myocytes (Chapleau and Sabharwal, 2011; Coote, 2013; Stewart et al., 2012). ACh binds to M_2R on these cells, initiating a branched intracellular signaling pathway mediated by inhibitory ($G_{i/o}$) G proteins, culminating in the activation of the K^+ channel I_{KACh}, as well as the suppression of the cAMP/PKA-dependent cation-selective ion channel (HCN/I_f) and voltage-gated Ca^{2+} channels (Difrancesco, 2010; DiFrancesco et al., 1989; Mangoni and Nargeot, 2008; Wickman and Clapham, 1995).

The atrial I_{KACh} channel is a GIRK channel consisting of GIRK1 and GIRK4 subunits, in 1:1 stoichiometry (Corey et al., 1998; Krapivinsky et al., 1995a). I_{KACh} is gated by G protein $G\beta\gamma$ subunits liberated following M_2R activation (Logothetis et al., 1987; Wickman et al., 1994). Genetic ablation of either *Girk1* or *Girk4* in mice eliminated the I_{KACh} conductance in neonatal atrial myocytes, and yielded a modest increase in HR and decrease in HRV at baseline in adult animals (Bettahi et al., 2002; Wickman et al., 1998). Additionally, HR and HRV responses to ACh and CCh were diminished in isolated hearts from mice lacking GIRK1 or GIRK4 (Bettahi et al., 2002; Mesirca et al., 2013; Posokhova et al., 2013; Wickman et al., 1998).

While the parasympathetic impact on cardiac function is typically ascribed to its influence on the atria, SAN, and AVN, parasympathetic innervation of ventricular tissue is

also evident in mammals (Coote, 2013). In addition, profound effects of VNS on ventricular physiology have been noted in several species (Dobrzynski et al., 2002). For example, chronic VNS altered the electrophysiological properties of the heart and reduced susceptibility to ventricular arrhythmias in rats (Lee et al., 2016). Additionally, ACh shortened APD in human ventricular myocytes, in an atropine-sensitive manner (Koumi et al., 1997). This effect has been attributed to the activation of a GIRK channel (Dobrzynski et al., 2001, 2002; LaCroix et al., 2008; Yang et al., 2010b). Consistent with this premise, the ACh-induced decrease in APD and ERP in rat papillary muscle was blocked by tertiapin, and ACh triggered hyperpolarization and a reduction in APD in right ventricle recordings from wild-type but not *Girk4*$^{-/-}$ mice (Liang et al., 2014). In addition, a mutation in the human GIRK4/KCNJ5 gene underlies a congenital form of LQTS13, a ventricular repolarization disorder associated with arrhythmia, syncope, and sudden death (Wang et al., 2013a; Yang et al., 2010b)

While available evidence supports the contention that a GIRK channel contributes to the cholinergic influence on ventricular physiology, critical details remain unclear. Here, we examined the expression in mouse ventricle of genes implicated in atrial I_{KACh}-dependent signaling, and evaluated the impact of gene ablation on cholinergic signaling in ventricular myocytes. We present functional evidence that the GIRK channel in ventricular myocytes is a GIRK1/GIRK4 heteromer, and that it mediates the impact of cholinergic signaling on APD and excitability of these cells. We also probed the physiological impact of ventricular GIRK-dependent signaling using a novel ventricle-specific *Girk1*$^{-/-}$ mouse line. Our findings reveal that, despite the contribution of GIRK channels to the CCh-dependent acceleration of repolarization and decrease in ventricular myocyte excitability, ventricular GIRK-dependent signaling does not exert a significant impact on HR, HRV, or susceptibility to ventricular arrhythmias in mice.

3.2 Methods

Animals. All experimental procedures involving mice were approved by the Institutional Animal Care and Use Committee of the University of Minnesota, and were conducted in accordance with guidelines set by the National Institute of Health. The generation of *Girk1*$^{-/-}$, *Girk4*$^{-/-}$, *Rgs6*$^{-/-}$, and *Girk1*$^{fl/fl}$ mice was described previously (Bettahi et al., 2002; Marron Fernandez de Velasco et al., 2017a; Posokhova et al., 2010; Wickman et al., 1998). *Girk1*$^{fl/fl}$ mice were crossed with MLC2VCre(+) (Chen et al., 1998) mice to generate the MLC2VCre:*Girk1*$^{fl/fl}$ line. B6.Cg-Gt(ROSA)26Sortm14(CAG-tdTomato)Hze/J (Ai14-tdTomato) reporter mice were purchased from The Jackson Laboratory (Bar Harbor, ME) and crossed with MLC2VCre(+) mice. Mice were group-housed on a 12-h light/dark cycle, and given free access to food and water and were used for experiments at age 8–12 wk.

Quantitative RT-PCR. Total RNA was isolated from freshly isolated atrial and ventricular tissue samples from adult C57BL/6J mice using the RNeasy fibrous tissue kit (Qiagen; Germantown, MD), according to manufacturer recommendations. Reverse transcription was performed using iScript™ cDNA Synthesis Kit (Bio-Rad Laboratories; Hercules, CA). Quantitative PCR was performed in a StepOnePlus Real Time PCR System (Applied Biosystems; Foster City, CA), with the Fast SYBR Green Master Mix (ThermoFisher Scientific; Waltham, MA). The following amplification program was used: 95 °C/20 s followed by 40 cycles of 95 °C/3 s, 60 °C/30 s. Intron-spanning primer pairs were as follows: M_2R: 5′-GCCAGACTCCACCAGAT-3′ (forward) and 5′-CCATTGTTCGAGGAGTTAGTT-3′ (reverse); GIRK1: 5′-AAACTCACTCTCATGTTCCG-3′ (forward) and 5′-TCCAGTTCAAGTTGGTCAAG-3′ (reverse); GIRK4: 5′-GAGTTCGAAGTTGTGGTCATA-3′ (forward) and 5′-GCACCTCTGTATCCATGTAAG-3′ (reverse); RGS6: 5′-CTGACATTGTACAGTGGCTTAT-3′ (forward) and 5′-

GAGAACATGGTCTGAGATTGG-3′ (reverse). The specificity of the GIRK1, GIRK4, and RGS6 reactions was assessed with a melting curve at the end of the program, and confirmed using samples from *Girk1*$^{-/-}$, *Girk4*$^{-/-}$, and *Rgs6*$^{-/-}$ mice, respectively. Samples were tested in duplicate, and the average of replicates was used in the final data analysis. GAPDH (Mm_Gapd_2_SG QuantiTect primers; Qiagen) was used as internal control in each sample.

Cell culture. SAN cells and ventricular myocytes were isolated as described43,68. Mice were injected intraperitoneally (I.P.) with heparin (250 U) and then anesthetized with ketamine (100 mg/kg) and xylazine (10 mg/kg). To obtain SAN cells, hearts were excised into Tyrode's solution (in mM): 140 NaCl, 5.4 KCl, 1.2 KH_2PO_4, 1.0 $MgCl_2$, 1.8 $CaCl_2$, 5.55 glucose, 5 HEPES, pH 7.4 with NaOH. SAN-containing tissue was excised into a modified Tyrode's solution containing (in mM): 140 NaCl, 5.4 KCl, 1.2 KH_2PO_4, 0.2 $CaCl_2$, 50 taurine, 18.5 glucose, 5 HEPES, 0.1% BSA, pH 6.9 with NaOH, with elastase (0.3 mg/mL, Worthington Biochemical Corp., Lakewood, NJ) and collagenase II (0.21 mg/mL; Sigma Aldrich, St. Louis, MO). SAN tissue was digested at 37 °C for 30 min and then washed three times in a solution containing (in mM): 100 L-glutamic acid/potassium salt, 10 L-aspartic acid/potassium salt, 25 KCl, 10 KH_2PO_4, 2 $MgSO_4$, 20 taurine, 5 creatine, 0.5 EGTA, 20 glucose, 5 HEPES, 0.1% BSA, pH 7.2 with KOH. SAN tissue was then triturated and plated on laminin-coated coverslips (25 μg/mL) and used within 8 h.

Ventricular myocytes were extracted by excising hearts into ice-cold cell isolation buffer (in mM): 118 NaCl, 4.8 KCl, 25 HEPES, 1.2 KH_2PO_4, 1.2 $MgSO_4$, 11 glucose, 30 taurine, 10 2,3-butanedione monoxime, pH 7.4 (with NaOH). The aorta was subsequently cannulated and hearts were then retrogradely perfused using a Langendorff apparatus with warm cell isolation buffer supplemented with collagenase II (620 U/mL; Worthington Biochemical Corp.). After a 10 min digestion, the heart was taken off the cannula and the atria were removed. The ventricles were cut into pieces and triturated. Samples were then

transferred to a stop buffer consisting of cell isolation buffer supplemented with 2.5% BSA, 0.1 mM $CaCl_2$, 5%FBS; where $CaCl_2$ was added in three, 5 min increments to reach a final $CaCl_2$ concentration of 1.6 mM. The cell suspension was then transferred to media consisting of M199, 0.2% BSA, 26.2 mM sodium bicarbonate, 25 mM HEPES, insulin-transferrin-sodium-selenite solution (1X), 5% FBS, penicillin (1000 U), streptomycin (1 mg), pH 7.4 (with NaOH); and plated on laminin-coated coverslips (25 μg/mL) and used within 8 h.

Whole-cell electrophysiology. Coverslips containing adult SAN cells or ventricular myocytes were transferred to a perfusion chamber and electrophysiological recordings were conducted as described (Posokhova et al., 2010). SAN cells were identified as thin, striated cells with capacitance values between 20–40 pF. Ventricular myocytes were identified as quiescent, rod-shaped cells with capacitance values ranging from 100–250 pF. Whole-cell currents and voltages were measured with hardware (Axopatch-700B amplifier, Digidata 1440A) and software (pCLAMP v. 10.4) from Molecular Devices (Sunnyvale, CA). All currents were low-pass filtered at 0.1 kHz, sampled at 5 kHz, and stored on computer hard disk for analysis. The liquid-junction potential, predicted to be −17 mV using JPCalc software (Molecular Devices), was not corrected. CCh-induced currents were measured at a holding potential of −70 mV. Borosilicate patch pipettes were filled with (in mM): 130 K-gluconate, 2 $MgCl_2$, 1.1 EGTA, 5 HEPES, 2 Na_2ATP, 5 phosphocreatine, and 0.3 Na-GTP, pH 7.2 (with KOH). Whole-cell access was achieved in a low-K^+ bath solution consisting of (in mM): 130 NaCl, 5.4 KCl, 1 $CaCl_2$, 1 $MgCl_2$, 5.5 glucose, 5 HEPES/NaOH, pH 7.4. A high-K+ bath solution (+/−CCh) consisting of (in mM): 120 NaCl, 25 KCl, 1 CaCl2, 1 MgCl2, 5.5 glucose, 5 HEPES/NaOH, pH 7.4 was applied via ValveLink 8.2 rapid perfusion system (AutoMate Scientific, Berkeley, CA). Activation and deactivation time constants were extracted from appropriate regions of current traces, which were fit with a 1-term Boltzmann equation. Rheobase was evaluated in current-

clamp mode in low-K^+ bath solution by injecting increasing steps (5 pA/500 ms) of depolarizing current, starting at 0 pA, until an action potential spike was elicited. APD_{20}, APD_{50}, APD_{70}, and APD_{90} were measured from the average of 10 spikes elicited by injecting a supra-threshold current (1 nA/5 ms) into the cell. The % change in APD and rheobase after CCh perfusion was measured as with the follows: ((baseline − post-CCh/baseline) × 100). Only those experiments in which the access resistances were stable and low (<20 MΩ) were included in the final analysis.

Microscopy. Hearts were fixed with 4% paraformaldehyde in PBS at 4 °C for 16–24 h, transferred to a 10% sucrose/PBS solution at 4 °C for 24 h, and then transferred to a solution of 30% sucrose/PBS solution at 4 °C for at least 48 h. 20 μm thick slices were cut by cryostat at −20 °C and slices were mounted and stained with ProLong Gold Antifade reagent with DAPI (ThermoFisher Scientific; Waltham, MA). Fluorescent images were captured with an Olympus BX51W1 upright microscope with Disk Spinning Unit, using a 2X objective and digital CCD camera (C10600-10B, Hamamatsu Photonic System Corp; Bridgewater, NJ). Images were processed with Metamorph Advanced 7.7.7.0 (Molecular Devices).

In vivo ECG recordings. Mice were anesthetized with 1.5% isoflurane supplemented with an air mixture of 40% O2/60% N2 to sustain stable HR. Platinum needle ECG electrodes connected to an IX-ECG-12 recorder (iWorx; Dover, NH) were placed subcutaneously into each limb. Baseline HR was recorded for 10 min, at which point CCh (1.0 mg/kg I.P.) was administered. HR and HRV analysis was performed on 1-min bins of stable recording from minutes 9–10 (baseline) and 15–16 min (post-CCh), using Kubios HRV 3.02 software (Tarvainen et al., 2014). Artifact detection/correction was utilized to reduce the impact of ectopic and skipped beats (either AV block or RR intervals which differ from the neighboring RR intervals by over 25%) on HR and HRV analysis. The frequency bands for HRV analysis were defined as very low frequency (VLF), <0.4;

low frequency (LF), 0.4–1.5 Hz; and high frequency (HF), 1.5–5.0 Hz; using a 120 s window with a 50% overlap for Fast Fourier Fransform spectrum analysis using Welch's periodogram method. Arrhythmic events were defined as instances of AV block (P wave with no corresponding QRS complex) and/or instances of tachycardia (at least 3–5 beats). PR and QT intervals were analyzed from the average of 100 cycles from either lead I or lead II during these segments, using LabScribe v3 software, only from recordings where the noise level was sufficiently low to clearly delineate the beginning and end of the indicated waveform deflections. The QT interval was corrected for changes in RR interval using the following formula: QTc = SQRT[QT/(RR/100)] (Mitchell et al., 1998).

Ex vivo burst pacing. Hearts were excised and submerged in cardioplegic solution (in mM): 280 glucose, 13.44 KCl, 12.6 $NaHCO_3$, and 34 mannitol. The aorta was subsequently cannulated and retrogradely perfused with warm (37±1 °C), oxygenated Tyrode's (in mM): 130 NaCl, 1.8 $CaCl_2$, 4 KCl, 1.0 $MgCl_2$, 1.2 NaH_2PO_4, 24 $NaHCO_3$, 5.5 glucose, pH 7.4. Once hearts had been allowed to stabilize for 10 min, burst pacing at decreasing basic cycle lengths (BCL) (100 BCL down to 10 BCL, step-size 10) was applied 3 times to determine susceptibility to VT or VF at baseline via a stimulating electrode placed at the base of the left ventricle. Once the protocol was finished, 3 μM CCh was perfused into the hearts. After a 2–5 min stabilization period, the burst pacing protocol was run once again. Analysis was done using LabChart v7.3.8 software (ADInstruments; Colorado Springs, Colorado), where occurrences of VT lasting at least 7–8 beats, were tallied before and after CCh infusion.

Statistical analysis. All data are presented as the mean ± SEM. Statistical analyses were performed using Prism 5 (GraphPad Software, Inc.; La Jolla, CA) software. Male and female mice were used in all studies, and groups were balanced for sex. Data were analyzed with Student's two-tailed t-test (unpaired and paired), Fisher's exact test, 1-way ANOVA, and 2-way ANOVA with repeated measures, as appropriate. For studies involving

2-way ANOVA analysis, only the interaction is reported if one was detected. The Bonferroni multiple comparison post hoc test was used following 1-way or 2-way ANOVA analyses, if justified. The level of significance was set at $P < 0.05$.

3.3 Results

3.3.1 Expression of I_{KACh}-dependent signaling pathway elements in mouse atria and ventricle

Expression of key elements of the atrial M_2R-I_{KACh} signaling pathway, including GIRK1, GIRK4, M_2R, and RGS6, has been detected in ventricular tissue from many mammalian species (Dobrzynski et al., 2001, 2002; Wickman et al., 2002; Yang et al., 2010b, 2010a, 2013). A study in the rat heart revealed higher expression in atria than ventricle for GIRK1, GIRK4, and RGS6 (McGrath and de Bold, 2009). We sought to confirm these findings in the mouse by comparing the expression levels of these targets, as well as M_2R, in the atria and ventricle of adult mice using quantitative RT-PCR. We found that GIRK1, GIRK4, M_2R, and RGS6 mRNAs were all present in mouse ventricular tissue, but that the levels of all targets were lower (4- to 10-fold) than those found in mouse atrial tissue (**Figure 3.1**).

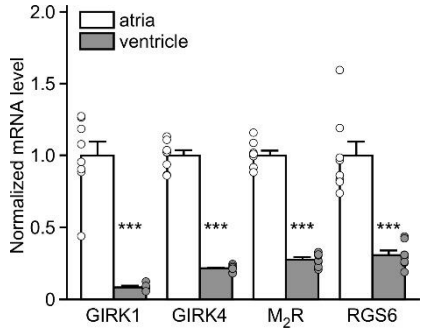

Figure 3.1. Expression of I_{KACh}-dependent signaling elements in mouse atria and ventricle.

mRNA levels of GIRK1 ($t_{14} = 9.4$, ***$P < 0.001$), GIRK4 ($t_{14} = 21.2$, ***$P < 0.001$), M_2R ($t_{13} = 18.6$, ***$P < 0.001$), and RGS6 ($t_{14} = 6.7$, ***$P < 0.001$), and in atria and ventricle from adult C57BL/6J mice, compared using an unpaired Student's *t*-test. mRNA levels of each target were normalized to the level of GAPDH mRNA measured in each sample. Ventricular mRNA levels for each target was normalized to the level present in atrial samples (n = 7–8 samples per tissue, per target).

3.3.2 Evidence of a GIRK1/GIRK4 heteromer in mouse ventricular myocytes

Previous work suggests that a GIRK4-containing GIRK channel is present in rodent ventricle (Kovoor et al., 2001; Liang et al., 2014). While GIRK1/GIRK4 heteromeric channels are thought to mediate the atrial I_{KACh} conductance, some evidence suggests that GIRK4 homomeric channels may contribute as well (Bender et al., 2001; Corey and Clapham, 1998). To assess the relative contributions of GIRK1 and GIRK4 to the GIRK channel activity in ventricle, we measured whole-cell currents induced by CCh in ventricular myocytes from wild-type mice, and from mice lacking GIRK1 or GIRK4. Ventricular myocytes express a prominent constitutive K^+ current (I_{K1}) that masks the ACh/CCh-induced GIRK current under normal whole-cell recording conditions, due to K^+ accumulation and/or depletion (Beckmann et al., 2008). As such, we included a low concentration of Ba^{2+} (5 μM) in our bath solution to selectively suppress I_{K1}, while preserving any potential GIRK channel activity. Indeed, 5 μM Ba^{2+} did not suppress the CCh-induced GIRK current in wild-type SAN cells; indeed, currents were slightly larger in the presence Ba^{2+} (**Supplementary Figure 3S1**).

CCh (100 μM) evoked reliable currents in ventricular myocytes from adult wild-type mice, but not in myocytes from *Girk1*$^{-/-}$ or *Girk4*$^{-/-}$ mice (**Figure 3.2a,b**). Since GIRK1 is unable to form functional homomeric channels (Hedin et al., 1996; Kennedy et al., 1996, 1999; Krapivinsky et al., 1995a; Ma et al., 2002), this observation supports the contention that GIRK1 and GIRK4 assemble to form the GIRK channel in mouse ventricular myocytes. The peak density of the CCh-induced GIRK current was ~5–10 fold smaller in ventricular myocytes, however, as compared to currents reported in SAN cells (Wydeven et al., 2014b). Additionally, the CCh-induced current activation and deactivation kinetics were significantly slower for the ventricular GIRK channel as compared to the atrial GIRK channel (**Figure 3.2c,d**) (Wydeven et al., 2014b). Furthermore, the ventricular GIRK current was more than an order of magnitude less sensitive to CCh ($EC_{50} = 4.8 \pm 0.6$ μM;

Figure 3.2e) than the SAN cell GIRK current ($EC_{50} = 0.25 \pm 0.03\ \mu M$) (Wydeven et al., 2014b), reminiscent of the lower ACh sensitivity of the GIRK conductance in human ventricular myocytes as compared to atrial myocytes (Koumi and Wasserstrom, 1994).

3.3.3 Influence of RGS6 on GIRK-dependent signaling in ventricular myocytes

The M_2R-I_{KACh} signaling pathway in atrial myocytes and SAN cells is negatively regulated by RGS6 (Posokhova et al., 2010, 2013; Wydeven et al., 2014b; Yang et al., 2010a). Indeed, in SAN cells and atrial myocytes from mice lacking RGS6, GIRK currents evoked by CCh exhibited slower deactivation kinetics and an increased sensitivity to CCh (Wydeven et al., 2014b; Yang et al., 2010a). To test whether ventricular GIRK-dependent signaling is negatively regulated by RGS6, we compared CCh-induced GIRK currents in ventricular myocytes from adult wild-type and *Rgs6*$^{-/-}$ mice. Current densities were slightly, but significantly, larger in ventricular myocytes from *Rgs6*$^{-/-}$ mice as compared to wild-type controls (**Figure 3.2a,b**). No effect of Rgs6 ablation, however, was seen on activation (**Figure 3.2c**) or deactivation (**Figure 3.2d**) kinetics of the CCh-induced, ventricular GIRK current. Moreover, the EC_{50} for CCh-induced activation of the GIRK current was comparable in ventricular myocytes from wild-type and *Rgs6*$^{-/-}$ mice **(Figure 3.2e**). Thus, the impact of RGS6 on ventricular GIRK-dependent signaling is limited to a modest negative regulation of peak current density.

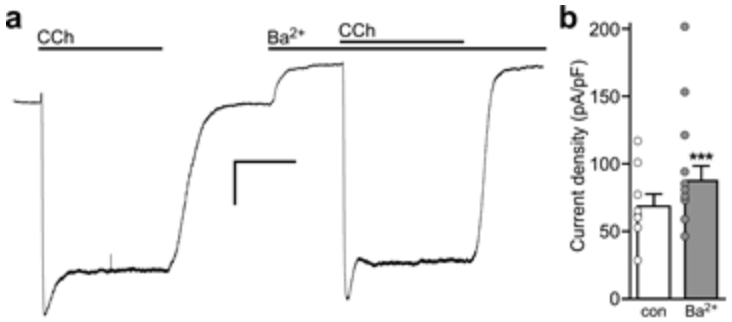

Supplementary Figure 3.S1. Impact of extracellular Ba^{2+} on CCh-induced GIRK current in mouse SAN cells

(**a**) Whole-cell current (V_{hold}= -70 mV) evoked by carbachol (CCh, 10 μM) in an adult wild-type SAN cell, in the absence or presence of 5 μM extracellular Ba^{2+}. Scale: 0.5 nA/10 s. (**b**) Summary of CCh-induced current density in adult wild-type SAN cells, measured in the absence (con) and presence (Ba^{2+}) of 5 μM Ba^{2+} (t_8=5.5, ****P*<0.001, n=9 cells/3 mice; paired Student's *t*-test).

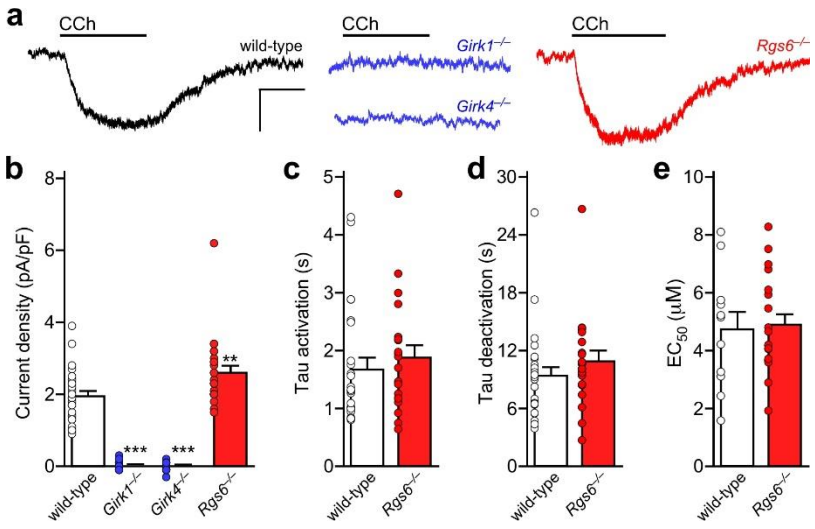

Figure 3.2. Carbachol-induced GIRK currents in adult mouse ventricular myocytes. (**a**) Whole-cell currents (V_{hold} = −70 mV) evoked by carbachol (CCh, 100 μM) in a high-K^+ bath solution (containing 5 μM $BaCl_2$) in adult ventricular myocytes from wild-type, *Girk1*$^{-/-}$, *Girk4*$^{-/-}$, and *Rgs6*$^{-/-}$ mice. Scale: 0.1 nA/10 s. (**b**) Summary of maximal CCh-induced current density in adult ventricular myocytes from wild-type (n = 28 cells/6 mice), *Girk1*$^{-/-}$ (n = 23 cells/4 mice), *Girk4*$^{-/-}$ (n = 21 cells/4 mice), and *Rgs6*$^{-/-}$ mice (n = 24 cells/6 mice); open symbols overlapping the bars denote individual data points. One-way ANOVA analysis revealed an effect of genotype on CCh-induced current density ($F_{3,92}$ = 110.6, P < 0.001). Symbols: **, ***P < 0.01 and 0.001, respectively, vs. wild-type. (c,d) Summary of activation (**c**; t_{44} = 0.7, P = 0.51) and deactivation (**d**); t_{44} = 1.1, P = 0.28) kinetics for the CCh-induced current in ventricular myocytes from wild-type (n = 25 cells/6 mice) and *Rgs6*$^{-/-}$ mice (n = 21 cells/6 mice), compared across genotypes using an unpaired Student's *t*-test. (**e**) Summary of EC_{50} values derived from concentration-response experiments for the CCh-induced current in adult ventricular myocytes from wild-type vs. *Rgs6*$^{-/-}$ mice. The EC_{50} for current activation by CCh did not differ between wild-type (4.8 ± 0.6 μM, n = 11 cells/4 mice) and *Rgs6*$^{-/-}$ (4.9 ± 0.4 μM, n = 19 cells/4 mice) ventricular myocytes, as determined using an unpaired Student's *t*-test (t_{28} = 0.20, P = 0.84).

3.3.4 Influence of GIRK channels on ventricular myocyte APD and excitability

To test whether I_{KACh} modulates ventricular myocyte excitability and repolarization, we evaluated the change in rheobase and APD induced by CCh (100 μM) in ventricular myocytes from wild-type and *Girk4*$^{-/-}$ mice. The CCh-induced decrease in ventricular myocyte excitability (increase in rheobase) was larger in ventricular myocytes from wild-type than *Girk4*$^{-/-}$ mice (**Figure 3.3a**). And, although there was no significant difference in the CCh-induced shortening of APD_{20}, APD_{50}, and APD_{70} between ventricular myocytes from wild-type and *Girk4*$^{-/-}$ mice (**Figure 3.3b–e**), the CCh-induced decrease in APD_{90} was blunted in ventricular myocytes from *Girk4*$^{-/-}$ mice (**Figure 3.3f**). Thus, GIRK channels contribute to the cholinergic regulation of excitability and repolarization of adult mouse ventricular myocytes.

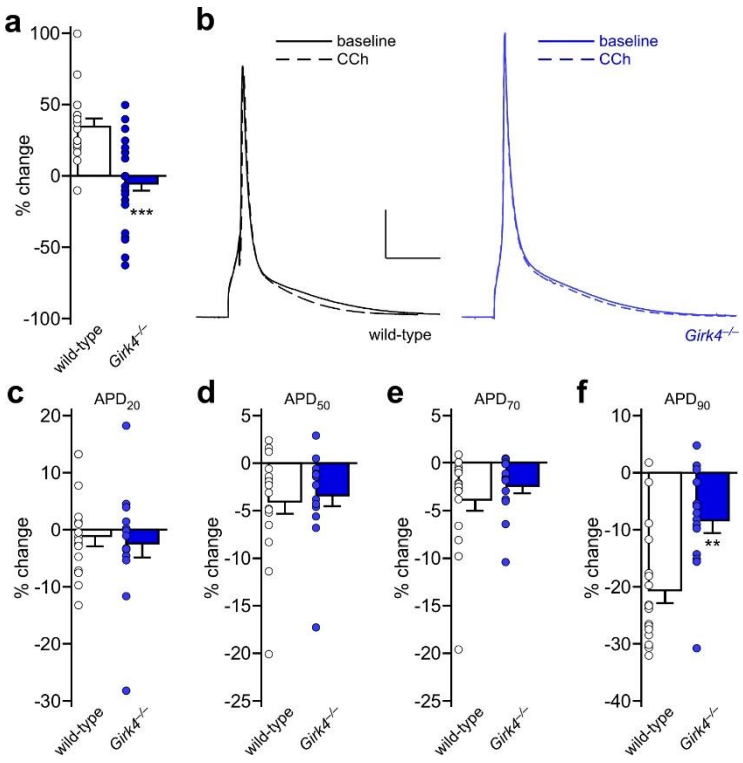

Figure 3.3. GIRK channel contribution to the cholinergic regulation of mouse ventricular myocyte repolarization and excitability.
(**a**) Change in rheobase evoked by CCh (100 μM) in adult wild-type (n = 19 cells/5 mice) and *Girk4*$^{-/-}$ (n = 26 cells/6 mice) ventricular myocytes, compared using an unpaired Student's *t*-test ($t_{43} = 5.1$, ***$P < 0.001$). (**b**) Action potentials evoked by current injection in wild-type and *Girk4*$^{-/-}$ ventricular myocytes, at baseline (solid line) and in the presence of CCh (100 μM, dashed line). Scale: 20 mV/25 ms. (**c**–**f**) Summary of the percentage change in APD_{20} ($t_{29} = 0.37$, $P = 0.72$), APD_{50} ($t_{29} = 0.38$, $P = 0.71$), APD_{70} ($t_{29} = 0.97$, $P = 0.34$), and APD_{90} ($t_{29} = 3.5$, **$P < 0.01$) evoked by CCh in wild-type (n = 17 cells/6 mice) and *Girk4*$^{-/-}$ (n = 14 cells/5 mice) ventricular myocytes, compared using an unpaired Student's *t*-test.

3.3.5. Generation and characterization of mice lacking GIRK channels in ventricle

To probe the impact of ventricular GIRK channel on cardiac physiology, we crossed a conditional Girk1 knockout mouse (*Girk1*$^{fl/fl}$) (Marron Fernandez de Velasco et al., 2017a) with a ventricle-specific Cre driver line (MLC2VCre) (Chen et al., 1998), PMID: 9550726). We first verified the ventricular specificity of Cre-dependent gene ablation conferred by the MLC2VCre driver line using a Cre-dependent fluorescent reporter mouse line (**Figure 3.4a,b**). We next evaluated the functional impact and cell specificity of *Girk1* ablation by measuring CCh-induced whole-cell currents in SAN cells and ventricular myocytes from MLC2VCre(−):*Girk1*$^{fl/fl}$ and MLC2VCre(+):*Girk1*$^{fl/fl}$ mice. CCh-induced current density in adult ventricular myocytes from MLC2VCre(+):*Girk1*$^{fl/fl}$ mice was significantly smaller than responses measured in ventricular myocytes from MLC2VCre(−):*Girk1*$^{fl/fl}$ littermates (**Figure 3.4c,d**). We observed no difference, however, in CCh-induced current density in SAN cells from adult MLC2VCre(+):*Girk1*$^{fl/fl}$ and MLC2VCre(−):*Girk1*$^{fl/fl}$ mice (**Figure 3.4e**). Thus, GIRK channel activity is selectively suppressed in ventricular myocytes from MLC2VCre(+):*Girk1*$^{fl/fl}$ mice.

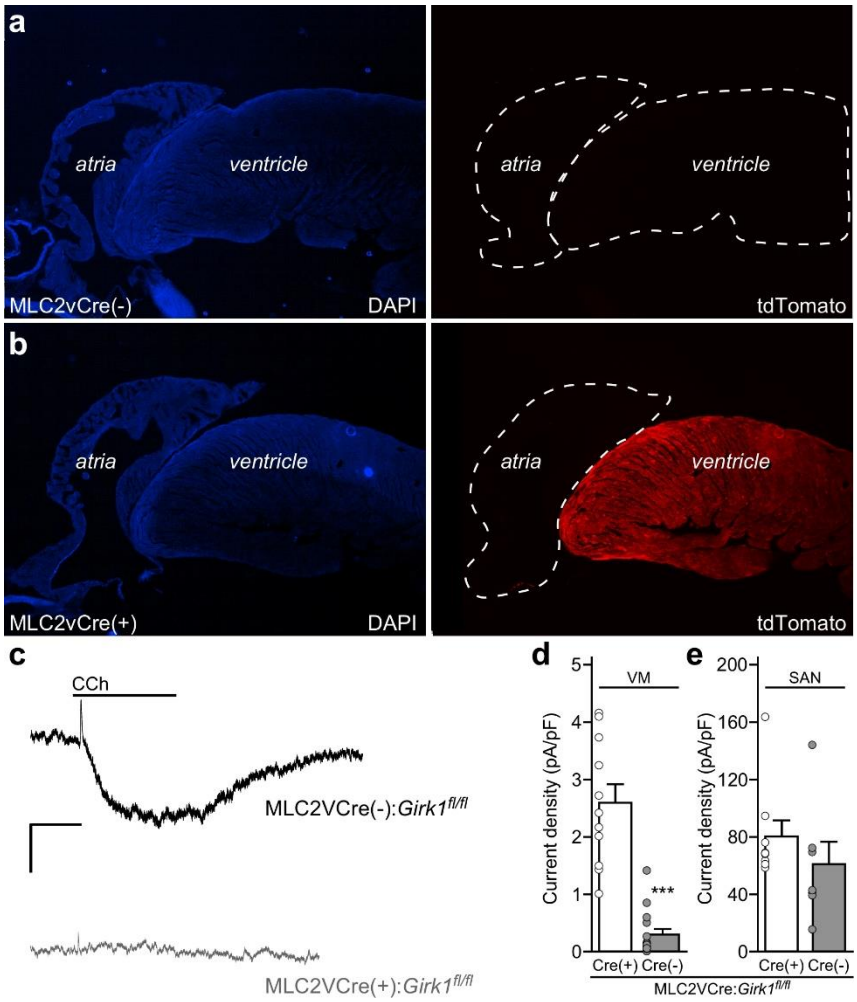

Figure 3.4. Characterization of mice lacking GIRK channels in the ventricle.
(**a**,**b**) Sections of the heart from MLC2VCre(−):Ai14-tdTomato and MLC2VCre(+):Ai14-tdTomato mice, labeled with the nuclear stain DAPI (left panels), showing restricted Cre-dependent gene expression (tdTomato, right panels) in the ventricle of MLC2VCre(+) mice. (**c**) Whole-cell currents (V_{hold} = − 70 mV) evoked by CCh (100 μM) in a high-K^+ bath solution (containing 5 μM $BaCl_2$) in adult ventricular myocytes from MLC2VCre(−):*Girk1*$^{fl/fl}$ and MLC2VCre(+):*Girk1*$^{fl/fl}$ mice. Scale: 0.2 nA/10 s. (**d**) Summary of CCh-induced current densities in MLC2VCre(−):*Girk1*$^{fl/fl}$ (n =11 cells/2 mice) and MLC2VCre(+):*Girk1*$^{fl/fl}$ (n = 15 cells/2 mice) ventricular myocytes (VM), compared with an unpaired Student's *t*-test (t_{24} = 7.5, ***P < 0.001). (**e**) Summary of CCh-induced current densities in adult SAN cells from MLC2VCre(−):*Girk1*$^{fl/fl}$ (n = 9 cells/3 mice) and MLC2VCre(+):*Girk1*$^{fl/fl}$ (n = 7 cells/2 mice) mice, compared with an unpaired Student's *t*-test (t_{14} = 1.1, P = 0.31).

3.3.6 Impact of ventricle-specific GIRK channel ablation on cardiac physiology

To discern the impact of ventricle-specific GIRK channel ablation on cardiac physiology, we evaluated electrocardiogram (ECG) recordings from anesthetized MLC2VCre(+):*Girk1*$^{fl/fl}$ and MLC2VCre(−):*Girk1*$^{fl/fl}$ mice, as well as wild-type and constitutive *Girk4*$^{-/-}$ mice. We measured HR (**Figure 3.5**) and HRV (**Figures 3.6** and **3.7**), as well as specific waveform parameters (PR, QT, and QTc intervals; **Supplementary Table 3.S1**), at baseline and following systemic administration of CCh (1.0 mg/kg I.P.). At baseline, HR was slightly higher in *Girk4*$^{-/-}$ mice relative to wild-type controls, but this difference did not reach the level of statistical significance (**Figure 3.5a–c**). Similarly, no significant difference in baseline HR was observed in MLC2VCre(+):*Girk1*$^{fl/fl}$ mice relative to MLC2VCre(−):*Girk1*$^{fl/fl}$ controls (**Figure 3.5d**). As expected, CCh decreased HR in wild-type mice, and this effect was significantly smaller in *Girk4*$^{-/-}$ mice (**Figure 3.5a–c**). In contrast, CCh-induced bradycardia was comparable in MLC2VCre(+):*Girk1*$^{fl/fl}$ and MLC2VCre(−):*Girk1*$^{fl/fl}$ mice (**Figure 3.5d**). Arrhythmic events, defined as instances of AV block or tachycardic episodes, were also quantified before and after CCh injection (**Supplementary Figure 3.S2**). While no arrhythmic events were observed at baseline for any genotype, wild-type mice exhibited more arrhythmic events than *Girk4*$^{-/-}$ mice after CCh injection. Both MLC2VCre(+):*Girk1*$^{fl/fl}$ mice and MLC2VCre(−):*Girk1*$^{fl/fl}$ mice exhibited a similar frequency of arrhythmic events after CCh injection.

We next evaluated HRV, examining the root mean square of successive differences (RMSSD) in R-R interval before and after CCh injection. While baseline RMSSD in *Girk4*$^{-/-}$ mice was slightly lower in comparison to wild-type mice, this difference did not reach the level of statistical significance (**Figure 3.6a–c**). Consistent with published data (Posokhova et al., 2013), the CCh-induced increased in RMSSD was significantly blunted in *Girk4*$^{-/-}$ mice relative to wild-type controls (**Figure 3.6c**). MLC2VCre(+):*Girk1*$^{fl/fl}$

and MLC2VCre(−):*Girk1*$^{fl/fl}$ mice displayed comparable RMSSD values, both prior to and after CCh injection (**Figure 3.6c**).

Frequency domain analysis can offer a more sensitive measure of the relative contributions of the sympathetic and parasympathetic branches of the ANS to HRV (Gehrmann et al., 2000). While power in the VLF range (<0.4 Hz) at baseline did not differ between wild-type and *Girk4*$^{-/-}$ mice, CCh increased VLF power in wild-type but not *Girk4*$^{-/-}$ mice (**Figure 3.7a**, left). In the LF range (0.4–1.5 Hz), *Girk4*$^{-/-}$ mice exhibited reduced power relative to wild-type controls at baseline and, in contrast to wild-type mice, a lack of increase induced by CCh (**Figure 3.7b**, left). In the HF range (1.5–5.0 Hz), we observed no difference between wild-type and *Girk4*$^{-/-}$ mice at baseline. Interestingly, CCh administration decreased power in this frequency range in wild-type mice, but not *Girk4*$^{-/-}$ mice (**Figure 3.7c**, left). No difference in power in VLF, LF, and HF domains was observed between MLC2VCre(+):*Girk1*$^{fl/fl}$ and MLC2VCre(−):*Girk1*$^{fl/fl}$ mice, either at baseline or after CCh administration (**Figure 3.7a–c**, right).

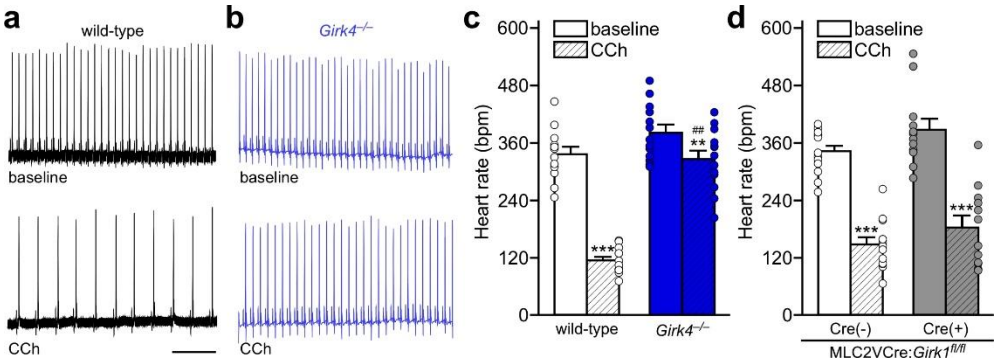

Figure 3.5. HR analysis of constitutive and ventricle-specific *Girk*$^{-/-}$ mice.
(**a**,**b**) Segments of ECG recordings from anesthetized wild-type (**a**) and *Girk4*$^{-/-}$ (**b**) mice, at baseline and after injection of CCh (1.0 mg/kg I.P.). Scale: 1 s. (**c**) Summary of HR data at baseline and after injection of CCh for wild-type (n = 12) and *Girk4*$^{-/-}$ (n = 13) mice. Two-way ANOVA analysis revealed an interaction between genotype and treatment ($F_{1,23} = 54.8$, $P < 0.001$). Symbols: **,***$P < 0.01$ and 0.001, respectively, vs. baseline (within genotype); $^{\#\#}P < 0.01$ vs. wild-type (within treatment). (**d**) Summary of HR data at baseline and after injection of CCh for MLC2VCre(+):*Girk1*$^{fl/fl}$ (n = 13) and MLC2VCre(−):*Girk1*$^{fl/fl}$ (n = 12) littermates. There was a significant main effect of treatment ($F_{1,23} = 173.1$, $P < 0.001$), but no main effect of genotype ($F_{1,23} = 3.6$, $P = 0.070$), or interaction between genotype and treatment ($F_{1,23} = 0.09$, $P = 0.77$). Symbols: ***$P < 0.001$ vs. baseline (within genotype).

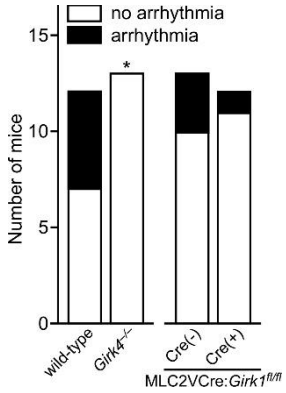

Supplementary Figure 3.S2. Impact of constitutive and ventricle-specific *Girk*$^{-/-}$ ablation on the frequency of arrhythmic events seen after CCh administration
Summary of arrhythmic events (instances of AV block or tachycardia) following systemic CCh administration (1.0 mg/kg I.P.) in wild-type and *Girk4*$^{-/-}$ mice, as well as MLC2VCre(-):*Girk1*$^{fl/fl}$ and MLC2VCre(+):*Girk1*$^{fl/fl}$ mice. Fisher's exact test revealed a significant difference (*P<0.05) in the frequency of arrhythmic events observed in wild-type and *Girk4*$^{-/-}$ mice, but no difference (P=0.59) in the frequency of arrhythmic events between MLC2VCre(-):*Girk1*$^{fl/fl}$ and MLC2VCre(+):*Girk1*$^{fl/fl}$ mice.

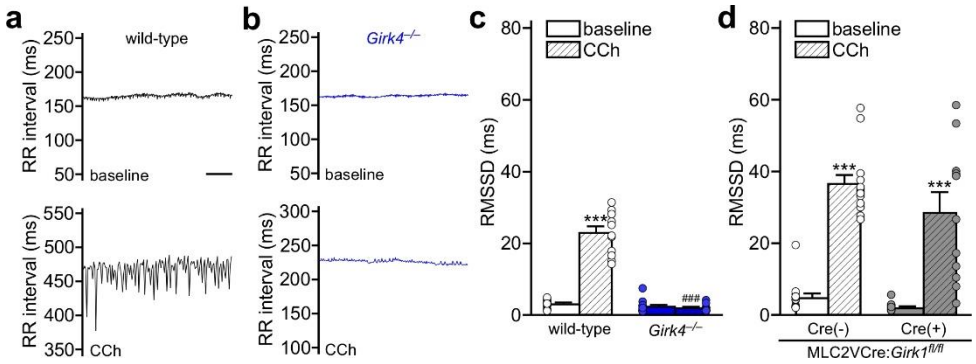

Figure 3.6. Time-domain HRV analysis of constitutive and ventricle-specific *Girk*$^{-/-}$ mice.

(**a**,**b**) RR tachograms for anesthetized wild-type (**a**) and *Girk4*$^{-/-}$ (**b**) mice, at baseline and following injection of CCh (1.0 mg/kg I.P.). Scale: 10 s. (**c**) Summary of RMSSD data at baseline and following injection of CCh for wild-type (n = 12) and *Girk4*$^{-/-}$ (n=13) mice. Two-way ANOVA analysis revealed an interaction between genotype and treatment ($F_{1,23} = 158.7$, $P < 0.001$). Symbols: ***$P < 0.001$ vs. baseline (within genotype); ###$P < 0.001$ vs. wild-type (within treatment). (**d**) Summary of RMSSD data at baseline and following injection of CCh for MLC2VCre(−):*Girk1*$^{fl/fl}$ (n = 13) and MLC2VCre(+):*Girk1*$^{fl/fl}$ (n = 12) mice. There was a significant main effect of treatment ($F_{1,23} = 96.3$, $P < 0.001$), but no main effect of genotype ($F_{1,23} = 3.2$, $P = 0.087$) or interaction between genotype and treatment ($F_{1,23} = 0.66$, $P = 0.43$). Symbols: ***$P < 0.001$ vs. baseline (within genotype).

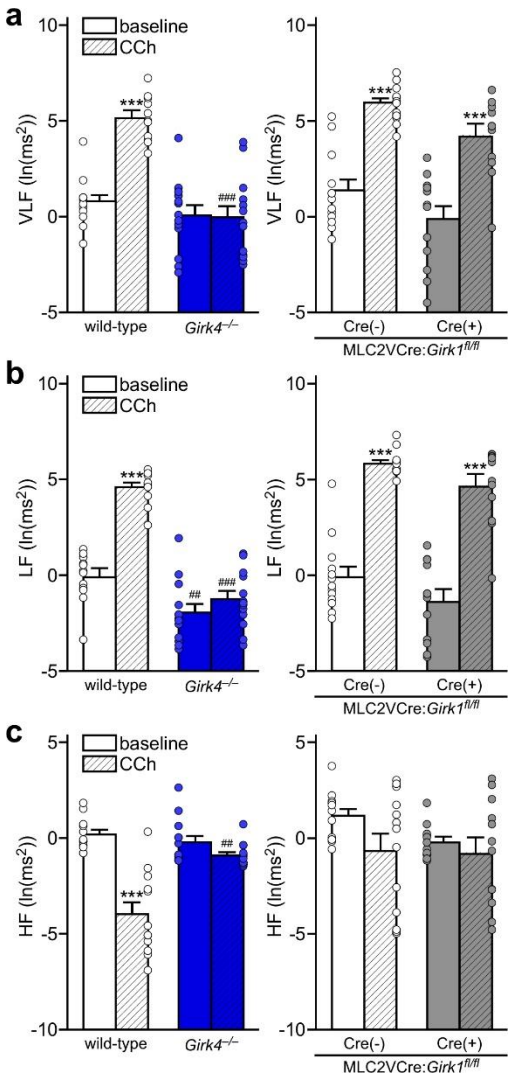

Figure 3.7. Frequency domain HRV analysis in constitutive and ventricle-specific *Girk*$^{-/-}$ mice.

(**a**) Power in the VLF (< 0.4 Hz) range at baseline and following injection of CCh (1.0 mg/kg I.P.). Two-way ANOVA analysis revealed an interaction between genotype and treatment ($F_{1,23} = 36.3$, $P < 0.001$) for wild-type (n = 12) and *Girk4*$^{-/-}$ (n = 13) mice (left panel). While main effects of treatment ($F_{1,23} = 51.0$, $P < 0.001$) and genotype ($F_{1,23} = 13.77$, $P < 0.01$) were observed for MLC2VCre(−):*Girk1*$^{fl/fl}$ (n = 13) and MLC2VCre(+):*Girk1*$^{fl/fl}$ (n = 12) mice (right panel), there was no interaction between genotype and treatment ($F_{1,23} = 0.01$, $P = 0.90$). Symbols: ***$P < 0.001$ vs. baseline (within genotype); $^{\#\#\#}P < 0.001$ vs. wild-type (within treatment). (**b**) Power in the LF (0.4–1.5 Hz) range at baseline and following injection of CCh (1.0 mg/kg i.p.). Two-way ANOVA analysis revealed an interaction between genotype and treatment ($F_{1,23} = 41.6$, $P < 0.001$) for wild-type and *Girk4*$^{-/-}$ mice (left panel). While main effects of treatment ($F_{1,23} = 113.1$, $P < 0.001$) and genotype ($F_{1,23} = 8.8$, $P < 0.01$) were observed for MLC2VCre(−):*Girk1*$^{fl/fl}$ and MLC2VCre(+):*Girk1*$^{fl/fl}$ mice (right panel), there was no interaction between genotype and treatment ($F_{1,23} = 0.02$, $P = 0.88$). Symbols: ***$P < 0.001$ vs. baseline (within genotype); $^{\#\#,\#\#\#}P < 0.01$ and 0.001, respectively, vs. wild-type (within treatment). (**c**) Power in the HF (1.5–5.0 Hz) range at baseline and following injection of CCh (1.0 mg/kg i.p.). Two-way ANOVA analysis

revealed an interaction between genotype and treatment ($F_{1,23} = 37.5$, $P < 0.001$) for wild-type and *Girk4*$^{-/-}$ mice (left panel). There were no main effects of treatment ($F_{1,23} = 2.7$, $P = 0.11$) or genotype ($F_{1,23} = 1.8$, $P = 0.19$) for MLC2VCre(−):*Girk1*$^{fl/fl}$ and MLC2VCre(+):*Girk1*$^{fl/fl}$ mice (right panel), nor was there an interaction between genotype and treatment ($F_{1,23} = 0.8$, $P = 0.38$). Symbols: ***$P < 0.001$ vs. baseline (within genotype). $^{\#\#}P < 0.01$ vs. wild-type (within treatment).

With respect to key parameters of the ECG waveform (**Supplementary Table 3.S1**), no significant genotype differences were observed for PR and QT intervals at baseline. CCh significantly prolonged both the PR and QT intervals in wild-type mice, and this effect was blunted in *Girk4*$^{-/-}$ mice. PR and QT intervals were also prolonged in MLC2VCre(+):*Girk1*$^{fl/fl}$ and MLC2VCre(−):*Girk1*$^{fl/fl}$ mice after CCh administration, but there was no difference between genotypes. We also evaluated the corrected QT (QTc) interval, a measure that can account for the influence of HR on the QT interval (Mitchell et al., 1998), using a variation of the human QT correction formula that assumes a typical RR interval for a conscious mouse under normal conditions (100 ms). We observed no difference in QTc interval between wild-type and *Girk4*$^{-/-}$ mice, or MLC2VCre(+):*Girk1*$^{fl/fl}$ or MLC2VCre(−):*Girk1*$^{fl/fl}$ mice, at baseline. Interestingly, while CCh administration had no effect on QTc interval in wild-type mice, it lengthened this interval in *Girk4*$^{-/-}$ mice. QTc interval was not prolonged after CCh injection, however, in either MLC2VCre(+):*Girk1*$^{fl/fl}$ or MLC2VCre(−):*Girk1*$^{fl/fl}$ mice.

Genotype	Baseline			CCh		
	PR (ms)	QT (ms)	QTc (ms)	PR (ms)	QT (ms)	QTc (ms)
wild-type	47.9±3.4	59.1±2.2	45.6±1.4	67.2±5.3[a]	99.5±4.8[a]	45.2±3.4
Girk4$^{-/-}$	48.1±1.2	63.0±2.0	49.8±0.9	56.2±1.3[a,b]	80.8±3.6[a,c]	57.2±1.0[a,d]
MLC2VCre(-)	46.8±1.0	65.8±2.2	49.3±1.9	58.1±2.4[a]	100.3±5.4[a]	50.5±2.3
MLC2VCre(+)	47.2±1.1	63.0±2.9	49.0±1.6	55.3±1.4[a]	113.2±11.5[a]	53.3±3.3

Supplementary Table 3.S1. ECG waveform analysis for constitutive and ventricle-specific *Girk*$^{-/-}$ mice

Summary of PR, QT, and QTc intervals before and after CCh injection (1.0 mg/kg). Group sizes ranged from 5-11 mice per genotype. Two-way ANOVA analysis revealed an interaction between genotype and treatment ($F_{1,19}$=28.8, P<0.001) for PR interval in wild-type and *Girk4*$^{-/-}$ mice. There was a main effect of treatment ($F_{1,22}$=74.5, P<0.001) mice, but no main effect of genotype ($F_{1,22}$=0.6, P=0.50) or interaction between genotype and treatment ($F_{1,22}$=2.5, P=0.10) for the PR interval in MLC2VCre(+):*Girk1*$^{fl/fl}$ and MLC2VCre(-):*Girk1*$^{fl/fl}$ mice. Two-way ANOVA analysis revealed an interaction between genotype and treatment ($F_{1,14}$=20.4, P<0.001) for QT interval in wild-type and *Girk4*$^{-/-}$ mice. There was a main effect of treatment ($F_{1,11}$=66.9, P<0.001), but no main effect of genotype ($F_{1,11}$=0.5, P=0.50) or interaction between genotype and treatment ($F_{1,11}$=2.3, P=0.20) for the QT interval in MLC2VCre(+):*Girk1*$^{fl/fl}$ and MLC2VCre(-):*Girk1*$^{fl/fl}$ mice. Two-way ANOVA analysis revealed an interaction between genotype and treatment ($F_{1,14}$=14.6, P<0.01) for QTc interval in wild-type and *Girk4*$^{-/-}$ mice. No main effect of treatment ($F_{1,11}$=3.4, P=0.091) or genotype ($F_{1,11}$=0.2, P=0.69), or interaction between genotype and treatment ($F_{1,11}$=1.2, P=0.30), was found for QTc interval for MLC2VCre(+):*Girk1*$^{fl/fl}$ and MLC2VCre(-):*Girk1*$^{fl/fl}$ mice. Symbols: [a]P<0.001 vs. baseline (within parameter); [b,c,d]P<0.05, 0.01, and 0.001, respectively, vs. wild-type (CCh).

3.3.7. Impact of ventricle-specific GIRK channel ablation on pacing-induced ventricular arrhythmia

To investigate the contribution of the ventricular GIRK channel to ventricular arrhythmogenesis, isolated hearts from MLC2VCre(+):*Girk1*$^{fl/fl}$ and MLC2VCre(−):*Girk1*$^{fl/fl}$ mice, as well as wild-type and constitutive *Girk4*$^{-/-}$ mice, were subjected to burst pacing in the absence and presence of CCh to discern differences in susceptibility to VT or VF (**Figure 3.8a**). There was no significant difference in the incidence of pacing-induced VT/VF at baseline between wild-type and *Girk4*$^{-/-}$ hearts (**Figure 3.8b**, left). Similarly, hearts from MLC2VCre(+):*Girk1*$^{fl/fl}$ and MLC2VCre(−):*Girk1*$^{fl/fl}$ mice did not differ in the incidence of VT/VF in response to pacing stimuli at baseline. After CCh perfusion, there was, again, no significant difference in incidence of pacing-induce VT/VF between wild-type and *Girk4*$^{-/-}$ hearts (**Figure 3.8b**, right). Likewise, no difference was observed in the incidence of pacing-induced VT/VF between MLC2VCre(+):*Girk1*$^{fl/fl}$ and MLC2VCre(−):*Girk1*$^{fl/fl}$ hearts. Collectively, these observations suggest that loss of the ventricular GIRK channel does not impact susceptibility to pacing-induced ventricular arrhythmias.

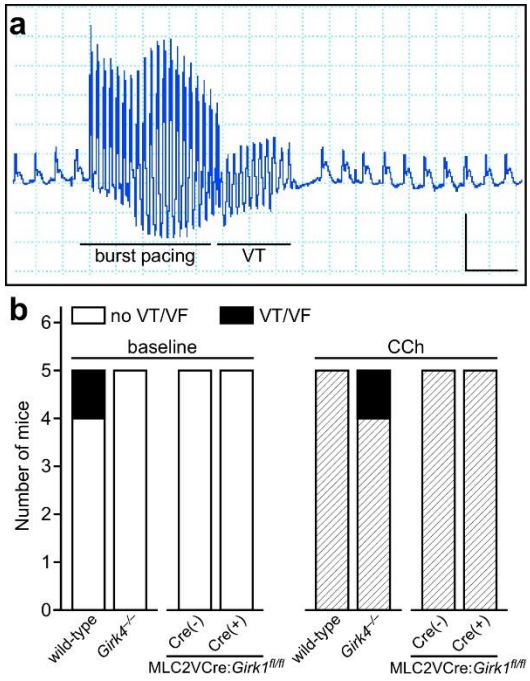

Figure 3.8. Susceptibility to pacing-induced ventricular arrhythmias in constitutive and ventricle-specific *Girk*$^{-/-}$ mice.
(**a**) Recording of a VT episode after infusion of CCh (3 μM) and burst pacing of the left ventricle. Scale: 0.5 V/0.2 s. (**b**) Summary of the number of mice exhibiting VT/VF episodes after burst pacing of the left ventricle at baseline (left) and after CCh perfusion (right). Fisher's exact test revealed no differences in the occurrence of VT/VF episodes between wild-type and *Girk4*$^{-/-}$ mice, either at baseline (P = 1.0) or after CCh administration (P = 1.0). We did not observe any incidents of VT/VF in MLC2VCre(−):*Girk1*$^{fl/fl}$ or MLC2VCre(+):*Girk1*$^{fl/fl}$ mice, either at baseline or after CCh administration.

3.4 Discussion

In this study, we present evidence that that GIRK channel found in adult mouse ventricular myocytes is, like the channel described previously in atrial myocytes and SAN cells, a GIRK1/GIRK4 heteromultimeric channel. Nevertheless, the GIRK current in ventricular myocytes exhibited several properties that differed from the GIRK current described previously in atrial myocytes and SAN cells (Posokhova et al., 2010; Wydeven et al., 2014b). Notably, the ventricular GIRK current was smaller and less sensitive to CCh. The differences in GIRK conductance between atrial and ventricular myocytes could be due to increased expression and/or influence of a negative regulator of GIRK-dependent signaling in ventricle. Our data suggest that increased ventricular expression or influence of RGS6, however, does not explain the functional differences between the mouse atrial and ventricular GIRK conductance. Indeed, RGS6 mRNA levels were substantially lower in ventricle than in atria. Moreover, *Rgs6* ablation did not enhance the CCh sensitivity or alter the kinetics of the ventricular GIRK current. It is possible that other RGS proteins account for the differences observed between in atrial and ventricular GIRK-dependent signaling in the mouse heart. Alternatively, elements of the GIRK-dependent signaling pathway may be compartmentalized in distinct fashion in the atria and ventricle, or additional positive and/or negative regulatory elements that impact I_{KACh}-dependent signaling remain to be discovered.

A recent study reported that the ACh-induced shortening of ventricular APD_{90} was diminished in isolated hearts from *Girk4*$^{-/-}$ mice, suggesting that a GIRK4-containing GIRK channel facilitates ventricular repolarization in the mouse heart (Liang et al., 2014). Consistent with this premise, we observed a significant impact of *Girk4* ablation on the CCh-induced shortening of APD_{90} in isolated ventricular myocytes from adult mice. Our efforts in isolated ventricular myocytes also revealed that *Girk4* ablation attenuates the

CCh-induced decrease in ventricular myocyte excitability. These results support our contention that the GIRK channel in ventricular myocytes contributes to the cholinergic regulation of ventricular myocyte APD and excitability.

I_{KACh} is a critical downstream mediator of parasympathetic effects on atrial physiology and HR regulation. Previous studies with ECG telemetry and isolated mouse hearts have shown that a loss of I_{KACh} correlates with altered baseline measures and diminished responses to pharmacologic manipulations that enhance or mimic parasympathetic input to the heart (Bettahi et al., 2002; Mesirca et al., 2013; Posokhova et al., 2013; Wickman et al., 1998). Here, we replicated several reported observations in *Girk4*$^{-/-}$ mice, including the attenuation of CCh-induced bradycardia. While we did not see a significant baseline tachycardia in *Girk4*$^{-/-}$ mice in this study, this may reflect an influence of anesthesia. We additionally observed evidence of diminished HRV at baseline (LF), and after CCh administration (RMSSD, VLF, and LF), in *Girk4*$^{-/-}$ mice. Our parallel evaluation of mice lacking GIRK channels selectively in ventricle indicate that most, if not all, of the cardiac phenotypes reported in constitutive *Girk1*$^{-/-}$ or *Girk4*$^{-/-}$ mice are attributable to a loss of atrial I_{KACh}. Surprisingly, we found that CCh decreased power in the HF domain in wild-type mice, but not in *Girk4*$^{-/-}$ mice. As fluctuations in HR due to respiration contribute to power in the HF range (Tsai et al., 2012), our observation could reflect a contribution of a GIRK4-containing GIRK channel to the cholinergic regulation of respiration. The CCh-induced decrease in HF power was not significant in MLC2VCre(−):*Girk1*$^{fl/fl}$ mice, however, suggesting that this parameter may not be a reliable indicator of the GIRK channel contribution to HRV in this frequency range.

Despite the fact that GIRK channels contribute to the inhibitory influence of CCh on ventricular myocytes, we did not see an obvious impact of ventricular GIRK channel ablation on QT or QTc intervals, at baseline or following CCh injection. It should be noted that previous attempts to model Long QT syndrome in mice have not reliably yielded mice

with prolonged QT intervals (Salama and London, 2007). For example, mice lacking KvLQT1, the gene associated with LQT1 in large mammals, do not consistently display prolonged QT intervals (Salama and London, 2007). We also cannot exclude the possibility that the influence of ventricular GIRK channel becomes more relevant in pathological conditions such as myocardial infarction or sympathetic stress. We did see a surprising prolongation of the QTc interval after CCh administration in *Girk4*$^{-/-}$ mice that was not seen in wild-type controls. While this observation may reflect a failure of the QT correction to adequately compensate for the impact of HR on QT interval or a limitation of this approach in mice under anesthesia (Boukens et al., 2014; Roussel et al., 2016), the finding is also consistent with the possibility that CCh modulates another effector that exerts an opposing influence from the GIRK channel on the QT interval. Importantly, since MLC2VCre(+):*Girk1*$^{fl/fl}$ and MLC2VCre(−):*Girk1*$^{fl/fl}$ mice exhibited similar QT and QTc intervals at baseline and after CCh administration, the selective prolongation of QTc interval in *Girk4*$^{-/-}$ mice presumably reflects an influence of GIRK channels outside of the ventricle.

I_{KACh}-dependent signaling has been linked to a variety of atrial rhythm disorders (Li et al., 2016; Mesirca et al., 2014, 2016a). Both genetic ablation of *Girk4* and pharmacological inhibition of GIRK channels can restore normal cardiac rhythm in multiple genetic models of supraventricular arrhythmia (Mesirca et al., 2014, 2016a). For example, genetic ablation of *Girk4* in mouse models of sick sinus syndrome and AV block reduces the number of ACh-induced arrhythmic episodes in these mice (Mesirca et al., 2016a). Additionally, fewer arrhythmic events were observed in *Girk4*$^{-/-}$ mice treated with CCh as compared to wild-type controls (this study), and *Girk4*$^{-/-}$ mice were resistant to pacing-induced AF (Kovoor et al., 2001). Studies in human AF patients further implicate I_{KACh} in supraventricular arrhythmogenesis. Atrial myocytes from human AF patients displayed both a significant reduction in I_{KACh} expression and an attenuation of CCh-induced

shortening of atrial APD (Dobrev et al., 2001). CCh-induced I_{KACh} currents were also smaller in atrial myocytes from AF patients, whereas constitutive GIRK channel activity was elevated (Dobrev et al., 2001, 2002, 2005). Remodeling involving I_{KACh} has also been observed in a “tachy-paced” dog model, where atrial tachycardia increased basal I_{KACh} channel activity (Voigt et al., 2007); this adaptation correlated with a decrease in ERP and an increase in AF duration. Collectively, these studies highlight the therapeutic potential associated with blocking or suppressing atrial I_{KACh} in multiple distinct atrial arrhythmias.

I_{KACh} antagonists have been proposed for use in the treatment of AF and other supraventricular rhythm disorders (Bhave et al., 2010; Li et al., 2009a, 2016; Mesirca et al., 2016a; Tanaka and Hashimoto, 2007). Recently, a novel family of direct-acting, small molecule activators and inhibitors of GIRK channels has been identified, members of which act selectively on GIRK1-containing GIRK channels such as I_{KACh} (Kaufmann et al., 2013; Ramos-Hunter et al., 2013; Wen et al., 2013). While a direct-acting I_{KACh} antagonist could prove useful in the treatment of atrial rhythm disorders, suppressing GIRK channel activity in the ventricle could pose a significant risk. We did not, however, observe a difference in susceptibility to pacing-induced ventricular arrhythmias in either the constitutive or ventricle-specific GIRK channel ablation models, arguing that a loss of ventricular GIRK channel does not predispose to ventricular arrhythmias. However, given the noted differences in the ionic currents underlying ventricular repolarization in mice and humans (Boukens et al., 2014), further studies are needed to determine whether inhibition of the human ventricular GIRK channel is also without effect. Nonetheless, our data support the contention that targeting I_{KACh} for atrial arrhythmias, via with selective inhibitors or genetic approaches, may constitute a safe alternative to existing anti-arrhythmic therapies that predispose patients to fatal ventricular disorders (Li et al., 2009a).

Chapter 4

Characterization of VU0468554, a selective inhibitor of cardiac GIRK channels

4.1 Introduction

GIRK channels are critical mediators of cell excitability (Lüscher and Slesinger, 2010). GIRK channels are activated by the Gβγ subunit of inhibitory G proteins ($G_{i/o}$) released upon GPCR activation (Huang et al., 1997; Krapivinsky et al., 1995b; Wickman et al., 1994). Gβγ binding to GIRK channels increases GIRK channel gating resulting in cell hyperpolarization. GIRK channels are highly expressed in cardiac and neuronal tissue and play central roles in the regulation of HR and neurotransmission (Lee et al., 2018; Luján et al., 2014; Wickman et al., 1998).

Cardiac GIRK channels are heterotetrameric complexes made up of GIRK1 and GIRK4 subunits in 1:1 stoichiometry (Corey et al., 1998; Corey and Clapham, 1998; Krapivinsky et al., 1995a). GIRK channels are expressed in atrial and nodal tissue, where they mediate much of the effect of parasympathetic signaling to the heart (Bettahi et al., 2002; Lee et al., 2018; Mesirca et al., 2013; Wickman et al., 1998). Muscarinic (M_2R) receptor activation of GIRK channels in sinoatrial nodal (SAN) cells results in slowing of the firing rate, resulting in bradycardia (Lee et al., 2018 (**Chapter 2**); Mesirca et al., 2013). Studies utilizing both global and atrial/SAN specific ablation of GIRK channels demonstrate that GIRK channels mediate a significant portion of the effects of vagal input on mouse HR and HRV (Lee et al., 2018 (**Chapter 2**); Wickman et al., 1998). Cardiac

GIRK channel activation also results in a pronounced shortening of APD and ERP and hyperpolarizes atrial myocytes (Wang et al., 2013b). GIRK channels are also expressed at relatively low levels in ventricular tissue (Anderson et al., 2018 (**Chapter 3**); Dobrzynski et al., 2001, 2002; Yang et al., 2010b), and there is evidence that they mediate, in part, M_2R and A_1R shortening of APD and ERP (Anderson et al., 2018 (**Chapter 3**); Liang et al., 2014).

Increased GIRK channel activity in cardiac tissue has been implicated in the pathophysiology of nodal and atrial rhythm disorders. A mutation in GNB2, the gene encoding Gβ2, results in exaggerated GIRK-dependent signaling and has been identified in human patients with familial sinus node dysfunction (Long et al., 2020; Stallmeyer et al., 2017). Furthermore, increased GIRK channel activity has been linked to human patients with chronic AF (Dobrev et al., 2005; Voigt et al., 2007). Indeed, a study using a combination of optical mapping and immunoblotting revealed that regions of the human atria associated with Ado-induced AF initiation and maintenance, otherwise known as re-entry drivers, were localized to areas with co-expression of GIRK4 and A_1R in the human atria (Li et al., 2016). Similar observations were reported in the mouse, where genetic ablation of a negative regulator of GIRK-dependent signaling, RGS6, leads to an increase in susceptibility in pacing-induced AF (Posokhova et al., 2013).

Both pharmacological inhibition and genetic ablation of GIRK channels have been shown to rescue and/or terminate certain supraventricular arrhythmias in relevant mammalian models. Pharmacological inhibition of GIRK channels by TTQ, terminates both pharmacologically and vagally induced AF in canines (Hashimoto et al., 2006). Conversely, mice lacking cardiac GIRK channels are resistant to both pacing-induced AF and arrhythmias induced by VNS (Kovoor et al., 2001; Lee et al., 2018 (**Chapter 2**)). Additionally, genetic ablation of *Girk4* rescues symptoms of sick sinus syndrome and AV block in mouse models of nodal dysfunction (Mesirca et al., 2014, 2016a). Intriguingly,

while loss K^+ channel activity is normally associated with an increase in ventricular arrhythmia susceptibility (Ramalho and Freitas, 2018; Vandenberg et al., 2012), ablation of GIRK channels in ventricular tissue does not appear to increase the susceptibility to ventricular arrhythmia (Anderson et al., 2018 (**Chapter 2**)). Collectively, these studies highlight the potential of targeting cardiac GIRK channels as a safe therapeutic intervention for relevant rhythm disorders

Currently, subunit-specific pharmacological tools for studying the physiology of GIRK channels are lacking and this has impeded efforts to assess the therapeutic potential of targeting specific GIRK channel subtypes. However, a group of novel small-molecule modulators selective for GIRK1-containing GIRK channels has been identified (Wen et al., 2013) . This group includes the compounds ML297 and VU0810464, activators that display selectivity for GIRK1/GIRK2 channels, the predominant subtype in neurons, over GIRK1/GIRK4 channels (Vo et al., 2019; Wydeven et al., 2014a). Here, we describe and evaluate a novel GIRK1/GIRK4-selective inhibitor, VU0468554, identified from high-throughput screening of small molecule modulators with a similar chemical scaffold as ML297. Our work here in native cell types and the isolated heart suggests that VU0468554 is a promising GIRK1/GIRK4-selective inhibitor that could serve as a template for the development of new therapeutics for cardiac arrhythmias.

4.2 Materials and Methods

Animals. Animal experiments were approved by the Institutional Animal Care and Use Committee at the University of Minnesota. Both inbred and purchased (Jackson Laboratory, Bar Harbor, ME) male and female C57BL/6J mice were used for whole-cell electrophysiology and isolated heart studies. Generation of *Girk1*$^{-/-}$, *Girk2*$^{-/-}$, and *Girk4*$^{-/-}$ mice was described previously (Bettahi et al., 2002; Signorini et al., 1997; Wickman et al., 1998).

SAN cell culture. SAN cells were isolated from adult (8–12 wk) mice as described (Anderson et al., 2018 (**Chapter 3**)). Briefly, mice were anaesthetized with ketamine (100 mg/kg I.P.) and xylazine (10 mg/kg I.P.), and hearts were excised into Tyrode's solution. SAN-containing tissue was excised into a modified Tyrode's solution containing (in mM) 140 NaCl, 5.4 KCl, 1.2 KH_2PO_4, 0.2 $CaCl_2$, 50 taurine, 18.5 glucose, 5 HEPES, and 0.1% BSA (pH 6.9), with elastase (0.3 mg/mL, Worthington Biochemical Corp., Lakewood, NJ) and collagenase II (0.21 mg/mL). After digestion for 30 min at 37 °C, SAN tissue was triturated in wash solution and plated onto laminin-coated coverslips. After plating, SAN cells were used within 8 h.

Cultured hippocampal neurons. Primary cultures of hippocampal neurons were prepared as described (Vo et al., 2019). Briefly, extracted hippocampi from neonatal (P0–4 pups were placed into an ice-cold modified HBSS (Thermo Fisher), 10 mM HEPES-NaOH pH 7.3 (Thermo Fisher), 0.02% (w/v) Pluronic F-127, and 1.5 μM Thallos-AM (TEFlabs, Austin, TX). The tissue was digested for 20 min with papain and DNAse I at 37 °C with occasional inversion. Hippocampi were mechanically dissociated in growth medium containing Neural-basal A medium, 2% B27 supplement, 0.5 mM Glutamax, and antibiotic/antimycotic (Thermo Fisher Scientific) using trituration in 1 mL pipettes. Neurons were pelleted via centrifugation and plated onto 8 mm glass coverslips precoated with

poly-l-lysine in 48-well plates. Neurons were maintained in culture in a humidified 5% CO_2 incubator at 37 °C, and half of the medium was replaced with fresh growth medium every 3–4 d. Neurons were kept in culture for 10–14 d before experimentation.

Electrophysiology. Coverslips containing hippocampal neurons or SAN cells were transferred to a chamber containing a low-K^+ bath solution consisting of (in mM) 130 NaCl, 5.4 KCl, 1 $CaCl_2$, 1 $MgCl_2$, 5.5 D-glucose, and 5 HEPES/NaOH (pH 7.4). Pyramidal-shaped neurons with capacitance values between 80 and 200 pF were targeted for hippocampal recordings. SAN cells were identified as thin, striated cells with capacitance values 15-40 pF. Fire-polished borosilicate patch pipettes were filled with K-gluconate pipette solution containing (in mM) 140 K-gluconate, 2 $MgCl_2$, 1.1 EGTA, 5 HEPES, 2 Na_2-ATP, 0.3 Na-GTP, and 5 Na-phosphocreatine (pH 7.2). Cells were held in voltage-clamp mode at −70 mV once whole-cell access was achieved. The liquid-junction potential was predicted to be −17 mV using JPCalc software (Molecular Devices, LLC, Sunnyvale, CA), and was not corrected for. GIRK-dependent currents were measured in a high-K^+ bath solution containing (in mM) 120 NaCl, 25 KCl, 1 $CaCl_2$, 1 $MgCl_2$, 5.5 D-glucose, and 5 HEPES/NaOH (pH 7.4). VU0468554 and ML297 were dissolved in first in DMSO and then diluted into the high-K^+ bath solution. Baclofen and CCh were diluted in the high-K^+ bath solution. Compounds were applied directly to the recorded cell using a ValveLink 8.2 rapid perfusion system (AutoMate Scientific, Inc.; Berkeley, CA). For hippocampal recordings, whole-cell currents were measured with hardware (Axopatch-200B amplifier, Digidata 1322A) and software (pCLAMP v. 8.2) from Molecular Devices. Recordings for SAN cells experiments were obtained with hardware (Axopatch-700B amplifier, Digidata 1440A) and software (pCLAMP v. 10.4) from Molecular Devices. Only experiments in which the access resistances were stable and low (<20 MΩ) were included in the analysis.

Isolated Heart. Hearts were excised and placed into ice-cold, oxygenated Tyrode's solution and the aorta was quickly cannulated. Cannulated hearts were then placed into a warm (37±1 ºC) Tyrode's bath, and iWorx (Dover, NH) platinum recording electrodes were placed near/on the surface of the heart. Oxygenated Tyrode's solution was then perfused at 2-3 mL/min and a baseline HR was recorded for 10 min. After the baseline HR was acquired, 1 μM CCh was perfused and allowed to stabilize for 15 min. While CCh was still being perfused, a bolus injection of either vehicle (1:100 DMSO) or VU0468554 (10 μM) was injected through a port in the Langendorf apparatus. The ECG signal was acquired with LabScribe v.3 software (iWorx; Dover, NH), and filtered as appropriate. The derivative of that channel was computed to account for movements in baseline and to amplify the signal for subsequent analysis. A 15-s segment from each time point (baseline, CCH, 5 min post, 10 min post) was then exported to Kubios HRV v.2 (Tarvainen et al., 2014) for HR analysis, utilizing artifact correction as appropriate.

Statistical analysis. All data were analyzed using Prism v.8.2.1 software (GraphPad Software; San Diego, CA) and are presented as mean ± SEM. The level of statistical significance was set at $p < 0.05$. Specific statistical analyses are denoted within the figure legends.

4.3 Results

4.3.1 Identification and characterization of VU0468554, a selective inhibitor of GIRK1/4 channels

VU0468554 was discovered through structure-activity relationship (SAR) investigations using the GIRK1-selective agonist ML297 as a chemical scaffold to identify novel GIRK channel activators and inhibitors (Wen et al., 2013) (**Figure 4.1**). Novel activators and inhibitors were assessed using a thallium(Tl^+)-flux based assay, which involves loading cells with Tl^+-sensitive dye to exploit the ability of Tl^+ to pass through K^+ channels, resulting in a fluorescent readout of channel activity (David Weaver, 2018). Inhibition was normalized to the inhibition displayed by SCH23390, a D1 receptor antagonist which also displays off-target GIRK channel inhibition (Terry and Katz, 1994; Wen et al., 2013). In this assay, VU0468554 exhibited 93% inhibition in GIRK1/2-expressing HEK cells and 67% inhibition in GIRK1/4-expressing HEK cells (Wen et al., 2013). VU0468554 also displayed a promising selectivity profile, exhibiting more potent inhibition in GIRK1/4 expressing HEK cells (IC_{50}: 0.85 μM) in comparison to GIRK1/2 expressing HEK cells (IC_{50}: 2.6 μM) (Wen et al., 2013).

4.3.2 VU0468554 preferentially inhibits cardiac GIRK channels

The GIRK1/4 selectivity profile of VU0468554 displayed in HEK cells prompted further investigation of the impact of VU0468554 on GIRK-dependent signaling in native cell types. Using mouse SAN cells, which express the GIRK1/4 channel subtype (Krapivinsky et al., 1995a), we measured the ability of VU0468554 to reverse GIRK-dependent currents elicited by muscarinic receptor activation. A saturating concentration of the CCh (10 μM) elicited large, inward currents in SAN cells from wild-type mice (**Figure 4.2A**). These currents are absent in SAN cells from *Girk4*$^{-/-}$ mice, indicating that the

response is GIRK-dependent (**Figure 4.2A**). VU0468554 reversed CCh-induced GIRK currents in SAN cells in a dose-dependent manner, inhibiting approximately 73% of the CCh-induced response at the highest dose tested (10 μM; **Figure 4.2A,C,D**).

In addition to modulating cardiomyocyte excitability, GIRK channels are expressed widely in the nervous system and are major contributors to inhibitory signaling in neurons (Luján and Aguado, 2015; Mayfield et al., 2015). Therefore, we next explored the ability of VU0468554 to reverse GIRK-dependent responses in cultured hippocampal (HPC) neurons, which express the GIRK1/2 channel subtype (Wydeven et al., 2012, 2014a). Selective activation of $GABA_B$ receptors with baclofen (100 μM) elicited robust currents in hippocampal neurons from C57BL/6J mice that were not present in neurons from *Girk2*$^{-/-}$ mice, indicating that the baclofen-induced response under these assay conditions is completely GIRK-dependent (**Figure 4.2B**). VU0468554 dose-dependently inhibited baclofen-induced currents in HPC neurons with a comparable potency as seen in SAN cells (**Figure 4.2D,E**). However, at a maximal concentration, VU0468554 inhibited only about 20% of baclofen-induced currents, which is significantly smaller than the % inhibition of GIRK currents in SAN cells (**Figure 4.2C**). Therefore, VU0468554 displays a significantly more efficacious block of cardiac GIRK channels over neuronal GIRK channels.

We next assessed whether the actions of VU0468554 in SAN cells were GIRK1-dependent as well. Application of VU0468554 (10 μM) resulted in a small reversible increase in the holding current (**Figure 4.3A,B**), likely due to antagonism of constitutive GIRK channel activity. Indeed, this change in holding current was entirely absent in SAN cells from *Girk1*$^{-/-}$ mice (**Figure 4.3F,G**). Thus, the effects of VU0468554 are sensitive for GIRK1-containing channels.

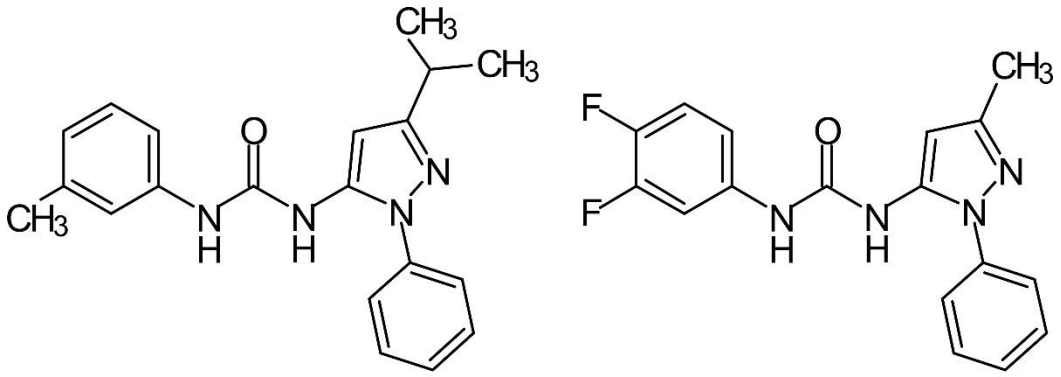

Figure 4.1. Chemical structure of VU0468554 and ML297
Structure of VU0468554 (left) which was discovered from SAR investigations using ML297(right) as a chemical scaffold for chemical optimization (Wen et al., 2013).

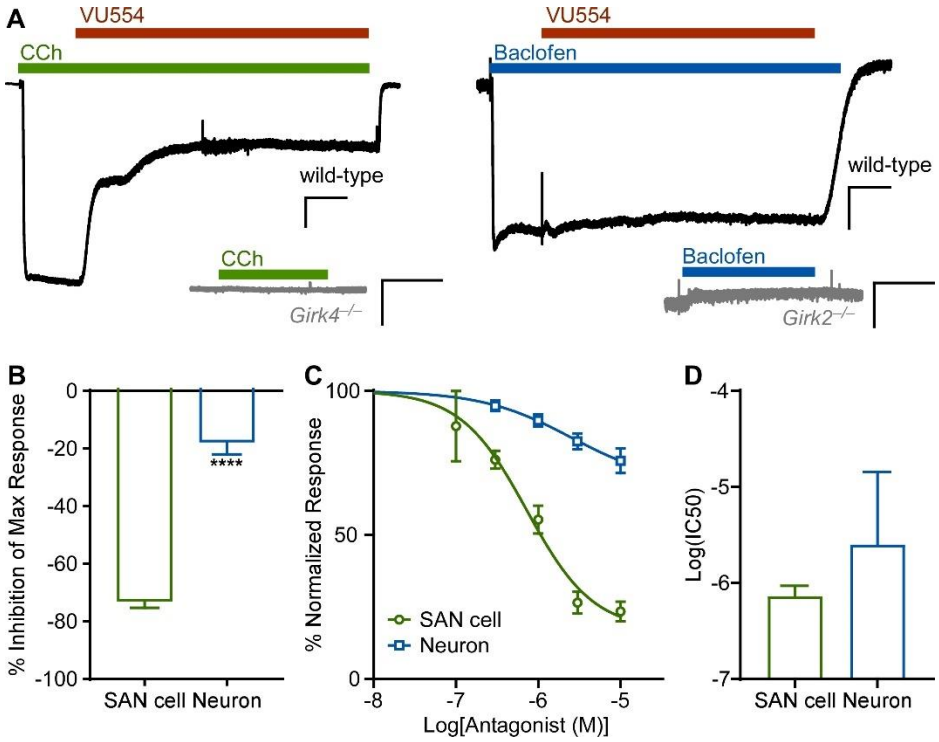

Figure 4.2. VU0468554 preferentially blocks cardiac GIRK channels over neuronal GIRK channels

(**A**)Representative whole-cell CCh-induced currents (V_{hold}= -70 mV) (left) and baclofen-induced currents (right) reversed by perfusion of a maximal concentration of VU0468554 (10 μM) in either SAN cells (left) or HPC neurons (right) from wildtype mice (top) or *Girk*$^{-/-}$ mice (bottom). Scale bars: 10 s/500 pA. (**B**) Summary of the % inhibition of maximal currents evoked by either CCh (SAN cells) or baclofen (HPC neurons). Statistical analysis revealed a significant difference (t_{15}=11.8; ****P<0.0001; unpaired t-test) in the % inhibition between responses in wild-type SAN cells (n=9 cells/4 mice) and wild-type HPC neurons (n=8 cells). (**C**) Summary of concentration-dependent inhibition of CCh-induced in SAN cells (n=10 cells/4 mice) and baclofen-induced currents in cultured HPC neurons from wild-type mice (n=7 cells). (**D**) Summary of the Log(IC_{50}) of VU0468554 from concentration-dependent inhibition of CCh-induced in SAN cells. Statistical analysis revealed no significant difference (t_{15}=0.8; P=0.41; unpaired t-test) in the Log(IC_{50}) of VU0468554 on CCh- and Baclofen- induced currents in wild-type SAN cells (n=10 cells /4 mice) and wildtype HPC neurons (n=7 cells).

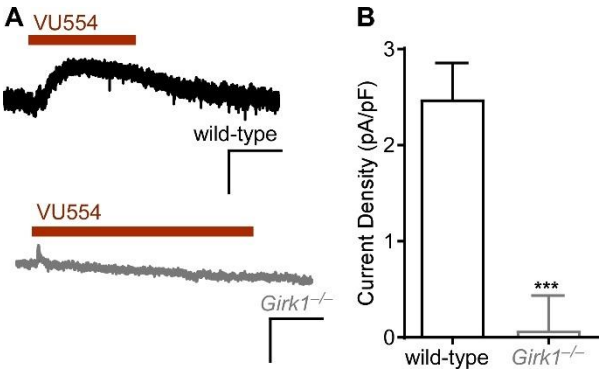

Figure 4.3. VU0468554 is sensitive for GIRK1-containing channels
(**A**)Representative currents evoked by VU0468554 (10 μM) SAN cells from wild-type (top) and *Girk1*$^{-/-}$ (bottom) mice. Scale bars: 5 s/100 pA. (**B**)Summary of the current density of responses evoked by VU0468554 (10 mM) in wild-type and *Girk1*$^{-/-}$ SAN cells. Statistical analysis revealed a significant difference (t_{21}=4.4; ***P<0.0001; unpaired t-test) in the % inhibition between responses in wild-type SAN cells (n=9 cells /3 mice) and *Girk1*$^{-/-}$ SAN cells (n=14 cells /4 mice).

4.3.3 VU0468554 exhibits un-competitive inhibition of Gβγ-dependent GIRK channel activity

Next, we investigated the mechanism of inhibition exhibited by VU0468554. We performed CCh concentration-response experiments in the presence or absence of a maximally effective dose of VU0468554 (10 μM) and examined both efficacy and potency of CCh (**Figure 4.4A-C**). Addition of VU0468554 decreased the maximal response induced by CCh, and this effect was not overcome by higher concentrations of CCh (**Figure 4.4B**), suggesting that VU0468554 inhibits GPCR-induced GIRK channel activity in a non-competitive manner. We also observed a slight decrease in potency, as evidence by increase in EC_{50} of CCh-induced responses (**Figure 4.4C**). This finding is consistent with an "un-competitive" mechanism of inhibition, where the inhibition of VU0468554 relies upon formation of a GIRK channel:Gβγ complex.

ML297 is a GIRK1-dependent agonist that activates GIRK channels independent of Gβγ (Wydeven et al., 2014a), presumably via direct binding. Therefore, we next examined if VU0468554 inhibits ML297-induced, receptor-independent activation of cardiac GIRK channels. We measured measuring ML297 concentration-response experiments in the presence or absence of 10 μM VU0468554 (**Figure 4.4D**). A significant decrease in the efficacy of ML297 in the presence of VU0468554 was observed (**Figure 4.4F**), suggesting that VU0468554 inhibition of ML297 is likely non-competitive. Addition of VU0468554 did decrease the potency of ML297, however, this effect was not significant (**Figure 4.4E**).

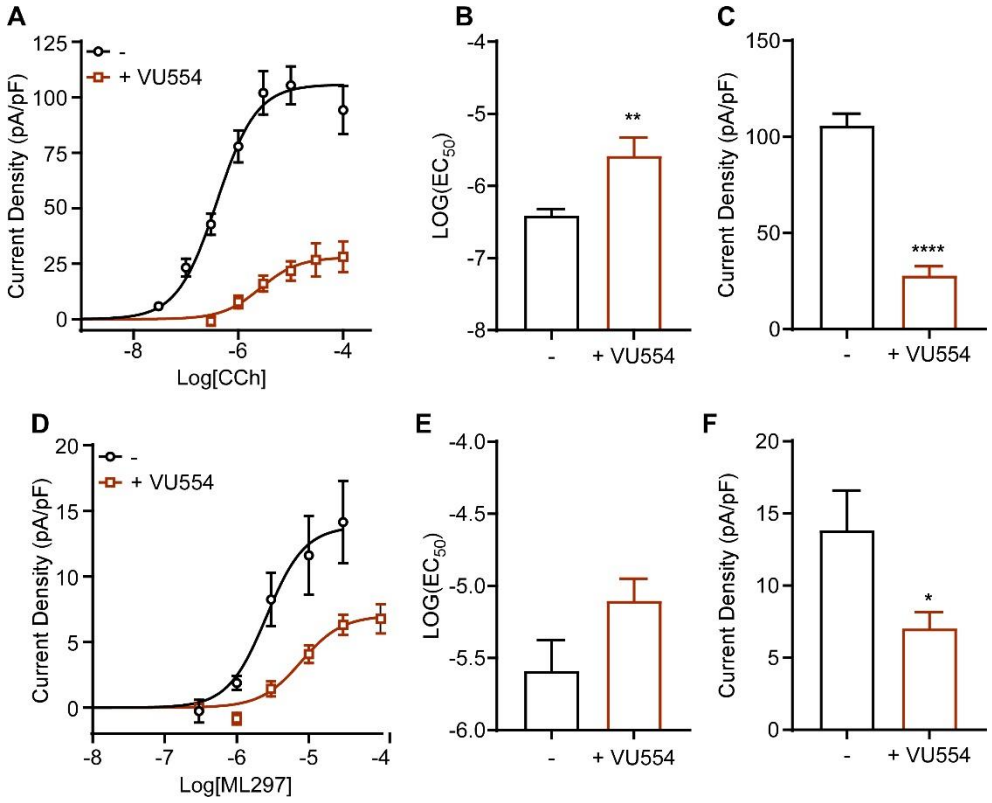

Figure 4.4. Mechanism of VU0468554 inhibition of GIRK-dependent responses in SAN cells

(**A**) Summary of concentration-dependent experiments of CCh-induced currents in wildtype SAN cells in the presence (n=11 cells /3 mice) or absence of 10 μM VU0468554 (n=17 cells /4 mice). (**B**) Summary of the Log(EC_{50}) from concentration-dependent of CCh-induced currents in wildtype SAN cells. Statistical analysis revealed a significant difference (t_{26}=3.6; ***P*<0.01; unpaired *t*-test) in the Log(EC_{50}) of CCh-induced currents in presence (n=11 cells /3 mice) or absence (n=17 cells /4 mice) of 10 μM VU0468554 in wildtype SAN cells. (**C**) Summary of the top (maximal response, pA/pF) of the nonlinear regression fits of the concentration-dependent CCh-induced responses in wildtype SAN cells. Statistical analysis revealed a significant difference (t_{26}=8.8; *****P*<0.0001; unpaired *t*-test) in the maximal current density of CCh-induced currents in presence (n=11 cells /3 mice) or absence (n=17 cells /4 mice) of 10 μM VU0468554 in wildtype SAN cells. (**D**) Summary of concentration dependent experiments of ML297-induced currents in wildtype SAN cells in the presence (n=14 cells /4 mice) or absence of 10 μM VU0468554 (n=10 cells /2 mice). (**E**) Summary of the Log(EC_{50}) from concentration-dependent of ML297-induced currents in wildtype SAN cells. Statistical analysis revealed a significant difference (t_{20}=1.9; *P*=0.08; unpaired *t*-test) in the Log(EC_{50}) of ML297-induced currents in presence (n=14 cells /4 mice) or absence (n=10 cells /2 mice) of 10 μM VU0468554 in wildtype SAN cells. (**F**) Summary of the top (maximal response, pA/pF) of the nonlinear regression fits of the concentration-dependent ML297-induced responses in wildtype SAN cells. Statistical analysis revealed a significant difference (t_{20}=2.7; **P*<0.05; unpaired *t*-test) in the maximal current density of ML297-induced currents in presence (n=14 cells /4 mice) or absence (n=10 cells /2 mice) of 10 μM VU0468554 in wildtype SAN cells.

4.3.4. VU0468554 reverses GIRK-mediated bradycardia in the isolated heart

We next investigated whether the reversal in CCh-induced GIRK currents elicited by VU0468554 in SAN cells translated to a block of GIRK-dependent bradycardia evoked by muscarinic activation. We obtained baseline HR from isolated wild-type and *Girk4*$^{-/-}$ mouse hearts. We then perfused the hearts with 1 μM CCh and compared the decrease in HR in wild-type and *Girk4*$^{-/-}$ mouse hearts. The decrease in HR upon perfusion of 1 μM CCh was significantly blunted in *Girk4*$^{-/-}$ mouse hearts (**Figure 4.5B**). After the HR reduction upon CCh perfusion had stabilized, VU0468554 (10 μM) or vehicle (1:100 DMSO) was administered and HR data at 5 min and 10 min post-injection was analyzed. Injection of VU0468554 reversed CCh-induced bradycardia by approximately 60 bpm (or 20% recovery) at 5 min post-injection (**Figure 4.5A-C**) and 50 bpm (or 16% recovery) at 10 min post-injection. We did not see a significant effect of vehicle injection on wild-type HR (**Figure 4.5**). Notably, we did not observe an impact of VU0468554 on the minimal CCh-induced bradycardia from isolated hearts from *Girk4*$^{-/-}$ mice, indicating that the impact of VU0468554 is likely due to its actions on GIRK channels (**Figure 4.5B**). These results show that 10 μM VU0468554 reverse approximately 1/3 of GIRK-mediated bradycardia elicited by muscarinic activation.

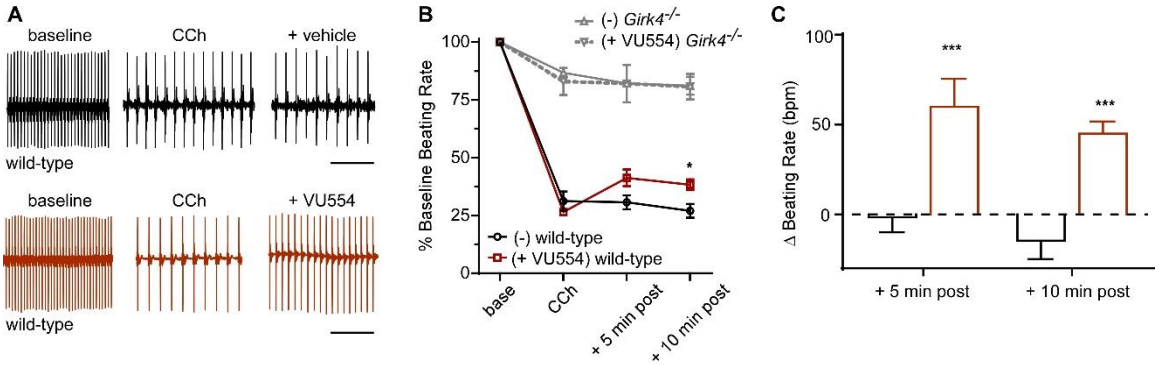

Figure 4.5. VU0468554 partially reverses GIRK-dependent bradycardia in the isolated heart

(**A**) Representative isolated heart recordings from wild-type mice showing HRs at baseline (left), after CCh perfusion (middle), and 5 min post-injection (right) while CCh is still being perfused. Top traces were from heart that was administered the vehicle alone (~1:100 DMSO), while the bottom traces were administered VU0468554 (~ 10 μM). (**B**) Summary of the % baseline beating rate of isolated hearts from wildtype and *Girk4*$^{-/-}$ mice. Unpaired t-test revealed a significant difference in the % baseline beating rate after CCh perfusion between isolated hearts from wildtype (n=10) and *Girk4*$^{-/-}$ (n=5) mice was detected (t_{13}=23.3, ****P<0.0001). Two-way ANOVA comparing the effect of treatment and time-point in wild-type mouse hearts revealed a significant interaction between time point and treatment ($F_{2,18}$=11.9; ***P<0.001) in the % inhibition. Post-hoc analysis revealed a significant difference between vehicle (n=6) and treatment (n=5) at 10 min post injection in wild-type mice (*P<0.05). Two-way ANOVA comparing the effect of treatment and time-point in *Girk4*$^{-/-}$ mouse hearts (vehicle, n=3; treatment, n=2) revealed no significant effect of treatment ($F_{2,3}$=0.1; P=0.8), time point ($F_{2,6}$=2.1; P=0.2) or interaction ($F_{2,6}$=0.5; P=0.61). (**C**) Summary of the Δbeating rate (bpm) of isolated hearts from wildtype mice. Two-way ANOVA revealed a significant effect of treatment ($F_{1,9}$=31.4; ***P<0.001), but not of time point $F_{1,9}$=2.5;P=0.15 and no interaction between the two was detected $F_{1,9}$=0.01; P=0.92)

4.4 Discussion

Here, we describe the characterization of a novel cardiac GIRK channel inhibitor, VU0468554. VU0468554 is selective for cardiac over neuronal GIRK channels, as evidenced by both previous work in GIRK channel-expressing HEK cells (Wen et al., 2013) and work here in primary culture models. The inhibition of cardiac GIRK channels resulted in a modest, yet significant, reversal of GIRK-dependent bradycardia elicited by muscarinic receptor activation. Therefore, VU0468554 represents a novel, exciting new pharmacological tool for selective targeting of GIRK1/4 channels.

VU0468554 displayed favorable maximal inhibition in native cell types, demonstrating nearly 60-80% antagonism of CCh-induced GIRK currents in SAN cells, yet only about 20% inhibition of baclofen-induced currents in HPC neurons. Intriguingly, we saw no significant difference in the potency between cardiac and neuronal inhibition of GIRK channels. This differs from previous observations in HEK cells, where VU0468554 exhibited a nearly 3x more potent inhibition in GIRK1/4 expressing HEK cells over GIRK1/2 expressing HEK cells. These discrepancies could arise from differences in how inhibition was measured in each assay. The thallium-flux based assay measured inhibition of basal activity of HEK cells transfected with either GIRK1/4 or GIRK1/2. In this study, we measured differences in inhibition of GPCR-activated GIRK-currents in native cell types. Furthermore, HEK cells lacking certain tissue-dependent signaling elements which influence GIRK channel gating and sub-cellular localization, such as RGS proteins (Doupnik, 2015) and synapse-associated proteins (SAPs) (Lunn et al., 2007). Thus, work here highlights the importance of experimentation in native cell types of tissues of interest.

GIRK channels are critical mediators of the effects of muscarinic activation on cardiomyocytes (Anderson et al., 2018; Bettahi et al., 2002; Lee et al., 2018; Wickman et al., 1998). Our work shows that VU0468554 can inhibit both G$\beta\gamma$-dependent (CCh-

induced) GIRK responses as well as basal GIRK channel activity, which is Gβγ-independent (Kienitz et al., 2014). Furthermore concentration-response experiments revealed evidence of non-competitive inhibition of Gβγ-dependent responses. We did note a significant shift in the potency (EC_{50}) of CCh-induced responses upon addition of VU0468554, suggesting additional un-competitive inhibition, where VU0468554 exhibits greater affinity for GIRK channels in complex with Gβγ.

VU0468554 was discovered from a family of compounds related to the previously characterized GIRK1-dependent agonist, ML297, which activates GIRK channels independent of Gβγ (Wydeven et al., 2014a). Site-mutagenesis studies revealed 2 distinct residues, one found in the GIRK1 pore helix and the other in the second membrane-spanning domain, that are necessary for ML297 activation of GIRK1-containing GIRK channels (Wydeven et al., 2014a). Our results here show that, like ML297, VU0468554 is a GIRK1-dependent GIRK channel modulator. However, we did not see strong evidence for competitive inhibition of ML297 by VU0468554, suggesting that even though ML297 and VU0468554 are from the same family of compounds, the binding sites may be unique. Thus, future studies utilizing site mutagenesis may provide a clearer picture of the mode of GIRK channel inhibition by VU0468554.

While VU0468554 exhibited a strong block of GIRK channel activity in isolated SAN cells, we observed only approximately 30% block of GIRK-dependent bradycardia elicited by muscarinic receptor activation in the isolated heart. This is likely due to solubility issues with the compound, which precipitates out of aqueous solution at concentrations over 10 μM. Higher concentrations may be necessary to reach the maximal inhibition of GIRK-dependent bradycardia by VU0468554 in the isolated heart model. Therefore, VU0468554 may serve as a lead compound for future iterations with improved solubility,

allowing for higher concentrations to be reached and used for further preclinical assessments.

Previous work has investigated the potential of GIRK channel inhibitors for the treatment of cardiac arrhythmias. TTQ (Jin and Lu, 1999), which is relatively selective for GIRK channels at nanomolar concentrations (Jin et al., 1999), has been shown to suppress atrial tachyarrhythmias in canines subjected to pacing-induced cardiac remodeling while not affecting ventricular physiology (Cha et al., 2006). NIP-142 was identified and shown to inhibit GIRK currents at low concentrations (EC_{50} =0.64 μM) and hERG channels at higher concentrations (EC_{50}=44 μM); it also reverses CCh and Ado-induced shortening of APD (Matsuda et al., 2006). Similar to the effects of TTQ, NIP-142 has been shown to terminate and prevent re-initiation of both AF and atrial flutter in atrial canine preparations (Hidehiko et al., 2002).

Against this background of existing GIRK channel blockers, VU0468554 is unique in its relatively selective inhibition of cardiac over neuronal GIRK channels. As previously mentioned, GIRK channels are widely throughout the CNS and play a critical role in mediating inhibitory signaling in discrete neuronal populations (Luján et al., 2014). Accordingly, a loss of GIRK-dependent signaling in the brain has been associated with several neurological disorders such as mood-related disorders, addiction, and epilepsy (Luján et al., 2014). Indeed, the dosing of the GIRK channel inhibitor BMS914392, previously known as NTC-801, was reduced by a factor of 3 in a study in human patients with AF due to severe CNS side effects (MacHida et al., 2011; Podd et al., 2016; Yamamoto et al., 2014). One possible explanation given concerning the CNS side effects was that BMS914392 may be blocking GIRK-dependent signaling in the brain. Thus, efforts to develop novel GIRK channel inhibitors for as a therapeutic intervention for related arrhythmias would ideally be selective for cardiac GIRK channels over neuronal GIRK channels, like VU0468554.

While GIRK channel activity has been widely implicated in arrhythmias such as nodal dysfunction and AF (Ehrlich et al., 2007, 2008; Mesirca et al., 2014, 2016a, 2016b) a lack of atrial GIRK channel has been linked to additional cardiac disorders. For example, *Girk4*$^{-/-}$ mice have been reported to experience resting tachycardia as observed via ECG telemetry (Posokhova et al., 2013). Furthermore, *Girk4*$^{-/-}$ mice also exhibit an increase in the amount of time necessary for HR to recover from sympathetic stimulation from either stress, exercise, or pharmacological stimulation (Mesirca et al., 2013). Prolonged recovery to sympathetic stimulation is associated with an increased risk for adverse cardiac outcomes such as myocardial infarction (Nissinen et al., 2003; White and Raven, 2014). Thus, a selective GIRK1/4 agonist may have potential utility in these scenarios. Future work could identify such an agonist similarly to how VU0468554 was discovered.

In conclusion, VU0468554 represents a novel lead compound as a GIRK1/4 selective inhibitor. VU0468554 and/or future iterations with improved solubility could prove incredibly useful as not only a new pharmacological tool for studying GIRK channels, but also have therapeutic implications in relevant cardiac arrhythmia models. Future work could evaluate the utility of VU0468554 and future iterations in mammalian models of supraventricular arrhythmias.

Acknowledgments: This work was made possible due to the contributions of Dr. David Weaver and Dr. Corey Hopkins who provided both ML297 and VU468554 for the studies contained in this chapter. Additionally, I would like to recognize the contributions of Baovi Vo of the Wickman lab who contributed data with VU468554 in HPC neurons.

Chapter 5

GPCR-dependent biasing of GIRK channel signaling dynamics by RGS6 in mouse sinoatrial nodal cells.

Anderson A, Masuho I, Marron Fernandez de Velasco E, Nakano A, Birnbaumer L, Martemyanov K, Wickman K (2020). Network of RGS-G protein interactions biases potency and efficacy of GPCR selectivity in mouse sinoatrial nodal cells. Proc. Natl. Acad. Sci. USA. 117(25):14522-14531

Author contributions: A.A., K.A.M., and K.W. designed research; A.A., I.M., and E.M.F.d.V. performed research; I.M., A.N., L.B., and K.A.M. contributed new reagents/analytic tools; A.A., I.M., E.M.F.d.V., and K.W. analyzed data; and A.A., I.M., A.N., L.B., K.A.M., and K.W. wrote the paper. All authors reviewed the manuscript.

5.1 Introduction

GPCRs constitute the largest family of cell surface receptors in the mammalian genome, and they mediate the influence of a diverse array of ligands on cell signaling, organ physiology, and behavior (Hauser et al., 2017). GPCRs evoke biological responses by coupling to a limited array of heterotrimeric G proteins, which then regulate the activity of a relatively small pool of effectors. Mechanisms underlying the compartmentalization of G protein dependent signaling pathways in native cell types are not well-understood.

Regulation of HR offers an opportunity to investigate how different GPCRs engage intracellular signaling networks to shape a critical physiological response. Activation of the parasympathetic branch of the ANS elicits bradycardia (Dyavanapalli et al., 2016), an effect mediated by the ACh-induced activation of M_2R on sinoatrial nodal SAN cells (Dhein et al., 2001). M_2R activation stimulates inhibitory G proteins, which then modulate the activity of downstream effectors, including GIRK channels (Logothetis et al., 1987; Sakmann et al., 1983; Wickman et al., 1994). The cardiac GIRK channel is a heterotetramer consisting of GIRK1 and GIRK4 subunits (Corey et al., 1998; Corey and Clapham, 1998; Krapivinsky et al., 1995a). Studies involving *Girk1*$^{-/-}$ and *Girk4*$^{-/-}$ mice have shown that activation of cardiac GIRK channels mediates most of the parasympathetic impact on HR, as well as atrial and AV impulse conduction (Bettahi et al., 2002; Lee et al., 2018; Mesirca et al., 2013; Wickman et al., 1998). Cardiac GIRK channels are also activated by Ado, an autacoid generated under ischemic conditions that activates A_1R, resulting in GIRK-dependent bradycardia (Belardinelli et al., 1988; Layland et al., 2014; Mustafa et al., 2009; Wickman et al., 1998). The ability of Ado to suppress HR and AV impulse conduction is exploited clinically to treat and diagnose supraventricular tachycardias (Layland et al., 2014).

GPCR-dependent signaling dynamics are influenced by RGS proteins (Woodard et al., 2015). RGS proteins possess GAP catalytic activity that accelerates the intrinsic GTP hydrolysis rate of $G\alpha$ subunits. Previous work from our group and others has identified RGS6 as a critical negative regulator of M_2R-GIRK signaling in mouse SAN cells and atrial myocytes (Posokhova et al., 2010; Wydeven et al., 2014b; Yang et al., 2010a). RGS6 is a member of the R7 RGS sub-family of RGS proteins, members of which form obligate dimers with the atypical $G\beta$ subunit $G\beta5$ (Anderson et al., 2009). Genetic ablation of *Rgs6* in mice increased GIRK channel sensitivity to muscarinic receptor activation, prolonged the deactivation rate of currents elicited by CCh, and enhanced CCh-induced bradycardia (Posokhova et al., 2010; Wydeven et al., 2014b; Yang et al., 2010a). The extent to which RGS6 regulates A_1R-GIRK signaling in the heart is currently unknown.

Here, we probed the functional compartmentalization of GPCR-dependent signaling by investigating signaling engaged by M_2R and A_1R activation in SAN cells. Despite converging on a common effector, M_2R-GIRK and A_1R-GIRK signaling pathways display notable differences in amplitude and kinetics. Using an array of knockout mouse lines, as well as electrophysiological, molecular, and optical imaging approaches, we found that the differences in M_2R-GIRK and A_1R-GIRK signaling dynamics in mouse SAN cells can be explained by GPCR-specific coupling biases for inhibitory G protein isoforms and the $G\alpha_o$ substrate specificity of RGS6.

5.2 Methods

5.2.1 Main-Text Methods

Animals. All procedures involving mice were approved by the Institutional Animal Care and Use Committee of the University of Minnesota, and experiments were conducted in accordance with guidelines set by the NIH. The generation of *Girk4*$^{-/-}$ and *Rgs6*$^{-/-}$ mice was described previously (Wickman et al., 1998; Wydeven et al., 2014b). C57BL/6J mice, bred on site or purchased from The Jackson Laboratory, were used as wild-type controls for these studies. Mice lacking either $G\alpha_o$ or $G\alpha_{i2}$ selectively in atrial/SAN tissue were generated by crossing the SLNCre driver mouse line (Nakano et al., 2011) with floxed versions of either $G\alpha_o$ (Ang et al., 2016) or $G\alpha_{i2}$ (Sebastian et al., 2013), resulting in SLNCre:$G\alpha_o^{fl/fl}$ and SLNCre:$G\alpha_{i2}^{fl/fl}$ mouse lines, respectively. Male and female mice were group-housed on a 12-h light/dark cycle, given free access to food and water, and used for experiments at ages 8 to 12 wk.

SAN Cell Culture and Recordings. SAN cells were prepared for electrophysiological analysis as described (Anderson et al., 2018) (**Chapter 3**). See section **5.2.2** for further details.

Isolated Heart Recordings. Hearts were excised and placed into ice-cold, oxygenated Tyrode's solution, and the aorta was quickly cannulated. Cannulated hearts were then placed into a warm (37 ± 1 °C) Tyrode's bath, and iWorx platinum recording electrodes were placed near/on the surface of the heart. Oxygenated Tyrode's solution was then perfused at 2 to 3 mL/min, and a baseline HR was recorded. Increasing concentrations of CCh or CPA (Tocris Bioscience) were then perfused via peristaltic pump for at least 15 min per dose. The ECG signal was acquired with LabScribe v.3 software (iWorx) and filtered as appropriate. The derivative of that channel was computed to account for movements in baseline and to amplify the signal for subsequent analysis. A

30-s segment from the last minute of exposure to each agonist dose was then exported to Kubios HRV v.2 (Tarvainen et al., 2014) for HR analysis, utilizing artifact correction as appropriate.

Quantitative RT-PCR. Total RNA was isolated from freshly isolated atrial tissue samples from adult wild-type mice and *Rgs6*$^{-/-}$ mice using the RNeasy fibrous tissue kit (Qiagen), according to manufacturer recommendations. Reverse transcription of 1.2 μg of total RNA per sample was performed using Maxima H Minus First Strand cDNA Synthesis Kit (ThermoFisher Scientific). Quantitative PCR was performed in a QuantStudio3 Real Time PCR System (Applied Biosystems) with the Fast SYBR Green Master Mix (ThermoFisher Scientific). See SI Appendix for further details, including target-specific primer sequences, reaction conditions, and analysis information.

Fast Kinetic BRET Assay. HEK293T/17 cells were grown in Dulbecco's Modified Eagle Media (Thermo Fisher Scientific) supplemented with 10% fetal bovine serum (Millipore Sigma), minimum Eagle's medium nonessential amino acids, 1 mM sodium pyruvate, and antibiotics (100 units/mL penicillin and 100 mg/mL streptomycin) at 37 °C in a humidified incubator containing 5% CO2. Culture dishes (3.5 cm) were incubated for 10 min at 37 °C with 1 mL of 10 mg/mL growth-factor–reduced Matrigel (BD Biosciences) in culture medium. For transfection, cells were seeded into 3.5-cm dishes at a density of 2 × 106 cells/dish. After 2 h, expression constructs (total 5 μg/dish) were added to the cells using PLUS (5 μg/dish) and Lipofectamine LTX (6 μL/dish) reagents (Thermo Fisher Scientific). BRET measurements of Venus-Gβ1γ2 and masGRK3ct-Nluc-HA were performed to measure G protein activation by M_2R and A_1R, or the GAP activity of RGS6/Gβ5 in living cells, as described (Masuho et al., 2015b, 2015a). See SI Appendix for further details, including information about DNA constructs and transfection as well as BRET assay procedures and analysis.

Statistical Analysis. All data were analyzed using Prism v.8.2.1 software (GraphPad Software) and are presented as mean ± SEM. Statistical outliers were identified and excluded with Grubb's outlier test. The level of statistical significance was set at $P < 0.05$. Specific statistical analyses are denoted within the figure legends.

5.2.2 Supplementary Methods

SAN cell culture. Adult male and female mice (8-10 wk) were anesthetized with intraperitoneal (i.p) ketamine (100 mg/Kg) and xylazine (10 mg/Kg). Hearts were excised into Tyrode's solution (in mM): 140 NaCl, 5.4 KCl, 1.2 KH2PO4, 1.0 $MgCl_2$, 1.8 $CaCl_2$, 5.55 glucose, 5 HEPES (pH 7.4 with NaOH). SAN-containing tissue was excised into a modified Tyrode's solution containing (in mM): 140 NaCl, 5.4 KCl, 1.2 KH_2PO_4, 0.2 $CaCl_2$, 50 taurine, 18.5 glucose, 5 HEPES, 0.1% BSA (pH 6.9 with NaOH) with elastase (0.3 mg/mL, Worthington Biochemical Corp., Lakewood, NJ) and collagenase II (0.21 mg/mL; Sigma Aldrich, St. Louis, MO). SAN tissue was digested at 37 °C for 30 min and then washed three times in a solution containing (in mM): 100 L-glutamic acid/potassium salt, 10 L-aspartic acid/potassium salt, 25 KCl, 10 KH_2PO_4, 2 $MgSO_4$, 20 taurine, 5 creatine, 0.5 EGTA, 20 glucose, 5 HEPES, 0.1% BSA (pH 7.2 with KOH). SAN tissue was then brought up to a volume of 500 μL of KB solution and triturated; 50 μL of the SAN cell containing solution was plated on each laminin-coated coverslips (25 μg/mL) and used within 8 h. In some experiments, SAN cells were treated with pertussis toxin (5 μg/mL; Tocris Bioscience, Bristol, UK) for 4-6 h prior to recordings.

Electrophysiology. Whole-cell currents and voltages were measured with hardware (Axopatch700B amplifier, Digidata 1440A) and software (pCLAMP v. 10.4) from Molecular Devices (Sunnyvale, CA). SAN cells were identified as thin, striated cells with capacitance values between 15–45 pF. Currents evoked by Ado (Sigma-Aldrich, St. Louis, MO), CCh (Sigma-Aldrich, St. Louis, MO), and ML297 (a generous gift from Dr. C. David

Weaver and Dr. Corey Hopkins) were measured at a holding potential of −70 mV. Borosilicate patch pipettes were filled with (in mM): 140 K-gluconate, 2 $MgCl_2$, 1.1 EGTA, 5 HEPES, 2 Na_2ATP, 5 phosphocreatine, and 0.3 Na-GTP (pH 7.2 with KOH). Whole-cell access was achieved in a low-K^+ bath solution consisting of (in mM): 130 NaCl, 5.4 KCl, 1 $CaCl_2$, 1 $MgCl_2$, 5.5 glucose, 5 HEPES/NaOH (pH 7.4). A high-K^+ bath solution (+/−CCh, Ado, or ML297) consisting of (in mM): 120 NaCl, 25 KCl, 1 $CaCl_2$, 1 $MgCl_2$, 5.5 glucose, 5 HEPES/NaOH (pH 7.4) was applied via ValveLink 8.2 rapid perfusion system (AutoMate Scientific, Berkeley, CA). Current reversal with TTQ (Alomone Labs, Jerusalem, Israel) was measured in the presence of CCh or Ado. Activation and deactivation time constants were extracted from appropriate regions of stable current traces and were fit with a 1-term Boltzmann equation: $f(x) = \sum_{i=1}^{n} \frac{A_i}{1+e^{-x/\tau_i}} + C$.

Only those experiments in which the access resistances were stable and low (<20 MΩ) were included in the final analysis.

Quantitative RT-PCR. The following amplification program was used: 95 °C/20 s followed by 40 cycles of 95 °C/3 s, 60 °C/30 s. Intron-spanning primer pairs were as follows:

A_1R: 5'-CAGAGCTCCATCCTGGCTCT-3' (forward)

5'-CGCTGAGTCACCACTGTCTTG-3' (reverse)

M_2R: 5′-GCCAGACTCCACCAGAT-3′ (forward)

5′-CCATTGTTCGAGGAGTTAGTT-3′ (reverse)

GIRK1: 5′-AAACTCACTCTCATGTTCCG-3′ (forward)

5′-TCCAGTTCAAGTTGGTCAAG-3′ (reverse)

GIRK4: 5′-GAGTTCGAAGTTGTGGTCATA-3′ (forward)

5′-GCACCTCTGTATCCATGTAAG-3′ (reverse)

RGS6: 5′-CTGACATTGTACAGTGGCTTAT-3′ (forward)

5′-GAGAACATGGTCTGAGATTGG-3′ (reverse)

The specificity of all reactions was assessed with a melting curve at the end of the program. Samples were tested in triplicate, and the average of replicates was used in the final data analysis. GAPDH (Mm_Gapd_2_SG QuantiTect primers; Qiagen) was used as an internal control in each sample.

cDNA constructs. A_1R (AY136746), M_2R (AF498916), $G\alpha_{oB}$ (AH002708), $G\alpha_z$ (J03260), $G\alpha_{11}$ (AF493900), $G\alpha_{14}$ (NM_004297), $G\alpha_{15}$ (AF493904), $G\alpha_s$ long isoform ($G\alpha_{sL}$) (NM_000516), $G\alpha_{olf}$ (AF493893), $G\alpha_{12}$ (NM_007353), $G\alpha_{13}$ (NM_006572), RGS6 (NM_004296), and $G\beta5S$ (NM_006578) in pcDNA3.1(+) were purchased from cDNA Resource Center (www.cDNA.org). Flag-tagged dopamine D2 receptors (NM_000795) containing the hemagglutinin signal sequence (KTIIALSYIFCLVFA) at the N-terminus was a gift from Dr. Abraham Kovoor. The pCMV5 plasmids encoding rat $G\alpha_{oA}$, rat $G\alpha_{i1}$, rat $G\alpha_{i2}$, rat $G\alpha_{i3}$, human $G\alpha_q$, and bovine $G\alpha_s$ short isoform ($G\alpha_{sS}$) were gifts from Dr. Hiroshi Itoh. Venus 156-239- $G\beta1$ (amino acids 156-239 of Venus fused to a GGSGGG linker at the N terminus of $G\beta1$ without the first methionine (NM_002074)) and Venus 1-155-$G\gamma2$ (amino acids 1-155 of Venus fused to a GGSGGG linker at the N terminus of $G\gamma2$ (NM_053064)) were gifts from Dr. Nevin A. Lambert (Hollins et al., 2009). Flag-tagged Ric-8A (NM_053194) in pcDNA3.1 was a gift from Dr. Jean-Pierre Montmayeur (Fenech et al., 2009). Flag-tagged Ric-8B (NM_183172 with one missense mutation (A1586G)) in pcDNA3.1 was a gift from Dr. Bettina Malnic (Von Dannecker et al., 2006). The masGRK3ct-Nluc-HA constructs were constructed by introducing HA tag at the C-terminus of masGRK3ct-Nluc reported previously (Masuho et al., 2015b). PTX-S1 constructs were reported previously (Raveh et al., 2010). GenBank accession numbers for each sequence are given in parentheses.

Fast kinetic BRET assay. The GPCR (M_2R (6), A_1R (1), and dopamine D2 receptor (D_2R) (1)), $G\alpha$ ($G\alpha_{oA}$ (2), $G\alpha_{oB}$ (1), $G\alpha_{i1}$ (1), $G\alpha_{i2}$ (2), $G\alpha_{i3}$ (1.5), $G\alpha_z$ (1.5), $G\alpha_q$ (2), $G\alpha_{11}$ (2),

$G\alpha_{14}$ (4), $G\alpha_{15}$ (2), $G\alpha_s$ short (6), $G\alpha_s$ long (4), $G\alpha_{olf}$ (6), $G\alpha_{12}$ (3), or $G\alpha_{13}$ (4)), Venus 156-239-Gβ1 (1), Venus 1-155- Gγ2 (1), and BRET donor (masGRK3ct-Nluc-HA (1)) were transfected with RGS6 (1) and Gβ5s (1) constructs; the number in parentheses indicates the ratio of transfected DNA (ratio 1 = 0.21 μg). $G\alpha_{14/15}$ and $G\alpha_{olf}$ were transfected with Ric-8A (1) and Ric-8B (1), respectively. A construct carrying catalytic subunit of pertussis toxin (PTX-S1) were transfected with $G\alpha_z$, Gαs subfamily, $G\alpha_q$ subfamily, and $G\alpha_{12/13}$ subfamily to inhibit the possible coupling of endogenous $G_{i/o}$ to GPCRs. An empty vector (pcDNA3.1(+)) was used to normalize the amount of transfected DNA. After transfection (16-24 h), HEK293T/17 cells were washed once with BRET buffer (Dulbecco's Phosphate-Buffered Saline containing 0.5 mM $MgCl_2$ and 0.1% glucose) and detached by gentle pipetting over the monolayer. Cells were harvested with centrifugation at 500xg for 5 min and resuspended in BRET buffer. Approximately 50,000 to 100,000 cells per well were distributed in 96-well flat-bottomed white microplates (Greiner Bio-One, Kremsmünster, Austria). The Nluc substrate furimazine was purchased from Promega (Madison, WI) and used according to manufacturer specifications. BRET measurements were made using a microplate reader (POLARstar Omega; BMG Labtech, Offenburg, Germany) equipped with two emission photomultiplier tubes, allowing for detection of two emissions simultaneously with a highest possible resolution of 20 ms per data point. All measurements were performed at room temperature. The BRET signal was determined by calculating the ratio of the light emitted by the Venus-G$\beta1\gamma2$ (535 nm with a 30 nm band path width) over the light emitted by the masGRK3ctNluc-HA (475 nm with a 30 nm band path width). The average baseline value (basal BRET ratio) recorded prior to agonist stimulation was subtracted from the experimental BRET signal values and obtained ΔBRET ratio. The time constants (tau) of the activation and deactivation phases were obtained by fitting a single exponential curve to the traces with Clampfit 10.3. k_{GAP} rate constants were determined by subtracting the basal deactivation rate from the deactivation

rate measured in the presence of exogenous RGS protein. Obtained k_{GAP} rate constants were used to quantify GAP activity

5.3 Results

5.3.1 A_1R-GIRK and M_2R-GIRK signaling distinctions in mouse SAN cells

We began by measuring whole-cell currents evoked by a saturating concentration of either Ado (10 μM) or CCh (10 μM) in isolated SAN cells from C57BL/6J (wild-type) mice (**Figure 5.1**). Both agonists reliably evoked currents in SAN cells from wild-type, but not in SAN cells from congenic *Girk4*$^{-/-}$ mice (**Figure 5.1A,B**), indicating that the evoked responses were mediated by GIRK channel activation. Currents elicited by Ado in wild-type SAN cells were smaller than CCh-induced currents (**Figure 5.1C**) and did not exhibit acute desensitization (**Figure 5.1D**). In addition, activation and deactivation rates of Ado-induced GIRK currents were slower than those of CCh induced responses (**Figure 5.1E,F**).

5.3.2. RGS6 exerts a GPCR-dependent influence on GIRK-dependent signaling

In parallel, we explored the impact of *Rgs6* ablation on Ado- and CCh-induced currents in SAN cells. While Ado-induced currents were significantly larger in SAN cells from *Rgs6*$^{-/-}$ mice relative to wild-type controls (**Figure 5.1A,C**), there was no impact of *Rgs6* ablation on CCh-induced current amplitudes (**Figure 5.1B,C**). *Rgs6* ablation also exerted a GPCR-dependent impact on response kinetics. Loss of RGS6 correlated with prolonged activation rate of Ado-induced currents (**Figure 5.1E**), but there was no impact on deactivation rate (**Figure 5.1F**). In contrast, and consistent with published reports (Posokhova et al., 2010; Wydeven et al., 2014b), there was no impact of Rgs6 ablation on the activation rate of CCh-induced currents (**Figure 5.1F**), but deactivation rate was prolonged (**Figure 5.1F**). Acute desensitization of CCh- and Ado-induced currents was not impacted by Rgs6 ablation (**Figure 5.1D**). Thus, RGS6 normally suppresses the

amplitude and accelerates the activation rate of A_1R-GIRK signaling in mouse SAN cells, while accelerating the deactivation rate of M_2R-GIRK signaling.

Ado-induced currents in SAN cells from *Rgs6*$^{-/-}$ mice were completely reversed by the GIRK channel inhibitor TTQ (300 nM; **Supplementary Figure 5.S1**) (Jin et al., 1999; Jin and Lu, 1999), indicating that the enhanced Ado-induced responses in these cells involves an increase in GIRK-dependent signaling. There was no difference in GIRK1, GIRK4, or A_1R mRNA levels in atrial tissue samples containing the SAN region from wild-type and *Rgs6*$^{-/-}$ mice (**Supplementary Figure 5.S2**). Additionally, GIRK channel currents evoked by ML297, a direct and selective activator of GIRK1-containing GIRK channels (Kaufmann et al., 2013; Wydeven et al., 2014a), were modestly but significantly smaller in SAN cells from *Rgs6*$^{-/-}$ mice (**Supplementary Figure 5.S3**). Thus, the increase in Ado-induced GIRK currents in SAN cells from *Rgs6*$^{-/-}$ mice does not appear to be linked to an increase in the expression of A_1R or GIRK channels.

To address the impact of *Rgs6* ablation on the sensitivity of M_2R-GIRK and A_1R-GIRK signaling pathways, we measured GIRK currents evoked by increasing concentrations of Ado and CCh in SAN cells from wild-type and *Rgs6*$^{-/-}$ mice. While there was no impact of Rgs6 ablation on the sensitivity of GIRK channels to Ado (**Figure 5.2A-C**), GIRK channels in SAN cells from *Rgs6*$^{-/-}$ mice were more sensitive to CCh than GIRK channels in SAN cells from wild-type controls (**Figure 5.2D-F**) (Wydeven et al., 2014b). Thus, RGS6 decreases GIRK channel sensitivity to CCh, but not Ado, in SAN cells.

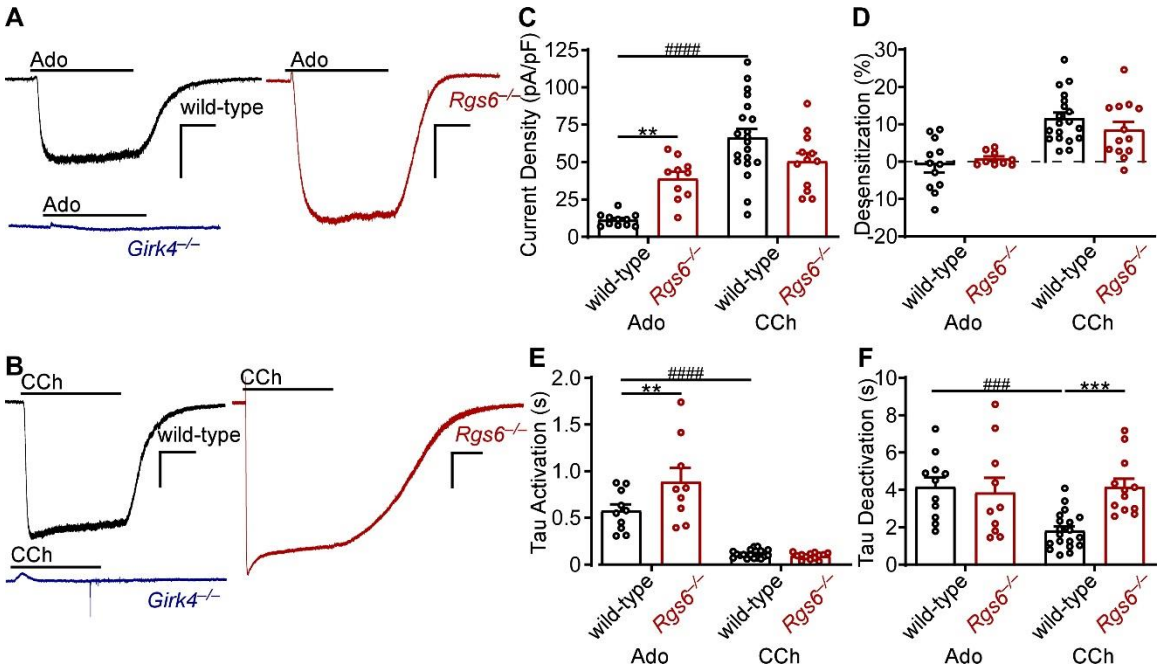

Figure 5.1. Ado- and CCh-induced GIRK currents in SAN cells.
(**A** and **B**) Whole-cell currents (V_{hold} = −70 mV) evoked by Ado (10 μM; **A**) or CCh (10 μM; **B**) in SAN cells from wild-type (Left, black) and *Rgs6*$^{-/-}$ (Right, red) mice; these currents were not observed in SAN cells from *Girk4*$^{-/-}$ mice (Bottom, blue). (Scale bars: 5 s/500 pA.) (**C**) Peak current density of responses elicited by Ado (Left) and CCh (Right) in SAN cells from wild-type (black) and *Rgs6*$^{-/-}$ (red) mice. There was a significant interaction between genotype and agonist ($F_{1,49}$ = 14.9, P < 0.001; two-way ANOVA); group sizes ranged from 10 to 20 cells (5–7 mice). **P < 0.01 wild-type vs. *Rgs6*$^{-/-}$ (within agonist); $^{\#\#\#\#}P$ < 0.0001 Ado vs. CCh (wild-type). (**D**) Acute desensitization of responses elicited by Ado (Left) and CCh (Right) in SAN cells from wild-type (black) and *Rgs6*$^{-/-}$ (red) mice. Statistical analysis revealed a main effect of agonist ($F_{1,49}$ = 30.4, P < 0.0001; two-way ANOVA), but no main effect of genotype ($F_{1,49}$ = 0.13, P = 0.72; two-way ANOVA) or genotype x agonist interaction ($F_{1,49}$ = 1.6, P = 0.21; two-way ANOVA); group sizes ranged from 9 to 19 cells (5–7 mice). (**E**) Activation rates of responses elicited by Ado (Left) and CCh (Right) in SAN cells from wild-type (black) and *Rgs6*$^{-/-}$ (red) mice. Statistical analysis revealed a genotype x agonist interaction ($F_{1,45}$ = 6.8, P < 0.05; two-way ANOVA); group sizes ranged from 9 to 17 cells (5–7 mice). **P < 0.01 wild-type vs. *Rgs6*$^{-/-}$ (within agonist); $^{\#\#\#\#}P$ < 0.0001 Ado vs. CCh (wild type). (**F**) Deactivation rates of responses elicited by Ado (Left) and CCh (Right) in SAN cells from wild-type (black) and *Rgs6*$^{-/-}$ (red) mice. Statistical analysis revealed a genotype x agonist interaction ($F_{1,48}$ = 8.0, P < 0.01; two-way ANOVA); group sizes ranged from 12 to 19 cells (5–7 mice). ***P < 0.001 wild-type vs. *Rgs6*$^{-/-}$ (within agonist); $^{\#\#\#}P$ < 0.001 Ado vs. CCh (wild type).

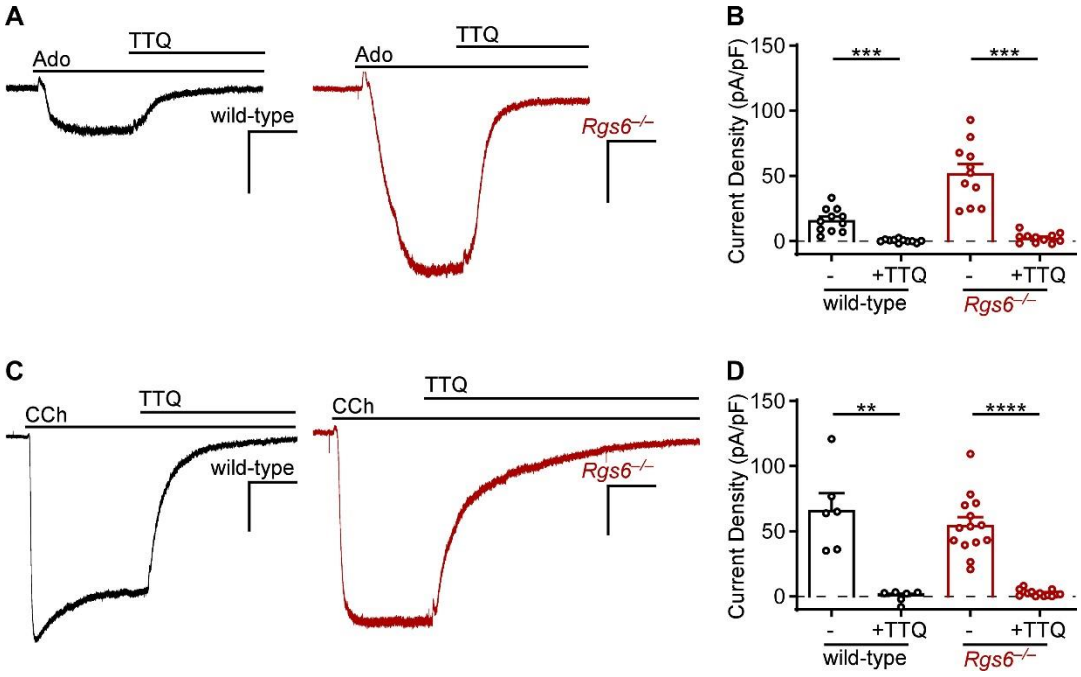

Supplemental Figure 5.S1. GIRK-dependence of Ado- and CCh-induced currents. **(A)** The GIRK channel blocker TTQ (300 nM) reversed whole-cell currents evoked by Ado (10 μM) in SAN cells from wild-type and *Rgs6*$^{-/-}$ mice. **(B)** Peak current density of Ado-induced currents (-/+ TTQ) in SAN cells from wild-type (n=11 cells/3 mice) and *Rgs6*$^{-/-}$ (n=11 cells/3 mice) mice. There was a significant difference in the peak current density of Ado-induced currents before and after TTQ perfusion in SAN cells isolated from wild-type (t_{10}=5.6, ***P< 0.001; paired t-test) and *Rgs6*$^{-/-}$ (t_{10}=8.2, ****P<0.0001; paired t-test) mice. **(C)** TTQ (300 nM) reversed whole-cell currents evoked by CCh (10 μM) in SAN cells from wild-type and *Rgs6*$^{-/-}$ mice. **(D)** Peak current density of CCh-induced currents (-/+ TTQ) in SAN cells from wild-type (n=6 cells/3 mice) and *Rgs6*$^{-/-}$ (n=14 cells/4 mice) mice. There was a significant difference in the peak current density of CCh-induced currents before and after TTQ perfusion in SAN cells from wild-type (t_5=5.3, **P<0.01; paired t-test) and *Rgs6*$^{-/-}$ (t_{13}=8.7, ****P<0.0001; paired t-test) mice.

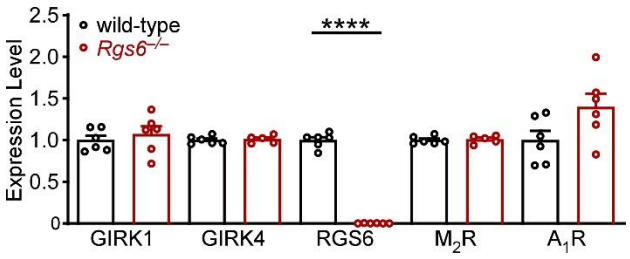

Supplemental Figure 5.S2. Impact of *Rgs6* ablation on the expression of GPCR-GIRK signaling elements.
mRNA levels of GIRK1 (t_{10}=0.7, p=0.52), GIRK4 (t_9=0.4, p=0.72), RGS6 (t_{10}=27.4, ****P<0.0001), M_2R (t_9=0.3, p=0.76), and A_1R (t_{10}=2.0, p=0.07) in atrial/SAN tissue samples from wild-type (black) and *Rgs6*$^{-/-}$ (red) mice, compared using unpaired student's *t*-tests. mRNA levels of each target were normalized to the level of GAPDH mRNA measured in each sample, and the mRNA levels for each target in *Rgs6*$^{-/-}$ samples were normalized to the level present in wild-type samples (n=5–6 samples per tissue and target).

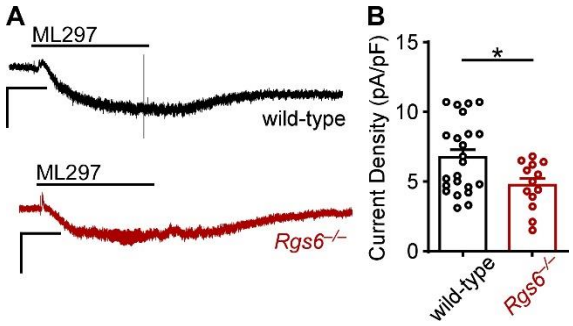

Supplemental Figure 5.S3. ML297-induced currents in wild-type and *Rgs6*$^{-/-}$ SAN cells.
(A) Representative whole-cell currents evoked by ML297 (10 μM) in SAN cells from wild-type (top) and *Rgs6*$^{-/-}$ (bottom) mice. Scale bars: 5 s/200 pA. **(B)** There was a modest but significant decrease in the peak ML297-induced current density in SAN cells from *Rgs6*$^{-/-}$ (n=13 cells/4 mice) as comparison to wild-type (n=23 cells/4 mice) mice (t_{34}=2.5, **P*<0.05; unpaired *t*-test).

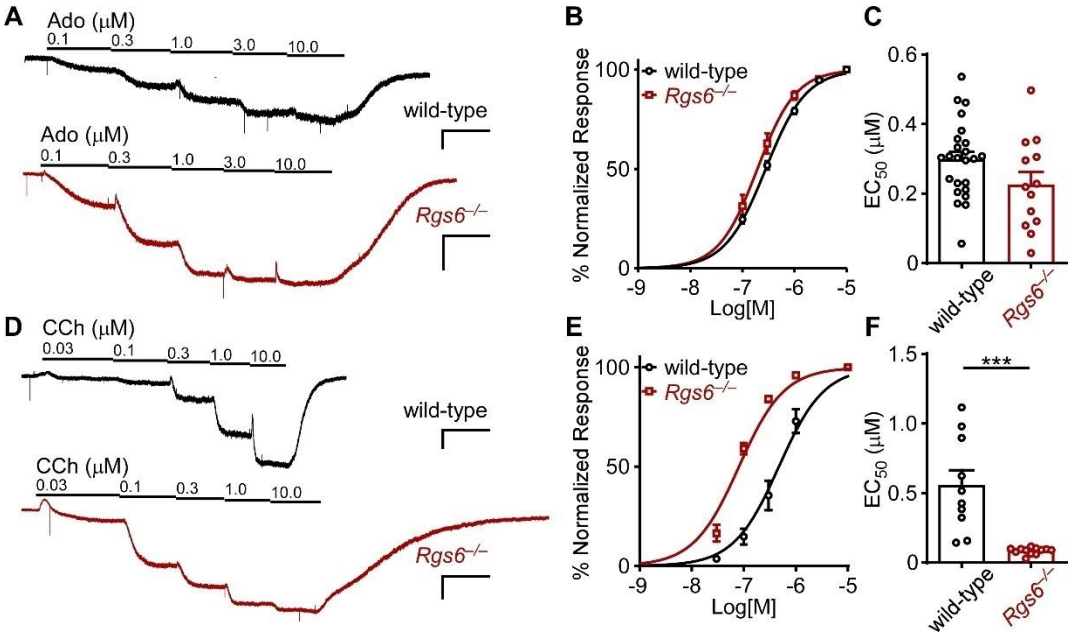

Figure 5.2. Impact of Rgs6 ablation on GIRK channel sensitivity to CCh and Ado. (**A**) Concentration-response experiments for Ado in SAN cells from wild-type (Scale bars: Top, 10 s/200 pA.) and *Rgs6*$^{-/-}$ (Scale bars: Bottom, 10 s/500 pA.) mice. (**B** and **C**) Summary of concentration-response experiments for Ado-induced currents in SAN cells from wild-type and *Rgs6*$^{-/-}$ mice. There was no difference in EC_{50} values for Ado-induced currents in SAN cells from wild-type (n = 24 cells/7 mice) and *Rgs6*$^{-/-}$ (n = 13 cells/5 mice) mice (t_{35} = 1.8, P = 0.08; unpaired t test). (**D**) Concentration-response experiments for CCh-induced currents in SAN cells from wild-type (Scale bars: Top, 10 s/200 pA.) and *Rgs6*$^{-/-}$ (Scale bars: Bottom, 10 s/500 pA.) mice. (**E** and **F**) Summary of concentration-response experiments of CCh-induced currents in SAN cells from wild-type and *Rgs6*$^{-/-}$ mice. The EC_{50} values for CCh-induced currents in SAN cells from *Rgs6*$^{-/-}$ (n = 12 cells/4 mice) mice were lower than the EC_{50} values measured in wild-type counterparts (n = 10 cells/4 mice) (t_{20} = 4.8, ***P < 0.001; unpaired t test).

5.3.3. RGS6 impacts GIRK-dependent bradycardia in a GPCR-dependent manner

We also evaluated the impact of *Rgs6* ablation on the bradycardic effect of A_1R and M_2R activation using an isolated heart model (**Figure 5.3**). Both the stable A_1R agonist CPA (**Figure 5.3A,B**) and CCh (**Figure 5.3C,D**) evoked dose-dependent decreases in HR in wild-type hearts. The bradycardic effect of CPA and CCh was strongly diminished in hearts from *Girk4*$^{-/-}$ mice (**Figure 5.3B,D**), suggesting that M_2R- and A_1R-induced bradycardia is largely dependent on GIRK channel activation. The magnitude of CPA-induced bradycardia was larger in *Rgs6*$^{-/-}$ as compared to wild-type hearts (**Figure 5.3B**), but there was no detectable shift in CPA potency. While CCh-induced bradycardia was also more pronounced in *Rgs6*$^{-/-}$ hearts (Posokhova et al., 2010, 2013; Wydeven et al., 2014b), there was a clear leftward shift in the dose-response curve (**Figure 5.3D**). Thus, the results from the isolated heart model mirror the results obtained isolated SAN cells, indicating that RGS6 exerts a prominent negative influence on A_1R-GIRK signaling amplitude and M_2R-GIRK signaling sensitivity.

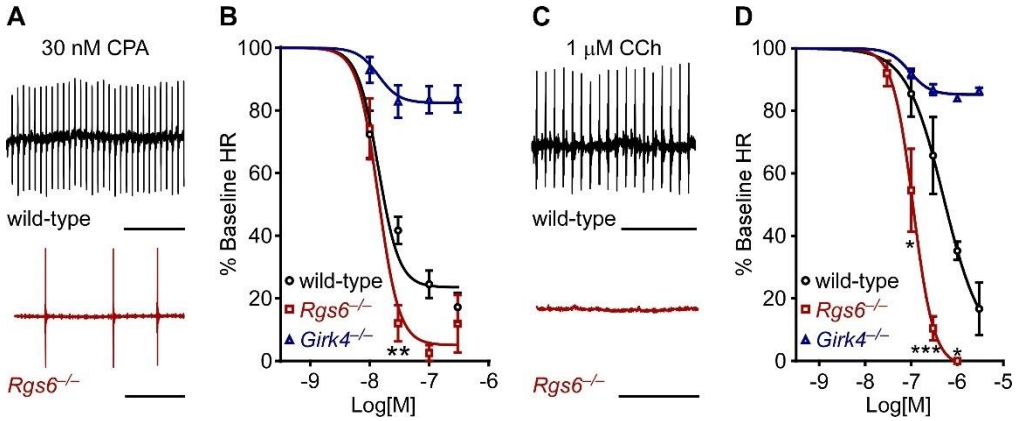

Figure 5.3. CPA- and CCh-induced bradycardia in isolated hearts from wild-type and *Rgs6*$^{-/-}$ mice.

(**A**) Segments of ECG traces from isolated wild-type (Top) and *Rgs6*$^{-/-}$ (Bottom) hearts perfused with the A_1R-selective agonist CPA (30 nM). (Scale bar: 5 s.) (**B**) Percentage decrease in HR (relative to baseline) following perfusion of increasing concentrations of CPA in hearts from wild-type (n = 6), *Rgs6*$^{-/-}$ (n = 7), and *Girk4*$^{-/-}$ (n = 4) mice; there was a genotype x CPA concentration interaction for wild-type and *Rgs6*$^{-/-}$ hearts ($F_{4,44}$ = 2.81; P < 0.05; two-way ANOVA with repeated measures). **P < 0.01 wild type vs. *Rgs6*$^{-/-}$. (**C**) Segments of ECG traces of isolated wild-type (Top) and *Rgs6*$^{-/-}$ (Bottom) hearts perfused with CCh (1 μM). (Scale bar: 5 s.) (**D**) Percentage decrease in HR (relative to baseline) following perfusion of increasing concentrations of CCh in hearts from wild-type (n = 3), *Rgs6*$^{-/-}$ (n = 5), and *Girk4*$^{-/-}$ (n = 6) mice; there was a genotype x CCh concentration interaction for wild-type and *Rgs6*$^{-/-}$ hearts ($F_{3,18}$ = 5.1, P < 0.05; two-way ANOVA with repeated measures). *P < 0.05 and ***0.001, respectively, wild type vs. *Rgs6*$^{-/-}$.

5.3.4. RGS6 limits the access of A_1R to GIRK channels

The differential impact of Rgs6 ablation on M_2R-GIRK and A_1R-GIRK signaling in mouse SAN cells could reflect the coupling of the GPCRs to separate pools of GIRK channels. To test this possibility, we examined whether Ado-induced currents were occluded by a maximal CCh-induced GIRK channel response. In both wild-type and *Rgs6*$^{-/-}$ SAN cells, Ado failed to evoke an additive current during application of a saturating concentration of CCh (**Figure 5.4A,B**). When the order of agonist application was reversed, CCh evoked an additive current during the Ado induced response (**Figure 5.4C**). The size of the CCh-induced additive response was substantially smaller, however, in SAN cells from *Rgs6*$^{-/-}$ mice (**Figure 5.4D**). Indeed, the Ado-induced GIRK current occluded nearly all of the CCh-induced response. Collectively, these findings show that M_2R and A_1R couple to a shared pool of GIRK channels in SAN cells, and that RGS6 effectively limits the access of A_1R to GIRK channels in these cells.

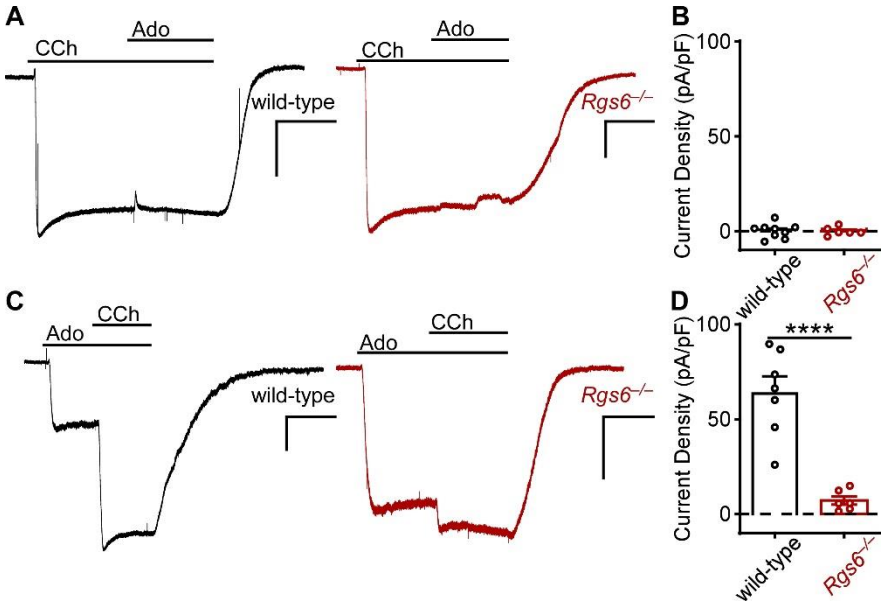

Figure 5.4. Occlusion of CCh- and Ado-induced GIRK currents.
(**A**) Occlusion experiments showing whole-cell currents elicited by a maximal concentration of CCh (10 μM), followed by Ado application (10 μM) in SAN cells from wild-type (Left) and *Rgs6*$^{-/-}$ (Right) mice. (Scale bars: 10 s/500 pA.) (**B**) There was no difference in the Ado-induced additive response in SAN cells isolated from wild-type (n = 9 cells/4 mice) and *Rgs6*$^{-/-}$ (n = 6 cells/5 mice) mice (t_{13} = 0.11, P = 0.91; unpaired t test). (**C**) Occlusion experiments showing whole-cell currents elicited by a maximal concentration of Ado (10 μM), followed by CCh application (10 μM) in SAN cells from wild-type (Left) and *Rgs6*$^{-/-}$ (Right) mice. (Scale bars: 10 s/500 pA.) (**D**) There was a significant difference in the CCh-induced additive response in SAN cells from wild-type (n = 7 cells/4 mice) and *Rgs6*$^{-/-}$ (n = 6 cells/4 mice) mice (t_{11} = 6.0; ****P < 0.0001; unpaired t test).

5.3.5. M_2R and A_1R display overlapping but distinct G protein coupling preferences

We next investigated whether the utilization of different $G\alpha$ isoforms by M_2R and A_1R could explain the differences in GIRK channel-dependent signaling and modulation by RGS6. Treatment with pertussis toxin abolished CCh and Ado-induced currents in wild-type SAN cells (**Supplementary Figure 5.S4**), indicating that M_2R and A_1R-GIRK signaling pathways are mediated by inhibitory ($G_{i/o}$) G proteins. To probe the inhibitory G protein coupling preferences for M_2R and A_1R, we employed a Bioluminescence Resonance Energy Transfer (BRET) assay to measure G protein activation in response to GPCR stimulation in living cells (**Figure 5.5A**) (Masuho et al., 2015b). We quantified maximal BRET response amplitudes and G protein activation rates for M_2R and A_1R, in the presence of specific G protein isoforms (**Figure 5.5B**). Analysis of BRET amplitudes showed that both M_2R and A_1R can activate all members of the $G_{i/o}$ sub-family, as well as G15 (**Figure 5.5C**). M_2R displayed faster activation rates with $G\alpha_o$ relative to $G\alpha_i$ isoforms, however, while A_1R exhibited similar activation rates for $G\alpha_o$ and $G\alpha_i$ isoforms (**Figure 5.5D**). Since G protein activation rates closely reflect the catalytic activity of GPCRs (Masuho et al., 2013), whereas amplitudes in the BRET assay could be influenced by intrinsic differences in the extent of heterotrimer dissociation (Digby et al., 2008) we relied on activation rate as a proxy for $G\alpha$ coupling preferences for M_2R and A_1R. Accordingly, M_2R exhibits a coupling preference for $G\alpha_o$ over $G\alpha_i$, whereas A_1R does not discriminate between the inhibitory G protein isoforms.

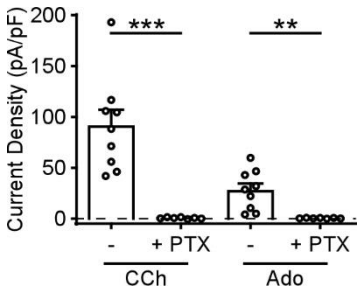

Supplemental Figure 5.S4. Impact of pertussis toxin (PTX) on CCh- and Ado-induced currents.
Summary of CCh- and Ado-induced current densities from control (-; n=9 cells/4 mice) or PTX-treated (+ PTX; n=7 cells/3 mice) wild-type SAN cells. PTX treatment (5 μg/mL; 4-6 h) abolished CCh-induced (t_{14}=5.1, ***p<0.001; unpaired t-test) and Ado-induced (t_{14}=3.7, **p<0.01; unpaired t-test) currents.

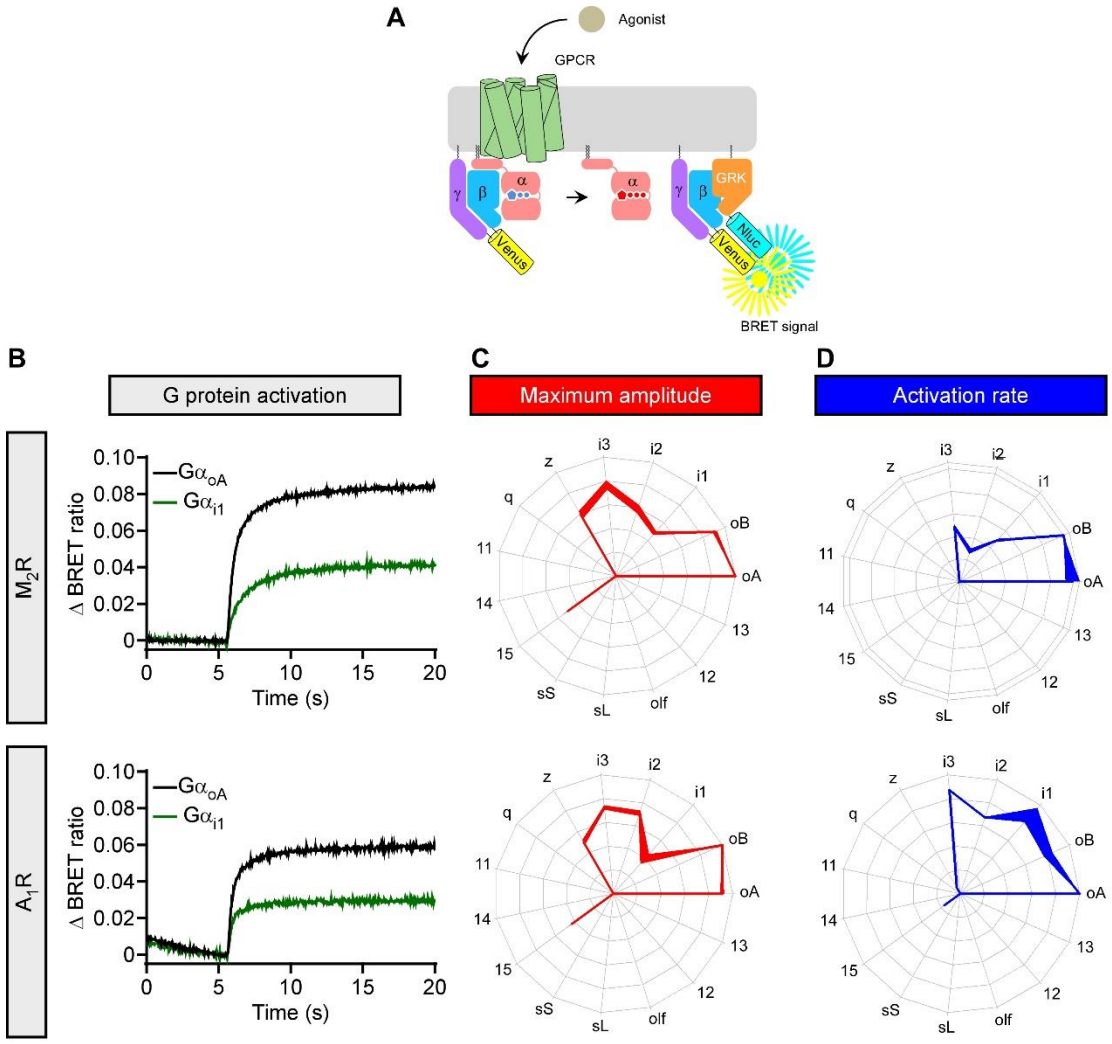

Figure 5.5. G protein coupling preferences of M_2R and A_1R.
(**A**) Schematic representation of the BRET assay for real-time optical imaging of G protein activity. Agonist-induced activation of a GPCR leads to the dissociation of Gα-GTP and Venus-Gβγ subunits. The released Venus-Gβγthen interacts with the Gβγ effector mimetic masGRK3ct-Nluc-HA to produce the BRET signal. (**B**) Representative real-time monitoring of G protein activation by M_2R (Top) or A_1R (Bottom). HEK293T/17 cells were transfected with the BRET sensor pair (A) and GPCR, together with either $G\alpha_{oA}$ (black) or $G\alpha_{i1}$ (green). Acetylcholine (100 μM) or Ado (100 μM) was applied at the 5-s time point, and the BRET signal was followed across time. (**C** and **D**) G protein coupling summary diagrams for M_2R and A_1R. Maximum amplitudes (red) and activation rate constants (blue) for 15 different G proteins were normalized to the largest value and plotted in the wheel diagrams. Line thickness represents the SEM of three technical replicates performed independently.

5.3.6. $G\alpha_o$ is the preferred substrate for RGS6 GAP activity

Given the distinct G protein isoform coupling preferences displayed by M_2R and A_1R, and the differential impact of RGS6 on G protein-mediated regulation of GIRK channels, we next tested whether the RGS6 exhibits a G protein isoform preference for its catalytic activity. The G protein deactivation rates of all $G\alpha_{i/o}$ members were measured in the presence of RGS6/Gβ5 using a modified version of the BRET assay (**Figure 5.6A**). The D2 dopamine receptor (D_2R), dopamine, and haloperidol were chosen for this study due to previous work showing that D_2R can efficiently activate all $G\alpha_{i/o}$ G proteins and that GTPase activity is the rate-limiting step in response deactivation for this combination of receptor and ligands (Masuho et al., 2013). Consistent with results from a study involving purified RGS6/Gβ5 and G proteins (Hooks et al., 2003), RGS6/Gβ5 strongly accelerated the deactivation of $G\alpha_{oA/B}$, while showing only weak activity toward $G\alpha_{i1\text{-}3}$ isoforms and no activity toward $G\alpha_z$ (**Figure 5.6B,C**). Thus, $G\alpha_o$ is the preferred substrate for RGS6 and its GAP activity.

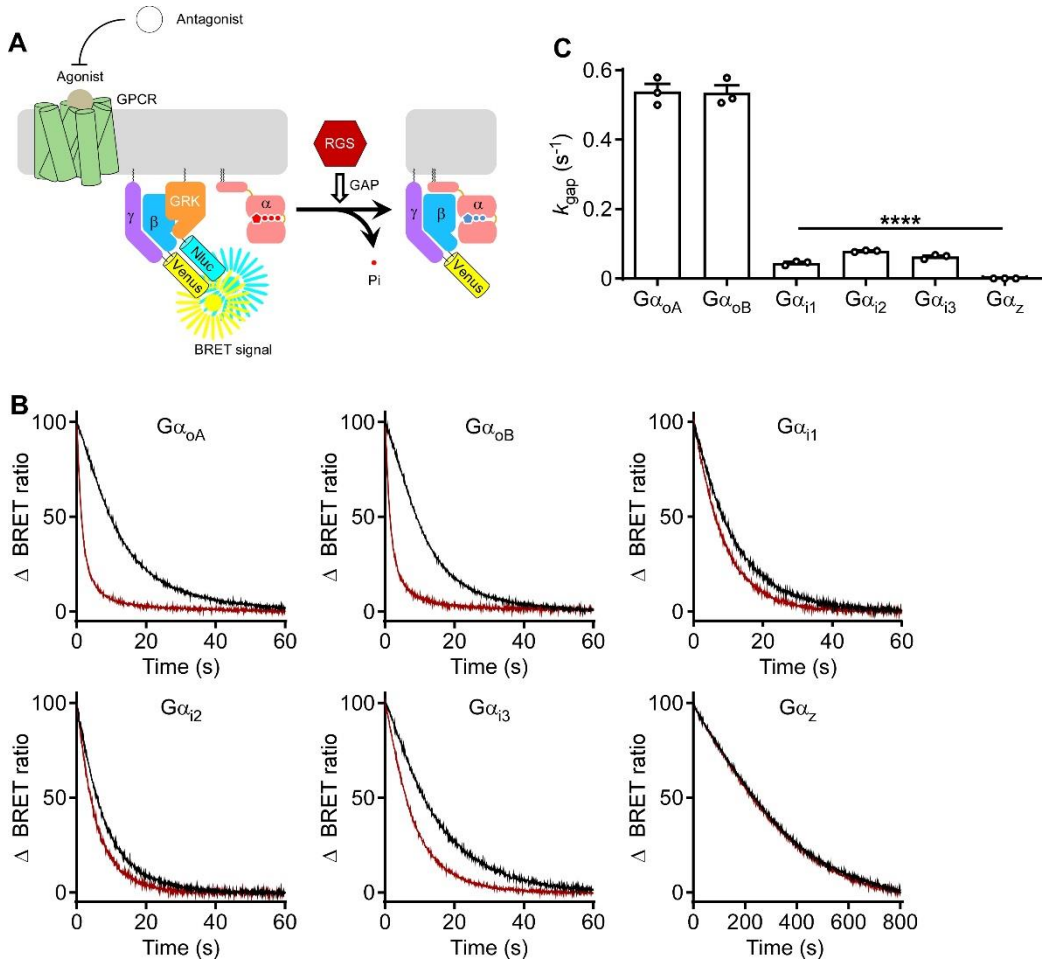

Figure 5.6. Gα substrate specificity of RGS6/Gβ5.
(**A**) Schematic representation of the BRET assay for measuring RGS GAP activity. Application of antagonist after G protein activation by a GPCR agonist initiates the deactivation of G proteins, decreasing the BRET signal. (**B**) Real-time monitoring of G protein deactivation. HEK293T/17 cells were transfected with D_2R, Gα, Venus-Gβγ, and masGRK3ct-Nluc-HA with (red) or without (black) RGS6/Gβ5. Dopamine (100 μM) and haloperidol (100 μM) were applied to activate D_2R and initiate G protein deactivation, respectively. Representative data from three independent experiments are shown. (**C**) Comparison of k_{GAP} activity of RGS6/Gβ5 on the Gi/o isoforms ($F_{5,12} = 372.6$, $P < 0.0001$; one-way ANOVA). ****$P < 0.0001$ vs. $G\alpha_o$ isoforms.

5.3.7. $G\alpha_o$ and $G\alpha_{i2}$ ablation impact GIRK-dependent signaling in a GPCR-dependent manner

Previous work utilizing constitutive or conditional knockout mice has implicated $G\alpha_o$ and $G\alpha_{i2}$ isoforms in HR regulation (Ang et al., 2016; Sebastian et al., 2013; Zuberi et al., 2008). Accordingly, we crossed an atrial-specific Cre driver line (SLNCre (Nakano et al., 2011)) with conditional $G\alpha_o$ ($G\alpha_o^{fl/fl}$ (Ang et al., 2016)) or $G\alpha_{i2}$ ($G\alpha_{i2}^{fl/fl}$ (Sebastian et al., 2013)) knockout mice, to generate mice lacking $G\alpha_o$ (SLNCre:$G\alpha_o^{fl/fl}$) or $G\alpha_{i2}$ (SLNCre:$G\alpha_{i2}^{fl/fl}$) in atrial (including SAN) tissue. We then recorded currents evoked by CCh or Ado in SAN cells from Cre(+) and Cre(-) littermates (**Figure 5.7**). While maximal CCh-induced currents and desensitization were smaller in SLNCre(+):$G\alpha_o^{fl/fl}$ SAN cells compared to Cre(-) littermates (**Figure 5.7A-C**), Ado-induced currents and desensitization were not impacted by $G\alpha_o$ ablation (**Figure 5.7F-H**). $G\alpha_{i2}$ ablation had no impact on CCh- or Ado-induced response amplitudes or desensitization (**Figure 5.7B,C,G,H**). Loss of $G\alpha_o$ prolonged activation and deactivation rates of CCh-induced GIRK currents, whereas $G\alpha_{i2}$ ablation was without effect (**Figure 5.7D,E**). The deactivation rate of Ado-induced GIRK currents was also prolonged by $G\alpha_o$ ablation (**Figure 5.7J**), but interestingly, the activation rate of Ado-induced GIRK currents was accelerated by $G\alpha_{i2}$ ablation (**Figure 5.7I**). Collectively, these results align with observations that M_2R signals preferentially through $G\alpha_o$, whereas A_1R does not discriminate between $G\alpha_o$ and $G\alpha_i$. Moreover, the lack of impact of $G\alpha_{i2}$ ablation on the CCh- and Ado-induced GIRK current deactivation rates is consistent with the $G\alpha_o$ substrate preference of RGS6.

Lastly, we evaluated the impact of $G\alpha_o$ or $G\alpha_{i2}$ ablation on GIRK channel sensitivity to CCh and Ado. While the loss of $G\alpha_o$ did not impact GIRK channel sensitivity to CCh (**Figure 5.8A-C**), $G\alpha_{i2}$ ablation increased the sensitivity of GIRK channels to CCh. Conversely, $G\alpha_o$ ablation increased GIRK channel sensitivity to Ado, whereas $G\alpha_{i2}$ ablation was without effect (**Figure 5.8D-F**). Thus, loss of $G\alpha_o$ increases the sensitivity of

A_1R-GIRK channel signaling, whereas loss of $G\alpha_{i2}$ increases the sensitivity of M_2R-GIRK channel signaling.

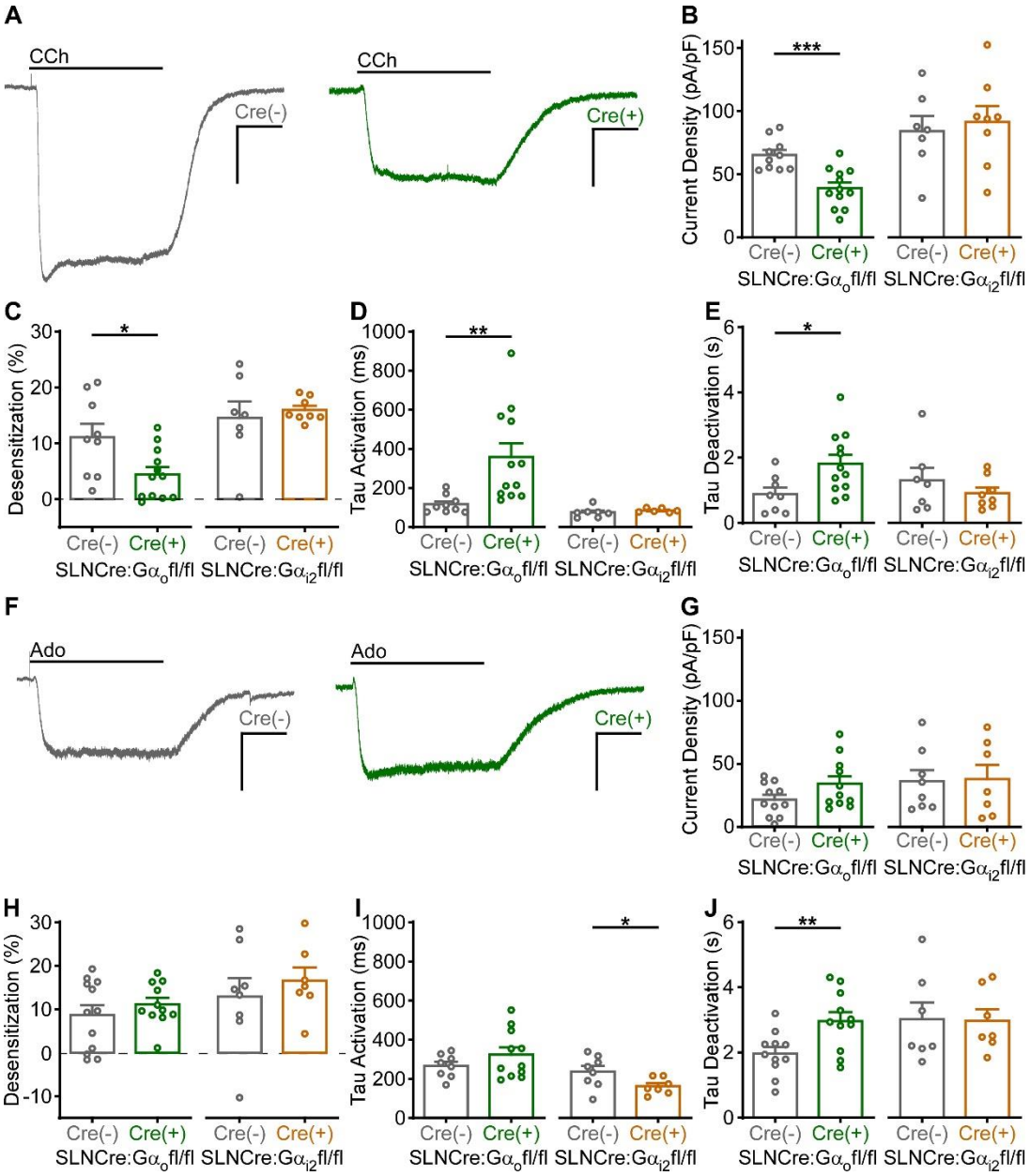

Figure 5.7. Impact of Gα$_o$ and Gα$_{i2}$ ablation on CCh- and Ado-induced GIRK currents. (**A**) Whole-cell currents evoked by CCh (10 μM) in SAN cells from SLNCre(−):Gα$_o^{fl/fl}$ (Left, gray) and SLNCre(+):Gα$_o^{fl/fl}$ (Right, green) mice. (Scale bars: 5 s/500 pA.) (**B** and **C**) Peak CCh-induced current density (t_{20} = 4.3, ***P < 0.001; unpaired t test) and current desensitization (t_{19} = 2.6, *P < 0.05; unpaired t test) were smaller in SAN cells from SLNCre(+):Gα$_o^{fl/fl}$ mice as compared to their SLNCre(−):Gα$_o^{fl/fl}$ counterparts; group sizes ranged from 9 to 12 cells (5 mice) per genotype. There was no difference in CCh-induced current density (t_{13} = 0.4, P = 0.69; unpaired t test) or desensitization (t_{13} = 0.5, P = 0.62; unpaired t test) in SAN cells from SLNCre(−):Gα$_{i2}^{fl/fl}$ mice and SLNCre(+):Gα$_{i2}^{fl/fl}$ mice; group sizes ranged from 7 to 8 cells (3 mice) per genotype. (**D** and **E**) Activation (t_{19} = 3.0, **P < 0.01; unpaired t test) and deactivation (t_{18} = 2.5, *P < 0.05; unpaired t test) rates of CCh-induced currents were prolonged in SAN cells from SLNCre(+):Gα$_o^{fl/fl}$ mice, relative to SLNCre(−):Gα$_o^{fl/fl}$ counterparts; group sizes ranged from 8 to 12 cells (5 mice) per

genotype. There was no difference in activation (t_{11} = 0.9, P = 0.38; unpaired t test) or deactivation (t_{13} = 1.0, P = 0.36; unpaired t test) rates of CCh-induced currents in SAN cells from SLNCre(−):$G\alpha_{i2}^{fl/fl}$ and SLNCre(+):$G\alpha_{i2}^{fl/fl}$ mice; group sizes ranged from 6 to 8 cells (3 mice) per genotype. (**F**) Whole-cell currents evoked by Ado (10 μM) in SAN cells from SLNCre(−):$G\alpha_{o}^{fl/fl}$ (Left, gray) and SLNCre(+):$G\alpha_{o}^{fl/fl}$ (Right, green) mice. (Scale bars: 5 s/500 pA.) (**G** and **H**) There was no difference in peak current density (t_{20} = 1.8, P = 0.08; unpaired t test) or desensitization (t_{21} = 0.9, P = 0.38; unpaired t test) of Ado-induced currents in SAN cells from SLNCre(−):$G\alpha_{o}^{fl/fl}$ and SLNCre(+):$G\alpha_{o}^{fl/fl}$ mice; group sizes ranged from 11 to 12 cells (4 mice) per genotype. There were no differences in Ado-induced current density (t_{13} = 0.1, P = 0.91; unpaired t test) or desensitization (t_{13} = 0.7, P = 0.51; unpaired t test) in SAN cells from SLNCre(−):$G\alpha_{i2}^{fl/fl}$ and SLNCre(+):$G\alpha_{i2}^{fl/fl}$ mice; group sizes ranged from 7 to 8 cells (3 mice) per genotype. (**I** and **J**) There was no difference in peak current density (t_{20} = 1.8, P = 0.08; unpaired t test) or desensitization (t_{21} = 0.9, P = 0.38; unpaired t test) of Ado-induced currents in SAN cells from SLNCre(−):$G\alpha_{o}^{fl/fl}$ and SLNCre(+):$G\alpha_{o}^{fl/fl}$ mice; group sizes ranged from 11 to 12 cells (4 mice) per genotype. There was an increase in activation rate (t_{13} = 2.2, *P < 0.05; unpaired t test) of Ado-induced currents in SAN cells from SLNCre(+):$G\alpha_{i2}^{fl/fl}$ mice as compared to SLNCre(−):$G\alpha_{i2}^{fl/fl}$ littermates. There was no difference in deactivation rate (t_{12} = 0.08, P = 0.94; unpaired t test) of Ado-induced currents in SAN cells from SLNCre(−):$G\alpha_{i2}^{fl/fl}$ and SLNCre(+):$G\alpha_{i2}^{fl/fl}$ mice; group sizes ranged from 7 to 8 cells (3 mice) per genotype.

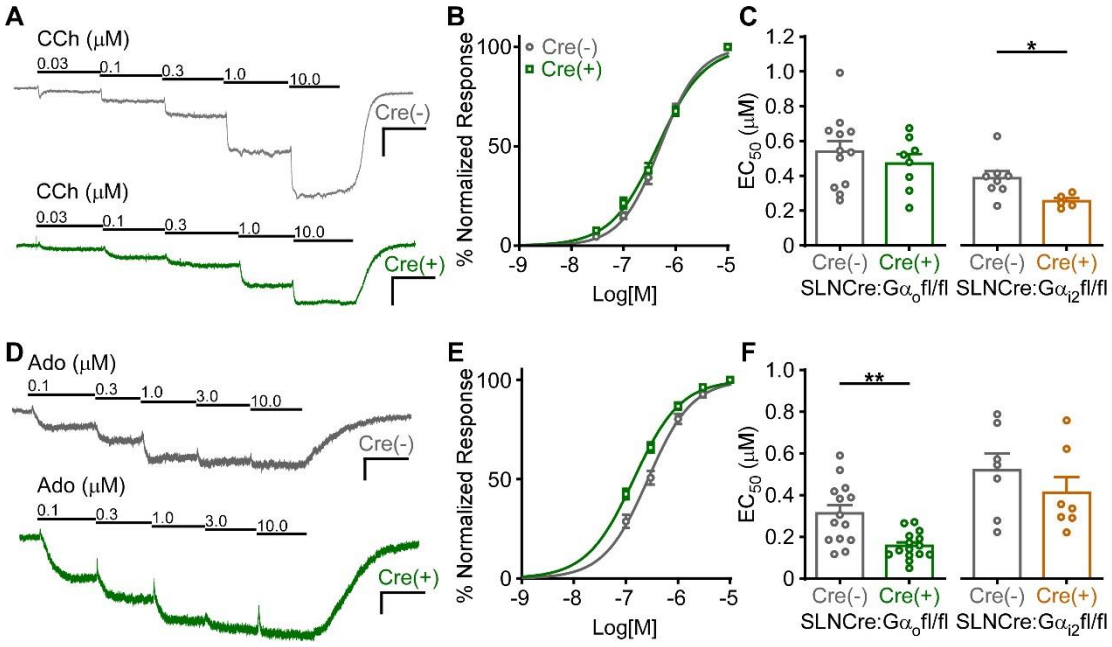

Figure 5.8. Impact of $G\alpha_o$ or $G\alpha_{i2}$ ablation on GIRK channel sensitivity to CCh and Ado.

(**A**) Concentration-response experiments of CCh-induced currents in SAN cells from SLNCre(−):$G\alpha_o^{fl/fl}$ (Top) and SLNCre(+):$G\alpha_o^{fl/fl}$ (Bottom) mice. (**B**) Summary of CCh sensitivity experiments in SAN cells from SLNCre(−):$G\alpha_o^{fl/fl}$ and SLNCre(+):$G\alpha_o^{fl/fl}$ mice. (**C**) There was no difference in EC_{50} values of CCh-induced GIRK currents in SAN cells from SLNCre(−):$G\alpha_o^{fl/fl}$ (n = 12 cells/3 mice) and SLNCre(+):$G\alpha_o^{fl/fl}$ (n = 8 cells/3 mice) mice (t_{18} = 0.8, P = 0.44; unpaired t test), but there was a decrease in the EC_{50} value in SAN cells from SLNCre(+):$G\alpha_{i2}^{fl/fl}$ (n = 5 cells/3 mice) compared to SLNCre(−):$G\alpha_{i2}^{fl/fl}$ (n = 8 cells/3 mice) mice (t_{11} = 2.5, *P < 0.05; unpaired t test). (**D**) Concentration-response experiments of Ado-induced GIRK currents in SAN cells from SLNCre(−):$G\alpha_o^{fl/fl}$ (Top) and SLNCre(+):$G\alpha_o^{fl/fl}$ (Bottom) mice. (**E**) Summary of concentration-response experiments of Ado-induced GIRK currents in SAN cells from SLNCre(−):$G\alpha_o^{fl/fl}$ and SLNCre(+):$G\alpha_o^{fl/fl}$ mice. (**F**) The EC_{50} value for Ado-induced signaling in SAN cells from SLNCre(+):$G\alpha_o^{fl/fl}$ (n = 15 cells/3 mice) mice was lower than that measured in SAN cells from SLNCre(−):$G\alpha_o^{fl/fl}$ (n = 12 cells/3 mice) mice (t_{25} = 3.3, **P < 0.01; unpaired t test), but there was no difference in EC_{50} value in SAN cells from SLNCre(−):$G\alpha_{i2}^{fl/fl}$ (n = 7 cells/3 mice) and SLNCre(+):$G\alpha_{i2}^{fl/fl}$ (n = 7 cells/3 mice) mice (t_{12} = 1.0, P = 0.35; unpaired t test).

5.4 Discussion

While M_2R and A_1R signal to a shared pool of GIRK channels in mouse SAN cells, the amplitude and kinetics of these signaling pathways are distinct. RGS6 exerts a GPCR dependent influence on GIRK-dependent signaling in mouse SAN cells, modulating the sensitivity and kinetics of M_2R-GIRK signaling, and the amplitude of A_1R-GIRK signaling. Innate GPCR-G protein coupling preferences appear to contribute to the distinctions in M_2R- and A_1R GIRK signaling pathways in SAN cells. Our data suggest that $G\alpha_o$ plays a more important role in mediating M_2R-GIRK than A_1R-GIRK signaling in mouse SAN cells. This, together with the strong $G\alpha_o$ substrate preference of RGS6, provides a plausible explanation for the GPCR dependent influence of RGS6 on GIRK-dependent signaling in mouse SAN cells.

A_1R-GIRK responses are smaller than M_2R-GIRK responses in mouse SAN cells; parallel observations have been noted in mouse, rat, and guinea pig atrial myocytes (Bünemann and Pott, 1995; Cho, 2010; Wellner-Kienitz et al., 2000). A maximal M_2R-induced GIRK response completely occludes the A_1R-GIRK response in SAN cells, suggesting that M_2R activation can elicit a maximal GIRK-dependent response, while A_1R activation can only engage a fraction of available GIRK channels. Different levels of M_2R and A_1R expression likely contribute to the differences in response amplitudes and activation kinetics. Indeed, over-expression of A_1R in rat atrial myocytes increased Ado-induced GIRK currents and accelerated current activation rate (Kienitz et al., 2011). Thus, the level of A_1R and/or G protein intermediate appears to limit A_1R-GIRK signaling amplitude in mouse SAN cells.

Considering the GAP activity of RGS6, *Rgs6* ablation should result in increased steady-state levels of activated $G\alpha_o$ (and $G\beta\gamma$) following M_2R and A_1R activation. Indeed, A_1R-GIRK response amplitudes were enhanced by Rgs6 ablation without up-regulation of

A_1R or GIRK channels. Thus, the amplitude of A_1R-GIRK signaling in mouse SAN cells is likely limited by the amount of activated G protein released by A_1R activation. Interestingly, loss of RGS6 had no impact on CCh-induced GIRK current amplitude, suggesting that the GIRK channel limits the M_2R-GIRK responses in these cells, a contention supported by our occlusion data. The enhanced sensitivity of GIRK channels to CCh in SAN cells from *Rgs6*$^{-/-}$ mice further suggests that the loss of RGS6 effectively increases the fraction of spare M_2R receptors in these cells. Interestingly, we recently reported an increase in M_2R-GIRK current amplitude in ventricular myocytes from *Rgs6*$^{-/-}$ mice, where expression M_2R is lower than in the atria (Anderson et al., 2018) (**Chapter 3**). Thus, RGS6 may impact GPCR-effector response amplitudes when the level of G protein, rather than effector, is limiting.

RGS proteins may also facilitate GIRK-dependent signaling in a GAP-independent manner. Mice heterozygous for an RGS-insensitive $G\alpha_o$, for example, exhibit blunted GIRK channel responses to mu opioid receptor (MOR) activation in some neurons (Anderson et al., 2018) (**Chapter 3**), suggesting that RGS proteins promote MOR-GIRK coupling. Notably, we observed a modest decrease in GIRK currents elicited by the GIRK channel activator ML297 in SAN cells from *Rgs6*$^{-/-}$ mice. Thus, RGS6 may facilitate efficient GIRK channel signaling in SAN cells, perhaps via physical interaction (Xie et al., 2010). The increase in A_1R-GIRK channel signaling seen with *Rgs6* ablation, however, suggests that this is not the main influence of RGS6 in SAN cells. Other work has called attention to the role of adaptor proteins, including R7BP and GPR158, in fine-tuning the influence of RGS proteins (Anderson et al., 2009; Jayaraman et al., 2009; Orlandi et al., 2015; Ostrovskaya et al., 2018). While R7BP or GPR158 expression has not been observed in the heart (Grabowska et al., 2008; Orlandi et al., 2012), an unknown adaptor protein(s) may influence the impact of RGS6/Gβ5 on GIRK-dependent signaling in cardiomyocytes.

Previous work has implicated $G\alpha_o$ in the bradycardic effects of A_1R and M_2R activation. For example, isolated hearts from mice with a global knockout of $G\alpha_o$, but not $G\alpha_{i2}$ or $G\alpha_{i3}$, exhibited diminished CCh-induced bradycardia (Duan et al., 2007). Additionally, work with ESDCs showed that the reduction in isoproterenol-stimulated beating rate elicited by M_2R and A_1R activation was exaggerated in cells containing an RGS-insensitive version of $G\alpha_o$ (Fu et al., 2006). Our finding that $G\alpha_o$ is a critical mediator of M_2R-GIRK signaling in mouse SAN cells, and that *Rgs6* ablation enhances both M_2R- and A_1R-mediated bradycardia, are in line with these reports. Interestingly, the enhanced A_1R-induced suppression of isoproterenol stimulated beating rate seen in ESDCs harboring a RGS-insensitive $G\alpha_o$ mutant was not blunted by TTQ, suggesting that this effect of A_1R activation may not be GIRK-dependent (Fu et al., 2006).This contrasts with our finding that A_1R-mediated bradycardia is absent in *Girk4*$^{-/-}$ mouse hearts. These discrepancies likely arise from the different cell types and model systems employed, where the relative complements of GPCRs, G proteins, effectors, and RGS proteins may differ.

There is little consensus on relevance of $G\alpha_{i2}$ to HR regulation. Mice with a global deletion of $G\alpha_{i2}$ exhibited diminished CCh-induced bradycardia, and resting tachycardia (Zuberi et al., 2008). Mice harboring an RGS-insensitive $G\alpha_{i2}$ displayed enhanced M_2R-induced bradycardia, and the enhanced effect of CCh on beating rate of ESDCs harboring this mutation was reversed by TTQ (Fu et al., 2006). These findings are consistent with a prominent role for $G\alpha_{i2}$ in mediating M_2R-GIRK signaling in SAN cells. Atrial myocytes from mice lacking $G\alpha_{i2}$ exhibited increased CCh-induced GIRK responses, however, which was attributed to increased GIRK subunit expression (Nobles et al., 2018). Moreover, mice lacking $G\alpha_{i2}$ selectively in the cardiac conduction system exhibited resting tachycardia but normal CCh-induced bradycardia (Sebastian et al., 2013). Thus, the impact of $G\alpha_{i2}$ ablation and RGS-insensitive $G\alpha_{i2}$ on CCh-induced bradycardia is model-

dependent and may reflect an indirect (non-cardiac) influence of $G\alpha_{i2}$ on HR regulation. Additionally, the impact of $G\alpha_{i2}$ on resting HR may be exerted through GIRK-independent mechanisms (Ye et al., 1999). For example, M_2R activation inhibits the hyperpolarization activated channel (I_f) by suppressing AC activity and cAMP production (Dhein et al., 2001). Interestingly, M_2R-I_f coupling is more sensitive than M_2R-GIRK signaling in SAN cells (DiFrancesco et al., 1989). Our data show that $G\alpha_o$ plays a critical role in M_2R-GIRK signaling. This pathway is subject to negative regulation by RGS6 and may, therefore, only be engaged by strong parasympathetic activation. $G\alpha_{i2}$, which is less susceptible to the GAP activity of RGS6, may mediate M_2R-I_f coupling during periods of weaker parasympathetic activity.

It is important to recognize that genetic ablation of an individual $G\alpha$ isoform redirects signaling to residual G protein isoforms. Ablation of $G\alpha_o$, for example, routes M_2R-GIRK signaling through $G\alpha_i$. In our hands, this yielded small CCh-induced GIRK currents with slow activation rates, reminiscent of Ado-induced GIRK currents in wild-type SAN cells. In contrast, routing A_1R-GIRK signaling through $G\alpha_i$ had no impact on Ado-induced current amplitude or activation kinetics. $G\alpha_o$ ablation did increase the sensitivity of GIRK channels to Ado, suggesting that (residual) $G\alpha_i$ is more efficient than $G\alpha_o$ at mediating A_1R-GIRK signaling in mouse SAN cells. Similarly, $G\alpha_{i2}$ ablation increased the sensitivity of GIRK channels to CCh, suggesting that (residual) $G\alpha_o$ is a more efficient mediator than $G\alpha_{i2}$ of M_2R-GIRK signaling in mouse SAN cells. The modest overall impact of $G\alpha_{i2}$ ablation, particularly on A_1R-GIRK signaling, is likely attributable to the presence of residual $G\alpha_{i1}$ and $G\alpha_{i3}$ isoforms (Nobles et al., 2018). Indeed, this likely explains why there was no impact of global ablation of any single G protein isoform ($G\alpha_o$, $G\alpha_{i2}$, $G\alpha_{i1/3}$) on GIRK-dependent bradycardia elicited by the A_1R agonist 2-Chloro-N-cyclopentyladenosine (CCPA) (Sebastian et al., 2013).

Ado can provoke AF through shortening of the ERP, an effect thought to be mediated by GIRK channel activation in atrial myocytes (Layland et al., 2014). Enhanced A_1R and GIRK channel expression are associated with increased bradycardia in a tachypacing induced chronic heart failure model in dogs (Long et al., 2020). Moreover, AF induced by A_1R activation or M_2R activation (via vagal nerve stimulation) is thought to be mediated in part by GIRK channel activity (Hashimoto et al., 2006; Li et al., 2016). While loss of GIRK4 in mice conferred resistance to pacing induced AF (Kovoor et al., 2001), *Rgs6* ablation resulted in a higher incidence of AF induction (Posokhova et al., 2013). Similar to the impact of *Girk4* ablation, peptides targeting specific $G\alpha_i$ isoforms reduced AF susceptibility during vagal nerve stimulation in dogs (Aistrup et al., 2009). These and related observations, together with our results, show that interventions that suppress the influence of inhibitory G protein signaling in atria, by targeting signaling mediators and regulators, or effectors, could prove beneficial for treatment of certain arrhythmias and heart failure.

Insights gained in this study are likely to be relevant to the compartmentalization of GPCR-dependent signaling in other cell types, including neurons. GIRK channel regulation by inhibitory GPCRs has been implicated in neurological disorders including epilepsy, pain and analgesia, anxiety and depression, and addiction (Luján et al., 2014; Lüscher and Slesinger, 2010). Neuronal GIRK-dependent signaling pathways regulated by $GABA_BR$, $5\text{-}HT_{1A}R$ and A_1R exhibit distinct amplitude and kinetic profiles, and are differentially susceptible to plasticity (Chung et al., 2009; Leaney, 2003; Marron Fernandez de Velasco et al., 2017b; Nassirpour et al., 2010). Our previous work has highlighted the integral role of RGS7, another member for the R7 RGS family, in modulating the kinetics and sensitivity of $GABA_BR$-GIRK signaling in hippocampal neurons (Fajardo-Serrano et al., 2013; Ostrovskaya et al., 2014, 2018; Xie et al., 2010). Furthermore, RGS7 prefers $G\alpha_o$ over $G\alpha_i$ as a substrate for its GAP activity (Masuho et al., 2013). Thus, GPCR-G

protein and RGS-G protein substrate preferences likely shape neuronal GPCR-GIRK signaling dynamics in neurons and may help the functional compartmentalization of these signaling pathways.

Chapter 6

Discussion

6.1 Summary of Findings

The pathogenesis of various rhythm disorders, including bradyarrhythmias, AF, nodal dysfunction, can be linked to disturbances in parasympathetic signaling to the heart (Dobrev et al., 2005; Li et al., 2016; Stallmeyer et al., 2017). GIRK channels are critical downstream effectors of parasympathetic signaling to the heart, representing an essential regulator of cardiomyocyte excitability. Therefore, understanding the details and physiology of GIRK-dependent signaling in the heart may provide a promising new therapeutic strategy.

This dissertation comprehensively investigates GIRK-dependent signaling in the heart and addresses previous gaps in knowledge. In **Chapter 2**, I provide a thorough description of the overlooked GIRK channel signaling in mouse ventricular myocytes and use a novel transgenic mouse line, MLC2VCre:*Girk1*$^{fl/fl}$, to elucidate the role of GIRK channels in ventricular physiology. Using a similar approach, **Chapter 3** demonstrates that atrial/nodal GIRK channels mediate nearly all of the effects of direct VNS on HR dynamics and arrhythmogenesis. These findings, in conjunction with the existing literature, highlight the potential of selective GIRK channel targeting for the treatment of supraventricular arrhythmias. Thus, in **Chapter 4**, I characterized the novel GIRK channel inhibitor, VU0468554, which demonstrated promising selectivity for cardiac GIRK channels. Lastly, while the regulation of M_2R-GIRK dependent signaling in the heart has been well described, a concerted effort to characterize A_1R-GIRK signaling in the SAN is less well

known. Therefore, work in **Chapter 5** sought to expand our understanding of the molecular details of GIRK-dependent signaling in SAN cells by comparing A_1R-GIRK and M_2R-GIRK dependent signaling. Here, I found that distinct GPCR-G protein coupling preferences, in combination with a strong substrate preference by RGS6, resulted in intriguing GPCR-dependent biasing of GIRK-dependent signaling in SAN cells. As a whole, my thesis highlights new molecular and physiological insights into GIRK channels function in cardiac tissue that can be leveraged for the development of novel cardiac pharmacotherapies

6.1.1 Atrial GIRK channels as key mediators of parasympathetic signaling to the heart

The release of ACh from parasympathetic post-ganglionic nerve terminals onto cardiomyocytes activates muscarinic receptors, culminating in decreased HR, conduction velocity, and contraction. Indeed, mice lacking M_2R exhibit dramatic attenuation of the bradycardic response to cholinergic stimulation (Stengel et al., 2000). There are several ion channels downstream of M_2R that to mediate these effects, including I_f, I_{CaL}, and GIRK channels. Work from DiFrancesco and colleagues has highlighted a concentration-dependence in the actions of ACh in mammalian SAN cells, where low concentrations activate I_f and high concentrations activate GIRK channels (DiFrancesco et al., 1989). However, it is unclear how these findings translate to physiological contributions to HR slowing. Indirect pharmacological stimulation of the vagus nerve through the baroreflex results in bradycardia and an increase in HRV which is blunted about 50% in *Girk4*$^{-/-}$ mice (Wickman et al., 1998). These results, however, are confounded by both potential pharmacological off-target effects and the presence of GIRK4 in neuronal populations upstream cardiac vagal neurons in the brainstem.

My work in **Chapter 2** addressed these limitations through a combination of approaches involving direct VNS and a novel mouse line lacking GIRK channels

selectively in atrial/SAN tissue (SLNCre:*Girk1*$^{fl/fl}$) (**Figure 2.1**) (Lee et al., 2018). Using this approach, I found that atrial/nodal GIRK channels are the main mediator of VNS-induced slowing of HR and increased HRV (**Figure 2.4-2.5**) (Lee et al., 2018). Notably, both of these effects were not seen in the presence of atropine, confirming the dependence of these responses on muscarinic activation. These results suggest that, in contrast to previous findings which suggested approximately 50% contribution (Wickman et al., 1998), GIRK channels are the main mediators of the effects of direct VNS on HR dynamics (Lee et al., 2018) (**Chapter 2**). These results align with recent work, where the overexpression of HCN4 in mice did not impact VNS-induced bradycardia in the absence of sympathetic stimulation (Kozasa et al., 2018). Our convergent findings might be explained by indirect muscarinic inhibition of I_f, which relies on inhibition of AC to decrease intracellular cAMP. Perhaps the I_f current plays a larger role in vagal slowing during tonic sympathetic activity, and, therefore, may be a critical molecular mechanism underlying the interplay of autonomic signaling known as “accentuated antagonism.”

Work in **Chapter 2** also highlighted the role of GIRK channels in mediating the arrhythmogenic effects of VNS on the mouse heart. Indeed, mice lacking GIRK channels in the atria/SAN (either selectively or globally) are resistant to arrhythmias initiated through VNS (**Figure 2.6**) (Lee et al., 2018). These results align with previous mammalian studies in which the application of GIRK channel blockade terminates arrhythmias induced by VNS (Hashimoto et al., 2006). These findings, in combination with those of **Chapter 3**, further bolster the proposal that cardiac GIRK channels represent a promising therapeutic target for the treatment of related cardiac arrhythmias.

6.1.2 Unique properties of GIRK-dependent signaling in the mouse ventricle

Previously, the presence and relevance of GIRK channels in mammalian ventricular tissue was unclear. (**Table 1.1**). Using a multi-disciplinary approach, work in

Chapter 3 provided the field with much-needed clarity regarding GIRK-dependent signaling in the mouse ventricle. I showed that mRNA for both GIRK1 and GIRK4 (in addition to M_2R and RGS6) is indeed present in ventricular tissue (**Figure 3.1**) (Anderson et al., 2018), though at considerably lower levels when compared to atrial tissue. Furthermore, application of 100 μM CCh evoked inward currents in isolated mouse ventricular myocytes. These currents were absent in ventricular myocytes from *Girk1*$^{-/-}$ and *Girk4*$^{-/-}$ mice (**Figure 3.2**) (Anderson et al., 2018). These results demonstrate GIRK channels in the ventricle exhibit a similar subunit composition to that of SAN/atrial tissue.

Additionally, work in **Chapter 3** highlighted several distinct characteristics of ventricular GIRK channel signaling which differ from previous observations in SAN cells and atrial myocytes. Ventricular GIRK channels were approximately an order of magnitude less sensitive to muscarinic activation than those present in SAN cells; thus a 10-fold higher concentration was necessary to evoke maximal GIRK channel activation in ventricular myocytes (**Figure 3.2**) (Anderson et al., 2018). Additionally, maximal CCh-induced currents were significantly smaller and exhibited significantly slower activation and deactivation kinetics in comparison to maximal currents elicited in SAN cells in previous studies (**Figure 3.2**) (Anderson et al., 2018; Posokhova et al., 2010; Wydeven et al., 2014b). Moreover, RGS6 ablation resulted in a slight, yet significant increase in the amplitude of CCh-induced responses, yet no impact on kinetics or sensitivity (**Figure 3.2**) (Anderson et al., 2018). While lower expression levels may explain some of these differences, these results could also suggest that currently unknown distinctions in the underlying functional compartmentalization of related signaling components of GIRK-dependent signaling between the atria and ventricle.

6.1.3 Impact of GIRK-dependent signaling in the mouse ventricle

Previous work has highlighted the impact of muscarinic activation in ventricular tissue. Optical mapping and sharp electrode recordings in rodents have demonstrated that muscarinic activation shortens APD and ERP and lowers the RMP of ventricular tissue and papillary muscle (Liang et al., 2014). Indeed, application of CCh shortened APD and increased the rheobase of individual mouse ventricular myocytes (**Figure 3.3**) (Anderson et al., 2018). Furthermore, these effects were blunted in myocytes from *Girk4*$^{-/-}$ mice, suggesting that GIRK channels mediate these effects, at least in part (**Figure 3.3**) (Anderson et al., 2018). To elucidate how GIRK channels contribute to general ventricular physiology, we developed the ventricular-specific GIRK knockout line (**Figure 3.4**) (Anderson et al., 2018). This selective knockout circumvents potential confounds due to differences in HR in constitutive *Girk*$^{-/-}$ mice (Wickman et al., 1998). Mice with ventricular GIRK ablation retain HR and HRV responses to muscarinic activation (**Figure 3.5-3.7**) (Anderson et al., 2018). ECG recordings from anesthetized MLC2VCre(+):*Girk1*$^{fl/fl}$ mice revealed no QT interval prolongation either at baseline or after CCh injection when compared to Cre(-) counterparts (**Supplementary Table 3.S1**). Additionally, I observed no increase in pacing-induced VT/VF in either global or ventricular specific GIRK channel ablation. Together, my findings suggest the loss of GIRK channel activity in ventricular tissue does not increase the risk of ventricular arrhythmogenesis (**Figure 3.8**) (Anderson et al., 2018). These results indicate that therapeutic interventions targeting GIRK channels in the context of supraventricular arrhythmias would not promote new arrhythmias in the ventricles, making cardiac GIRK channels a safer therapeutic target.

6.1.4 Characterization of novel GIRK1/4 selective inhibitor

Chapters 2 and **3**, in conjunction with previous literature, support inhibiting GIRK channel activity to treat supraventricular arrhythmias. However, GIRK channels are

prominently expressed through the CNS and represent critical mediators of neuronal inhibition (Mayfield et al., 2015). Therefore, therapeutic interventions leveraging GIRK channel activity to treat cardiac arrhythmias would, ideally, be selective for cardiac GIRK channels to avoid unwanted CNS-mediated side-effects. Accordingly, work in **Chapter 4** characterized the novel GIRK1-selective inhibitor, VU0468554. This novel inhibitor displays a significantly more efficacious block of GIRK-dependent currents in SAN cells in comparison to neuronal counterparts (~70% vs. ~20%) (**Figure 4.2**). Notably, no impact of VU0468554 was observed on the holding current of SAN cells isolated from *Girk1*$^{-/-}$ mice, suggesting that VU0468554-mediated inhibition is GIRK1-dependent (**Figure 4.3**). Concentration-response experiments revealed that the mechanism of inhibition of $G\beta\gamma$-activated GIRK currents by VU0468554 is likely "un-competitive" and, therefore, may have a greater affinity for the GIRK channel:$G\beta\gamma$ complex (**Figure 4.4**). Furthermore, VU0468554 blockade of cardiac GIRK channel activity resulted in a modest, yet significant reversal of muscarinic-induced bradycardia (**Figure 4.5**). Altogether, VU0468554 represents a novel GIRK1/4 selective inhibitor with potential therapeutic utility.

6.1.5 Intrinsic differences in A_1R-GIRK and M_2R-GIRK dependent signaling in mouse SAN cells

RGS proteins, namely RGS6, play a negative regulatory role in modulating M_2R-GIRK signaling (Stewart et al., 2012; Wydeven et al., 2014b; Yang et al., 2010a). In addition to M_2R activation, GIRK channels are also activated by other GPCRs, including A_1R. While A_1R and M_2R both signal through GIRK channels, these signaling pathways have unique regulation and underlying signaling components. For example, Ado-induced currents were smaller and uniquely regulated by G_q-coupled receptors, when compared to ACh-activated GIRK currents (Cho, 2010). Additionally, work with RGS-insensitive EDSCs and mice suggested that M_2R- and A_1R-GIRK signaling may utilize different G

proteins (Fu et al., 2006). Therefore, **Chapter 5** sought to expand and clarify the details of A_1R-GIRK and M_2R-GIRK signaling in SAN cells (Anderson et al., 2020). Ado-induced currents displayed smaller currents with slower activation and smaller deactivation currents than CCh-induced currents (**Figure 5.1**) (Anderson et al., 2020), similar to previous observations in atrial myocytes (Cho, 2010). Furthermore, I identified a striking difference between the regulation of A_1R-GIRK signaling and M_2R-GIRK signaling by RGS6. Genetic ablation of RGS6 resulted in enhanced Ado-induced current amplitudes, yet did not impact kinetics or sensitivity of Ado responses. These observations contrast with previous work, which demonstrated prolonged deactivation kinetics and enhanced channel sensitivity to CCh-induced currents in SAN cells from *Rgs6*$^{-/-}$ mice (Posokhova et al., 2010; Wydeven et al., 2014b). These observations were replicated in this study (**Figures 5.1** & **5.2**) (Anderson et al., 2020). These differences translated to enhancements in the efficacy of A_1R-GIRK mediated bradycardia and in the potency of M_2R-GIRK mediated bradycardia upon RGS6 ablation (**Figure 5.3**) (Anderson et al., 2020). Altogether, these results highlight that while A_1R and M_2R utilize the same effector, *i.e.,* GIRK channels, differences in signaling characteristics and regulation suggest potential divergences in the underlying signaling architecture.

6.1.6 GPCR and RGS G protein preferences bias signaling to GIRK channels in mouse SAN cells

Accordingly, further work in **Chapter 5** strove to elucidate the fundamental distinctions in A_1R-GIRK and M_2R-GIRK signaling and regulation in the SA node. Initial occlusion work revealed that A_1R and M_2R do indeed appear to signal through the same population of GIRK channels, albeit to differing extents (**Figure 5.4**) (Anderson et al., 2020). Moreover, removal of RGS6 resulted in near occlusion of the M_2R response by Ado. This suggests RGS6 normally restricts A_1R-GIRK signaling (**Figure 5.4**) (Anderson

et al., 2020). Additional work in HEK cells utilizing a BRET based assay revealed overlapping yet distinct preferences in the inhibitory G protein isoforms utilized by M_2R and A_1R. While A_1R displayed no discrimination between $G\alpha_o$ and $G\alpha_i$, M_2R exhibited a clear preference for $G\alpha_o$ over $G\alpha_i$ (**Figure 5.5**) (Anderson et al., 2020). Furthermore, additional work in the BRET assay revealed that $G\alpha_o$ is the preferred substrate for the GAP activity of RGS6 (**Figure 5.6**) (Anderson et al., 2020). To assess whether these differences translated to differences in M_2R- and A_1R-GIRK signaling directly in SAN cells, we developed novel mouse lines (SLNCre:$G\alpha_o^{fl/fl}$ and SLNCre:$G\alpha_{i2}^{fl/fl}$) with selective ablation of either $G\alpha_o$ or $G\alpha_{i2}$. Thus, the removal of either $G\alpha_o$ or $G\alpha_{i2}$ redirects GIRK-dependent signaling through the remaining $G_{i/o}$ isoforms (**Figure 5.7 & 5.8**) (Anderson et al., 2020). $G\alpha_{i2}$ ablation resulted in a minimal impact on M_2R-GIRK and A_1R-GIRK signaling in SAN cells. In contrast, $G\alpha_o$ ablation decreased the amplitude and slowed the kinetics of M_2R-GIRK responses, while enhancing the sensitivity and prolonging the deactivation rate of A_1R-GIRK signaling (**Figure 5.7 & 5.8**) (Anderson et al., 2020). Altogether, these results suggest that the substrate preference for $G\alpha_o$ by RGS6 uniquely biases the signaling dynamics of A_1R-GIRK and M_2R-GIRK signaling due to underlying G protein preferences by each receptor. The work contained in **Chapter 5** not only adds to our understanding of G protein isoform involvement in the regulation of HR, but also highlights potential avenues of selectively targeting specific receptor/GIRK interactions which could be exploited therapeutically.

6.2 Future Directions

The work in this dissertation provides new molecular and physiological insights into GIRK-dependent signaling in the heart while also providing an initial characterization of a novel GIRK1/4 selective inhibitor. Future work could build upon the findings contained in this thesis to add to our understanding of the GIRK-dependent signaling as an extension of parasympathetic signaling to the heart.

6.2.1 GIRK channel involvement in therapeutic aspects of VNS

Work in **Chapter 2** describes how GIRK channels present in in the atria and SAN mediate nearly all of the effects of direct VNS in the heart on HR, HRV, and arrhythmogenesis. An important limitation of this study, however, is that these effects were only tested at one relatively high level of stimulation which resulted in approximately 40% reduction in HR (**Figure 2.4**) and provoked arrhythmias in 70% of wild-type mice (**Figure 2.6**) (Lee et al., 2018). An interesting follow-up study could involve an investigation into the level GIRK channel engagement in the therapeutic effects of low-level VNS. The literature has highlighted numerous, potentially therapeutic roles for low level VNS in cardiac disorders such as ventricular arrhythmias and heart failure (Wang et al., 2019). Chronic low-level VNS can suppress ventricular arrhythmias in canine models of myocardial infarction (Nasi-Er et al., 2019; Sun et al., 2020; Yu et al., 2016). Similar findings have been observed in rats, where chronic VNS reduced the susceptibility of pacing-induced ventricular arrhythmias in the isolated heart (Lee et al., 2016; Sabbah et al., 2011). Additionally, low-level VNS can mitigate the remodeling observed in mammalian models of heart failure (Zhou et al., 2019). Considering previous work demonstrating a concentration-dependent impact of ACh on the involvement of downstream effectors (DiFrancesco et al., 1989), it is possible that differing levels of VNS

could produce similar results. Therefore, future work is necessary to determine the level of GIRK involvement in the therapeutic effects of low-level VNS.

6.2.2 VU554 analogues in therapeutic settings

The characterization of the novel GIRK inhibitor VU0468554 in **Chapter 4** includes both *in vitro* work in native cell types expressing GIRK channels of distinct subunit compositions and *ex vivo* assessment of GIRK-dependent bradycardia in the isolated heart. While these *in vitro* and *ex vivo* results are promising, *in vivo* preclinical work is necessary to fully evaluate the therapeutic potential of VU0468554. This could involve an initial, *in vivo* assessment of the effect of VU0468554 on muscarinic-induced bradycardia in the anesthetized mouse using a similar experimental design to the isolated heart study in **Figure 4.4**. Preliminary pharmacokinetic analysis from mice injected with 3 mg/kg VU0468554 revealed a promising pharmacokinetic profile for *in vivo* work with a maximum whole blood concentration of 23.3 ng/mL at 15 min post-injection and a half-life of 23.5 min. Additional studies in related cardiac arrhythmia models could also include *Rgs6*$^{-/-}$ mice, which display both a resting bradycardia and enhanced HR slowing in response to CCh, likely due to enhanced GIRK-dependent signaling (Posokhova et al., 2013). Furthermore, *Rgs6*$^{-/-}$ mice are significantly more prone to pacing-induced AF (Posokhova et al., 2013). Thus, experiments finding VU0468554 blocks/ameliorates these effects in this mouse model of bradycardia and AF in either *ex vivo* or *in vivo* work could be particularly informative. Additional relevant models could include mouse models of sick sinus node dysfunction and heart block developed by Dr. Mangoni and colleagues (Mesirca et al., 2014, 2016b, 2016a). These include mice with non-functioning HCN4 (I_f) or mice with ablation of $I_{Ca,L1.3}$. In both models, genetic ablation of *Girk4* has been shown to restore normal sinus rhythm. Therefore, both models represent ideal opportunities for testing of the therapeutic potential of VU0468554. Given the critical role GIRK channels

play in mediating inhibitory signaling in the CNS (Mayfield et al., 2015), these studies could be complimented by an *in vivo* assessment of VU0468554 impact on GIRK-related behaviors such as fear learning and anxiety-related behaviors (Victoria et al., 2016; Wydeven et al., 2014a) to investigate the potential for unwanted side-effects.

6.2.3 Molecular details underlying GIRK-dependent signaling in the ventricle

In **Chapter 3**, we observed that GIRK currents evoked by muscarinic activation in the mouse ventricle are dependent on both GIRK1 and GIRK4, similar to previous observations in SAN cells and atrial myocytes. However, CCh-induced currents in mouse ventricular myocytes displayed several unique characteristics in comparison to CCh-induced responses in SAN cells (**Figure 6.1**) (Anderson et al., 2018, 2020). CCh-induced currents in ventricular myocytes were significantly smaller and exhibit slower activation and deactivation kinetics (**Figure 6.1**) (Anderson et al., 2018, 2020). Furthermore, GIRK channels in ventricular myocytes were significantly less sensitive to CCh compared to SAN counterparts (**Figure 6.1**) (Anderson et al., 2018, 2020). While differences in the expression levels between SAN/atrial and ventricular tissue could explain some of these findings (**Figure 3.1**) (Anderson et al., 2018), an intriguing follow-up study could involve probing the inhibitory G protein isoforms underlying ventricular GIRK-dependent signaling. Given insights revealed in **Chapter 5** (Anderson et al., 2020), it is possible that the smaller, slower CCh-induced responses present in ventricular myocytes are due to a lack of $G\alpha_o$ involvement in ventricular tissue. Indeed, transcriptional analysis of rat cardiac tissue revealed a 2.31 fold decrease in $G\alpha_{o1}$ in ventricular tissue as compared to atrial tissue (McGrath and de Bold, 2009) Furthermore, the impact of *Rgs6* ablation on M_2R-GIRK signaling in ventricular myocytes (**Figure 3.2**) (Anderson et al., 2018) and A_1R-GIRK signaling in SAN cells, which does not appear to significantly engage $G\alpha_o$, (**Figure 5.1**) (Anderson et al., 2020) are noticeably similar. These studies could involve novel mouse

lines with ventricular ablation of either $G\alpha_o$ or $G\alpha_{i2}$ to redirect GIRK-dependent signaling in the ventricle through remaining $G_{i/o}$ isoforms, similar to **Figure 5.7** and **Figure 5.8** (Anderson et al., 2020). Furthermore, these efforts could expand to assess A_1R-GIRK dependent signaling in the ventricular tissue, given that adenosine and muscarinic agonists exhibit similar effects APD and ERP in ventricular tissue (Liang et al., 2014).

Relatedly, future work could also expand our knowledge on the signaling details of GIRK-dependent signaling by additional GPCRs in SAN tissue. Sphingosine-1-phosphate (S1P), for example, is a unique lipid produced intracellularly that can act as a S1P receptor ($S1P_{1-5}$) ligand when transported outside of the cell (Jozefczuk et al., 2020). S1P receptor activation results in HR slowing, an effect attributed to cardiac GIRK channel activation (Koyrakh et al., 2005; OCHI et al., 2006). Intriguingly, previous occlusion studies in guinea pig atrial myocytes revealed that while ACh-induced activation of GIRK channels occludes S1P activation of GIRK, reversing the order of agonist application (S1P then S1P+ACh), does not result in complete occlusion (OCHI et al., 2006), similar to our findings with Ado and CCh in mouse SAN cells (**Figure 5.4**) (Anderson et al., 2020). Therefore, it is possible that similar differences uncovered in **Chapter 5** concerning A_1R- and M_2R-GIRK dependent signaling to GIRK channels may be at present with S1P-dependent signaling. Future work using similar approaches utilized in **Chapter 5** could yield new insights into S1P-GIRK channel signaling.

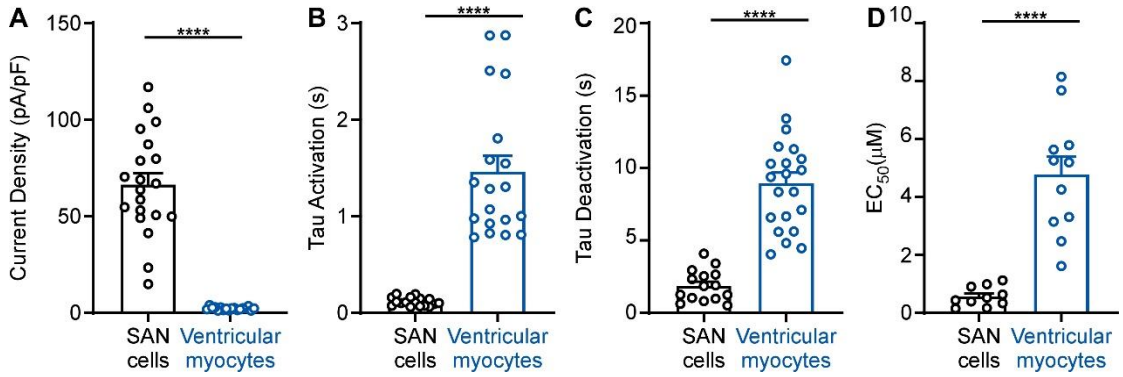

Figure 6.1. Comparison of CCh-induced currents in mouse SAN cells and ventricular myocytes.

Comparison of CCh-induced currents in SAN cells (10 μM) and ventricular myocytes (100 μM). Maximal amplitudes **(A)**, activation kinetics **(B)**, deactivation kinetics **(C)**, and sensitivity **(D)** of CCh-induced currents in SAN cells and ventricular myocytes analyzed using unpaired *t*-test with Welch's correction for unequal variances; ****$P<0.0001$

6.2.4 Implications for functional compartmentalization of neuronal GIRK signaling

As discussed in **Chapter 5**, a similar network of GPCR and RGS biases observed in GIRK-dependent signaling present in SAN cells may be present in neuronal GIRK channel signaling. RGS7, a member of the R7 RGS family along with RGS6, accelerates the kinetics and sensitivity of $GABA_BR$-GIRK dependent signaling in mouse HPC neurons, similar to the influence of RGS6 on M_2R-GIRK signaling in mouse SAN cells (Ostrovskaya et al., 2014, 2018; Xie et al., 2010). However, the influence of RGS7 on additional GPCR-GIRK signaling in HPC neurons, such as A_1R- and $5HT_{1A}R$-, remains unclear. Furthermore, the underlying $G_{i/o}$ isoforms which mediate signaling between various GPCR-GIRK signaling in HPC neurons are currently unknown.

As a follow-up to our findings in **Chapter 5**, I performed preliminary investigations to assess the contribution of $G\alpha_o$, the preferred substrate of RGS7 (Masuho et al., 2013), to $GABA_BR$-, A_1R-, and 5HTR-GIRK dependent signaling in HPC neurons. These efforts included a viral-Cre approach in cultured HPC neurons from neonatal $G\alpha_o^{fl/fl}$ mice (**Figure 6.2**). I found that viral ablation of $G\alpha_o$ from HPC neurons resulted in a significant reduction in the current amplitude and desensitization of maximal baclofen- and 5HT- evoked responses. In contrast, no impact was seen on maximal Ado-induced response amplitudes or desensitization (**Figure 6.2**). Similarly, the activation kinetics of $GABA_BR$-and 5HTR-GIRK responses where significantly prolonged, while A_1R-GIRK current activation kinetics were not impacted (**Figure 6.2**). Intriguingly, the deactivation kinetics of all three responses (baclofen, Ado, and 5HT) were all delayed upon removal of $G\alpha_o$ (**Figure 6.2**). I observed an increase in sensitivity of A_1R-GIRK responses (**Figure 6.3**), similar to findings in **Chapter 5**. Additionally, I observed a minimal, yet significant impact on 5HTR-GIRK sensitivity but no impact on $GABA_BR$-GIRK sensitivity (**Figure 6.3**). As a whole, these results would suggest that GPCR/G protein biases are likely present in neuronal GIRK-dependent signaling. Furthermore, these biases may be influenced by RGS7, which

has a substrate preference for $G\alpha_o$. Future work involving occlusion studies and recordings in HPC neurons from *Rgs7*$^{-/-}$ mice could further elucidate the underlying GIRK channel signaling architecture.

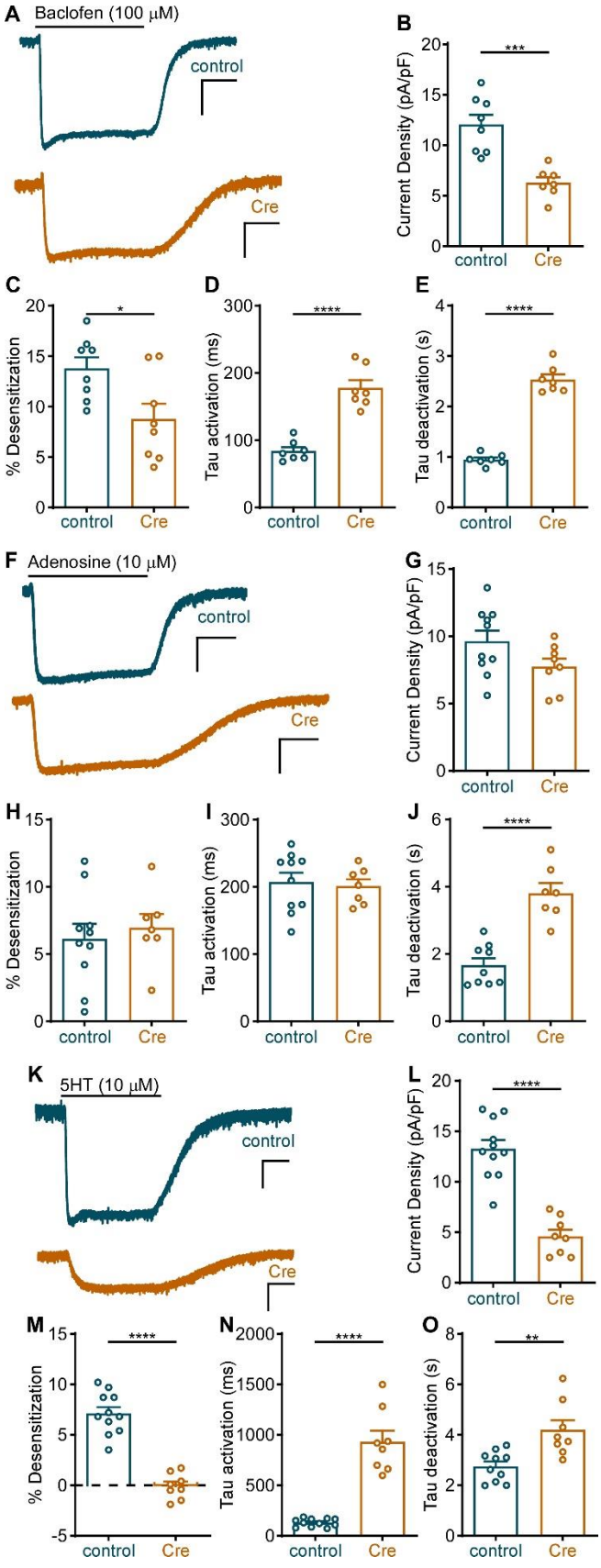
A
Baclofen (100 μM)
control
Cre
B
Current Density (pA/pF)
***
control
Cre
C
% Desensitization
*
D
Tau activation (ms)
****
E
Tau deactivation (s)
****
F
Adenosine (10 μM)
G
H
I
J
K
5HT (10 μM)
L
M
N
O
**

Figure 6.2. Impact of $G\alpha_o$ ablation on maximal agonist-induced GIRK currents in cultured HPC neurons.
Maximal-agonist induced currents in cultured HPC neurons from $G\alpha_o^{fl/fl}$. Cultured HPC neurons were infected with either a control virus (AAV8-CaMKIIa-mCherry-ΔCre) or a Cre expressing virus (AAV8-CaMKIIa-mCherry-Cre) **(A**, **F**, and **K).** Representative currents from baclofen (100 μM), Ado (10 μM), and 5HT (10 μM) in control-infected and Cre-infected HPC neurons (Scale bars: 5 s, 500 pA). Maximal agonist-induced current amplitudes **(B**, **G**, and **L)**, desensitization **(C**, **H** and **M),** activation kinetics **(D**, **I**, and **N)**, deactivation kinetics **(E**, **J**, and **O)**. Data analyzed using unpaired *t*-test; **P*<0.05, ***P*<0.01, ****P*<0.001, and *****P*<0.0001, respectively.

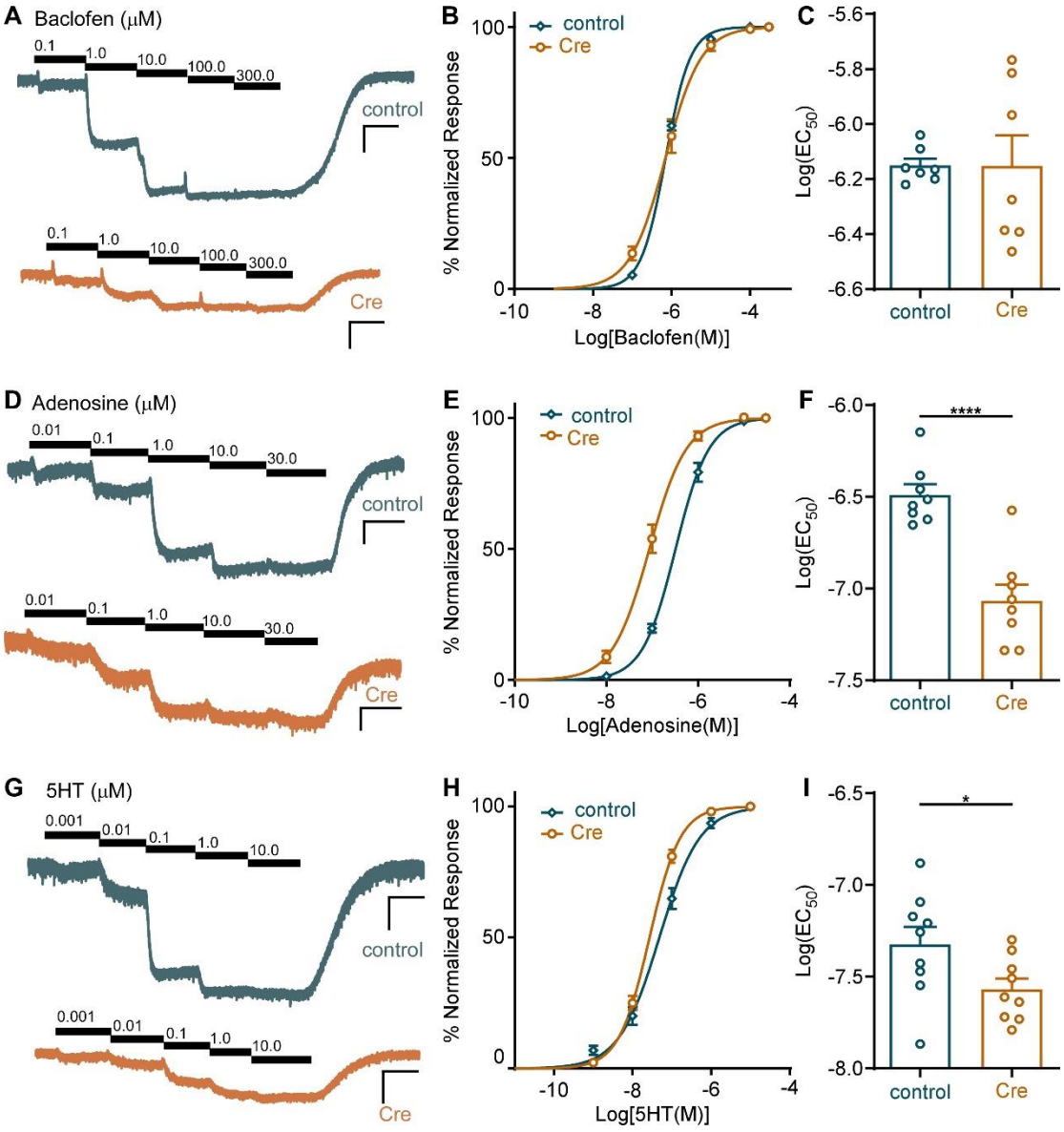

Figure 6.3. Impact of $G\alpha_o$ ablation on GIRK channel sensitivity to $GABA_BR$, A_1R, and 5HTR activation.

Cultured HPC neurons were infected with either a control virus (AAV8-CaMKIIa-mCherry-ΔCre) or a virus expressing Cre (AAV8-CaMKIIa-mCherry-Cre). **(A**, **D**, and **G)** Representative concentration-response experiments of baclofen-, Ado-, and 5HT-induced currents in control-infected and Cre-infected HPC neurons. **(B**, **E**, and **H)** Summary of concentration-response experiments **(B**, **E**, and **H)** and Log(EC_{50}) values **(C**, **F**, and **I)**. Data analyzed using unpaired t-test; **P*<0.05 and *****P*<0.0001, respectively.

6.3 Concluding Thoughts

In conclusion, the work contained in this thesis provides comprehensive insights into the physiological roles of GIRK-dependent signaling in the heart. While GIRK channels play an integral part in mediating parasympathetic regulation of HR dynamics via the vagus nerve (**Chapter 2**), loss of GIRK channel activity does not appear to increase the susceptibility to ventricular disorders (**Chapter 3**). Accordingly, this work includes the characterization a novel GIRK channel inhibitor that displays promising selectivity for cardiac GIRK channels over neuronal GIRK channels, which has important therapeutic implications (**Chapter 4**). Lastly, work in **Chapter 5** expanded on previous understandings of GIRK-dependent signaling in SAN cells to reveal an intricate network of underlying G protein biases and substrate preferences which shape GIRK-signaling dynamics. Altogether, cardiac GIRK channels and related signaling elements represent an attractive therapeutic target for the development of efficacious and safe treatments for cardiac arrhythmias.

Bibliography

Aistrup, G. L., Villuendas, R., Ng, J., Gilchrist, A., Lynch, T. W., Gordon, D., et al. (2009). Targeted G-protein inhibition as a novel approach to decrease vagal atrial fibrillation by selective parasympathetic attenuation. *Cardiovasc. Res.* 83, 481–92. doi:10.1093/cvr/cvp148.

Aksu, T., Guler, T. E., Yalin, K., Mutluer, F. O., Ozcan, K. S., and Calò, L. (2018). Catheter ablation of bradyarrhythmia: From the beginning to the future. *Am. J. Med. Sci.* 355, 252–265. doi:10.1016/j.amjms.2017.11.016.

Alboni, P., Holz, A., and Brignole, M. (2013). Vagally mediated atrioventricular block: Pathophysiology and diagnosis. *Heart* 99, 904–908. doi:10.1136/heartjnl-2012-303220.

AlMahameed, S. T., and Ziv, O. (2019). Ventricular arrhythmias. *Med. Clin. North Am.* 103, 881–895. doi:10.1016/j.mcna.2019.05.008.

Al-Zaiti, S., and Magdic, K. (2016) Paroxysmal supraventricular tachycardia: pathophysiology, diagnosis, and management. *Crit Care Nurs Clin North Am*. 3, 309-16. doi: 10.1016/j.cnc.2016.04.005.

Anderson, A., Kulkarni, K., Marron Fernandez de Velasco, E., Carlblom, N., Xia, Z., Nakano, A., et al. (2018). Expression and relevance of the G protein-gated K+ channel in the mouse ventricle. *Sci. Rep.* 8, 1192. doi:10.1038/s41598-018-19719-x.

Anderson, A., Masuho, I., Marron Fernandez de Velasco, E., Nakano, A., Birnbaumer, L., Martemyanov, K. A., et al. (2020). GPCR-dependent biasing of GIRK channel signaling dynamics by RGS6 in mouse sinoatrial nodal cells. *Proc. Natl. Acad. Sci.* 117, 202001270. doi:10.1073/pnas.2001270117.

Anderson, G. R., Posokhova, E., and Martemyanov, K. A. (2009). The R7 RGS protein family: Multi-subunit regulators of neuronal G protein signaling. *Cell Biochem. Biophys.* 54, 33–46. doi:10.1007/s12013-009-9052-9.

Andresen, M. C., and Kunze, D. L. (1994). Nucleus tractus solitarius—Gateway to neural circulatory control. *Annu. Rev. Physiol.* 56, 93–116. doi:10.1146/annurev.ph.56.030194.000521.

Ang, R., Abramowitz, J., Birnbaumer, L., Gourine, A. V., and Tinker, A. (2016). The role of GαO-mediated signaling in the rostral ventrolateral medulla oblongata in cardiovascular reflexes and control of cardiac ventricular excitability. *Physiol. Rep.* 4. doi:10.14814/phy2.12860.

Anumonwo, J. M. B., and Lopatin, A. N. (2010). Cardiac strong inward rectifier potassium channels. *J. Mol. Cell. Cardiol.* 48, 45–54. doi:10.1016/j.yjmcc.2009.08.013.

Bagliani, G., Della Rocca, D. G., De Ponti, R., Capucci, A., Padeletti, M., and Natale, A. (2018). Ectopic beats: Insights from timing and morphology. *Card. Electrophysiol. Clin.* 10, 257–275. doi:10.1016/j.ccep.2018.02.013.

Balse, E., and Eichel, C. (2018). “The cardiac sodium channel and its protein partners,” in *Handbook of Experimental Pharmacology* (Springer New York LLC), 73–99. doi:10.1007/164_2017_45.

Beaumont, E., Southerland, E. M., Hardwick, J. C., Wright, G. L., Ryan, S., Li, Y., et al. (2015). Vagus nerve stimulation mitigates intrinsic cardiac neuronal and adverse myocyte remodeling postmyocardial infarction. *Am. J. Physiol. - Hear. Circ. Physiol.* 309, H1198–H1206. doi:10.1152/ajpheart.00393.2015.

Beckmann, C., Rinne, A., Littwitz, C., Mintert, E., Bösche, L. I., Kienitz, M.-C., et al.

(2008). G protein-activated (GIRK) current in rat ventricular myocytes is masked by constitutive inward rectifier current. *Cell. Physiol. Biochem.* 21, 259–268. doi:10.1159/000129381.

Belardinelli, L., Giles, W. R., and West, A. (1988). Ionic mechanisms of adenosine actions in pacemaker cells from rabbit heart. *J. Physiol.* 405, 615–33. doi:10.1113/jphysiol.1988.sp017352.

Bender, K., Nasrollahzadeh, P., Timpert, M., Liu, B., Pott, L., and Kienitz, M.-C. (2008). A role for RGS10 in β-adrenergic modulation of G-protein-activated K^+ (GIRK) channel current in rat atrial myocytes. *J. Physiol.* 586, 2049–2060. doi:10.1113/jphysiol.2007.148346.

Bender, K., Wellner-Kienitz, M. C., Inanobe, A., Meyer, T., Kurachi, Y., and Pott, L. (2001). Overexpression of monomeric and multimeric GIRK4 subunits in rat atrial myocytes removes fast desensitization and reduces inward rectification of muscarinic K(+) current (I(K(ACh))). Evidence for functional homomeric GIRK4 channels. *J. Biol. Chem.* 276, 28873–80. doi:10.1074/jbc.M102328200.

Berlin, S., Tsemakhovich, V. A., Castel, R., Ivanina, T., Dessauer, C. W., Keren-Raifman, T., et al. (2011). Two distinct aspects of coupling between Gα i protein and G protein-activated K + channel (GIRK) revealed by fluorescently labeled Gα i3 protein subunits. *J. Biol. Chem.* 286, 33223–33235. doi:10.1074/jbc.M111.271056.

Bettahi, I., Marker, C. L., Roman, M. I., and Wickman, K. (2002). Contribution of the Kir3.1 subunit to the muscarinic-gated atrial potassium channel I_{KACh}. *J. Biol. Chem.* 277, 48282–48288. doi:10.1074/jbc.M209599200.

Bhave, G., Lonergan, D., Chauder, B. A., and Denton, J. S. (2010). Small-molecule modulators of inward rectifier K+ channels: Recent advances and future possibilities. *Future Med. Chem.* 2, 757–774. doi:10.4155/fmc.10.179.

Bibevski, S., and Dunlap, M. E. (2011). Evidence for impaired vagus nerve activity in heart failure. *Heart Fail. Rev.* 16, 129–35. doi:10.1007/s10741-010-9190-6.

Bigger, J. T., Fleiss, J. L., Steinman, R. C., Rolnitzky, L. M., Kleiger, R. E., and Rottman, J. N. (1992). Frequency domain measures of heart period variability and mortality after myocardial infarction. *Circulation* 85, 164–171. doi:10.1161/01.CIR.85.1.164.

Blomquist, T. M., Priola, D. V., and Romero, A. M. (1987). Source of intrinsic innervation of canine ventricles: A functional study. *Am. J. Physiol. - Hear. Circ. Physiol.* 252. doi:10.1152/ajpheart.1987.252.3.h638.

Blumer, J. B., Cismowski, M. J., Sato, M., and Lanier, S. M. (2005). AGS proteins: Receptor-independent activators of G-protein signaling. *Trends Pharmacol. Sci.* 26, 470–476. doi:10.1016/j.tips.2005.07.003.

Blumer, J. B., and Lanier, S. M. (2014). Activators of g protein signaling exhibit broad functionality and define a distinct core signaling triad. *Mol. Pharmacol.* 85, 388–396. doi:10.1124/mol.113.090068.

Bodi, I., Mikala, G., Koch, S. E., Akhter, S. A., and Schwartz, A. (2005). The L-type calcium channel in the heart: The beat goes on. *J. Clin. Invest.* 115, 3306–3317. doi:10.1172/JCI27167.

Boukens, B. J., Rivaud, M. R., Rentschler, S., and Coronel, R. (2014). Misinterpretation of the mouse ECG: “Musing the waves of Mus musculus.” *J. Physiol.* 592, 4613–4626. doi:10.1113/jphysiol.2014.279380.

Boyett, M. R., Kirby, M. S., Orchard, C. H., and Roberts, A. (1988). The negative inotropic effect of acetylcholine on ferret ventricular myocardium. *J. Physiol.* 404, 613–635. doi:10.1113/jphysiol.1988.sp017309.

Breitwieser, G. E., and Szabo, G. (1985). Uncoupling of cardiac muscarinic and β-adrenergic receptors from ion channels by a guanine nucleotide analogue. *Nature* 317, 538–540. doi:10.1038/317538a0.

Bukiya, A. N., Osborn, C. V., Kuntamallappanavar, G., Toth, P. T., Baki, L., Kowalsky, G., et al. (2015). Cholesterol increases the open probability of cardiac KACh currents. *Biochim. Biophys. Acta - Biomembr.* 1848, 2406–2413. doi:10.1016/j.bbamem.2015.07.007.

Bukiya, A. N., and Rosenhouse-Dantsker, A. (2017). Synergistic activation of G protein-gated inwardly rectifying potassium channels by cholesterol and PI(4,5)P 2. *Biochim. Biophys. Acta - Biomembr.* 1859, 1233–1241. doi:10.1016/j.bbamem.2017.03.023.

Bünemann, M., and Pott, L. (1995). Down-regulation of A1 adenosine receptors coupled to muscarinic K^+ current in cultured guinea-pig atrial myocytes. *J. Physiol.* 482 (Pt 1), 81–92. doi:10.1113/jphysiol.1995.sp020501.

Calloe, K., Goodrow, R., Olesen, S.-P., Antzelevitch, C., and Cordeiro, J. M. (2013). Tissue-specific effects of acetylcholine in the canine heart. *Am. J. Physiol. Circ. Physiol.* 305, H66–H75. doi:10.1152/ajpheart.00029.2013.

Calvillo, L., Vanoli, E., Andreoli, E., Besana, A., Omodeo, E., Gnecchi, M., et al. (2011). Vagal stimulation, through its nicotinic action, limits infarct size and the inflammatory response to myocardial Ischemia and reperfusion. *J. Cardiovasc. Pharmacol.* 58, 500–507. doi:10.1097/FJC.0b013e31822b7204.

Caulfield, M. P. (1993). Muscarinic receptors-characterization, coupling and function. *Pharmacol. Ther.* 58, 319–379. doi:10.1016/0163-7258(93)90027-B.

Cha, T. J., Ehrlich, J. R., Chartier, D., Qi, X. Y., Xiao, L., and Nattel, S. (2006). Kir3-based inward rectifier potassium current: Potential role in atrial tachycardia remodeling effects on atrial repolarization and arrhythmias. *Circulation* 113, 1730–1737. doi:10.1161/CIRCULATIONAHA.105.561738.

Chapleau, M. W., and Sabharwal, R. (2011). Methods of assessing vagus nerve activity and reflexes. *Heart Fail. Rev.* 16, 109–127. doi:10.1007/s10741-010-9174-6.

Charpentier, F., Mérot, J., Loussouarn, G., and Baró, I. (2010). Delayed rectifier K^+ currents and cardiac repolarization. *J. Mol. Cell. Cardiol.* 48, 37–44. doi:10.1016/j.yjmcc.2009.08.005.

Chatterjee, N. A., Chae, C. U., Kim, E., Moorthy, M. V., Conen, D., Sandhu, R. K., et al. (2017). Modifiable risk factors for incident heart failure in atrial fibrillation. *JACC Hear. Fail.* 5, 552–560. doi:10.1016/j.jchf.2017.04.004.

Chen, J., Kubalak, S. W., Minamisawa, S., Price, R. L., Becker, K. D., Hickey, R., et al. (1998). Selective requirement of myosin light chain 2v in embryonic heart function. *J. Biol. Chem.* 273, 1252–1256. doi:10.1074/jbc.273.2.1252.

Chen, P. S., and Tan, A. Y. (2007). Autonomic nerve activity and atrial fibrillation. *Hear. Rhythm* 4. doi:10.1016/j.hrthm.2006.12.006.

Chiou, C. W., Eble, J. N., and Zipes, D. P. (1997). Efferent vagal innervation of the canine atria and sinus and atrioventricular nodes: The third fat pad. *Circulation* 95, 2573–2584. doi:10.1161/01.CIR.95.11.2573.

Cho, H. (2010). Regulation of adenosine-activated GIRK channels by Gq-coupled receptors in mouse atrial myocytes. *Korean J. Physiol. Pharmacol.* 14, 145. doi:10.4196/kjpp.2010.14.3.145.

Cho, K.-I., Cha, T.-J., Lee, S.-J., Shim, I.-K., Zhang, Y. H., Heo, J.-H., et al. (2014). Attenuation of acetylcholine activated potassium current (I KACh) by simvastatin, not pravastatin in mouse atrial cardiomyocyte: possible atrial fibrillation preventing effects of statin. *PLoS One* 9, e106570. doi:10.1371/journal.pone.0106570.

Chugh, S. S., Reinier, K., Teodorescu, C., Evanado, A., Kehr, E., Al Samara, M., et al. (2008). Epidemiology of sudden cardiac death: clinical and research implications. *Prog. Cardiovasc. Dis.* 51, 213–228. doi:10.1016/j.pcad.2008.06.003.

Chung, H. J., Ge, W.-P., Qian, X., Wiser, O., Jan, Y. N., and Jan, L. Y. (2009). G protein-

activated inwardly rectifying potassium channels mediate depotentiation of long-term potentiation. *Proc. Natl. Acad. Sci. U. S. A.* 106, 635–40. doi:10.1073/pnas.0811685106.
Cifelli, C., Rose, R. A., Zhang, H., Voigtlaender-Bolz, J., Bolz, S.-S., Backx, P. H., et al. (2008). RGS4 regulates parasympathetic signaling and heart rate control in the sinoatrial node. *Circ. Res.* 103, 527–535. doi:10.1161/CIRCRESAHA.108.180984.
Cismowski, M. J., Takesono, A., Bernard, M. L., Duzic, E., and Lanier, S. M. (2001). Receptor-independent activators of heterotrimeric G-proteins. in *Life Sciences* (Elsevier Inc.), 2301–2308. doi:10.1016/S0024-3205(01)01019-0.
Coote, J. H. (2013). Myths and realities of the cardiac vagus. *J. Physiol.* 591, 4073–4085. doi:10.1113/jphysiol.2013.257758.
Coote, J. H., and Chauhan, R. A. (2016). The sympathetic innervation of the heart: Important new insights. *Auton. Neurosci. Basic Clin.* 199, 17–23. doi:10.1016/j.autneu.2016.08.014.
Corey, S., and Clapham, D. E. (1998). Identification of native atrial G-protein-regulated inwardly rectifying K^+ (GIRK4) channel homomultimers. *J. Biol. Chem.* 273, 27499–504. doi:10.1074/jbc.273.42.27499.
Corey, S., Krapivinsky, G., Krapivinsky, L., and Clapham, D. E. (1998). Number and stoichiometry of subunits in the native atrial G-protein-gated K^+ channel, IKACh. *J. Biol. Chem.* 273, 5271–8. doi:10.1074/jbc.273.9.5271.
Dahya, V., and Taigen, T. L. (2019). Pharmacologic and nonpharmacologic management of atrial fibrillation. *Med. Clin. North Am.* 103, 835–846. doi:10.1016/j.mcna.2019.04.004.
Dascal, N., Lim, N. F., Schreibmayer, W., Wang, W., Davidson, N., and Lester, H. A. (1993a). Expression of an atrial G-protein-activated potassium channel in Xenopus oocytes. *Proc. Natl. Acad. Sci. U. S. A.* 90, 6596–6600. doi:10.1073/pnas.90.14.6596.
Dascal, N., Schreibmayer, W., Lim, N. F., Wang, W., Chavkin, C., DiMagno, L., et al. (1993b). Atrial G protein-activated K^+ channel: expression cloning and molecular properties. *Proc. Natl. Acad. Sci. U. S. A.* 90, 10235–9. doi:10.1073/pnas.90.21.10235.
David Weaver, C. (2018). "Thallium flux assay for measuring the activity of monovalent cation channels and transporters," in *Methods in Molecular Biology* (Humana Press Inc.), 105–114. doi:10.1007/978-1-4939-7362-0_9.
De Biasi, M. (2002). Nicotinic mechanisms in the autonomic control of organ systems. *J. Neurobiol.* 53, 568–579. doi:10.1002/neu.10145.
Deng, W., Bukiya, A. N., Rodríguez-Menchaca, A. A., Zhang, Z., Baumgarten, C. M., Logothetis, D. E., et al. (2012). Hypercholesterolemia induces up-regulation of K_{ACh} cardiac currents via a mechanism independent of phosphatidylinositol 4,5-bisphosphate and Gβγ. *J. Biol. Chem.* 287, 4925–4935. doi:10.1074/jbc.M111.306134.
Dhein, S., van Koppen, C. J., and Brodde, O. E. (2001). Muscarinic receptors in the mammalian heart. *Pharmacol. Res.* 44, 161–82. doi:10.1006/phrs.2001.0835.
Difrancesco, D. (2010). The role of the funny current in pacemaker activity. *Circ. Res.* 106, 434–446. doi:10.1161/CIRCRESAHA.109.208041.
DiFrancesco, D., and Borer, J. S. (2007). The funny current: Cellular basis for the control of heart rate. *Drugs* 67, 15–24. doi:10.2165/00003495-200767002-00003.
DiFrancesco, D., Ducouret, P., and Robinson, R. B. (1989). Muscarinic modulation of cardiac rate at low acetylcholine concentrations. *Science* 243, 669–71. doi:10.1126/science.2916119.
Digby, G. J., Sethi, P. R., and Lambert, N. A. (2008). Differential dissociation of G

protein heterotrimers. *J. Physiol.* 586, 3325–3335. doi:10.1113/jphysiol.2008.153965.
Dobrev, D., Friedrich, A., Voigt, N., Jost, N., Wettwer, E., Christ, T., et al. (2005). The G protein-gated potassium current IK,ACh is constitutively active in patients with chronic atrial fibrillation. *Circulation* 112, 3697–3706. doi:10.1161/CIRCULATIONAHA.105.575332.
Dobrev, D., Graf, E., Wettwer, E., Himmel, H. M., Hála, O., Doerfel, C., et al. (2001). Molecular basis of downregulation of G-protein -coupled inward rectifying K+ current (ik,ach) in chronic human atrial fibrillation decrease in GIRK4 mrna correlates with reduced IK,ACh and muscarinic receptor-mediated shortening of action potentials. *Circulation* 104, 2551–2557. doi:10.1161/hc4601.099466.
Dobrev, D., Wettwer, E., Kortner, A., Knaut, M., Schüler, S., and Ravens, U. (2002). Human inward rectifier potassium channels in chronic and postoperative atrial fibrillation. *Cardiovasc. Res.* 54, 397–404. doi:10.1016/S0008-6363(01)00555-7.
Dobrzynski, H., Janvier, N. C., Leach, R., Findlay, J. B. C., and Boyett, M. R. (2002). Effects of ACh and adenosine mediated by Kir3.1 and Kir3.4 on ferret ventricular cells. *Am. J. Physiol. Circ. Physiol.* 283, H615–H630. doi:10.1152/ajpheart.00130.2002.
Dobrzynski, H., Marples, D. D. R., Musa, H., Yamanushi, T. T., Hendersonxyl, Z., Takagishi, Y., et al. (2001). Distribution of the muscarinic K^+ channel proteins Kir3.1 and Kir3.4 in the ventricle, atrium, and sinoatrial node of heart. *J. Histochem. Cytochem.* 49, 1221–1234. doi:10.1177/002215540104901004.
Doupnik, C. A. (2015). RGS redundancy and implications in GPCR-GIRK signaling. *Int. Rev. Neurobiol.* 123, 87–116. doi:10.1016/bs.irn.2015.05.010.
Doupnik, C. A., Davidson, N., and Lester, H. A. (1995). The inward rectifier potassium channel family. *Curr. Opin. Neurobiol.* 5, 268–77. doi:10.1016/0959-4388(95)80038-7.
Doupnik, C. A., Xu, T., and Shinaman, J. M. (2001). Profile of RGS expression in single rat atrial myocytes. *Biochim. Biophys. Acta* 1522, 97–107. doi:10.1016/s0167-4781(01)00342-6.
Draghici, A. E., and Taylor, J. A. (2016). The physiological basis and measurement of heart rate variability in humans. *J. Physiol. Anthropol.* 35. doi:10.1186/s40101-016-0113-7.
Duan, S. Z., Christe, M., Milstone, D. S., and Mortensen, R. M. (2007). Go but not Gi2 or Gi3 is required for muscarinic regulation of heart rate and heart rate variability in mice. *Biochem. Biophys. Res. Commun.* 357, 139–143. doi:10.1016/j.bbrc.2007.03.130.
Dusi, V., Zhu, C., and Ajijola, O. A. (2019). Neuromodulation approaches for cardiac arrhythmias: Recent advances. *Curr. Cardiol. Rep.* 21. doi:10.1007/s11886-019-1120-1.
Dyavanapalli, J., Dergacheva, O., Wang, X., and Mendelowitz, D. (2016). Parasympathetic vagal control of cardiac function. *Curr. Hypertens. Rep.* 18, 22. doi:10.1007/s11906-016-0630-0.
Ehrlich, J. R., Biliczki, P., Hohnloser, S. H., and Nattel, S. (2008). Atrial-selective approaches for the treatment of atrial fibrillation. *J. Am. Coll. Cardiol.* 51, 787–792. doi:10.1016/j.jacc.2007.08.067.
Ehrlich, J. R., Nattel, S., and Hohnloser, S. H. (2007). Novel anti-arrhythmic drugs for atrial fibrillation management. *Curr. Vasc. Pharmacol.* 5, 185–95. doi:10.2174/157016107781024073.
Eisner, D. A., Caldwell, J. L., Kistamás, K., and Trafford, A. W. (2017). Calcium and excitation-contraction coupling in the heart. *Circ. Res.* 121, 181–195.

doi:10.1161/CIRCRESAHA.117.310230.
El-Sherif, N., Caref, E. B., Chinushi, M., and Restivo, M. (1999). Mechanism of arrhythmogenicity of the short-long cardiac sequence that precedes ventricular tachyarrhythmias in the long QT syndrome. *J. Am. Coll. Cardiol.* 33, 1415–1423. doi:10.1016/S0735-1097(98)00700-1.
Fajardo-Serrano, A., Wydeven, N., Young, D., Watanabe, M., Shigemoto, R., Martemyanov, K. A., et al. (2013). Association of Rgs7/Gβ5 complexes with Girk channels and GABAB receptors in hippocampal CA1 pyramidal neurons. *Hippocampus* 23, 1231–45. doi:10.1002/hipo.22161.
Fenech, C., Patrikainen, L., Kerr, D. S., Grall, S., Liu, Z., Laugerette, F., et al. (2009). Ric-8A, a Galpha protein guanine nucleotide exchange factor potentiates taste receptor signaling. *Front. Cell. Neurosci.* 3, 11. doi:10.3389/neuro.03.011.2009.
Fu, D. guan (2015). Cardiac arrhythmias: Diagnosis, symptoms, and treatments. *Cell Biochem. Biophys.* 73, 291–296. doi:10.1007/s12013-015-0626-4.
Fu, Y., Huang, X., Zhong, H., Mortensen, R. M., D'Alecy, L. G., and Neubig, R. R. (2006). Endogenous RGS proteins and Gα subtypes differentially control muscarinic and adenosine-mediated chronotropic effects. *Circ. Res.* 98, 659–666. doi:10.1161/01.RES.0000207497.50477.60.
Gaborit, N., Le Bouter, S., Szuts, V., Varro, A., Escande, D., Nattel, S., et al. (2007). Regional and tissue specific transcript signatures of ion channel genes in the non-diseased human heart. *J. Physiol.* 582, 675–693. doi:10.1113/jphysiol.2006.126714.
Gatti, P. J., Johnson, T. A., McKenzie, J., Lauenstein, J. M., Gray, A., and Massari, V. J. (1997). Vagal control of left ventricular contractility is selectively mediated by a cranioventricular intracardiac ganglion in the cat. *J. Auton. Nerv. Syst.* 66, 138–144. doi:10.1016/S0165-1838(97)00071-4.
Geerling, J. C., Shin, J. W., Chimenti, P. C., and Loewy, A. D. (2010). Paraventricular hypothalamic nucleus: Axonal projections to the brainstem. *J. Comp. Neurol.* 518, 1460–1499. doi:10.1002/cne.22283.
Gehrmann, J., Hammer, P. E., Maguire, C. T., Wakimoto, H., Triedman, J. K., and Berul, C. I. (2000). Phenotypic screening for heart rate variability in the mouse. *Am. J. Physiol. - Hear. Circ. Physiol.* 279. doi:10.1152/ajpheart.2000.279.2.h733.
Go, A. S., Hylek, E. M., Phillips, K. A., Chang, Y. C., Henault, L. E., Selby, J. V., et al. (2001). Prevalence of diagnosed atrial fibrillation in adults: National implications for rhythm management and stroke prevention: The anticoagulation and risk factors in atrial fibrillation (ATRIA) study. *J. Am. Med. Assoc.* 285, 2370–2375. doi:10.1001/jama.285.18.2370.
Gordan, R., Gwathmey, J. K., and Xie, L.-H. (2015). Autonomic and endocrine control of cardiovascular function. *World J. Cardiol.* 7, 204–14. doi:10.4330/wjc.v7.i4.204.
Gorenek, B., Fisher, J. D., Kudaiberdieva, G., Baranchuk, A., Burri, H., Campbell, K. B., et al. (2020). Premature ventricular complexes: diagnostic and therapeutic considerations in clinical practice: A state-of-the-art review by the American College of Cardiology Electrophysiology Council. *J. Interv. Card. Electrophysiol.* 57, 5–26. doi:10.1007/s10840-019-00655-3.
Gourine, A. V., Machhada, A., Trapp, S., and Spyer, K. M. (2016). Cardiac vagal preganglionic neurones: An update. *Auton. Neurosci. Basic Clin.* 199, 24–28. doi:10.1016/j.autneu.2016.06.003.
Grabowska, D., Jayaraman, M., Kaltenbronn, K. M., Sandiford, S. L., Wang, Q., Jenkins, S., et al. (2008). Postnatal induction and localization of R7BP, a membrane-anchoring protein for regulator of G protein signaling 7 family-Gβ5 complexes in brain. *Neuroscience* 151, 969–982. doi:10.1016/j.neuroscience.2007.11.045.

Gurevich, V. V., and Gurevich, E. V. (2019). GPCR signaling regulation: The role of GRKs and arrestins. *Front. Pharmacol.* 10. doi:10.3389/fphar.2019.00125.
Harvey, R. D. (2012). “Muscarinic Receptor Agonists and Antagonists: Effects on Cardiovascular Function,” in *Handbook of experimental pharmacology*, 299–316. doi:10.1007/978-3-642-23274-9_13.
Harvey, R. D., and Belevych, A. E. (2003). Muscarinic regulation of cardiac ion channels. *Br. J. Pharmacol.* 139, 1074–1084. doi:10.1038/sj.bjp.0705338.
Hashimoto, N., Yamashita, T., and Tsuruzoe, N. (2006). Tertiapin, a selective I_{KACh} blocker, terminates atrial fibrillation with selective atrial effective refractory period prolongation. *Pharmacol. Res.* 54, 136–41. doi:10.1016/j.phrs.2006.03.021.
Hauser, A. S., Attwood, M. M., Rask-Andersen, M., Schiöth, H. B., and Gloriam, D. E. (2017). Trends in GPCR drug discovery: New agents, targets and indications. *Nat. Rev. Drug Discov.* 16, 829–842. doi:10.1038/nrd.2017.178.
He, C., Zhang, H., Mirshahi, T., and Logothetis, D. E. (1999). Identification of a potassium channel site that interacts with G protein betagamma subunits to mediate agonist-induced signaling. *J. Biol. Chem.* 274, 12517–24. doi:10.1074/jbc.274.18.12517.
Hedayat, M., Mahmoudi, M. J., Rose, N. R., and Rezaei, N. (2010). Proinflammatory cytokines in heart failure: Double-edged swords. *Heart Fail. Rev.* 15, 543–562. doi:10.1007/s10741-010-9168-4.
Hedin, K. E., Lim, N. F., and Clapham, D. E. (1996). Cloning of a Xenopus laevis inwardly rectifying K^+ channel subunit that permits GIRK1 expression of IKACh currents in oocytes. *Neuron* 16, 423–9. doi:10.1016/s0896-6273(00)80060-4.
Heeringa, J., Van Der Kuip, D. A. M., Hofman, A., Kors, J. A., Van Herpen, G., Stricker, B. H. C., et al. (2006). Prevalence, incidence and lifetime risk of atrial fibrillation: The Rotterdam study. *Eur. Heart J.* 27, 949–953. doi:10.1093/eurheartj/ehi825.
Hibino, H., Inanobe, A., Furutani, K., Murakami, S., Findlay, I., and Kurachi, Y. (2010). Inwardly rectifying potassium channels: Their structure, function, and physiological roles. *Physiol. Rev.* 90, 291–366. doi:10.1152/physrev.00021.2009.
Hidehiko, N., Akira, F., Naoki, F., Tomoyuki, M., Toru, Y., and Hiroshi, I. (2002). Effects of a novel class III antiarrhythmic agent, NIP-142, on canine atrial fibrillation and flutter. *Circ. J.* 66, 185–191. doi:10.1253/circj.66.185.
Hollins, B., Kuravi, S., Digby, G. J., and Lambert, N. A. (2009). The c-terminus of GRK3 indicates rapid dissociation of G protein heterotrimers. *Cell. Signal.* 21, 1015–1021. doi:10.1016/j.cellsig.2009.02.017.
Hooks, S. B., Waldo, G. L., Corbitt, J., Bodor, E. T., Krumins, A. M., and Harden, T. K. (2003). RGS6, RGS7, RGS9, and RGS11 stimulate GTPase activity of Gi family G-proteins with differential selectivity and maximal activity. *J. Biol. Chem.* 278, 10087–93. doi:10.1074/jbc.M211382200.
Hou, Y., Zhou, Q., and Po, S. S. (2016). Neuromodulation for cardiac arrhythmia. *Hear. Rhythm* 13, 584–592. doi:10.1016/j.hrthm.2015.10.001.
Huang, C. L., Feng, S., and Hilgemann, D. W. (1998). Direct activation of inward rectifier potassium channels by PIP2 and its stabilization by Gbetagamma. *Nature* 391, 803–6. doi:10.1038/35882.
Huang, C. L., Jan, Y. N., and Jan, L. Y. (1997). Binding of the G protein betagamma subunit to multiple regions of G protein-gated inward-rectifying K^+ channels. *FEBS Lett.* 405, 291–8. doi:10.1016/s0014-5793(97)00197-x.
Huang, C. L., Slesinger, P. A., Casey, P. J., Jan, Y. N., and Jan, L. Y. (1995). Evidence that direct binding of Gβγ to the GIRK1 G protein-gated inwardly rectifying K^+ channel is important for channel activation. *Neuron* 15, 1133–1143. doi:10.1016/0896-6273(95)90101-9.

Huang, W. A., Boyle, N. G., and Vaseghi, M. (2017). Cardiac innervation and the autonomic nervous system in sudden cardiac death. *Card. Electrophysiol. Clin.* 9, 665–679. doi:10.1016/j.ccep.2017.08.002.
Huang, W. A., Shivkumar, K., and Vaseghi, M. (2015). Device-based autonomic modulation in arrhythmia patients: the role of vagal nerve stimulation. *Curr. Treat. Options Cardiovasc. Med.* 17. doi:10.1007/s11936-015-0379-9.
Hullmann, J., Traynham, C. J., Coleman, R. C., and Koch, W. J. (2016). The expanding GRK interactome: Implications in cardiovascular disease and potential for therapeutic development. *Pharmacol. Res.* 110, 52–64. doi:10.1016/j.phrs.2016.05.008.
Inanobe, A., Fujita, S., Makino, Y., Matsushita, K., Ishii, M., Chachin, M., et al. (2001). Interaction between the RGS domain of RGS4 with G protein alpha subunits mediates the voltage-dependent relaxation of the G protein-gated potassium channel. *J. Physiol.* 535, 133–43. doi:10.1111/j.1469-7793.2001.t01-1-00133.x.
Ito, H., Ono, K., and Noma, A. (1994). Background conductance attributable to spontaneous opening of muscarinic K^+ channels in rabbit sino-atrial node cells. *J. Physiol.* 476.
Jayaraman, M., Zhou, H., Jia, L., Cain, M. D., and Blumer, K. J. (2009). R9AP and R7BP: traffic cops for the RGS7 family in phototransduction and neuronal GPCR signaling. *Trends Pharmacol. Sci.* 30, 17–24. doi:10.1016/j.tips.2008.10.002.
Jin, W., Klem, A. M., Lewis, J. H., and Lu, Z. (1999). Mechanisms of inward-rectifier K^+ channel inhibition by tertiapin-Q. *Biochemistry* 38, 14294–14301. doi:10.1021/bi991206j.
Jin, W., and Lu, Z. (1999). Synthesis of a stable form of tertiapin: a high-affinity inhibitor for inward-rectifier K^+ channels. *Biochemistry* 38, 14286–93. doi:10.1021/bi991205r.
Jozefczuk, E., Guzik, T. J., and Siedlinski, M. (2020). Significance of sphingosine-1-phosphate in cardiovascular physiology and pathology. *Pharmacol. Res.* 156. doi:10.1016/j.phrs.2020.104793.
Kanjhan, R., Coulson, E. J., Adams, D. J., and Bellingham, M. C. (2005). Tertiapin-Q blocks recombinant and native large conductance K^+ Channels in a use-dependent manner. *J. Pharmacol. Exp. Ther.* 314, 1353–1361. doi:10.1124/jpet.105.085928.
Karschin, C., Dissmann, E., Stühmer, W., and Karschin, A. (1996). IRK(1-3) and GIRK(1-4) inwardly rectifying K+ channel mRNAs are differentially expressed in the adult rat brain. *J. Neurosci.* 16, 3559–70. doi:10.1523/JNEUROSCI.16-11-03559.1996.
Katritch, V., Cherezov, V., and Stevens, R. C. (2013). Structure-function of the G protein–coupled receptor superfamily. *Annu. Rev. Pharmacol. Toxicol.* 53, 531–556. doi:10.1146/annurev-pharmtox-032112-135923.
Katsouras, G., Sakabe, M., Comtois, P., Maguy, A., Burstein, B., Guerra, P. G., et al. (2009). Differences in atrial fibrillation properties under vagal nerve stimulation versus atrial tachycardia remodeling. *Hear. Rhythm* 6, 1465–1472. doi:10.1016/j.hrthm.2009.07.034.
Kaufmann, K., Romaine, I., Days, E., Pascual, C., Malik, A., Yang, L., et al. (2013). ML297 (VU0456810), the first potent and selective activator of the GIRK potassium channel, displays antiepileptic properties in mice. *ACS Chem. Neurosci.* 4, 1278–1286. doi:10.1021/cn400062a.
Kennedy, A., Finlay, D. D., Guldenring, D., Bond, R., Moran, K., and McLaughlin, J. (2016). The cardiac conduction system: generation and conduction of the cardiac impulse. *Crit. Care Nurs. Clin. North Am.* 28, 269–279. doi:10.1016/j.cnc.2016.04.001.
Kennedy, M. E., Nemec, J., and Clapham, D. E. (1996). Localization and interaction of

epitope-tagged GIRK1 and CIR inward rectifier K^+ channel subunits. *Neuropharmacology* 35, 831–9. doi: 10.1016/0028-3908(96)00132-3.
Kennedy, M. E., Nemec, J., Corey, S., Wickman, K., and Clapham, D. E. (1999). GIRK4 confers appropriate processing and cell surface localization to G-protein-gated potassium channels. *J. Biol. Chem.* 274, 2571–82. doi:10.1074/jbc.274.4.2571.
Kienitz, M.-C., Littwitz, C., Bender, K., and Pott, L. (2011). Remodeling of inward rectifying K+ currents in rat atrial myocytes by overexpression of A1-adenosine receptors. *Basic Res. Cardiol.* 106, 953–966. doi:10.1007/s00395-011-0193-9.
Kienitz, M.-C., Mintert-Jancke, E., Hertel, F., and Pott, L. (2014). Differential effects of genetically-encoded Gβγ scavengers on receptor-activated and basal Kir3.1/Kir3.4 channel current in rat atrial myocytes. *Cell. Signal.* 26, 1182–1192. doi:10.1016/j.cellsig.2014.02.007.
Kofuji, P., Davidson, N., and Lester, H. A. (1995). Evidence that neuronal G-protein-gated inwardly rectifying K^+ channels are activated by G beta gamma subunits and function as heteromultimers. *Proc. Natl. Acad. Sci. U. S. A.* 92, 6542–6. doi:10.1073/pnas.92.14.6542.
Koumi, S., Sato, R., Nagasawa, K., and Hayakawa, H. (1997). Activation of inwardly rectifying potassium channels by muscarinic receptor-linked G protein in isolated human ventricular myocytes. *J. Membr. Biol.* 157, 71–81. doi:10.1007/s002329900217.
Koumi, S., and Wasserstrom, J. A. (1994). Acetylcholine-sensitive muscarinic K^+ channels in mammalian ventricular myocytes. *Am. J. Physiol. Circ. Physiol.* 266, H1812–H1821. doi:10.1152/ajpheart.1994.266.5.H1812.
Kovoor, P., Wickman, K., Maguire, C. T., Pu, W., Gehrmann, J., Berul, C. I., et al. (2001). Evaluation of the role of I(KACh) in atrial fibrillation using a mouse knockout model. *J. Am. Coll. Cardiol.* 37, 2136–43. doi:10.1016/s0735-1097(01)01304-3.
Koyrakh, L., Roman, M. I., Brinkmann, V., and Wickman, K. (2005). The heart rate decrease caused by acute FTY720 administration is mediated by the G protein-gated potassium channel I_{KACh}. *Am. J. Transplant.* 5, 529–536. doi:10.1111/j.1600-6143.2005.00754.x.
Kozasa, Y., Nakashima, N., Ito, M., Ishikawa, T., Kimoto, H., Ushijima, K., et al. (2018). HCN4 pacemaker channels attenuate the parasympathetic response and stabilize the spontaneous firing of the sinoatrial node. *J. Physiol.* 596, 809–825. doi:10.1113/JP275303.
Krapivinsky, G., Gordon, E. A., Wickman, K., Velimirović, B., Krapivinsky, L., and Clapham, D. E. (1995a). The G-protein-gated atrial K^+ channel I_{KAch} is a heteromultimer of two inwardly rectifying K^+-channel proteins. *Nature* 374, 135–141. doi:10.1038/374135a0.
Krapivinsky, G., Krapivinsky, L., Wickman, K., and Clapham, D. E. (1995b). G beta gamma binds directly to the G protein-gated K^+ channel, IKACh. *J. Biol. Chem.* 270, 29059–62. doi:10.1074/jbc.270.49.29059.
Kubo, Y., Reuveny, E., Slesinger, P. A., Jan, Y. N., and Jan, L. Y. (1993). Primary structure and functional expression of a rat G-protein-coupled muscarinic potassium channel. *Nature* 364, 802–6. doi:10.1038/364802a0.
Kumari, N., Gaur, H., and Bhargava, A. (2018). Cardiac voltage gated calcium channels and their regulation by β-adrenergic signaling. *Life Sci.* 194, 139–149. doi:10.1016/j.lfs.2017.12.033.
Kuß, J., Stallmeyer, B., Goldstein, M., Rinné, S., Pees, C., Zumhagen, S., et al. (2019). Familial sinus node disease caused by a gain of GIRK (G-protein activated inwardly rectifying K^+ channel) channel function. *Circ. Genomic Precis. Med.* 12, e002238. doi:10.1161/CIRCGEN.118.002238.

La Rovere, M. T., Pinna, G. D., Maestri, R., Robbi, E., Caporotondi, A., Guazzotti, G., et al. (2009). Prognostic implications of baroreflex sensitivity in heart failure patients in the beta-blocking era. *J. Am. Coll. Cardiol.* 53, 193–199. doi:10.1016/j.jacc.2008.09.034.

LaCroix, C., Freeling, J., Giles, A., Wess, J., and Li, Y. F. (2008). Deficiency of M2 muscarinic acetylcholine receptors increases susceptibility of ventricular function to chronic adrenergic stress. *Am. J. Physiol. - Hear. Circ. Physiol.* 294. doi:10.1152/ajpheart.00724.2007.

Layland, J., Carrick, D., Lee, M., Oldroyd, K., and Berry, C. (2014). Adenosine: physiology, pharmacology, and clinical applications. *JACC. Cardiovasc. Interv.* 7, 581–91. doi:10.1016/j.jcin.2014.02.009.

Leaney, J. L. (2003). Contribution of Kir3.1, Kir3.2A and Kir3.2C subunits to native G protein-gated inwardly rectifying potassium currents in cultured hippocampal neurons. *Eur. J. Neurosci.* 18, 2110–8. doi:10.1046/j.1460-9568.2003.02933.x.

Lee, S. W., Anderson, A., Guzman, P. A., Nakano, A., Tolkacheva, E. G., and Wickman, K. (2018). Atrial GIRK Channels Mediate the Effects of Vagus Nerve Stimulation on Heart Rate Dynamics and Arrhythmogenesis. *Front. Physiol.* 9, 943. doi:10.3389/fphys.2018.00943.

Lee, S. W., Li, Q., Libbus, I., Xie, X., Kenknight, B. H., Garry, M. G., et al. (2016). Chronic cyclic vagus nerve stimulation has beneficial electrophysiological effects on healthy hearts in the absence of autonomic imbalance. *Physiol. Rep.* 4, 1–8. doi:10.14814/phy2.12786.

Lesage, F., Duprat, F., Fink, M., Guillemare, E., Coppola, T., Lazdunski, M., et al. (1994). Cloning provides evidence for a family of inward rectifier and G-protein coupled K^+ channels in the brain. *FEBS Lett.* 353, 37–42. doi:10.1016/0014-5793(94)01007-2.

Li, D., Sun, H., and Levesque, P. (2009a). Antiarrhythmic drug therapy for atrial fibrillation: focus on atrial selectivity and safety. *Cardiovasc. Hematol. Agents Med. Chem.* 7, 64–75. doi:10.2174/187152509787047621.

Li, N., Csepe, T. A., Hansen, B. J., Sul, L. V., Kalyanasundaram, A., Zakharkin, S. O., et al. (2016). Adenosine-induced atrial fibrillation. *Circulation* 134, 486–498. doi:10.1161/CIRCULATIONAHA.115.021165.

Li, Y. F., LaCroix, C., and Freeling, J. (2009b). Specific subtypes of nicotinic cholinergic receptors involved in sympathetic and parasympathetic cardiovascular responses. *Neurosci. Lett.* 462, 20–23. doi:10.1016/j.neulet.2009.06.081.

Li, Y., Fu, X., Zhang, Z., and Yu, B. (2017). Knockdown of cardiac Kir3.1 gene with siRNA can improve bradycardia in an experimental sinus bradycardia rat model. *Mol. Cell. Biochem.* 429, 103–111. doi:10.1007/s11010-017-2939-7.

Liang, B., Nissen, J. D., Laursen, M., Wang, X., Skibsbye, L., Hearing, M. C., et al. (2014). G-protein-coupled inward rectifier potassium current contributes to ventricular repolarization. *Cardiovasc. Res.* 101, 175–184. doi:10.1093/cvr/cvt240.

Lloyd-Jones, D. M., Wang, T. J., Leip, E. P., Larson, M. G., Levy, D., Vasan, R. S., et al. (2004). Lifetime risk for development of atrial fibrillation: The framingham heart study. *Circulation* 110, 1042–1046. doi:10.1161/01.CIR.0000140263.20897.42.

Logothetis, D. E., Kurachi, Y., Galper, J., Neer, E. J., and Clapham, D. E. (1987). The βγ subunits of GTP-binding proteins activate the muscarinic K^+ channel in heart. *Nature* 325, 321–326. doi:10.1038/325321a0.

Lombardi, F., and Stein, P. K. (2011). Origin of heart rate variability and turbulence: An appraisal of autonomic modulation of cardiovascular function. *Front. Physiol.* 2 DEC. doi:10.3389/fphys.2011.00095.

Long, V. P., Bonilla, I. M., Baine, S., Glynn, P., Kumar, S., Schober, K., et al. (2020).

Chronic heart failure increases negative chronotropic effects of adenosine in canine sinoatrial cells via A1R stimulation and GIRK-mediated IKado. *Life Sci.* 240, 117068. doi:10.1016/j.lfs.2019.117068.

Lujan, H. L., Rivers, J. P., and DiCarlo, S. E. (2016). Complex and interacting influences of the autonomic nervous system on cardiac electrophysiology in conscious mice. *Auton. Neurosci.* 201, 24–31. doi:10.1016/j.autneu.2016.08.017.

Luján, R., and Aguado, C. (2015). "Localization and targeting of GIRK channels in mammalian central neurons," in *International Review of Neurobiology* (Academic Press Inc.), 161–200. doi:10.1016/bs.irn.2015.05.009.

Luján, R., Marron Fernandez de Velasco, E., Aguado, C., and Wickman, K. (2014). New insights into the therapeutic potential of Girk channels. *Trends Neurosci.* 37, 20–29. doi:10.1016/j.tins.2013.10.006.

Lunn, M. L., Nassirpour, R., Arrabit, C., Tan, J., Mcleod, I., Arias, C. M., et al. (2007). A unique sorting nexin regulates trafficking of potassium channels via a PDZ domain interaction. *Nat. Neurosci.* 10, 1249–1259. doi:10.1038/nn1953.

Lüscher, C., and Slesinger, P. A. (2010). Emerging roles for G protein-gated inwardly rectifying potassium (GIRK) channels in health and disease. *Nat. Rev. Neurosci.* 11, 301–315. doi:10.1038/nrn2834.

Ma, D., Zerangue, N., Raab-Graham, K., Fried, S. R., Jan, Y. N., and Jan, L. Y. (2002). Diverse trafficking patterns due to multiple traffic motifs in G protein-activated inwardly rectifying potassium channels from brain and heart. *Neuron* 33, 715–29. doi:10.1016/s0896-6273(02)00614-1.

MacHida, T., Hashimoto, N., Kuwahara, I., Ogino, Y., Matsuura, J., Yamamoto, W., et al. (2011). Effects of a highly selective acetylcholine-activated K^+ channel blocker on experimental atrial fibrillation. *Circ. Arrhythmia Electrophysiol.* 4, 94–102. doi:10.1161/CIRCEP.110.951608.

Macle, L., and Nattel, S. (2016). Arrhythmias in 2015: Advances in drug, ablation, and device therapy for cardiac arrhythmias. *Nat. Rev. Cardiol.* 13, 67–68. doi:10.1038/nrcardio.2015.196.

Mancia, G., and Grassi, G. (2014). The autonomic nervous system and hypertension. *Circ. Res.* 114, 1804–1814. doi:10.1161/CIRCRESAHA.114.302524.

Mangmool, S., and Kurose, H. (2011). G(i/o) protein-dependent and -independent actions of Pertussis Toxin (PTX). *Toxins (Basel).* 3, 884–99. doi:10.3390/toxins3070884.

Mangoni, M. E., and Nargeot, J. (2008). Genesis and regulation of the heart automaticity. *Physiol. Rev.* 88, 919–982. doi:10.1152/physrev.00018.2007.

Manolis, A. A., Manolis, T. A., Apostolopoulos, E. J., Apostolaki, N. E., Melita, H., and Manolis, A. S. (2020). The role of the autonomic nervous system in cardiac arrhythmias: The neuro-cardiac axis, more foe than friend? *Trends Cardiovasc. Med.* doi:10.1016/j.tcm.2020.04.011.

Marlene Hosey, M., Benovic, J. L., DebBurman, S. K., and Richardson, R. M. (1995). Multiple mechanisms involving protein phosphorylation are linked to desensitization of muscarinic receptors. *Life Sci.* 56, 951–955. doi:10.1016/0024-3205(95)00033-3.

Marron Fernandez de Velasco, E., Carlblom, N., Xia, Z., and Wickman, K. (2017a). Suppression of inhibitory G protein signaling in forebrain pyramidal neurons triggers plasticity of glutamatergic neurotransmission in the nucleus accumbens core. *Neuropharmacology* 117, 33–40. doi:10.1016/j.neuropharm.2017.01.021.

Marron Fernandez de Velasco, E., Zhang, L., N. Vo, B., Tipps, M., Farris, S., Xia, Z., et al. (2017b). GIRK2 splice variants and neuronal G protein-gated K+ channels: implications for channel function and behavior. *Sci. Rep.* 7, 1639. doi:10.1038/s41598-017-01820-2.

Masuho, I., Martemyanov, K. A., and Lambert, N. A. (2015a). Monitoring G protein activation in cells with BRET. *Methods Mol. Biol.* 1335, 107–13. doi:10.1007/978-1-4939-2914-6_8.

Masuho, I., Ostrovskaya, O., Kramer, G. M., Jones, C. D., Xie, K., and Martemyanov, K. A. (2015b). Distinct profiles of functional discrimination among G proteins determine the actions of G protein–coupled receptors. *Sci. Signal.* 8, ra123–ra123. doi:10.1126/scisignal.aab4068.

Masuho, I., Xie, K., and Martemyanov, K. A. (2013). Macromolecular composition dictates receptor and G protein selectivity of regulator of G protein signaling (RGS) 7 and 9-2 protein complexes in living cells. *J. Biol. Chem.* 288, 25129–42. doi:10.1074/jbc.M113.462283.

Matsuda, T., Ito, M., Ishimaru, S., Tsuruoka, N., Saito, T., Iida-Tanaka, N., et al. (2006). Blockade by NIP-142, an antiarrhythmic agent, of carbachol-induced atrial action potential shortening and GIRK1/4 channel. *J. Pharmacol. Sci.* 101, 303–310. doi:10.1254/jphs.FP0060324.

Mayfield, J., Blednov, Y. A., and Harris, R. A. (2015). "Behavioral and Genetic Evidence for GIRK Channels in the CNS: Role in Physiology, Pathophysiology, and Drug Addiction," in *International Review of Neurobiology* (Academic Press Inc.), 279–313. doi:10.1016/bs.irn.2015.05.016.

McGrath, M. F., and de Bold, A. J. (2009). Transcriptional analysis of the mammalian heart with special reference to its endocrine function. *BMC Genomics* 10. doi:10.1186/1471-2164-10-254.

McIntyre, S. D., Kakade, V., Mori, Y., and Tolkacheva, E. G. (2014). Heart rate variability and alternans formation in the heart: The role of feedback in cardiac dynamics. *J. Theor. Biol.* 350, 90–97. doi:10.1016/j.jtbi.2014.02.015.

McMorn, S. O., Harrison, S. M., Zang, W. J., Yu, X. J., and Boyett, M. R. (1993). A direct negative inotropic effect of acetylcholine on rat ventricular myocytes. *Am. J. Physiol. Circ. Physiol.* 265, H1393–H1400. doi:10.1152/ajpheart.1993.265.4.H1393.

Medina, I., Krapivinsky, G., Arnold, S., Kovoor, P., Krapivinsky, L., and Clapham, D. E. (2000). A Switch Mechanism for Gβγ Activation of I_{KACh}. *J. Biol. Chem.* 275, 29709–29716. doi:10.1074/jbc.M004989200.

Meijler, F. L., and Janse, M. J. (1988). Morphology and electrophysiology of the mammalian atrioventricular node. *Physiol. Rev.* 68, 608–647. doi:10.1152/physrev.1988.68.2.608.

Mendelowitz, D. (1996). Firing properties of identified parasympathetic cardiac neurons in nucleus ambiguus. *Am. J. Physiol. Circ. Physiol.* 271, H2609–H2614. doi:10.1152/ajpheart.1996.271.6.H2609.

Mesirca, P., Alig, J., Torrente, A. G., Müller, J. C., Marger, L., Rollin, A., et al. (2014). Cardiac arrhythmia induced by genetic silencing of 'funny' (f) channels is rescued by GIRK4 inactivation. *Nat. Commun.* 5, 4664. doi:10.1038/ncomms5664.

Mesirca, P., Bidaud, I., Briec, F., Evain, S., Torrente, A. G., Le Quang, K., et al. (2016a). G protein-gated I_{KACh} channels as therapeutic targets for treatment of sick sinus syndrome and heart block. *Proc. Natl. Acad. Sci.* 113, E932–E941. doi:10.1073/pnas.1517181113.

Mesirca, P., Bidaud, I., and Mangoni, M. E. (2016b). Rescuing cardiac automaticity in L-type Cav1.3 channelopathies and beyond. *J. Physiol.* 594, 5869–5879. doi:10.1113/JP270678.

Mesirca, P., Marger, L., Toyoda, F., Rizzetto, R., Audoubert, M., Dubel, S., et al. (2013). The G-protein–gated K^+ channel, I_{KACh}, is required for regulation of pacemaker activity and recovery of resting heart rate after sympathetic stimulation. *J. Gen. Physiol.* 142, 113–126. doi:10.1085/jgp.201310996.

Mihaylova, S., Killian, A., Mayer, K., Pullamsetti, S. S., Schermuly, R., and Rosengarten, B. (2012). Effects of anti-inflammatory vagus nerve stimulation on the cerebral microcirculation in endotoxinemic rats. *J. Neuroinflammation* 9. doi:10.1186/1742-2094-9-183.

Mitchell, G. F., Jeron, A., and Koren, G. (1998). Measurement of heart rate and Q-T interval in the conscious mouse. *Am. J. Physiol. - Hear. Circ. Physiol.* 274. doi:10.1152/ajpheart.1998.274.3.h747.

Miyasaka, Y., Barnes, M. E., Gersh, B. J., Cha, S. S., Bailey, K. R., Abhayaratna, W. P., et al. (2006). Secular trends in incidence of atrial fibrillation in Olmsted County, Minnesota, 1980 to 2000, and implications on the projections for future prevalence. *Circulation* 114, 119–125. doi:10.1161/CIRCULATIONAHA.105.595140.

Munger, T. M., Wu, L. Q., and Shen, W. K. (2014). Atrial fibrillation. *J. Biomed. Res.* 28, 1–17. doi:10.7555/JBR.28.20130191.

Mustafa, S. J., Morrison, R. R., Teng, B., and Pelleg, A. (2009). Adenosine receptors and the heart: role in regulation of coronary blood flow and cardiac electrophysiology. *Handb. Exp. Pharmacol.*, 161–88. doi:10.1007/978-3-540-89615-9_6.

Nakano, H., Williams, E., Hoshijima, M., Sasaki, M., Minamisawa, S., Chien, K. R., et al. (2011). Cardiac origin of smooth muscle cells in the inflow tract. *J. Mol. Cell. Cardiol.* 50, 337–45. doi:10.1016/j.yjmcc.2010.10.009.

Nasi-Er, B. guli, Wenhui, Z., HuaXin, S., Xianhui, Z., Yaodong, L., Yanmei, L., et al. (2019). Vagus nerve stimulation reduces ventricular arrhythmias and increases ventricular electrical stability. *PACE - Pacing Clin. Electrophysiol.* 42, 247–256. doi:10.1111/pace.13585.

Nassirpour, R., Bahima, L., Lalive, A. L., Lüscher, C., Luján, R., and Slesinger, P. A. (2010). Morphine- and CaMKII-dependent enhancement of GIRK channel signaling in hippocampal neurons. *J. Neurosci.* 30, 13419–30. doi:10.1523/JNEUROSCI.2966-10.2010.

Neff, R. A., Mihalevich, M., and Mendelowitz, D. (1998). Stimulation of NTS activates NMDA and non-NMDA receptors in rat cardiac vagal neurons in the nucleus ambiguus. *Brain Res.* 792, 277–282. doi:10.1016/S0006-8993(98)00149-8.

Nemec, J., Wickman, K., and Clapham, D. E. (1999). G βγ Binding Increases the Open Time of I KACh : Kinetic Evidence for Multiple G βγ Binding Sites. *Biophys. J.* 76, 246–252. doi:10.1016/S0006-3495(99)77193-6.

Nerbonne, J. M., and Kass, R. S. (2005). Molecular physiology of cardiac repolarization. *Physiol. Rev.* 85, 1205–1253. doi:10.1152/physrev.00002.2005.

Nishimura, M., Habuchi, Y., Hiromasa, S., and Watanabe, Y. (1988). Ionic basis of depressed automaticity and conduction by acetylcholine in rabbit AV node. *Am. J. Physiol. - Hear. Circ. Physiol.* 255. doi:10.1152/ajpheart.1988.255.1.h7.

Nissinen, S. I., Mäkikallio, T. H., Seppänen, T., Tapanainen, J. M., Salo, M., Tulppo, M. P., et al. (2003). Heart rate recovery after exercise as a predictor of mortality among survivors of acute myocardial infarction. *Am. J. Cardiol.* 91, 711–714. doi:10.1016/S0002-9149(02)03410-0.

Nobles, M., Montaigne, D., Sebastian, S., Birnbaumer, L., and Tinker, A. (2018). Differential effects of inhibitory G protein isoforms on G protein-gated inwardly rectifying K+ currents in adult murine atria. *Am. J. Physiol. Cell Physiol.* 314, C616–C626. doi:10.1152/ajpcell.00271.2016.

Noma, A., and Trautwein, W. (1978). Relaxation of the ACh-induced potassium current in the rabbit sinoatrial node cell. *Pflügers Arch. Eur. J. Physiol.* 377, 193–200. doi:10.1007/BF00584272.

Ochi, R., Momose, Y., Oyama, K., and Giles, W. (2006). Sphingosine-1-phosphate

effects on guinea pig atrial myocytes: Alterations in action potentials and K^+ currents. *Cardiovasc. Res.* 70, 88–96. doi:10.1016/j.cardiores.2006.01.010.
Odutayo, A., Wong, C. X., Hsiao, A. J., Hopewell, S., Altman, D. G., and Emdin, C. A. (2016). Atrial fibrillation and risks of cardiovascular disease, renal disease, and death: systematic review and meta-analysis. *BMJ* 354, i4482. doi:10.1136/bmj.i4482.
Ogrodowczyk, M., Dettlaff, K., and Jelinska, A. (2015). Beta-Blockers: Current State of Knowledge and Perspectives. *Mini-Reviews Med. Chem.* 16, 40–54. doi:10.2174/1389557515666151016125948.
Orlandi, C., Posokhova, E., Masuho, I., Ray, T. A., Hasan, N., Gregg, R. G., et al. (2012). GPR158/179 regulate G protein signaling by controlling localization and activity of the RGS7 complexes. *J. Cell Biol.* 197, 711–719. doi:10.1083/jcb.201202123.
Orlandi, C., Xie, K., Masuho, I., Fajardo-Serrano, A., Lujan, R., and Martemyanov, K. A. (2015). Orphan receptor GPR158 is an allosteric modulator of RGS7 catalytic activity with an essential role in dictating its expression and localization in the brain. *J. Biol. Chem.* 290, 13622–13639. doi:10.1074/jbc.M115.645374.
Ostrovskaya, O. I., Orlandi, C., Fajardo-Serrano, A., Young, S. M., Lujan, R., and Martemyanov, K. A. (2018). Inhibitory signaling to ion channels in hippocampal neurons is differentially regulated by alternative macromolecular complexes of RGS7. *J. Neurosci.* 38, 10002–10015. doi:10.1523/JNEUROSCI.1378-18.2018.
Ostrovskaya, O., Xie, K., Masuho, I., Fajardo-Serrano, A., Lujan, R., Wickman, K., et al. (2014). RGS7/Gβ5/R7BP complex regulates synaptic plasticity and memory by modulating hippocampal GABABR-GIRK signaling. *Elife* 3, e02053. doi:10.7554/eLife.02053.
Padeletti, L., and Bagliani, G. (2017). General introduction, classification, and electrocardiographic diagnosis of cardiac arrhythmias. *Card. Electrophysiol. Clin.* 9, 345–363. doi:10.1016/j.ccep.2017.05.009.
Papke, R. L. (2014). Merging old and new perspectives on nicotinic acetylcholine receptors. *Biochem. Pharmacol.* 89, 1–11. doi:10.1016/j.bcp.2014.01.029.
Peralta, E. G., Ashkenazi, A., Winslow, J. W., Smith, D. H., Ramachandran, J., and Capon, D. J. (1987). Distinct primary structures, ligand-binding properties and tissue-specific expression of four human muscarinic acetylcholine receptors. *EMBO J.* 6, 3923–3929. doi:10.1002/j.1460-2075.1987.tb02733.x.
Perry, C. A., Pravetoni, M., Teske, J. A., Aguado, C., Erickson, D. J., Medrano, J. F., et al. (2008). Predisposition to late-onset obesity in GIRK4 knockout mice. *Proc. Natl. Acad. Sci. U. S. A.* 105, 8148–8153. doi:10.1073/pnas.0803261105.
Petkovich, B. W., Vega, J., and Thomas, S. (2015). Vagal Modulation of Hypertension. *Curr. Hypertens. Rep.* 17. doi:10.1007/s11906-015-0532-6.
Pfaffinger, P. J., Martin, J. M., Hunter, D. D., Nathanson, N. M., and Hille, B. (1985). GTP-binding proteins couple cardiac muscarinic receptors to a K channel. *Nature* 317, 536–538. doi:10.1038/317536a0.
Piñol, R. A., Jameson, H., Popratiloff, A., Lee, N. H., and Mendelowitz, D. (2014). Visualization of oxytocin release that mediates paired pulse facilitation in hypothalamic pathways to brainstem autonomic neurons. *PLoS One* 9. doi:10.1371/journal.pone.0112138.
Podd, S. J., Freemantle, N., Furniss, S. S., and Sulke, N. (2016). First clinical trial of specific I_{KACh} blocker shows no reduction in atrial fibrillation burden in patients with paroxysmal atrial fibrillation: pacemaker assessment of BMS 914392 in patients with paroxysmal atrial fibrillation. *Europace* 18, 340–6. doi:10.1093/europace/euv263.

Posokhova, E., Ng, D., Opel, A., Masuho, I., Tinker, A., Biesecker, L. G., et al. (2013). Essential Role of the m2R-RGS6-IKACh Pathway in Controlling Intrinsic Heart Rate Variability. *PLoS One* 8, e76973. doi:10.1371/journal.pone.0076973.

Posokhova, E., Wydeven, N., Allen, K. L., Wickman, K., and Martemyanov, K. A. (2010). RGS6/Gβ5 Complex Accelerates I_{KACh} Gating Kinetics in Atrial Myocytes and Modulates Parasympathetic Regulation of Heart Rate. *Circ. Res.* 107, 1350–1354. doi:10.1161/CIRCRESAHA.110.224212.

Poth, K., Nutter, T. J., Cuevas, J., Parker, M. J., Adams, D. J., and Luetje, C. W. (1997). Heterogeneity of nicotinic receptor class and subunit mRNA expression among individual parasympathetic neurons from rat intracardiac ganglia. *J. Neurosci.* 17, 586–596. doi:10.1523/jneurosci.17-02-00586.1997.

Premchand, R. K., Sharma, K., Mittal, S., Monteiro, R., Dixit, S., Libbus, I., et al. (2016). Extended follow-up of patients with heart failure receiving autonomic regulation therapy in the ANTHEM-HF Study. *J. Card. Fail.* 22, 639–642. doi:10.1016/j.cardfail.2015.11.002.

Prystowsky, E. N., Naccarelli, G. V., Jackman, W. M., Rinkenberger, R. L., Heger, J. J., and Zipes, D. P. (1983). Enhanced parasympathetic tone shortens atrial refractoriness in man. *Am. J. Cardiol.* 51, 96–100. doi:10.1016/S0002-9149(83)80018-6.

Qin, M., Liu, X., Liu, T., Wang, T., and Huang, C. (2016). Potential role of regulator of G-protein signaling 5 in the protection of vagal-related bradycardia and atrial tachyarrhythmia. *J. Am. Heart Assoc.* 5, e002783. doi:10.1161/JAHA.115.002783.

Ramalho, D., and Freitas, J. (2018). Drug-induced life-threatening arrhythmias and sudden cardiac death: A clinical perspective of long QT, short QT and Brugada syndromes. *Rev. Port. Cardiol.* 37, 435–446. doi:10.1016/j.repc.2017.07.010.

Ramos-Hunter, S. J., Engers, D. W., Kaufmann, K., Du, Y., Lindsley, C. W., Weaver, C. D., et al. (2013). Discovery and SAR of a novel series of GIRK1/2 and GIRK1/4 activators. *Bioorg. Med. Chem. Lett.* 23, 5195–5198. doi:10.1016/j.bmcl.2013.07.002.

Randall, W. C., Ardell, J. L., Wurster, R. D., and Milosavljevic, M. (1987). Vagal postganglionic innervation of the canine sinoatrial node. *J. Auton. Nerv. Syst.* 20, 13–23. doi:10.1016/0165-1838(87)90077-4.

Raveh, A., Cooper, A., Guy-David, L., and Reuveny, E. (2010). Nonenzymatic rapid control of GIRK channel function by a G protein-coupled receptor kinase. *Cell* 143, 750–760. doi:10.1016/j.cell.2010.10.018.

Rishal, I., Keren-Raifman, T., Yakubovich, D., Ivanina, T., Dessauer, C. W., Slepak, V. Z., et al. (2003). Na^+ promotes the dissociation between $G\alpha_{GDP}$ and Gβγ, activating G protein-gated K^+ channels. *J. Biol. Chem.* 278, 3840–3845. doi:10.1074/jbc.C200605200.

Roussel, J., Champeroux, P., Roy, J., Richard, S., Fauconnier, J., Le Guennec, J. Y., et al. (2016). The complex QT/RR relationship in mice. *Sci. Rep.* 6. doi:10.1038/srep25388.

Rust, G., Burgunder, J. -M, Lauterburg, T. E., and Cachelin, A. B. (1994). Expression of neuronal nicotinic acetylcholine receptor subunit genes in the rat autonomic Nervous System. *Eur. J. Neurosci.* 6, 478–485. doi:10.1111/j.1460-9568.1994.tb00290.x.

Sabbah, H. N., Ilsar, I., Zaretsky, A., Rastogi, S., Wang, M., and Gupta, R. C. (2011). Vagus nerve stimulation in experimental heart failure. *Heart Fail. Rev.* 16, 171–178. doi:10.1007/s10741-010-9209-z.

Sakmann, B., Noma, A., and Trautwein, W. (1983). Acetylcholine activation of single muscarinic K^+ channels in isolated pacemaker cells of the mammalian heart. *Nature*

303, 250–253. doi:10.1038/303250a0.
Salama, G., and London, B. (2007). Mouse models of long QT syndrome. *J. Physiol.* 578, 43–53. doi:10.1113/jphysiol.2006.118745.
Saternos, H. C., Almarghalani, D. A., Gibson, H. M., Meqdad, M. A., Antypas, R. B., Lingireddy, A., et al. (2018). Distribution and function of the muscarinic receptor subtypes in the cardiovascular system. *Physiol. Genomics* 50, 1–9. doi:10.1152/physiolgenomics.00062.2017.
Schwartz, P. J. (1998). The autonomic nervous system and sudden death. *Eur. Heart J.* 19 Suppl F, F72-80.
Schwartz, P. J., and De Ferrari, G. M. (2011). Sympathetic-parasympathetic interaction in health and disease: abnormalities and relevance in heart failure. *Heart Fail. Rev.* 16, 101–7. doi:10.1007/s10741-010-9179-1.
Sebastian, S., Ang, R., Abramowitz, J., Weinstein, L. S., Chen, M., Ludwig, A., et al. (2013). The *in vivo* regulation of heart rate in the murine sinoatrial node by stimulatory and inhibitory heterotrimeric G proteins. *Am. J. Physiol. Integr. Comp. Physiol.* 305, R435–R442. doi:10.1152/ajpregu.00037.2013.
Shen, M. J., and Zipes, D. P. (2014). Role of the autonomic nervous system in modulating cardiac arrhythmias. *Circ. Res.* 114, 1004–1021. doi:10.1161/CIRCRESAHA.113.302549.
Shih, H. T. (1994). Anatomy of the action potential in the heart. *Texas Hear. Inst. J.* 21, 30–41.
Shu, J., Zhou, J., Patel, C., and Yan, G. X. (2009). Pharmacotherapy of cardiac arrhythmias - Basic science for clinicians. *PACE - Pacing Clin. Electrophysiol.* 32, 1454–1465. doi:10.1111/j.1540-8159.2009.02526.x.
Signorini, S., Liao, Y. J., Duncan, S. A., Jan, L. Y., and Stoffel, M. (1997). Normal cerebellar development but susceptibility to seizures in mice lacking G protein-coupled, inwardly rectifying K^+ channel GIRK2. *Proc. Natl. Acad. Sci. U. S. A.* 94, 923–927. doi:10.1073/pnas.94.3.923.
Smith, S., Rossignol, P., Willis, S., Zannad, F., Mentz, R., Pocock, S., et al. (2016). Neural modulation for hypertension and heart failure. *Int. J. Cardiol.* 214, 320–330. doi:10.1016/j.ijcard.2016.03.078.
Stallmeyer, B., Kuß, J., Kotthoff, S., Zumhagen, S., Vowinkel, K., Rinné, S., et al. (2017). A mutation in the G-protein gene *GNB2* causes familial sinus node and atrioventricular conduction dysfunction. *Circ. Res.* 120, e33–e44. doi:10.1161/CIRCRESAHA.116.310112.
Stancák, B. (1998). Pathophysiologic mechanisms of atrial rhythm disorders. II. Atrial flutter. *Vnitr. Lek.* 44, 722–6.
Standish, A., Enquist, L. W., and Schwaber, J. S. (1994). Innervation of the heart and its central medullary origin defined by viral tracing. *Science (80-.).* 263, 232–234. doi:10.1126/science.8284675.
Stengel, P. W., Gomeza, J., Wess, J., and Cohen, M. L. (2000). M(2) and M(4) receptor knockout mice: muscarinic receptor function in cardiac and smooth muscle in vitro. *J. Pharmacol. Exp. Ther.* 292, 877–85.
Stewart, A., and Fisher, R. A. (2015). “Introduction: G Protein-coupled Receptors and RGS Proteins,” in *Progress in Molecular Biology and Translational Science* (Elsevier B.V.), 1–11. doi:10.1016/bs.pmbts.2015.03.002.
Stewart, A., Huang, J., and Fisher, R. A. (2012). RGS proteins in heart: brakes on the vagus. *Front. Physiol.* 3, 95. doi:10.3389/fphys.2012.00095.
Stuesse, S. L., and Fish, S. E. (1984). Projections to the cardioinhibitory region of the nucleus ambiguus of rat. *J. Comp. Neurol.* 229, 271–278. doi:10.1002/cne.902290211.

Suh, B.-C., and Hille, B. (2008). PIP_2 Is a necessary cofactor for ion channel function: How and why? . *Annu. Rev. Biophys.* 37, 175–195. doi:10.1146/annurev.biophys.37.032807.125859.
Sun, H., Nasi-Er, B. G., Wang, X., Zhang, L., Lu, Y., Zhou, X., et al. (2020). Tragus nerve stimulation suppresses post-infarction ventricular arrhythmia by modulating autonomic activity and heterogeneities of cardiac receptor distribution. *Med. Sci. Monit.* 26. doi:10.12659/MSM.922277.
Sweeney, M. O., Ruetz, L. L., Belk, P., Mullen, T. J., Johnson, J. W., and Sheldon, T. (2007). Bradycardia pacing-induced short-long-short sequences at the onset of ventricular tachyarrhythmias. A possible mechanism of proarrhythmia? *J. Am. Coll. Cardiol.* 50, 614–622. doi:10.1016/j.jacc.2007.02.077.
Szentandrassy, N., Nagy, D., Hegyi, B., Magyar, J., Banyasz, T., and P. Nanasi, P. (2015). Class IV antiarrhythmic agents: New compounds using an old strategy. *Curr. Pharm. Des.* 21, 977–1010. doi:10.2174/1381612820666141029105910.
Tai, C. T., and Chen, S. A. (2009). Electrophysiological mechanisms of atrial flutter. *J. Chinese Med. Assoc.* 72, 60–67. doi:10.1016/S1726-4901(09)70024-3.
Takao, K., Yoshii, M., Kanda, A., Kokubun, S., and Nukada, T. (1994). A region of the muscarinic-gated atrial K^+ channel critical for activation by G protein beta gamma subunits. *Neuron* 13, 747–55. doi:10.1016/0896-6273(94)90041-8.
Takesono, A., Nowak, M. W., Cismowski, M., Duzic, E., and Lanier, S. M. (2002). Activator of G-protein signaling 1 blocks GIRK channel activation by a G-protein-coupled receptor: apparent disruption of receptor signaling complexes. *J. Biol. Chem.* 277, 13827–30. doi:10.1074/jbc.M201064200.
Tanaka, H., and Hashimoto, N. (2007). A multiple ion channel blocker, NIP-142, for the treatment of atrial fibrillation. *Cardiovasc. Drug Rev.* 25, 342–356. doi:10.1111/j.1527-3466.2007.00025.x.
Tarvainen, M. P., Niskanen, J.-P., Lipponen, J. A., Ranta-Aho, P. O., and Karjalainen, P. A. (2014). Kubios HRV--heart rate variability analysis software. *Comput. Methods Programs Biomed.* 113, 210–20. doi:10.1016/j.cmpb.2013.07.024.
Terry, P., and Katz, J. L. (1994). A comparison of the effects of the D1 receptor antagonists SCH 23390 and SCH 39166 on suppression of feeding behavior by the D1 agonist SKF38393. *Psychopharmacology (Berl).* 113, 328–333. doi:10.1007/BF02245205.
Touhara, K. K., and MacKinnon, R. (2018). Molecular basis of signaling specificity between GIRK channels and GPCRs. *Elife* 7. doi:10.7554/eLife.42908.
Tsai, M. L., Chen, C. C., Yeh, C. J., Chou, L. M., and Cheng, C. H. (2012). Frequency ranges of heart rate variability related to autonomic nerve activity in the mouse. *Clin. Exp. Hypertens.* 34, 182–190. doi:10.3109/10641963.2011.577492.
Turker, I., Ai, T., Itoh, H., and Horie, M. (2017). Drug-induced fatal arrhythmias: Acquired long QT and Brugada syndromes. *Pharmacol. Ther.* 176, 48–59. doi:10.1016/j.pharmthera.2017.05.001.
Uijtdehaage, S. H. J., and Thayer, J. F. (2000). Accentuated antagonism in the control of human heart rate. *Clin. Auton. Res.* 10, 107–110. doi:10.1007/BF02278013.
Vandenberg, J. I., Perry, M. D., Perrin, M. J., Mann, S. A., Ke, Y., and Hill, A. P. (2012). hERG K(+) channels: structure, function, and clinical significance. *Physiol. Rev.* 92, 1393–1478. doi:10.1152/physrev.00036.2011.
Victoria, N. C., Marron Fernandez de Velasco, E., Ostrovskaya, O., Metzger, S., Xia, Z., Kotecki, L., et al. (2016). G Protein-Gated K+ Channel Ablation in Forebrain Pyramidal Neurons Selectively Impairs Fear Learning. *Biol. Psychiatry* 80, 796–806. doi:10.1016/j.biopsych.2015.10.004.
Vo, B. N., Abney, K. K., Anderson, A., Marron Fernandez de Velasco, E., Benneyworth,

M. A., Daniels, J. S., et al. (2019). VU0810464, a non-urea G protein-gated inwardly rectifying K^+ (Kir3/GIRK) channel activator, exhibits enhanced selectivity for neuronal Kir3 channels and reduces stress-induced hyperthermia in mice. *Br. J. Pharmacol.* 176, 2238–2249. doi:10.1111/bph.14671.

Voigt, N., Abu-Taha, I., Heijman, J., and Dobrev, D. (2014). Constitutive Activity of the Acetylcholine-Activated Potassium Current IK,ACh in Cardiomyocytes. *Advances in pharmacology*, 393–409. doi:10.1016/B978-0-12-417197-8.00013-4.

Voigt, N., Heijman, J., Trausch, A., Mintert-Jancke, E., Pott, L., Ravens, U., et al. (2013). Impaired Na^+-dependent regulation of acetylcholine-activated inward-rectifier K^+ current modulates action potential rate dependence in patients with chronic atrial fibrillation. *J. Mol. Cell. Cardiol.* 61, 142–152. doi:10.1016/j.yjmcc.2013.03.011.

Voigt, N., Maguy, A., Yeh, Y.-H., Qi, X., Ravens, U., Dobrev, D., et al. (2007). Changes in IK,ACh single-channel activity with atrial tachycardia remodelling in canine atrial cardiomyocytes. *Cardiovasc. Res.* 77, 35–43. doi:10.1093/cvr/cvm051.

Von Dannecker, L. E. C., Mercadante, A. F., and Malnic, B. (2006). Ric-8B promotes functional expression of odorant receptors. *Proc. Natl. Acad. Sci. U. S. A.* 103, 9310–4. doi:10.1073/pnas.0600697103.

Wallukat, G. (2002). The β-adrenergic receptors. *Herz* 27, 683–690. doi:10.1007/s00059-002-2434-z.

Wang, F., Liu, J., Hong, L., Liang, B., Graff, C., Yang, Y., et al. (2013a). The phenotype characteristics of type 13 long QT syndrome with mutation in KCNJ5 (Kir3.4-G387R). *Hear. Rhythm* 10, 1500–1506. doi:10.1016/j.hrthm.2013.07.022.

Wang, J., Irnaten, M., Neff, R. A., Venkatesan, P., Evans, C., Loewy, A. D., et al. (2006). Synaptic and Neurotransmitter Activation of Cardiac Vagal Neurons in the Nucleus Ambiguus. *Ann. N. Y. Acad. Sci.* 940, 237–246. doi:10.1111/j.1749-6632.2001.tb03680.x.

Wang, X., Liang, B., Skibsbye, L., Olesen, S.-P., Grunnet, M., and Jespersen, T. (2013b). GIRK channel activation via adenosine or muscarinic receptors has similar effects on rat atrial electrophysiology. *J. Cardiovasc. Pharmacol.* 62, 192–198. doi:10.1097/FJC.0b013e3182965221.

Wang, Y., Po, S. S., Scherlag, B. J., Yu, L., and Jiang, H. (2019). The role of low-level vagus nerve stimulation in cardiac therapy. *Expert Rev. Med. Devices* 16, 675–682. doi:10.1080/17434440.2019.1643234.

Weis, W. I., and Kobilka, B. K. (2018). The molecular basis of G protein–coupled receptor activation. *Annu. Rev. Biochem.* 87, 897–919. doi:10.1146/annurev-biochem-060614-033910.

Wellner-Kienitz, M. C., Bender, K., Meyer, T., Bünemann, M., and Pott, L. (2000). Overexpressed A1 adenosine receptors reduce activation of acetylcholine-sensitive K^+ current by native muscarinic M2 receptors in rat atrial myocytes. *Circ. Res.* 86, 643–648. doi:10.1161/01.RES.86.6.643.

Wen, W., Wu, W., Romaine, I. M., Kaufmann, K., Du, Y., Sulikowski, G. A., et al. (2013). Discovery of 'molecular switches' within a GIRK activator scaffold that afford selective GIRK inhibitors. *Bioorg. Med. Chem. Lett.* 23, 4562–4566. doi:10.1016/j.bmcl.2013.06.023.

Wess, J., Liu, J., Blin, N., Yun, J., Lerche, C., and Kostenis, E. (1997). Structural basis of receptor/G protein coupling selectivity studied with muscarinic receptors as model systems. in *Life Sciences* (Life Sci), 1007–1014. doi:10.1016/S0024-3205(97)00041-6.

White, D. W., and Raven, P. B. (2014). Autonomic neural control of heart rate during dynamic exercise: Revisited. *J. Physiol.* 592, 2491–2500. doi:10.1113/jphysiol.2014.271858.

Whorton, M. R., and MacKinnon, R. (2011). Crystal Structure of the Mammalian GIRK2 K+ Channel and Gating Regulation by G Proteins, PIP_2, and Sodium. *Cell* 147, 199–208. doi:10.1016/j.cell.2011.07.046.
Wickman, K., and Clapham, D. E. (1995). Ion channel regulation by G proteins. *Physiol. Rev.* 75, 865–885. doi:10.1152/physrev.1995.75.4.865.
Wickman, K. D., Iñiguez-Lluhi, J. A., Davenport, P. A., Taussig, R., Krapivinsky, G. B., Linder, M. E., et al. (1994). Recombinant G-protein βγ-subunits activate the muscarinic-gated atrial potassium channel. *Nature* 368, 255–257. doi:10.1038/368255a0.
Wickman, K., Karschin, C., Karschin, A., Picciotto, M. R., and Clapham, D. E. (2000). Brain localization and behavioral impact of the G-protein-gated K^+ channel subunit GIRK4. *J. Neurosci.* 20, 5608–5615. doi:10.1523/JNEUROSCI.20-15-05608.2000.
Wickman, K., Nemec, J., Gendler, S. J., and Clapham, D. E. (1998). Abnormal heart rate regulation in GIRK4 knockout mice. *Neuron* 20, 103–14. doi:10.1016/s0896-6273(00)80438-9.
Wickman, K., Pu, W. T., and Clapham, D. E. (2002). Structural characterization of the mouse Girk genes. *Gene* 284, 241–250. doi:10.1016/S0378-1119(01)00884-8.
Willars, G. B. (2006). Mammalian RGS proteins: Multifunctional regulators of cellular signalling. *Semin. Cell Dev. Biol.* 17, 363–376. doi:10.1016/j.semcdb.2006.03.005.
Woodard, G. E., Jardín, I., Berna-Erro, A., Salido, G. M., and Rosado, J. A. (2015). Regulators of G-protein-signaling proteins: Negative modulators of G-protein-coupled receptor signaling. *Int. Rev. Cell Mol. Biol.* 317, 97–183. doi:10.1016/bs.ircmb.2015.02.001.
Wydeven, N., Marron Fernandez de Velasco, E., Du, Y., Benneyworth, M. A., Hearing, M. C., Fischer, R. A., et al. (2014a). Mechanisms underlying the activation of G-protein-gated inwardly rectifying K^+ (GIRK) channels by the novel anxiolytic drug, ML297. *Proc. Natl. Acad. Sci.* 111, 10755–10760. doi:10.1073/pnas.1405190111.
Wydeven, N., Posokhova, E., Xia, Z., Martemyanov, K. A., and Wickman, K. (2014b). RGS6, but not RGS4, is the dominant regulator of G protein signaling (RGS) modulator of the parasympathetic regulation of mouse heart rate. *J. Biol. Chem.* 289, 2440–9. doi:10.1074/jbc.M113.520742.
Wydeven, N., Young, D., Mirkovic, K., and Wickman, K. (2012). Structural elements in the Girk1 subunit that potentiate G protein-gated potassium channel activity. *Proc. Natl. Acad. Sci.* 109, 21492–21497. doi:10.1073/pnas.1212019110.
Xie, K., Allen, K. L., Kourrich, S., Colón-Saez, J., Thomas, M. J., Wickman, K., et al. (2010). Gβ5 recruits R7 RGS proteins to GIRK channels to regulate the timing of neuronal inhibitory signaling. *Nat. Neurosci.* 13, 661–663. doi:10.1038/nn.2549.
Xie, X., Lee, S. W., Johnson, C., Ippolito, J., Kenknight, B. H., and Tolkacheva, E. G. (2014). Intermittent vagal nerve stimulation alters the electrophysiological properties of atrium in the myocardial infarction rat model. in *2014 36th Annual International Conference of the IEEE Engineering in Medicine and Biology Society, EMBC 2014* (Institute of Electrical and Electronics Engineers Inc.), 1575–1578. doi:10.1109/EMBC.2014.6943904.
Yamamoto, W., Hashimoto, N., Matsuura, J., Machida, T., Ogino, Y., Kobayashi, T., et al. (2014). Effects of the selective KACh channel blocker NTC-801 on atrial fibrillation in a canine model of atrial tachypacing. *J. Cardiovasc. Pharmacol.* 63, 421–427. doi:10.1097/FJC.0000000000000065.
Yang, J., Huang, J., Maity, B., Gao, Z., Lorca, R. A., Gudmundsson, H., et al. (2010a). RGS6, a modulator of parasympathetic activation in heart. *Circ. Res.* 107, 1345–1349. doi:10.1161/CIRCRESAHA.110.224220.
Yang, J., Maity, B., Huang, J., Gao, Z., Stewart, A., Weiss, R. M., et al. (2013). G-protein

inactivator RGS6 mediates myocardial cell apoptosis and cardiomyopathy caused by doxorubicin. *Cancer Res.* 73, 1662–1667. doi:10.1158/0008-5472.CAN-12-3453.
Yang, Y., Yang, Y., Liang, B., Liu, J., Li, J., Grunnet, M., et al. (2010b). Identification of a Kir3.4 mutation in congenital long QT syndrome. *Am. J. Hum. Genet.* 86, 872–80. Available at: http://www.ncbi.nlm.nih.gov/pubmed/20560207 [Accessed January 29, 2019].
Ye, C., Sowell, M. O., Vassilev, P. M., Milstone, D. S., and Mortensen, R. M. (1999). Galpha(i2), Galpha(i3)and Galpha(o) are all required for normal muscarinic inhibition of the cardiac calcium channels in nodal/atrial-like cultured cardiocytes. *J. Mol. Cell. Cardiol.* 31, 1771–81. doi:10.1006/jmcc.1999.1015.
You, C. X., and Liu, C. F. (2019). Premature Ventricular Contractions and Cardiomyopathy. *Cardiol. Rev.* 27, 322–326. doi:10.1097/CRD.0000000000000262.
Yu, L., Wang, S., Zhou, X., Wang, Z., Huang, B., Liao, K., et al. (2016). Chronic Intermittent low-level stimulation of tragus reduces cardiac autonomic remodeling and ventricular arrhythmia inducibility in a post-infarction canine model. *JACC Clin. Electrophysiol.* 2, 330–339. doi:10.1016/j.jacep.2015.11.006.
Yuill, K. H., and Hancox, J. C. (2002). Characteristics of single cells isolated from the atrioventricular node of the adult guinea-pig heart. *Pflugers Arch. Eur. J. Physiol.* 445, 311–320. doi:10.1007/s00424-002-0932-8.
Zaza, A., Robinson, R. B., and DiFrancesco, D. (1996). Basal responses of the L-type Ca2+ and hyperpolarization-activated currents to autonomie agonists in the rabbit sino-atrial node. *J. Physiol.* 491, 347–355. doi:10.1113/jphysiol.1996.sp021220.
Zhang, H., He, C., Yan, X., Mirshahi, T., and Logothetis, D. E. (1999). Activation of inwardly rectifying K^+ channels by distinct Ptdlns(4,5)P2 interactions. *Nat. Cell Biol.* 1, 183–188. doi:10.1038/11103.
Zhang, Y., and Mazgalev, T. N. (2011). Arrhythmias and vagus nerve stimulation. *Heart Fail. Rev.* 16, 147–161. doi:10.1007/s10741-010-9178-2.
Zhang, Y., Popović, Z. B., Bibevski, S., Fakhry, I., Sica, D. A., Van Wagoner, D. R., et al. (2009). Chronic vagus nerve stimulation improves autonomic control and attenuates systemic inflammation and heart failure progression in a canine high-rate pacing model. *Circ. Hear. Fail.* 2, 692–699. doi:10.1161/CIRCHEARTFAILURE.109.873968.
Zhou, L., Filiberti, A., Humphrey, M. B., Fleming, C. D., Scherlag, B. J., Po, S. S., et al. (2019). Low-level transcutaneous vagus nerve stimulation attenuates cardiac remodelling in a rat model of heart failure with preserved ejection fraction. *Exp. Physiol.* 104, 28–38. doi:10.1113/EP087351.
Zhu, C., Hanna, P., Rajendran, P. S., and Shivkumar, K. (2019). Neuromodulation for Ventricular tachycardia and atrial fibrillation: A Clinical Scenario-Based Review. *JACC Clin. Electrophysiol.* 5, 881–896. doi:10.1016/j.jacep.2019.06.009.
Zuberi, Z., Birnbaumer, L., and Tinker, A. (2008). The role of inhibitory heterotrimeric G proteins in the control of in vivo heart rate dynamics. *Am. J. Physiol. Integr. Comp. Physiol.* 295, R1822–R1830. doi:10.1152/ajpregu.90625.2008.